

# **Development of *Mycobacterium tuberculosis* DNA gyrase as a target for antibacterial chemotherapy**

---

Shantanu Karkare

John Innes Centre

September 2010

This thesis is submitted in partial fulfilment of the requirements of the degree of Doctor of Philosophy at the University of East Anglia.

© This copy of the thesis has been supplied on condition that anyone who consults it is understood to recognise that its copyright rests with the author and that no quotation from the thesis, nor any information derived therefrom, may be published without the authors prior, written consent.

## ABSTRACT

Bacterial DNA gyrase is one of the proven targets for antibacterial chemotherapy. It is a type II DNA topoisomerase found in all bacteria. Most of our current information is related to the enzyme from *Escherichia coli* (*E. coli*), a Gram-negative bacterium, with limited information about the gyrase from *Mycobacterium tuberculosis* (*M. tuberculosis*), a Gram-positive bacterium. The emergence of multidrug-resistant tuberculosis (MDR-TB) and extremely drug-resistant tuberculosis (XDR-TB) with no new classes of drugs has posed a great challenge for the effective and short-term treatment of tuberculosis. Thus, it has become important to understand and investigate established drug targets, such as DNA gyrase, in *M. tuberculosis*. Although there are similarities between the gyrases from these two bacteria, there are key differences, which can be potentially exploited for identifying new drugs for tuberculosis. This work describes the identification of a putative Ca<sup>2+</sup>-binding site in *M. tuberculosis* GyrA and discovery of naphthoquinones as novel inhibitors of DNA gyrase.

In the absence of a complete crystal structure for *M. tuberculosis* GyrA, a homology model was constructed for biochemical and site-directed mutagenesis experiments involving the putative Ca<sup>2+</sup>-binding site. These experiments indicate that Ca<sup>2+</sup> has a potential regulatory role in *M. tuberculosis*. Virtual screening was performed to identify novel inhibitors targeting the Ca<sup>2+</sup>-binding site.

Diospyrin, a naphthoquinone was identified as a potent inhibitor of DNA gyrase. This work has demonstrated that diospyrin inhibits DNA gyrase with a novel mechanism and that the GyrB N-terminal domain is the potential target site. Docking studies were performed to predict the diospyrin-binding site in GyrB.

# TABLE OF CONTENTS

ABSTRACT .....	2
LIST OF FIGURES .....	7
LIST OF TABLES .....	14
ACKNOWLEDGEMENTS .....	17
Chapter 1: General Introduction.....	18
1.1 Tuberculosis .....	18
1.2 DNA topology.....	22
1.3 Biological significance of DNA topology.....	24
1.4 DNA topoisomerases .....	25
1.4.1 Introduction .....	25
1.4.2 Type IA topoisomerases.....	28
1.4.3 Structure of type IA topoisomerase.....	30
1.4.4 Mechanism of action of type IA topoisomerase .....	32
1.4.5 Type IB topoisomerases .....	33
1.4.6 Mechanism of action of type IB topoisomerases .....	35
1.4.7 Type II DNA topoisomerases.....	37
1.4.8 Structure of Type IIA topoisomerases .....	38
1.4.9 ATP hydrolysis by type II topoisomerases .....	41
1.4.10 Mechanism of type IIA topoisomerases.....	41
1.5 DNA gyrase.....	44
1.5.1 Introduction .....	44
1.5.2 DNA gyrase strand passage mechanism .....	49
1.5.3 DNA wrapping by DNA gyrase.....	49
1.5.4 DNA cleavage-religation reaction by DNA gyrase .....	50
1.5.5 ATP hydrolysis by DNA gyrase .....	52
1.5.6 DNA gyrase in eukaryotes .....	54
1.6 Type IIB topoisomerases .....	54
1.7 DNA gyrase inhibitors .....	56
1.7.1 Fluoroquinolones .....	57
1.7.2 Aminocoumarins .....	66
1.7.3 Simocyclinones .....	69
1.7.4 Cyclothialidine .....	71
1.7.5 GSK299423.....	73
1.7.6 CcdB.....	75

1.7.7 Microcin B17 .....	76
1.8 Other proteinaceous inhibitors .....	78
1.9 Aim of the project .....	80
Chapter 2: Materials & Methods.....	81
2.1 Bacteriology .....	81
2.1.1 <i>E. coli</i> and <i>M. smegmatis</i> strains.....	81
2.1.2 Media and antibiotics .....	82
2.1.3 Preparation of electrocompetent <i>M. smegmatis</i> cells.....	83
2.1.4 Preparation of chemically competent <i>E. coli</i> cells.....	84
2.1.5 Transformation.....	84
2.2 Molecular biology methods.....	85
2.2.1 Oligonucleotides .....	85
2.2.2 Preparation of supercoiled and relaxed pBR322*.....	87
2.2.3 Plasmid DNA purification.....	88
2.2.4 DNA concentration determination .....	88
2.2.5 PCR and cloning .....	89
2.2.6 Site-directed mutagenesis.....	90
2.2.7 RT-PCR (reverse-transcriptase).....	92
2.2.8 Agarose gel electrophoresis .....	92
2.2.9 DNA sequencing .....	93
2.3 Protein Methods .....	94
2.3.1 Purification of <i>M. tuberculosis</i> DNA gyrase and mutants.....	94
2.3.2 SDS-PAGE.....	95
2.3.3 Dialysis.....	96
2.3.4 Protein concentration .....	97
2.3.5 Protein concentration determination .....	97
2.3.6 Limited Proteolysis .....	98
2.3.7 Electroblothing & Edman sequencing .....	98
2.3.8 Peptide mass fingerprinting by Orbitrap mass spectrometer .....	99
2.3.9 Circular dichroism.....	100
2.4 Enzyme assays .....	102
2.4.1 DNA supercoiling, relaxation, and decatenation assays.....	102
2.4.2 DNA wrapping assay .....	102
2.4.3 Promoter activity assay ( $\beta$ -galactosidase activity assay).....	103
2.5 Biophysical techniques.....	104
2.5.1 ICP-AES.....	104

2.5.2 Nano-ESI MS .....	106
2.5.3 BIAcore .....	107
2.5.4 Protein crystallography .....	108
2.6 Bioinformatics software .....	109
2.6.1 Clustal W and MUSCLE.....	109
2.6.2 PSIPRED.....	110
2.6.3 PROSITE .....	110
2.6.4 Phyre and BioInfoBank MetaServer .....	110
2.6.5 Insight II.....	111
2.6.6 AutoDock Vina 1.0.2 .....	111
2.6.7 Discovery Studio 2.5.5.....	112
Chapter 3: Unique features of <i>M. tuberculosis</i> DNA gyrase .....	113
3.1 Purification of <i>M. tuberculosis</i> DNA gyrase .....	114
3.2 Bioinformatics analysis of <i>M. tuberculosis</i> DNA gyrase.....	115
3.3 <i>M. tuberculosis</i> GyrB promoter analysis .....	116
3.3.1 RT-PCR for <i>M. tuberculosis</i> GyrB transcript .....	117
3.3.2 Mass spectrometric analysis.....	120
3.3.3 GyrB N40Δ deletion mutant .....	121
3.3.4 Promoter analysis .....	125
3.4 A putative Ca <sup>2+</sup> -binding site in DNA gyrase.....	130
3.4.1 EF-hand Ca <sup>2+</sup> - binding domain .....	133
3.4.2 Model for the Ca <sup>2+</sup> - binding site .....	138
3.5 Conclusion .....	144
Chapter4 : Investigation of a putative Ca <sup>2+</sup> -binding site in <i>M. tuberculosis</i> GyrA	148
4.1 Bacterial DNA gyrase Ca <sup>2+</sup> selectivity.....	149
4.2 Ca <sup>2+</sup> -assisted Mg <sup>2+</sup> - dependent enzyme .....	153
4.3 SDM of the Ca <sup>2+</sup> -binding site .....	163
4.4 Effect of EGTA on the activity of mutants .....	174
4.5 Limited Proteolysis of GyrA.....	177
4.6 Virtual screening at the Ca <sup>2+</sup> -binding site .....	183
4.6.1 Introduction.....	183
4.6.2 Docking-based virtual screening.....	184
4.7 Conclusion .....	192
Chapter 5 : Identification and characterization of novel gyrase inhibitors .....	196
5.1 Introduction.....	197
5.2 Quinolines .....	198

5.3 Aaptamines and marine extracts .....	201
5.4 Naphthoquinones .....	205
5.5 Targets for naphthoquinones.....	208
5.6 Naphthoquinones inhibits DNA gyrase .....	211
5.7 <i>E. coli</i> Inhibitory activity .....	219
5.8 Diospyrin binding site .....	220
5.8.1 <i>M. tuberculosis</i> GyrB-diospyrin complex.....	221
5.8.2 <i>E. coli</i> GyrB43-diospyrin complex .....	225
5.9 Limited Proteolysis .....	229
5.10 Surface plasmon resonance .....	233
5.11 ATP competition assay .....	239
5.12 <i>M. tuberculosis</i> GyrB43- diospyrin complex.....	241
5.13 Discussion .....	247
Chapter 6: General Discussion.....	252
6.1 Introduction .....	252
6.2 <i>M. tuberculosis</i> GyrB promoter analysis .....	253
6.3 Putative Ca <sup>2+</sup> -binding site .....	254
6.4 Novel DNA gyrase inhibitors.....	261
APPENDIX.....	265
Crystallisation trials .....	266
ABBREVIATIONS.....	269
REFERENCES .....	270

## LIST OF FIGURES

Figure 1.1: <i>M. tuberculosis</i> stained with Zein-Neelsen stain.....	18
Figure 1.2: A global map showing the estimated TB incidence rates by country in 2007.....	20
Figure 1.3 : Mechanism of action of different TB drugs. ....	21
Figure 1.4: Significance of DNA topoisomerase.. ....	26
Figure 1.5: Classification of Topoisomerase based on structure and mechanism. ....	27
Figure 1.6: Domain alignment of type IA topoisomerase showing the structural diversity.....	30
Figure 1.7: Structure of <i>E. coli</i> topo III and <i>Archaeoglobus fulgidus</i> reverse gyrase. ....	31
Figure 1.8: General mechanism of action of type I topoisomerase.....	33
Figure 1.9: Detailed mechanism of human topoisomerase I.....	35
Figure 1.10: Structure of human topoI .....	36
Figure 1.11: Reactions catalysed by typeII topoisomerases .....	37
Figure 1.12: Domain organisation of type IIA topoisomerases .....	39
Figure 1.13: Conserved functional domains in type II topoisomerases. ....	40
Figure 1.14: Two-gate mechanism for type II A topoisomerase .....	42
Figure 1.15: Crystal structures of different domains of <i>E. coli</i> DNA gyrase.....	43
Figure 1.16: Electrostatic map of the GyrB' dimer and DNA duplex.....	47
Figure 1.17: Crystal structures of different domains of <i>M. tuberculosis</i> DNA gyrase .....	48
Figure 1.18: Crystal structures of GyrA C-terminal domain. ....	50
Figure 1.19: The two-metal ion mechanism for cleavage-religation reaction .....	51
Figure 1.20: Interaction between GyrB24 and ATP showing hydrogen-bonds with different residues. ....	52
Figure 1.21: Crystal structure of apo topo VI .....	55
Figure 1.22 : The DNA gyrase reaction and sites of action of gyrase inhibitors.....	56
Figure 1.23: Structures of fluoroquinolones. ....	58
Figure 1.24: Crystal structure of the topo IV-DNA-moxifloxacin complex.....	59
Figure 1.25: Quinolone-topo IV cleavage complex.....	60
Figure 1.26: <i>S. aureus</i> DNA gyrase in complex with ciprofloxacin and DNA .....	60

Figure 1.27: MfpA, Qnr homologue found in <i>M. tuberculosis</i> .....	65
Figure 1.28: The three main naturally-occurring aminocoumarins: novobiocin, clorobiocin, and coumermycin A <sub>1</sub> . .....	67
Figure 1.29: Overlap of the novobiocin (green) and ADPNP (red) binding site at <i>E. coli</i> GyrB N-terminus (GyrB24). .....	68
Figure 1.30: Simocyclinone D8 binds to GyrA59. ....	70
Figure 1.31: Cyclothialidine inhibits the ATPase activity of the GyrB subunit. ....	72
Figure 1.32: GSK299423 a novel DNA gyrase inhibitor.....	74
Figure 1.33: CcdB with multiple interacting partners: CcdA and DNA gyrase. ....	76
Figure 1.34: MccB17 chemical structure and gene cluster.....	77
Figure 2.1: Flowchart for the protein refolding experiment. ....	97
Figure 2.2: CD spectra of poly-L-lysine at pH 11.1 and placental collagen.....	101
Figure 2.3: Illustration of ICP-AES for the detection of metals or cations.....	105
Figure 2.4: Electrospray ionisation process. ....	107
Figure 3.1: SDS-PAGE (12%) of DNA gyrase subunits purified by affinity chromatography.....	114
Figure 3.2: Enzyme activity of purified <i>M. tuberculosis</i> DNA gyrase. ....	115
Figure 3.3: Multiple sequence alignment of bacterial GyrB using ClustalW 1.83..	116
Figure 3.4: RT- PCR for <i>M. tuberculosis</i> GyrB transcripts.....	119
Figure 3.5: Orbitrap analysis of <i>M. tuberculosis</i> GyrB.....	121
Figure 3.6: Different fractions of GyrB N40Δ deletion mutant purified by HisTrap .....	122
Figure 3.7: Effect of GyrB N40Δ on the decatenation activity of <i>M. tuberculosis</i> DNA gyrase.....	123
Figure 3.8: Effect of GyrB N40Δ on the supercoiling and relaxation activity of <i>M. tuberculosis</i> DNA gyrase .....	124
Figure 3.9: Promoters of <i>M. tuberculosis</i> DNA gyrase. ....	125
Figure 3.10: Screen capture of Artemis analysis of <i>gyr</i> promoter elements.....	126
Figure 3.11: Colonies of <i>M. smegmatis</i> mc <sup>2</sup> -155 obtained by transformation of the cells with pSM-128, pSM-128-Met and pSM-128-Val plasmids .....	128

Figure 3.12: $\beta$ -galactosidase activity recorded from the crude extract of <i>M. smegmatis</i> mc <sup>2</sup> -155 cells transformed with pSM-128, pSM-128-Val and pSM-128-Met respectively. ....	129
Figure 3.13: DNA gyrase is the only type II topoisomerase in <i>M. tuberculosis</i> .....	131
Figure 3.14: Multiple sequence alignment of bacterial GyrA using ClustalW 1.83	131
Figure 3.15: Multiples sequence alignment for GyrA from <i>B. melitensis</i> , <i>M. tuberculosis</i> and <i>C. diphtheriae</i> . ....	132
Figure 3.16: The two major groups of EF-hands .....	134
Figure 3.17: The non-cannonical EF-hand Ca <sup>2+</sup> -binding sites.....	136
Figure 3.18: Illustration of differences between canonical and pseudo-EF hand....	137
Figure 3.19: Sequence alignment for <i>M. tuberculosis</i> GyrA. ....	139
Figure 3.20: Homology model of <i>M. tuberculosis</i> GyrA Ca <sup>2+</sup> -binding site (MtGyrA-1H71) based on the psychrophilic metalloprotease from <i>Pseudomonas sp.</i> (PDB code: 1H71). ....	141
Figure 3.21: Homology model of <i>M. tuberculosis</i> GyrA Ca <sup>2+</sup> -binding site (MtGyrA-1BQB) based on <i>Staphylococcus aureus</i> metalloproteinase (PDB code: 1BQB)....	142
Figure 3.22: Difference between the 3-D environments of the GyrA Ca <sup>2+</sup> -binding site and the <i>Staphylococcus aureus</i> metalloproteinase (PDB id: 1BQB) template..	144
Figure 3.23: The predicted Ca <sup>2+</sup> -binding site in between the N- and C-terminal domains of <i>M. tuberculosis</i> DNA gyrase. ....	147
Figure 4.1: <i>E. coli</i> and <i>M. tuberculosis</i> DNA gyrase supercoiling assay in the presence of 6 mM Mg <sup>2+</sup> and Ca <sup>2+</sup> .....	149
Figure 4.2: Supercoiling assay of <i>M. tuberculosis</i> and <i>E. coli</i> hybrid enzyme in the presence of 6 mM Mg <sup>2+</sup> and 6 mM Ca <sup>2+</sup> .....	150
Figure 4.3: Effect of EGTA dialysis on the supercoiling and decatenation activity of <i>M. tuberculosis</i> DNA gyrase.....	154
Figure 4.4: DNA relaxation assay in the presence and absence of 1 mM Ca <sup>2+</sup> .....	155
Figure 4.5: Time-course experiment to demonstrate the difference in the relaxation activity of GyrA dialysed in the absence and presence of EGTA.....	156
Figure 4.6: Experimental plan for protein refolding experiment. ....	157
Figure 4.7: Effect of protein refolding in the presence and absence of EGTA on the supercoiling and relaxation activity of DNA gyrase.....	162

Figure 4.8: Effect of protein refolding in the presence and absence of EGTA on the decatenation activity of DNA gyrase. ....	163
Figure 4.9: Double mutation in the Ca <sup>2+</sup> - binding site. ....	164
Figure 4.10: Quadruple mutation in the Ca <sup>2+</sup> - binding site. ....	164
Figure 4.11: Acidic amino-acids in MtGyrA-1H71 and MtGyrA-1BQB model that were mutated to alanine in side-directed mutagenesis experiments. ....	165
Figure 4.12: Effect of double (GyrA E508A, D509A) and quadruple mutations. ...	167
Figure 4.13: Effect of quadruple mutation (GyrA D504A, E508A, D509A, E514A) on the supercoiling activity under different assay conditions. ....	168
Figure 4.14: No significant effect of double (GyrA E508A, D509A) and quadruple mutations (GyrA D504A, E508A, D509A, E514A) on the relaxation activity .....	169
Figure 4.15: Decatenation activity of the wild-type and quadruple mutant. ....	170
Figure 4.16: Far-UV (180-260 nm) CD spectra of wild-type GyrA and GyrA D504A, E508A, D509A, E514A .....	171
Figure 4.17: The effect of quadruple mutation (D504A, E508A, D509A, and E514A) on DNA wrapping around GyrA. ....	173
Figure 4.18: Effect of EGTA on the supercoiling and relaxation activity of the mutants. ....	175
Figure 4.19: Far-UV (180-260 nm) CD spectra of wild-type GyrA (dialysed in 1 mM EGTA) and GyrA D504A, E508A, D509A, E514A (dialysed in 1 mM EGTA) .....	176
Figure 4.20: Tryptic digest of the <i>M. tuberculosis</i> GyrA in the absence of Ca <sup>2+</sup> and in the presence of Ca <sup>2+</sup> .....	178
Figure 4.21: Tryptic digest of the <i>M. tuberculosis</i> GyrB in the absence of Ca <sup>2+</sup> and in the presence of Ca <sup>2+</sup> .....	179
Figure 4.22: Trypsin digestion profile of <i>M. tuberculosis</i> GyrA in the presence and absence of Ca <sup>2+</sup> at 30 min time. ....	180
Figure 4.23: Molecular weight estimation of the bands. ....	181
Figure 4.24: The sequence coverage of band 2&8 (~47-kDa). ....	182
Figure 4.25: Virtual screening of NCI diversity set II. ....	185
Figure 4.26: List of 51 hit compounds from the virtual screening of NCI diversity set II centered at the Ca <sup>2+</sup> -binding site in <i>M. tuberculosis</i> GyrA. ....	186

Figure 4.27: Inhibitory activity of the 10 selected compounds (100 $\mu$ M) against the supercoiling and relaxation activity of <i>M. tuberculosis</i> DNA gyrase.....	187
Figure 4.28: Chemical structures of 10 selected compounds from the virtual screening that were tested for their inhibitory activity in a standard supercoiling and relaxation assay. ....	189
Figure 4.29: Predicted binding modes for ligands ZINC01572309 and ZINC01639634. ....	190
Figure 4.30: Predicted binding modes for ligands ZINC01690699 and ZINC13130018. ....	191
Figure 4.31: Representation of the domains affected during the trypsin digestion in the presence of 3 mM $Ca^{2+}$ .....	195
Figure 5.1: Similar pharmacore of the fluoroquinolones and quinolines.....	198
Figure 5.2: Inhibitory activity of chloroquine and Mefloquine. ....	200
Figure 5.3: DNA cleavage assay in the presence of chloroquine and mefloquine (B) in the absence of ATP. ....	201
Figure 5.4: Aptos, a marine sponge and a natural source of Aaptamine. ....	202
Figure 5.5: Aaptamines and marine extracts.....	203
Figure 5.6: Inhibitory activity of aaptamine and kaempferol.....	204
Figure 5.7: <i>E. natalensis</i> , a medicinal plant and a natural source of naphthoquinones. ....	205
Figure 5.8: Naphthoquinones studied for their activity against mycobacterial DNA gyrase. ....	206
Figure 5.9: Structural similarities between 7-methyljuglone and menaquinone.....	209
Figure 5.10: Mycothiol reductase (Mtr) target for naphthoquinones.....	210
Figure 5.11: Supercoiling inhibition assay of 7-methyljuglone and diospyrin against wild-type <i>M. tuberculosis</i> DNA gyrase. ....	212
Figure 5.12: Supercoiling inhibition assay of neodiospyrin, isodiospyrin, menadione and shinanolone against wild-type <i>M. tuberculosis</i> DNA gyrase.....	213
Figure 5.13: Relaxation and decatenation inhibition assays of 7-methyljuglone and diospyrin respectively against <i>M. tuberculosis</i> DNA gyrase.....	214
Figure 5.14: Inhibition of <i>E. coli</i> DNA gyrase supercoiling activity in the presence of 7-methyljuglone and diospyrin. ....	216

Figure 5.15: DNA cleavage assay in the presence of different concentrations of 7-methyljuglone and diospyrin and in the presence of 1 mM ATP. ....	217
Figure 5.16: DNA cleavage assay in the presence of 7-methyljuglone and diospyrin in the absence of ATP. ....	218
Figure 5.17: In-vitro inhibitory activity of diospyrin against <i>E. coli</i> NR698 .....	219
Figure 5.18: Mass spectrometry spectrum of <i>M. tuberculosis</i> GyrB monomer (79-kDa).....	222
Figure 5.19: Mass spectrometry spectrum of <i>M. tuberculosis</i> GyrB in the presence of an 8-fold excess of diospyrin. ....	223
Figure 5.20: Mass spectrometry spectrum of <i>M. tuberculosis</i> GyrB in the presence of a 16-fold excess of diospyrin. ....	224
Figure 5.21: Mass spectrometry spectrum for protein-diospyrin complex. ....	225
Figure 5.22: Representation of GyrB functional domains. ....	226
Figure 5.23: Mass spectrometry spectrum of <i>E. coli</i> GyrB43. ....	226
Figure 5.24: Mass spectrometry of <i>E. coli</i> GyrB43 in the presence of a 16-fold excess of diospyrin. ....	227
Figure 5.25: Mass spectrometry spectrum of <i>E. coli</i> GyrB47. ....	228
Figure 5.26: Mass spectrometry spectrum of <i>E. coli</i> GyrB47 in the presence of a 16-fold excess of diospyrin. ....	229
Figure 5.27: Tryptic digest of the <i>M. tuberculosis</i> GyrA and <i>M. tuberculosis</i> GyrB in the presence and absence of diospyrin.....	230
Figure 5.28: Tryptic digest of <i>E. coli</i> GyrA and <i>E. coli</i> GyrB43 in the presence and absence of diospyrin.....	232
Figure 5.29: Surface plasmon resonance data showing binding of novobiocin to <i>E. coli</i> GyrB43 and <i>M. tuberculosis</i> GyrB .....	234
Figure 5.30: Surface plasmon resonance data showing binding of diospyrin to <i>E. coli</i> GyrB43.....	235
Figure 5.31: Surface plasmon resonance data shows novobiocin binding to <i>M. tuberculosis</i> GyrA and GyrB. ....	236
Figure 5.32: Experimental design for studying competition between novobiocin and diospyrin.....	237

Figure 5.33: Raw surface plasmon resonance data showing a series of 100 nM novobiocin injections followed by series of diospyrin injections. ....	238
Figure 5.34: Effect of ATP concentration on the extent of inhibition. ....	240
Figure 5.35: Potential diospyrin binding sites in the model structure of <i>M. tuberculosis</i> GyrB43 .....	243
Figure 5.36: Top 2 scoring poses of the diospyrin at site 1+2 referred to as pose-1+2.1 and pose- 1+2.2.....	245
Figure 5.37: Site-5, potential binding site for diospyrin with a deep cleft like binding pocket. ....	246
Figure 5.38: Docked diospyrin at site-5 forming 3 hydrogen bonds with Thr294, Thr302 and His 303.....	246
Figure 5.39: Potential binding site of diospyrin described as site-5 with the docked molecule. ....	250
Figure 5.40: <i>E. coli</i> GyrB43 superimposed over modeled <i>M. tuberculosis</i> GyrB43 with diospyrin docked at site-5. ....	250
Figure 6.1: Model proposed for the regulation of DNA supercoiling.....	258
Figure 6.2: Conformational changes in <i>M. tuberculosis</i> GyrA due to quadruple mutation (GyrA D504A, E508A, D509A, E514A), Ca <sup>2+</sup> and EGTA.....	260

# LIST OF TABLES

Table 1.1: Diversity of topoisomerases in the cellular world. ....	28
Table 1.2: Mutations in the DNA gyrase subunit conferring resistance to fluoroquinolones. ....	64
Table 2.1: The list of <i>E. coli</i> and <i>M. smegmatis</i> strains used in the study. ....	81
Table 2.2: PCR primers for generating PCR products that were cloned into vectors. .....	85
Table 2.3: Oligonucleotides designed in order to introduce mutations into expression plasmid pET20- <i>gyrA</i> . ....	86
Table 2.4: Oligonucleotide for RT-PCR. ....	86
Table 2.5: Typical thermocycler program used for amplifying sequences for promoter analysis. ....	90
Table 2.6: Typical thermocycler program used for side-directed mutagenesis. ....	91
Table 2.7: Typical thermocycler program used for RT-PCR. ....	92
Table 2.8: Typical thermocycler program used DNA sequencing. ....	93
Table 2.9: Composition of resolving and stacking gels of a 12.5 % SDS-PAGE. ....	95
Table 2.10: Instrument setting for ICP-AES. ....	105
Table 4.1: Summary of supercoiling activity of wild-type and hybrid enzymes in the presence $Mg^{2+}$ and $Ca^{2+}$ .....	151
Table 4.2: Summary of the activity of hybrid enzymes from different sources. ....	152
Table 4.3: ICP-AES Estimation of $Ca^{2+}$ and $Mg^{2+}$ in native and refolded <i>M.</i> <i>tuberculosis</i> GyrA. ....	159
Table 4.4: ICP-AES Estimation of $Ca^{2+}$ and $Mg^{2+}$ in <i>M. tuberculosis</i> GyrA dialysed or refolded in the presence of 1 mM EGTA. ....	160
Table 4.5: Summary table for the effect of EGTA dialysis and refolding on the enzyme activity. ....	161
Table 4.6: Sequence coverage and molecular weights for bands (1- 10). ....	181
Table 4.7: AutoDock Vina v1.0.2 calculated free energy of binding (FEB), number of rotatable bonds (#RotBonds), calculated hydrophobicity distribution (XLOGP) and molecular topological polar surface area (TPSA). ....	192

Table 5.1: IC <sub>50</sub> values for chloroquine and mefloquine based on supercoiling and relaxation assays.....	200
Table 5.2: Antituberculosis activity and cytotoxicity of 7-methyljuglone and its derivatives. ....	207
Table 5.3: Substrate properties of naphthoquinones with <i>M. tuberculosis</i> Mtr.....	211
Table 5.4: DNA supercoiling IC <sub>50</sub> values for naphthoquinones.....	215
Table 5.5: DNA relaxation and decatenation IC <sub>50</sub> values for naphthoquinones. ....	215
Table 5.6: Summary results of diospyrin binding studies using nano- ESI-MS.....	221
Table 5.7: Five docking sites in the <i>M. tuberculosis</i> GyrB43 model.....	244
Table 5.8: DNA supercoiling IC <sub>50</sub> values for Quinolines, Aaptamines and naphthoquinones. ....	248
Table 5.9: IC <sub>50</sub> values of 7-methyljuglone and diospyrin based on supercoiling, relaxation and decatenation assay. ....	248
Table 5.10: Percentage of cysteine residues present in <i>E. coli</i> and <i>M. tuberculosis</i> DNA gyrase.....	251

**This thesis is dedicated to the God Almighty, my family and all those people who are suffering with tuberculosis.**

## ACKNOWLEDGEMENTS

The work presented in this thesis was carried out in the laboratory of Professor A. Maxwell in the Department of Biochemistry, John Innes Centre, Norwich (UK). First of all I would like to thank Tony for his guidance throughout the course of my Ph.D. and giving me the freedom to plan my research. I would also like to thank Ms. Lesley Mitchenall and Dr. Nick Burton for sharing the best moments of my PhD and for helpful discussions.

I would like thank my collaborators whose cooperation has made it possible to work on multi-disciplinary aspects of this project: Prof. Namrita Lall, (University of Pretoria, South Africa) and Prof. Mark Hamann, PhD (The University of Mississippi) for providing compounds for my work on novel inhibitors; Dr. Faridoon Yousafzai, (Computational and Systems Biology, John Innes Centre, UK), Dr. Lora Mak (Theoretical Systems Biology, Institute of Food Research, UK) for providing computational biology support and help with molecular structure; Dr. Adam McKay, (University College London), Dr. Amanda Brown, Prof. Tanya Parish (Barts and The London School of Medicine and Dentistry), Dr. Sandra Greive (University of Cambridge, UK), Ms. Fiona Husband (Institute of Food Research, UK) for providing scientific guidance and assistance in my project.

I would also like to thank members of my supervisory committee, Prof. Rob Field, Dr. David Lawson, Dr. Richard Morris for their guidance.

Big thanks also go to Ms. Sarah Tolland for always making it possible for me to attend conferences and presentations. I also thank the members and colleagues of the Biological Chemistry department for being supportive. I cannot forget the staff at Library (Ms. Rachel Lewis & Mr. Chris Groom) who provided all the support I needed during my thesis writing stage.

I also thank my 'Columbian mom' Ms. Maria A. Farah and my 'Kenyan sister' Dorice Agol for always being with me on this journey. I thank my family members for all the support. As I submit this thesis I am fulfilling my Grandpa's dream, I am sure he will be proud of it. My mom, papa, nana and my sister all have taken lot of efforts and made sacrifices while I was enjoying my scientific exploration. And finally thank you God for all your grace.

## Chapter 1: General Introduction

### 1.1 Tuberculosis

Tuberculosis (TB) is an infectious disease caused by the Gram-positive actinobacteria *Mycobacterium tuberculosis* (*M. tuberculosis*). It is an intracellular pathogen with high lipid content in the cell wall. It is also a slow-growing obligate aerobe. The Zein-Neelsen acid-fast staining procedure is used for microscopic examination of the bacteria because of its lipid-rich cell wall (**Figure 1.1**). TB infection first affects the lungs (pulmonary TB) and then spreads to lymph nodes affecting bones, kidneys and causing meningitis. It is a droplet infection that spreads by breathing droplets in the air containing the TB bacteria.

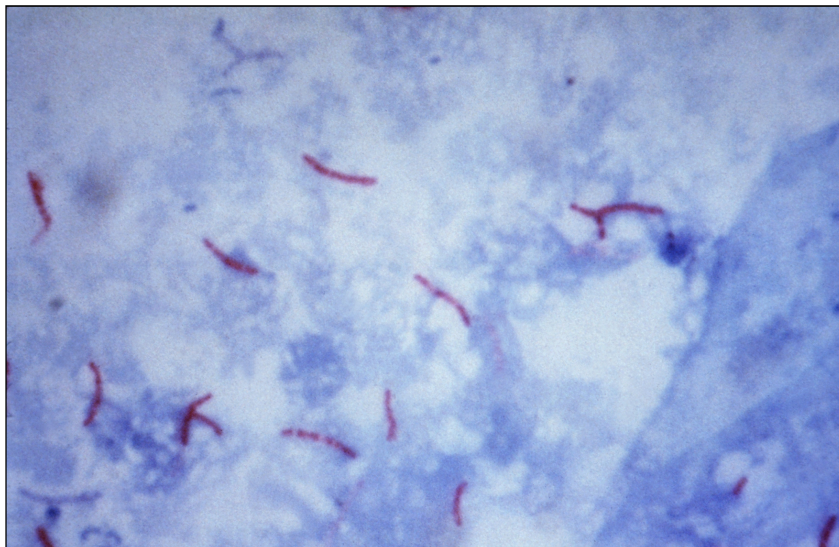


**Figure 1.1:** *M. tuberculosis* stained with Zein-Neelsen stain (Young *et al.*, 2008).

TB is a serious public health problem worldwide due to the AIDS epidemics, the advent of multidrug-resistant tuberculosis (MDR-TB) and extremely-drug resistant tuberculosis (XDR-TB) strains and the lack of new drugs in the market. Every year there are approximately 400,000 cases of MDR-TB, which is a specific form of drug-resistant TB. It occurs when the TB bacteria are resistant to at least isoniazid and rifampicin, the two most powerful anti-TB drugs. XDR-TB is a form of MDR-TB resistant to any fluoroquinolone, and at least one of the three second-line drugs (capreomycin, kanamycin, and amikacin).

WHO launched the DOTS programme (directly observed therapy, short courses) as a TB control strategy in 1994 (Young *et al.*, 2008). DOTS has relied on passive detection of microscopy smear-positive samples from patients. Although DOTS has been very successful at standardizing care practices and increasing cure rates, case-detection targets have been more difficult to achieve (Young *et al.*, 2008).

According to the latest WHO report published in 2009, 9.27 million new cases of TB occurred in 2007, 2 billion people are infected with TB, 12 million are co-infected with TB/HIV and two million people die every year. Asia (the south-east and western pacific regions) and Africa accounts for 55% and 31% respectively for all the cases worldwide. North & South America, eastern and Mediterranean regions also contribute to the global cases (**Figure 1.2**) (Bauquerez *et al.*, 2009). Though most cases of TB occur in Africa and Asia, in the UK about 8,000 cases of TB are reported each year and this number is rising slowly.

TB can be prevented by BCG (Bacillus Calmette-Guérin) vaccination, but it only protects between 70-80% of people who receive it. At present, the treatment time for TB is six to nine months with doses of multi-drug combinations. It has been nearly 35 years since the introduction of a new class of compounds for the TB treatment and until now, no significant advancements have been made in this area.

Based on the mechanism of action (**Figure 1.3**), the present antituberculosis drugs can be classified into following categories (Janin, 2007):

- 1. Inhibitors of DNA-based processes: Fluoroquinolones and Rifampicin.**
- 2. Inhibitors of protein synthesis: Streptomycin, Linezolid and Capreomycin.**
- 3. Peptidoglycan and arabinogalactam biosynthesis inhibitors: Ethambutol and Amoxicillin.**
- 4. Fatty acid biosynthesis inhibitors: Isoniazid, Pyrazinamide and PA-824.**

Drugs such as fluoroquinolone target DNA gyrase which is the focus of my research.

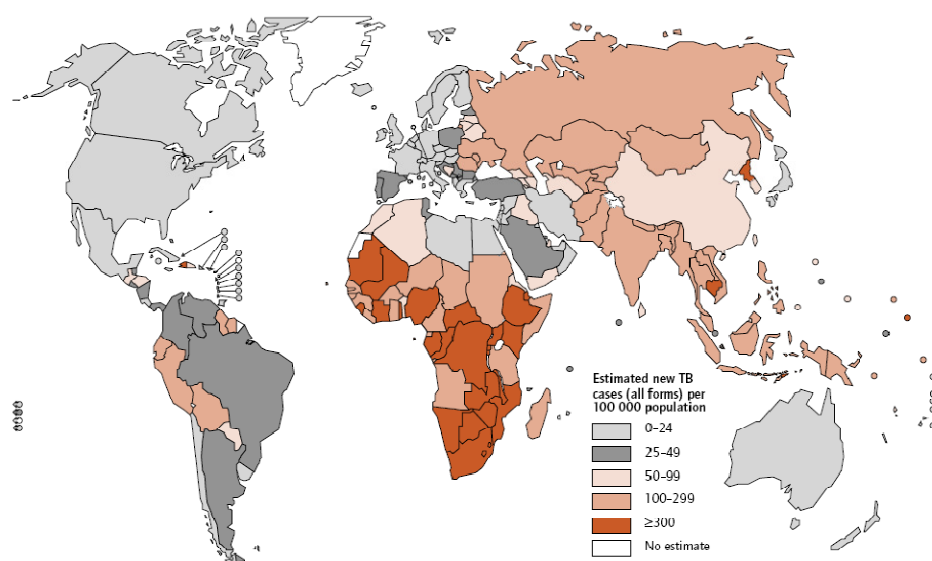


**Figure 1.2:** A global map showing the estimated TB incidence rates by country in 2007 (Bauquerez *et al.*, 2009).

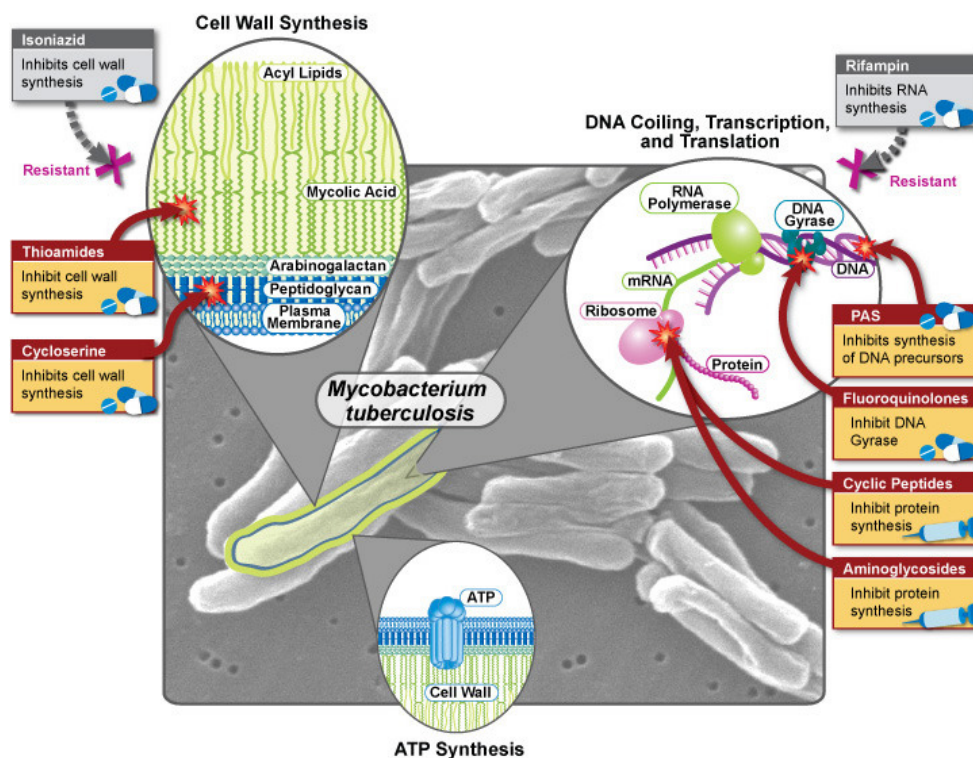


Figure 1.3 : Mechanism of action of different TB drugs.

(<http://www.nlm.nih.gov/medlineplus/tuberculosis.html>).

Despite the availability TB therapy, the emergence of MDR and XDR-TB has created demands for new effective drugs. Pharmaceutical companies have on-going programs in TB therapeutics, but it is not their primary focus. Active not-for-profit partnerships are playing important roles in accelerating the discovery and development of new TB drugs. For example, the TB Alliance and Bayer have signed an historic agreement to conduct a global clinical development program, seeking to register moxifloxacin for TB eradication. Moxifloxacin is a fluoroquinolone and an inhibitor of DNA gyrase.

## 1.2 DNA topology

DNA is the carrier of genetic information and it takes part in important cellular processes such as DNA replication and transcription. Several enzymes such as polymerases are involved in these processes and are sensitive to DNA topology for their activity. DNA topoisomerases have the ability to maintain DNA topology and solve topological problems that arise from processes such as transcription and DNA replication.

The determination of the structure of double-stranded DNA (Watson & Crick, 1953) in 1953 started the era of modern molecular biology. DNA is a right-handed 2 nm wide double-helical structure consisting of two strands of polynucleotide chain in opposite directions. The individual chains are joined together in pairs by double or triple hydrogen bonds between the purine and pyrimidine bases in each chain perpendicular to the helix axis ( $A = T$ ;  $G \equiv C$ ). According to the Watson and Crick model, there are ~10 base pairs (bp) for every turn of helix and a repeat distance of 3.4 nm for each successive turn. This form of the DNA double helix is known as the B-form. It is likely that the B-form represents the predominant conformation of DNA in cells; A- and Z-forms of DNA also exist. The existence of Z-form of DNA in vivo is debatable but the presence of A-DNA has been proposed at specific sites such as promoter regions (Shakkeed *et al.*, 1981) and transcription factor binding sites (Fairall *et al.*, 1989). Cruciforms, DNA triplexes and DNA quadruplexes are some other alternative DNA structures.

Bacterial plasmids, exists in a closed-circular form in which both the strands of the double-helical DNA are closed to form circles. This closed-circular DNA can be deformed under torsional stress to form supercoiled DNA (Sc). Supercoiling can be manifested as a change in twist (Tw) and / or a change in writhe (Wr). While twist is the number of double-helical turns in a given length of DNA, writhe quantifies the coiling of the path of a DNA helix in space. Each closed-circular DNA molecule has a linking number and it is called a topoisomer. Linking number (Lk) is the number of times the two strands of closed-circular DNA are linked.

$$\mathbf{Lk = Tw + Wr}$$

The Lk of closed circular DNA is changed through the breakage and the religation of one or both DNA strands. Positively supercoiled closed-circular DNA has a positive average linking difference ( $\Delta LK$ ), while negatively supercoiled closed-circular DNA has a negative average linking difference. The linking difference is the difference between the linking number of a particular topoisomer of closed-circular DNA (Lk) and the average linking number of relaxed DNA under given conditions ( $Lk^\circ = \text{No. bp/ helical repeat}$ ).  $Lk^\circ$  for the classical pBR322 plasmid is 415.3, if  $h = 10.5$  bp/turn under standard conditions (0.2 M NaCl, pH 7, 37°C).

$$\Delta Lk = Lk - Lk^\circ$$

Closed-circular DNA without any constraint of DNA helix and with average linking difference of zero is the relaxed DNA. Specific linking difference ( $\sigma$ ) compares the topological properties of DNA molecules of varying length. It is represented by the following equation.

$$\sigma = \Delta Lk / Lk^\circ$$

Double-stranded DNA can also form knots and catenanes. Knots were first observed in single- and double-stranded DNA (Liu *et al.*, 1976, Liu *et al.*, 1981). Catenanes were first observed in 1967 in the mitochondria of human cells (Clayton & Vinograd, 1967, Hudson & Vinograd, 1967). All these topological isomers (supercoiled DNA, relaxed DNA, knots and catenanes) of DNA can be studied by agarose gel electrophoresis. A closed-circular DNA molecule becomes more compact with increased writhe. As a result, compact DNA molecules migrate faster through the gels than topologically relaxed DNA molecules. DNA topoisomerases can interconvert between these different topological forms.

## 1.3 Biological significance of DNA topology

DNA topology is important for biological processes such as genome compaction, recombination, DNA replication, transcription, gene expression and chromosomal segregation. Genome compaction requires appropriate DNA topology, given the size of cells in which they are packaged. For example, the length of *E. coli* genome is ~1600  $\mu\text{M}$  enclosed in a rod-shaped cell that is ~1  $\mu\text{M}$  in diameter and ~3-5  $\mu\text{M}$  in length (Zimmerman, 2006). The DNA is negatively supercoiled and compacted into nucleoids in order to fit the *E. coli* chromosome within the cell. The nucleoids occupy less than 25% of the intracellular volume (Worcel & Burgi, 1972, Woldringh & Nanninga, 1985).

In case of eukaryotes the DNA forms nucleosomes consisting of 146 bp of DNA wrapped around the histone complex H2A/H2B/H3/H4 (Bates & Maxwell, 2005). This results in positive supercoils in the DNA which are then removed by topoisomerases to give negatively supercoiled DNA constrained within the nucleosomes (Bates & Maxwell, 2005). In prokaryotes, DNA gyrase introduces negative supercoils into DNA, which are then constrained by DNA-binding proteins. In eukaryotes, histones constrain the negative supercoiling of chromosomal DNA. Initiation of DNA replication requires unwinding of the DNA region forming the origin of replication. Negative supercoiling favours DNA unwinding and hence it is likely to favour the initiation of replication (Bates and Maxell, 2005). During the replication process, positive supercoils are formed ahead of the replication fork. These positive supercoils are likely to be removed by DNA gyrase and topo IV (Bates & Maxwell, 2005). Catenation may also result when two replication forks converge at the end of replication. Catenated DNA can be resolved by type II DNA topoisomerases. Both DNA gyrase and topo IV can decatenate DNA in *E. coli* (Steck & Drlica, 1984, Adams *et al.*, 1992). In case of *M. tuberculosis*, DNA gyrase performs efficient DNA decatenation in the absence of topo IV.

Similarly during transcription, movement of RNA polymerase results in positive and negative supercoiling ahead and behind the transcription bubble. This is called the ‘twin domain model for transcription’ (Liu & Wang, 1987). These positive and negative supercoils are removed by DNA gyrase and topo I respectively (**Figure 1.4**).

## 1.4 DNA topoisomerases

### 1.4.1 Introduction

DNA topoisomerases are a broad class of enzymes responsible for maintaining and manipulating the topological state of DNA (Corbett & Berger, 2003). These enzymes are required for vital processes in a cell such as DNA replication, transcription, recombination and chromatin remodeling; therefore they are found in all organisms including eukaryotes (yeast, plants, and animals), prokaryotes, viruses and archaea. Due to the important role played by topoisomerases in maintaining the cell viability, they are attractive clinical targets for antibiotics and chemotherapeutics (Maxwell, 2003). The first topoisomerase, *E. coli* topo I (*E. coli*  $\omega$  protein) was discovered in 1971 (Wang, 1971) followed by a second topoisomerase (eukaryotic type I) in 1972 (Champoux & Dulbecco, 1972).

Based on the mechanism of action, topoisomerases can be classified into two broad families, type I and type II. Type I topoisomerases cleave one strand, while type II cleave both strands, while manipulating the topological state of DNA. Both type I and type II topoisomerase can relax supercoiled DNA. This is important during transcription and DNA replication, which is when positive supercoils are generated ahead of RNA polymerase or DNA polymerase and negative supercoils are generated behind them (Liu & Wang, 1987, Cortes *et al.*, 2003) as shown in the **Figure 1.4B**. Type I and type II can also decatenate interlinked chromosomes formed during replication. Except prokaryotic type I topoisomerase and reverse gyrase, most DNA topoisomerases relax both negatively and positively supercoiled DNA. DNA gyrase and reverse gyrase are the only DNA topoisomerase that are able to introduce supercoils into DNA at the cost of ATP hydrolysis. While DNA gyrase introduces negative supercoils into DNA, reverse gyrase introduces positive supercoils.

Decatenation and unknotting are other topological simplification reactions that are catalysed by DNA topoisomerases. Decatenation involves unlinking two unlinked DNA plasmids and unknotting removes knots from circular plasmids.

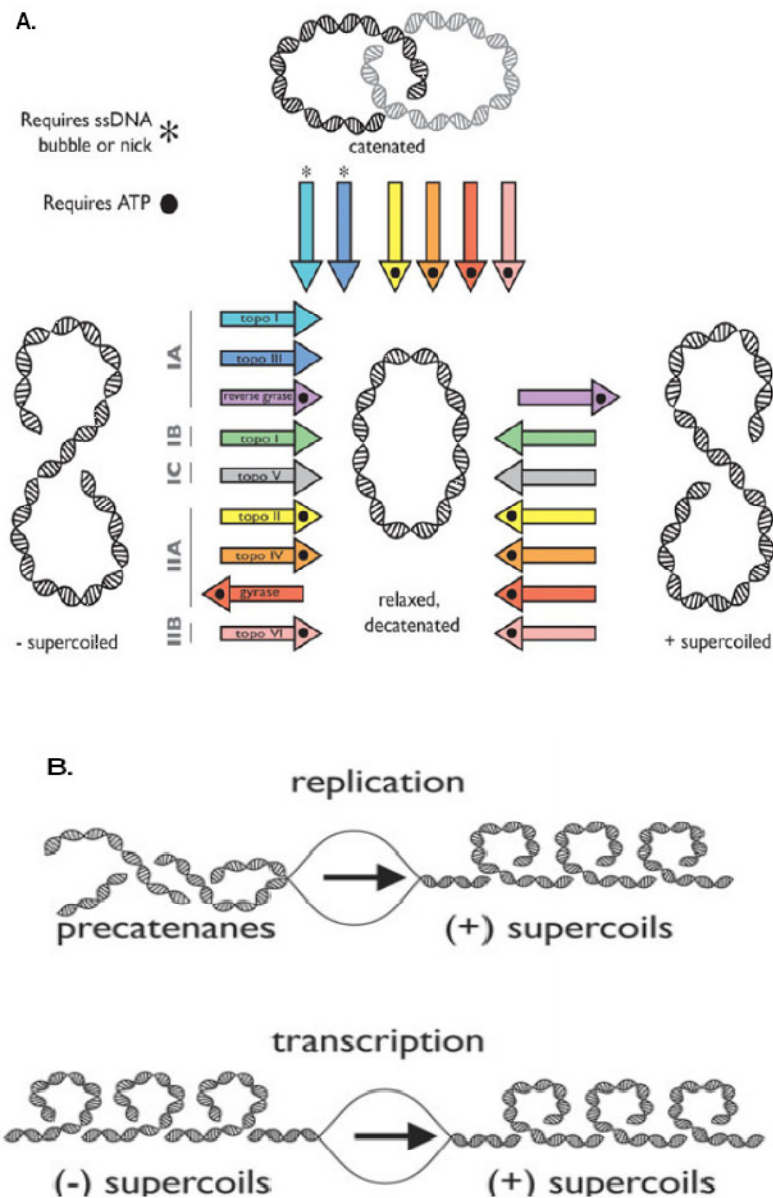


**Figure 1.4: Significance of DNA topoisomerase.** (A) Summary of different reactions catalysed by DNA topoisomerase. (B) DNA topoisomerase are required to resolve the changes in DNA topology during replication and transcription (Schoeffler & Berger, 2008).

As shown in **Figure 1.5** type I topoisomerases can be further subdivided into type IA and type IB, and type II into type IIA and type IIB based on structure and mechanism. The different types of topoisomerase can be found from single cell *E. coli* to higher eukaryotes. Within the bacterial world, topoisomerases are widely distributed. In *E. coli* four topoisomerases are found: DNA topoisomerase I, III (type IA), DNA gyrase and DNA topoisomerase IV (type IIA) (Wang, 2002, Wang, 1985). In some mesophilic bacteria topo III is absent. Other mesophiles have only two topoisomerases, one homologous to *E. coli* DNA gyrase and the second homologous to *E. coli* topo I. Reverse gyrase and topoisomerase V (type IB) are found in Hyperthermophiles. In Archaea, a reverse gyrase, a type IA topo, and topo VI are found. *Saccharomyces cerevisiae* and *Schizosaccharomyces pombe* have topo I (type IB), topo II (type IIA) and topo III (type IA). All higher eukaryotes have topo I and most have two type IIA isoforms (topo II $\alpha$ , topo II  $\beta$ ). They also contain two isoforms of topo III (topo III $\alpha$ , topo III  $\beta$ ). The distribution of DNA topoisomerase is summarised in Table 1.1.

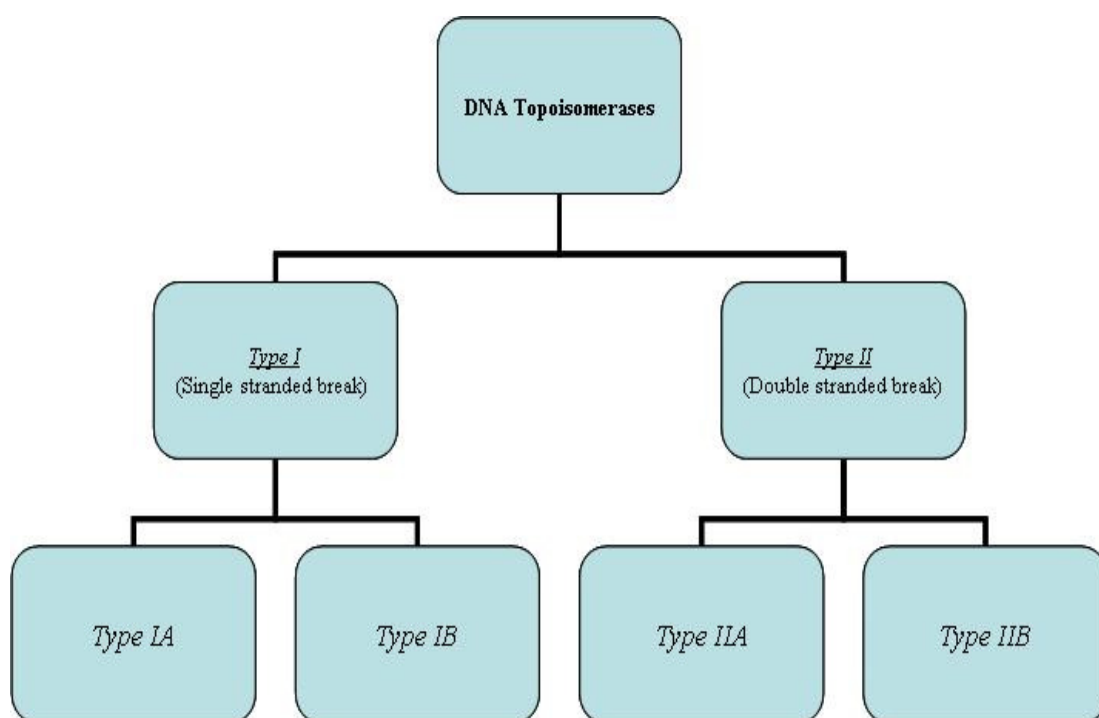


**Figure 1.5: Classification of Topoisomerase based on structure and mechanism.**

Organism	Type	Topoisomerase
Archaea	IA, IIB	Reverse gyrase, type IA topo and topo VI
<i>E. coli</i>	IA, IIA	Topo I, III, DNA gyrase and DNA topoisomerase IV
<i>M. tuberculosis</i>	IA, IIA	DNA gyrase, Topo I
Hyperthermophiles	IA, IB	Reverse gyrase, topoisomerase V
<i>Schizosaccharomyce. pombe</i> and <i>S. cerevisiae</i>	IA, IIA, IB	Topo I, topo II and topo III
Higher eukaryotes	IA, IIA, IB, IIB	Topo I, type IIA isoforms (topo II $\alpha$ , topo II $\beta$ ), topo III (topo III $\alpha$ , topo III $\beta$ ), topo VI

**Table 1.1: Diversity of topoisomerase in the cellular world.**

### 1.4.2 Type IA topoisomerases

Type IA topoisomerases form transient 5'-phospho-tyrosine covalent intermediates, releasing a free 3'-OH strand and allowing passage of the intact strand through the broken strand. The sub-type includes eubacterial DNA topoisomerase I, eubacterial DNA topoisomerase III, mammalian DNA topoisomerase III ( $\alpha/\beta$ ), eubacterial reverse gyrase and archaeal reverse gyrase. Type IA are able to relax negative supercoiling in the presence of  $Mg^{2+}$ , knot / unknot and catenate both single-stranded circles and double-stranded plasmids having nicks or gaps (Champoux, 2001).

All the members of this family share the following properties:

1. They are all monomers with the exception of the *Methanopyrus kandleri* topoV (Krah *et al.*, 1996) reverse gyrase.
2. DNA strand cleavage is accompanied by covalent attachment of one of the DNA ends to the enzyme through a 5' phosphodiester bond to the active site tyrosine.
3. Relaxation of negatively supercoiled DNA only in the presence of Mg<sup>2+</sup>.
4. Relaxation of negative supercoils does not go to completion and the change in the linking number is in the steps of one.
5. In addition to the ability to relax negative supercoils, these enzymes can catalyse the knotting, unkotting and interlinking of single-stranded circles as well as the knotting, unkotting, catenation and decatenation of gapped or nicked duplex DNA circles.

Besides the similarities, there are certain function and structural differences among the members of the family. For example *E. coli* topoisomerase III is much more effective at decatenation than topoisomerase I, and carries out this role in precatenane unlinking during DNA replication (DiGate & Marians, 1988, Hiasa *et al.*, 1994). In contrast to topoisomerase I, both *yeast* and *E. coli* topoisomerases III lack a Zn<sup>2+</sup>- binding domain altogether. Surprisingly human topoisomerase III has a Zn<sup>2+</sup>- binding domain with significant homology to that found in *E. coli* (Hanai *et al.*, 1996).

### 1.4.3 Structure of type IA topoisomerase

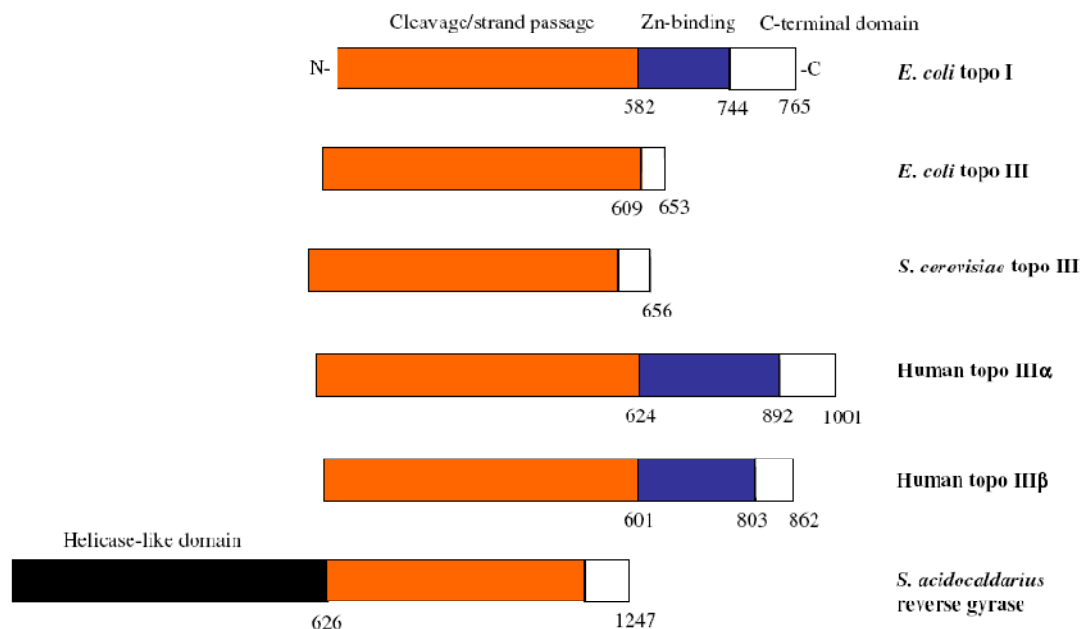


**Figure 1.6: Domain alignment of type IA topoisomerase showing the structural diversity (Bates & Maxwell, 2005).**

Within the same type IA subfamily there is diversity in the structure of the enzymes, as shown in the **Figure 1.6**. Type IA enzymes, like type IIA and IIB topoisomerases (**Figure 1.7**), have 5Y-CAP domains and Toprim domains (Corbett & Berger, 2004). Both these domains are important for DNA binding and cleavage. 5Y-CAP is a ‘winged-helix fold’ that bears the catalytic tyrosine residue that covalently attaches to the 5′ end of DNA (Corbett & Berger, 2004). The ‘Toprim’ domain is required for cleavage and has a cluster of acidic residues that are thought to form a binding site for  $Mg^{2+}$  ions (Corbett & Berger, 2004). These acidic residues are also brought close to the catalytic residues of the 5Y-CAP domains (Corbett & Berger, 2004). In addition to these domains, a CAP-like domain is present which is similar to the 5Y-CAP domain but it lacks the active-site tyrosine. This CAP-like domain, along with the 5Y-CAP domain, forms a hole in the centre of the protein having a diameter of  $\sim 25 \text{ \AA}$  (Corbett & Berger, 2004).

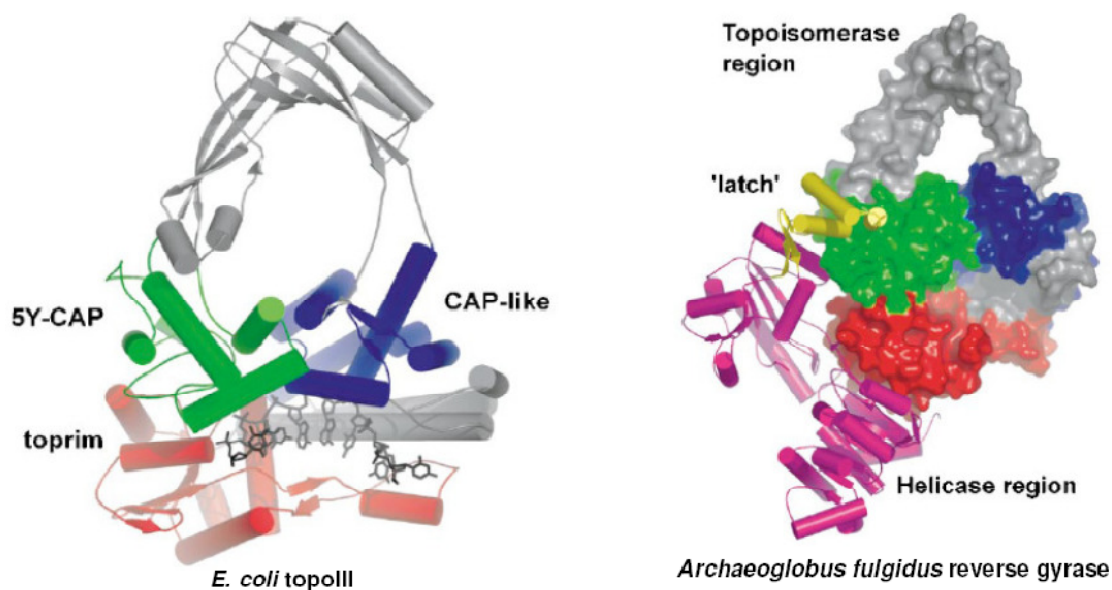


**Figure 1.7: Structure of *E. coli* topo III and *Archaeoglobus fulgidus* reverse gyrase (Corbett & Berger, 2004).**

There are some structural differences between the different members of type IA family. For example the *E. coli* topo I possess a 30-Da C-terminal region that bears five tandem  $Zn^{2+}$ -binding site, and the enzyme has been shown to bind up to two  $Mg^{2+}$  ions not observed in *E. coli* topo III. In the same way reverse gyrase, contains a distinctive helicase-like domain and a type IA topoisomerase domain in the same polypeptide. This distinct structure of reverse gyrase provides it the distinctive ability for ATP-dependent positive supercoiling of DNA.

Topo I from *M. tuberculosis* (Yang *et al.*, 1996, Annamalai *et al.*, 2009) and *M. smegmatis* (Bhaduri *et al.*, 1998) have also been purified and characterised. The gene encoding topo I in *M. tuberculosis* is 2700 nucleotide long encoding a 900 amino acid polypeptide with a molecular mass of 99,353 Da. The amino acid sequence identity in comparison to *E. coli* and *Synechococcus* topo I is 22 and 30% respectively. *M. tuberculosis* topo I like other topo Is relaxes negatively supercoiled DNA in a  $Mg^{2+}$ -dependent, ATP-independent reaction. However, there are differences between *M. tuberculosis* and *E. coli* at the structural and functional level. Unlike *E. coli* topo I it

does not contain a Zn<sup>2+</sup>-finger DNA binding motif in the C-terminal domain (Yang *et al.*, 1996) and is less efficient in removing negative supercoils from partially relaxed DNA. Interestingly like *E. coli*, *M. tuberculosis* topo I's preferred site for cleavage has a C nucleotide in the -4 position, with reference to its cleavage site (Annamalai *et al.*, 2009).

*M. smegmatis* topo I is the largest enzyme subunit (110-kDa) of the type IA family. It has all the typical properties of type I topoisomerases. However, like *M. tuberculosis* topo I it is different from the prototype *E. coli* topo I. It does not contain any bound Zn<sup>2+</sup> indicating the absence of the Zn<sup>2+</sup>-binding motif in DNA binding. Unlike *M. tuberculosis* DNA gyrase it is not inhibited by spermidine and is relatively stable at high temperatures. The enzyme activity is stimulated by single-strand DNA-binding protein (Sikder *et al.*, 2001, Bhaduri *et al.*, 1998). *M. smegmatis* topo I also has a specific cleavage site, which is a pentanucleotide motif (CG/TCT'T; † represents the cleavage site) (Sikder & Nagaraja, 2000). It has also been shown that the enzyme induced localized structural distortion upstream to the strong topoisomerase site (Bhaduri *et al.*, 2000) (Sikder & Nagaraja, 2001).

Topo I is a potential drug target. At present a lot of efforts are being directed to identify effective mycobacterial topo I inhibitors (Leelaram *et al.*, 2010). In the past diospyrin, a naphthoquinone (described in chapter 4) has been shown to inhibit eukaryotic topo I (Tazi *et al.*, 2005). At present topo I is one of the pipeline targets for the discovery of effective antibacterial at TB Alliance.

#### 1.4.4 Mechanism of action of type IA topoisomerase

The mechanism of action of type I A topoisomerase will be discussed by taking the example of *E. coli* topo I (**Figure 1.8**). A single strand of the DNA duplex (Li *et al.*, 2001) is cleaved followed by covalent bond formation between the active site tyrosine (Y319 in *E. coli* topo I) and the 5' phosphate of one of the free ends of the cleaved strand (Tse & Wang, 1980). In order to facilitate the intact strand passage, the protein domain, which possesses the active site tyrosine bound to the 5' end of the broken strand, moves to create a gap. Once the intact strand has been transported

through the gap, the broken strand is religated and the DNA is released. The linking number of the DNA changes by one with every round of strand passage. This mechanism has also been referred to as 'the enzyme-bridging model' (Champoux, 2001).

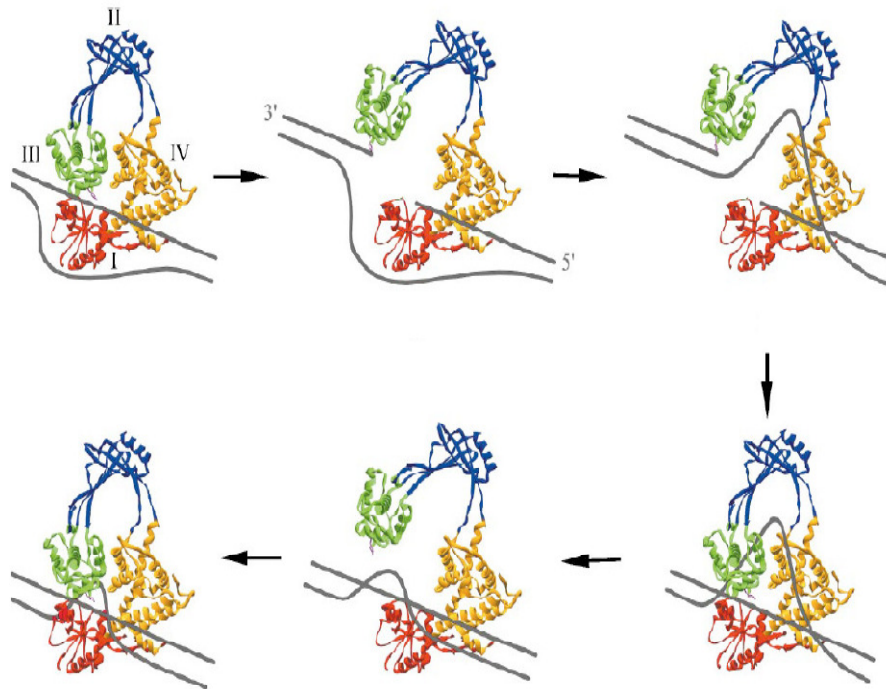


**Figure 1.8: General mechanism of action of type I topoisomerase demonstrating the single-stranded cleavage facilitating the strand passage for topological simplification (Champoux, 2001).**

### 1.4.5 Type IB topoisomerases

Type IB forms a 3'-phosphotyrosine covalent intermediate, releases the 5'-OH strand and leaves the broken strand free to rotate around the intact strand. This subtype includes eukaryotic DNA topoisomerase I, poxvirus DNA topoisomerase and eubacterial topoisomerase V (from *Methanopyrus*). Type IB can relax both negative and positive supercoils in a metal-independent process, unlike type IA topoisomerases. There are structural differences between the vacinina topo I (v-topoI) and human topo I

(h-topoI). Human topo I is larger (**Figure 1.10**) and has several extra domains (765 amino acids) in comparison to vaccinia topo I (314 amino acids). Human topo I has a highly charged and unstructured 24-kDa domain at its N-terminus (Stewart *et al.*, 1996). Although the function of this domain is not clear, it has shown to bind DNA downstream of the cleavage site to control DNA rotation (Lisby *et al.*, 2001).

There are three major sub domains (I, II, III) that wrap around the DNA duplex. Major portions of these domains comprise most of the IB/Int catalytic domain. The catalytic tyrosine of h-topoI (human) is present on a small 6-kDa domain at its C-terminus connected to the central body of the enzyme by a 7-kDa coiled linker elements. The linker region together with positively charged helices in sub domains I and II of the core region are thought to regulate the DNA rotation during the topoisomerase reaction (Lue *et al.*, 1995, Redinbo *et al.*, 2000, Stewart *et al.*, 1998). This arrangement of the catalytic residues is not found in v-topoI (virus) and it lacks the linker region.

Another type IB topoisomerase from the archeon *M. Kandleri* (110- kDa) is unique in structure and activity (Slesarev *et al.*, 1993). The 44-kDa N-terminal domain is similar to the IB/Int catalytic domain and the remaining 66-kDa has twelve 50 amino acid sequence repeats, each having helix-hairpin-helix DNA binding motifs (Belova *et al.*, 2001). Topo V activity is similar to the other type IB topoisomerase but topo V also aids enzyme processivity and possess apurinic site (AP) lyase activity (Belova *et al.*, 2001). A recently solved crystal structure of the N-terminal fragment of topoisomerase V shows no structural similarity with other type IB members, so it is not clear whether it should be classified as a member of type IB or as a separate family of type IC (Taneja *et al.*, 2006).

### 1.4.6 Mechanism of action of type IB topoisomerases

The crystal structures of several forms of the human enzyme with non-covalently and covalently bound DNA have been determined (Redinbo *et al.*, 1998, Redinbo *et al.*, 2000, Stewart *et al.*, 1998). These structures have provided clues to elucidate the enzyme mechanism. The energy for the relaxation mechanism is obtained from that stored in the supercoiled DNA. The unique structure of type IB allows it clamp DNA between sub domain I/II and sub domain III/C-terminal domain (**Figure 1.9 a,b**). DNA clamping is followed by single-strand cleavage and formation of a phosphotyrosine bond between the protein and the 3' end of the cleaved strand (Cheng *et al.*, 1998) (**Figure 1.9 c,d**). After the formation of DNA-topo, complex, controlled rotation of the helix duplex downstream of the cleavage site occurs and the enzyme opens up to allow this (**Figure 1.9 e**). This rotation of the helix duplex is important to relieve any torsional stress within the DNA substrate (Stewart *et al.*, 1998). Finally the 5' end of the cleaved DNA is reattached to the 3' end and the DNA is released (Cheng *et al.*, 1998).

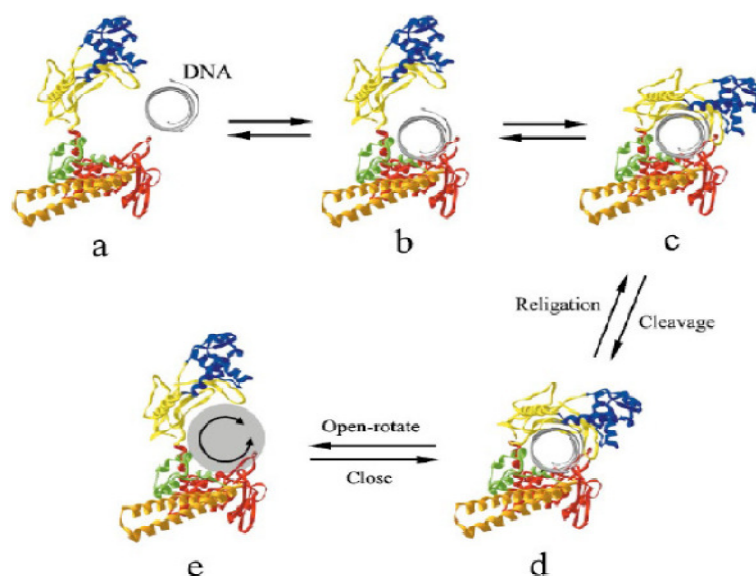


**Figure 1.9: Detailed mechanism of human topoisomerase I. (Champoux, 2001).**

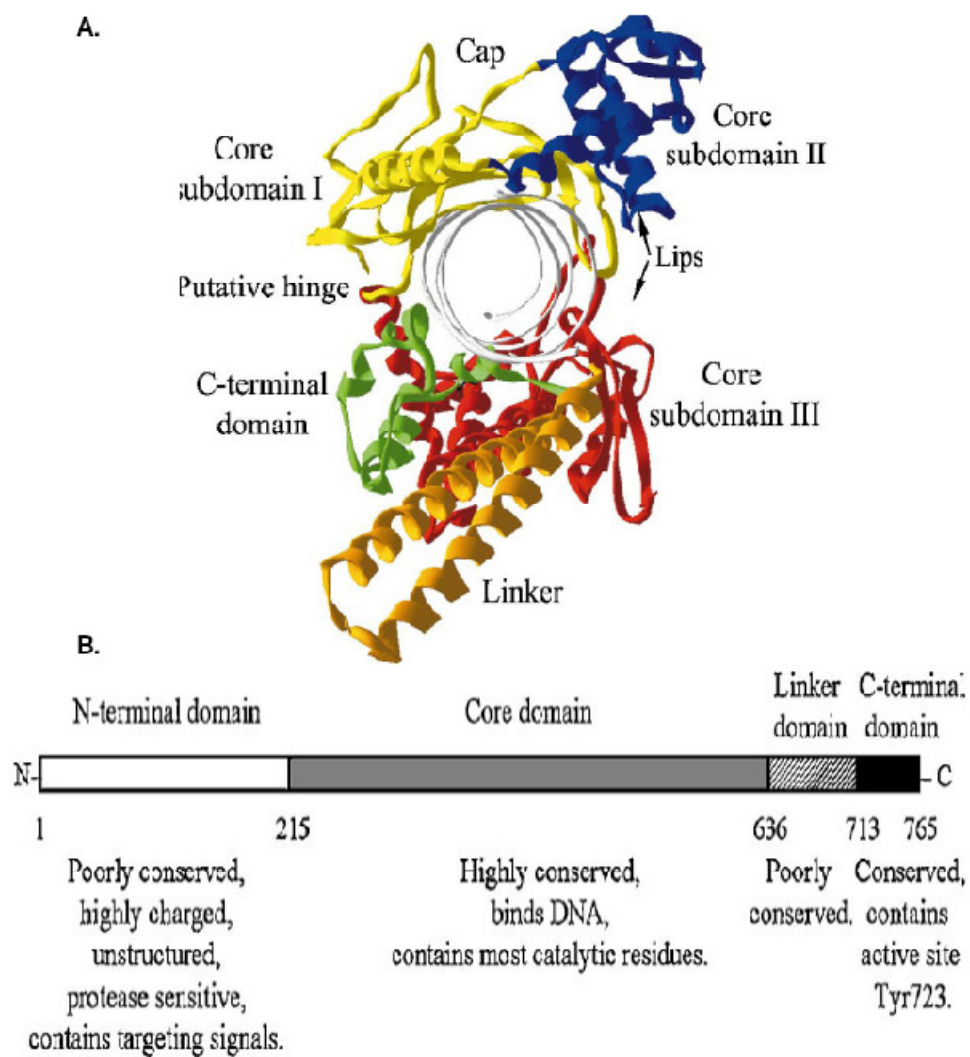


**Figure 1.10: Structure of human topoisomerase I.** (A) Human topoisomerase I bound with DNA (PDB code : 1A36) viewed down the DNA axis. (B) A cartoon of the Human topoisomerase I showing the features of different domains (Champoux, 2001).

### 1.4.7 Type II DNA topoisomerases

The enzymes in this category introduce double-strand breaks in a DNA duplex and allow the passage of another duplex through the break. Like type IA topoisomerases a covalent bond is formed between the tyrosine in the enzyme and the 5' phosphate of the DNA strands (Roca & Wang, 1992, Roca, 1995). The segment of DNA with the double-stranded breaks is called the G or 'gate' segment, and the DNA duplex transported through the gap in the G segment is called T or 'transported' segment. The broken ends of the G segment are religated after the passage of the T segment. All type II enzymes are ATP-dependent multimeric enzymes. The different topological reactions catalysed by type II topoisomerases are shown in the **Figure 1.11**.

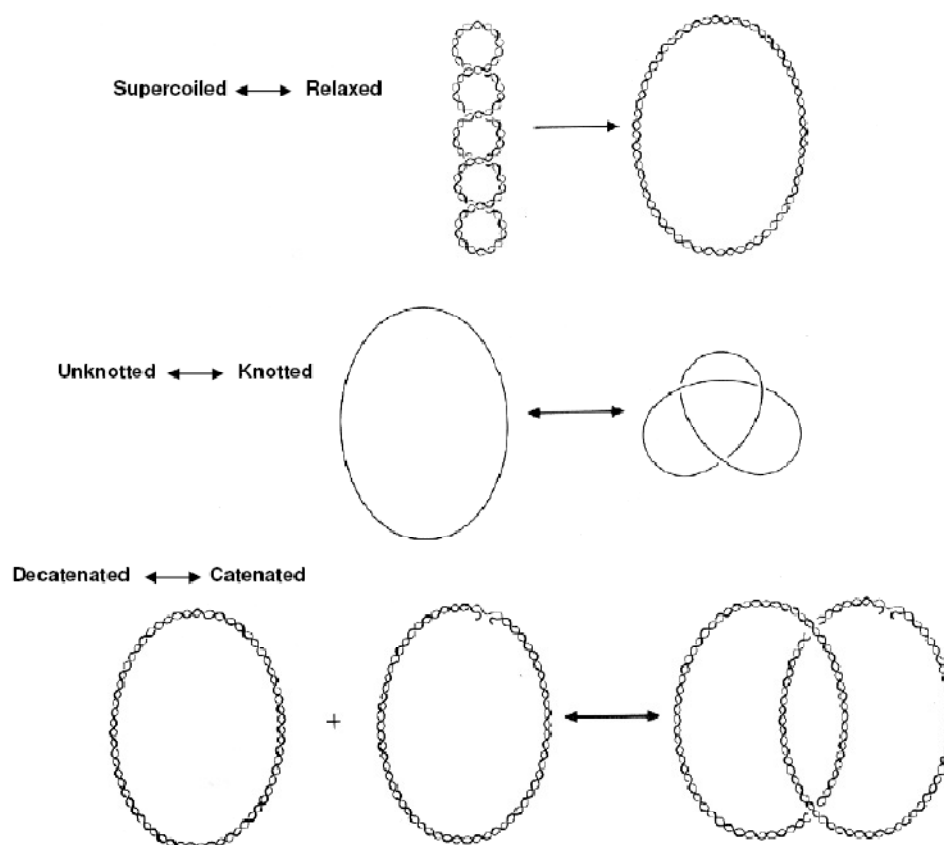


**Figure 1.11: Reactions catalysed by type-II topoisomerases (Bates & Maxwell, 2005).**

Type II topoisomerases are again divided into two families:

1. Type IIA includes bacterial DNA gyrase (*E. coli* and *M. tuberculosis*), topoisomerase IV (*E. coli* and *M. smegmatis*), and eukaryotic topoisomerase II.
2. Type IIB only includes topoisomerase VI. In the presence of ATP/Mg<sup>2+</sup> topoisomerase VI is able to relax both positively and negatively supercoiled DNA and decatenate DNA (Bergerat *et al.*, 1994, Buhler *et al.*, 2001).

Type II topoisomerase catalyse all the topological reactions such as supercoiling/relaxation, catenation / decatenation, knotting/ unknotting as shown in **Figure 1.11**. Depending on the location of G and T segments, different topological changes take place. When the G and T segments are located on the same DNA molecule then relaxation, knotting / unknotting of the DNA take place (Roca, 1995). However, if the G and T segments are located on different DNA molecules then catenation / decatenation take place.

#### 1.4.8 Structure of Type IIA topoisomerases

Type IIA topoisomerases are a diverse group of enzymes, which vary in subunit composition. For example, eukaryotic type II topoisomerases are homodimers and bacterial type II topoisomerases (topo IV and DNA gyrase) are heterotetramers. However, there are structural and sequence homologies between them (Figure 1.12). The B- and A- subunits of the bacterial type II topoisomerases are homologues to the N- and C-terminal halves of eukaryotic type II topoisomerases (Lynn *et al.*, 1986). This sequence and structural homology demonstrate evolutionary relationship between the prokaryotic and eukaryotic type II topoisomerases (Corbett & Berger, 2004, Champoux, 2001). Similarly the active-site tyrosine is present in a single polypeptide in the case of eukaryotic type II topoisomerases in a region which is equivalent to the GyrA/ ParC subunits in the case of bacterial type II topoisomerases (Champoux, 2001). Although the DNA gyrase core structure is similar to other type II topoisomerases, its C-terminus is different and has a DNA-binding domain with a  $\beta$ -propeller fold (Corbett *et al.*, 2004, Ruthenburg *et al.*, 2005). This domain is essential for the supercoiling activity of the enzyme and mediates the

wrapping of ~140 bp of DNA in a right-handed manner around the entire enzyme (Liu & Wang, 1978a).

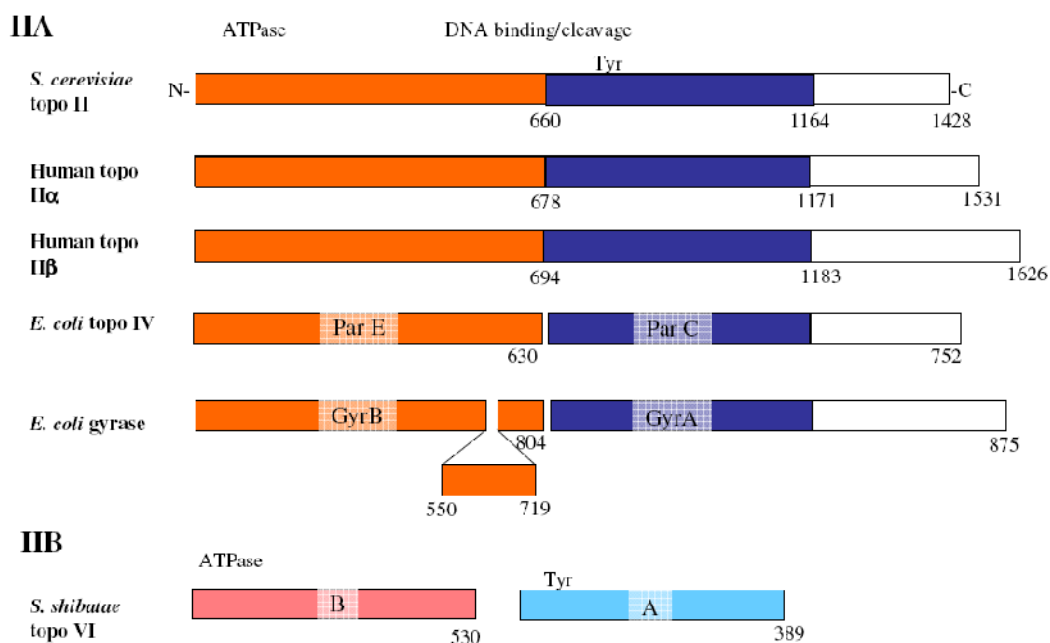


**Figure 1.12: Domain organisation of type IIA topoisomerases based upon sequence comparison and homology (Bates & Maxwell, 2005).**

Type IIA topoisomerases have functional domains that are conserved among the members and are present in type IA and IIB topoisomerases (**Figure 1.13**). For example the 5Y-CAP DNA and Toprim cleavage domain is present in type IA, IIA and IIB topoisomerases (Corbett & Berger, 2004). This domain has a winged-helix fold and possesses the active-site tyrosine, which binds to the 5' end of the cleaved DNA in the case of type II topoisomerases.

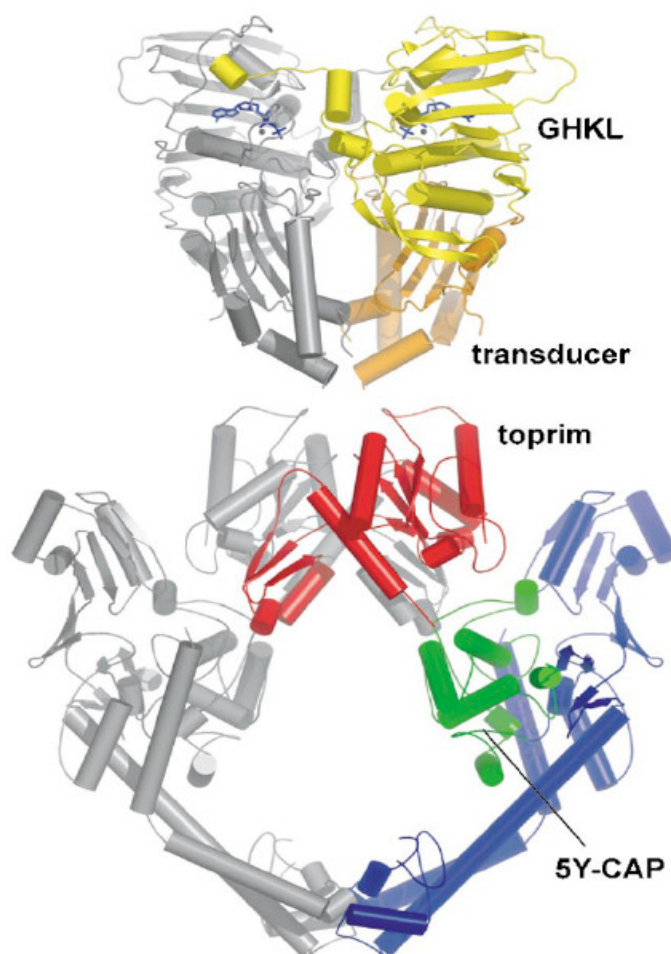


**Figure 1.13: Conserved functional domains in type II topoisomerases.** *The GHKL domain (yellow), transducer (orange), Toprim (red) and 5Y-CAP (green) are the conserved domains (Corbett & Berger, 2004).*

The Toprim (topoisomerase-primase) domain is approximately 100 amino acids and has two conserved motifs, one containing glutamate and other containing two conserved aspartates (DxD). The glutamate is essential for strand joining by topoisomerases and may act as a general base in nucleotide polymerisation by primases. The aspartates coordinate the  $Mg^{2+}$  and are important for the activity of the enzyme (Aravind *et al.*, 1998). The GHKL domain is important for the ATPase activity of type II topoisomerases. It is called GHKL due to its presence in DNA gyrase, Hsp90, CheA-family histidine kinases and MutL (Dutta & Inouye, 2000, Corbett & Berger, 2004). In type II topoisomerases, ATP-binding causes dimerisation of the

GHKL domains. The N-terminal arm from one GHKL domain reaches across the dimer interface and makes contacts with the ATP lid of the partner GHKL domain.

#### 1.4.9 ATP hydrolysis by type II topoisomerases

DNA gyrase hydrolyzes ATP to perform DNA supercoiling, which is an energetically unfavourable process. On the other hand, other type II topoisomerases that only relax DNA supercoils also hydrolyze ATP. Relaxation of supercoiled DNA is an energetically favourable process and hence it should not require ATP. It is proposed that ATP hydrolysis may be used to simplify distributions of DNA topoisomers below thermodynamic equilibrium levels (Rybenkov *et al.*, 1997), but the energy required for this process is low (Stuchinskaya *et al.*, 2009). A recent study related to topological simplification due to type II topoisomerases has shown that topological simplification is not altered by reducing the free energy available from ATP hydrolysis (varying ADP:ATP ratio) and it may be an evolutionary effect with no adaptive significance (Stuchinskaya *et al.*, 2009). It has also been proposed that the major role of ATP hydrolysis in the type II topoisomerase reaction is to enable the controlled separation of strong protein-protein interfaces. This prevents the formation of potential cytotoxic double-stranded breaks in DNA (Bates *et al.*, 2010).

#### 1.4.10 Mechanism of type IIA topoisomerases

Type IIA topoisomerases follow a two-gate mechanism for maintaining DNA topology (**Figure 1.14**). The reaction starts with the creation of a double-stranded break in DNA, which is called the gate segment or G segment, through which another DNA duplex is passed. The double-stranded break is created through nucleophilic attack of the DNA backbone and the formation of covalent bonds between the active site tyrosine in each monomer with the 5'-phosphates of the DNA strands (Roca, 1995, Roca & Wang, 1992). The broken ends of the G segment then make a way for the intact DNA duplex (transported segment or T segment) to be passed through the gap. This is brought about by conformational changes, which are induced by ATP binding. These conformational changes are transmitted across the enzyme which results in the capture of the T segment, closure of the N-gate, separation of the broken ends of the G

segment and closing of the C gate (Wang, 1998). After the passage of the T segment, the G segment is religated and the C-terminal gate opens to allow the T segment to exit the enzyme. When the G and T segments are located, on the same DNA molecule then either change in the level of supercoiling or knotting/ unknotting of DNA takes place (Roca, 1995, Tse *et al.*, 1980). On the contrary if the G and T segments are located on different DNA molecules then it leads to catenation/ decatenation of two DNA molecules (Roca, 1995). DNA relaxation takes place by reverse strand passage mechanism in DNA gyrase only. In this mechanism, the T segment enters through the opening at the C-gate; passes through the transient break in the G segment and exits through the open ATP-operated clamp (Williams & Maxwell, 1999b, Williams & Maxwell, 1999a).

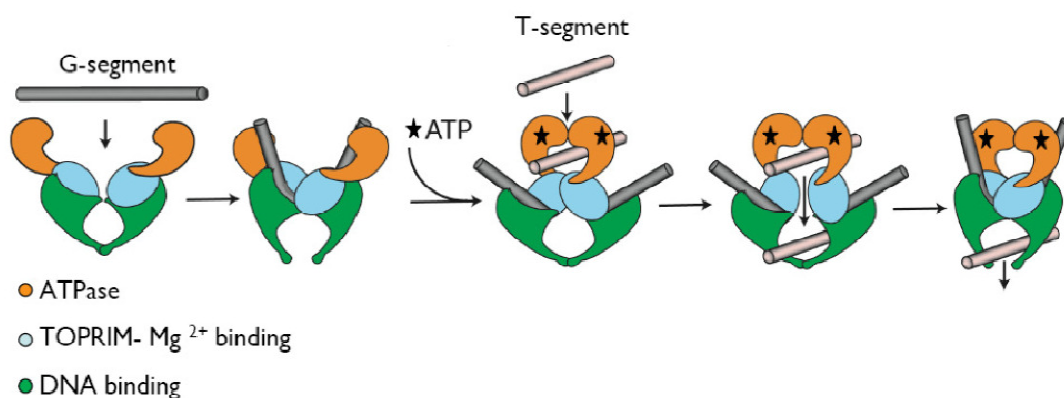


**Figure 1.14: Two-gate mechanism for type II A topoisomerase (Dong & Berger, 2007).**

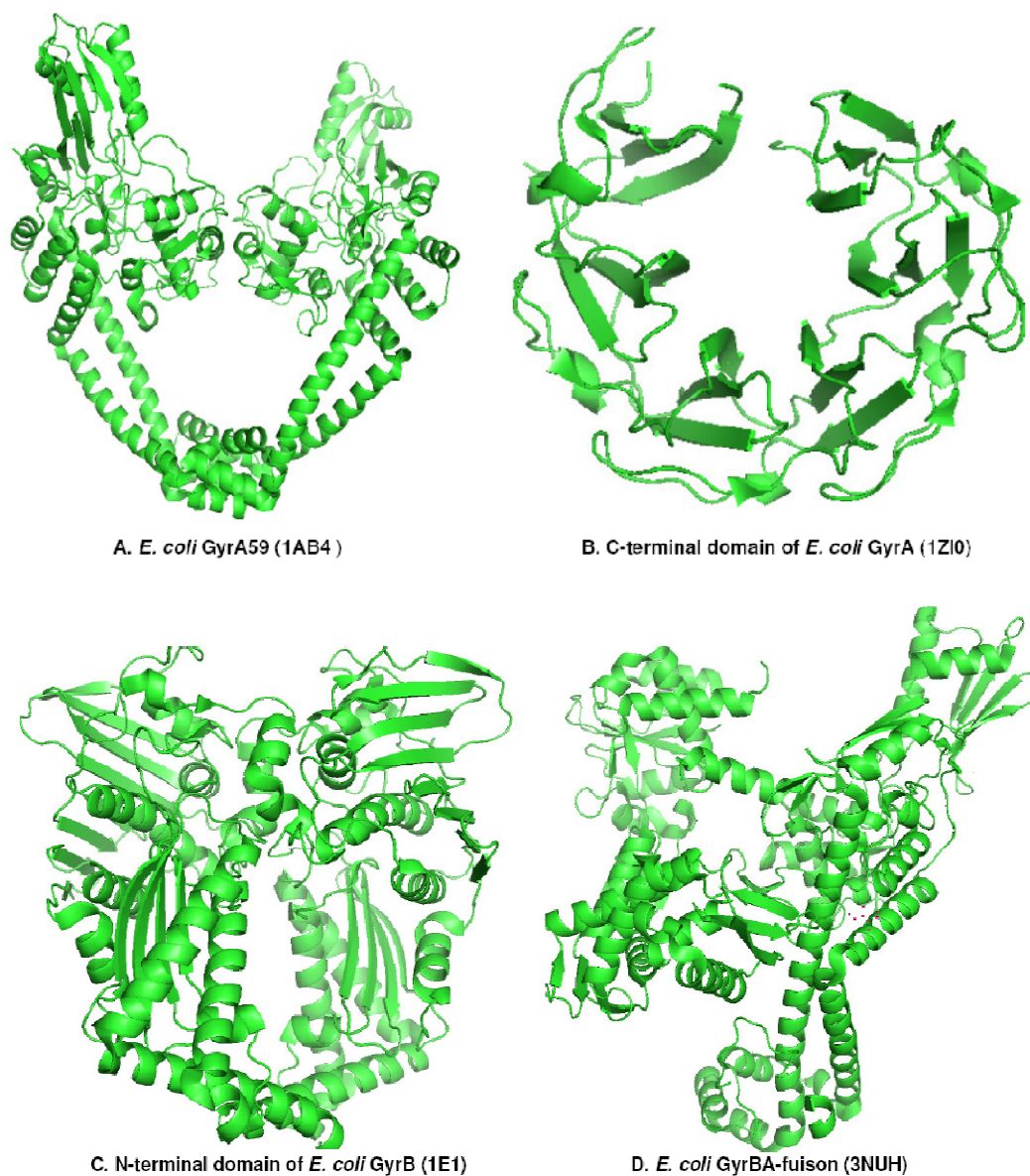


**Figure 1.15: Crystal structures of different domains of *E. coli* DNA gyrase.**

Structures have been solved for the (A) N-terminal (Morais Cabral *et al.*, 1997) and (B) C-terminal domains of *E. coli* GyrA (Ruthenburg *et al.*, 2005) as well as for the (C) N-terminal domain of *E. coli* GyrB (Brino *et al.*, 2000, Wigley *et al.*, 1991) and the (D) *E. coli* GyrBA-fusion (Schoeffler *et al.*, 2010). Structures were redrawn with PyMOL 1.01.

## 1.5 DNA gyrase

### 1.5.1 Introduction

DNA gyrase is a type IIA topoisomerase, which introduces negative supercoils into closed-circular DNA (Gellert *et al.*, 1976). DNA gyrases are found in all prokaryotes and in eukaryotes such as *Plasmodium falciparum*, *Plasmodium vivax* and *Arabidopsis thaliana*. *E. coli* DNA gyrase was the first type II topoisomerase to be discovered (Gellert *et al.*, 1976). The enzyme maintains the homeostatic balance of chromosomal superhelical density by catalysing the introduction of negative supercoiling into DNA, a prerequisite for replication and transcription, and relaxes positive supercoils generated ahead of the transcription complex. The DNA supercoiling mechanism involves transient breakage and resealing of both strands of DNA. It also catalyses catenation and decatenation of DNA rings, and knotting and unknotting of duplex DNA, but this activity is weaker in comparison to topo IV.

*E. coli* DNA gyrase is composed of two subunits of GyrA and two subunits of GyrB. The molecular weights of *E. coli* GyrA and GyrB are 97-kDa and 90-kDa respectively (Wang, 1985). The *E. coli* DNA gyrase domain boundaries have been well defined and characterised. GyrA is divided into a 64-kDa N-terminal domain (breakage-reunion domain) that contains the QRDR (Quinolone-resistance determining region), and a 33-kDa C-terminal domain around which the DNA is wrapped (Reece & Maxwell, 1989). The N-terminal domain forms a DNA-binding saddle known as the DNA breakage-reunion domain. It also forms a large 30-Å cavity that can accommodate a DNA duplex. The GyrA C-terminus adopts a  $\beta$ -propeller fold and is largely basic around the outside suggesting the involvement of the domain in DNA wrapping (Corbett & Berger, 2004, Liu & Wang, 1978a). GyrB is divided into a 43-kDa N-terminal ATPase domain (aminocoumarin interaction site) (Wigley *et al.*, 1991) and a 47-kDa C-terminal domain (Brown *et al.*, 1979, Gellert *et al.*, 1979, Adachi *et al.*, 1987) that interacts with GyrA and DNA. *E. coli* DNA gyrase has a 170 amino acid insertion within the C-terminal domain, in comparison to other bacterial DNA gyrase (*M. tuberculosis*) and type IIA topoisomerases. This insertion is important for the DNA binding capabilities of *E. coli* DNA gyrase (Chatterji *et al.*, 2000). Recently

it has been established that the insertion is important for DNA binding and communication between different functional domains (Schoeffler *et al.*, 2010). The crystal structures for different domains of *E. coli* gyrase subunits are available as shown in the **Figure 1.15**.

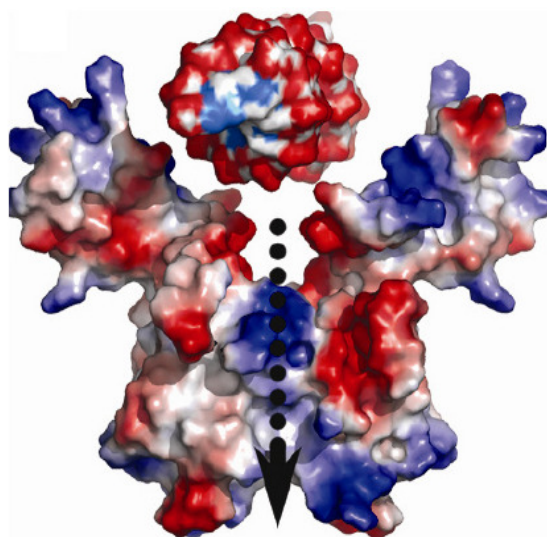
*M. tuberculosis* DNA gyrase is a validated target for anti-tubercular drug discovery, because its inhibition results in mycobactericidal activity (Mdluli & Ma, 2007). Inhibitors of this enzyme are also active against non-replicating, persistent mycobacterium, which may play a role in shortening the duration of TB therapy. The *M. tuberculosis* DNA gyrase genes have been cloned in *E. coli* (Madhusudan *et al.*, 1994, Takiff *et al.*, 1994). Based on the sequencing data and genome analysis, *M. tuberculosis* genes encoding DNA gyrase were identified as a *gyrB-gyrA* contig in which *gyrA* and *gyrB* encode the A and B subunits, respectively; they are organized as a bicistronic unit. The *gyrA* gene is located 34 nucleotides downstream of *gyrB*. Both the genes are transcribed from the promoter elements located upstream of *gyrB* coding sequence.

Like *E. coli* DNA gyrase, *M. tuberculosis* DNA gyrase is an A<sub>2</sub>B<sub>2</sub> tetramer. GyrA is ~97-kDa and 838 amino acids, while GyrB is ~72-kDa and 714 amino acids. The N-terminal domain of GyrB harbours the ATPase activity; the C-terminal domain of GyrB is the domain that interacts with GyrA and forms a complex capable of catalyzing DNA breakage and reunion. The N-terminal domain of GyrA is the catalytic centre of gyrase, which harbours the DNA cleavage–reunion activity, and the C-terminal domain of GyrA is involved in binding and wrapping the DNA. Recent research shows that Y577, R691 and R745 are among the key DNA-binding residues in the C-terminal domain of *M. tuberculosis* GyrA, and that the third blade of the GyrA C-terminal domain is the main DNA-binding region (Huang *et al.*, 2006). The pairwise comparisons of the gyrase proteins from *M. tuberculosis* and *M. smegmatis* showed that GyrA of *M. smegmatis* shares 88.5% identity and 93.9% similarity with that of *M. tuberculosis* at the amino acid level. *M. smegmatis* GyrB is also highly homologous (86% amino acid sequence identity) to *M. tuberculosis* GyrB protein.

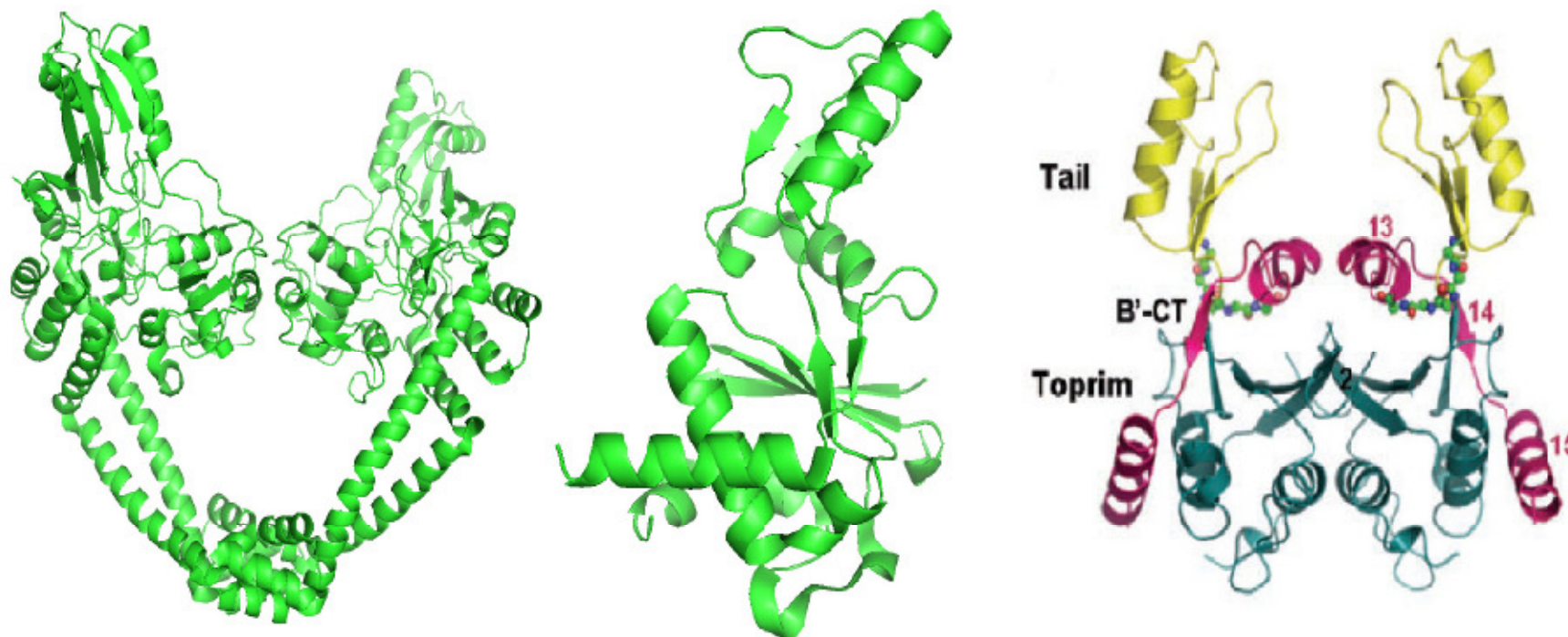
There are two structural differences between *E. coli* and *M. tuberculosis* DNA gyrase. There is an insertion of 170 amino acids within the Toprim fold of *E. coli* GyrB that is not present in *M. tuberculosis*. In order to understand the significance of this insertion, a crystal structure has been solved (PDB code: 3NUH) for this insert sequence along with the DNA binding and cleavage core of *E. coli* gyrase (Schoeffler *et al.*, 2010). The insert adopts a novel fold that contacts the associated GyrA subunit (**Figure 1.15, D**). Mutagenesis experiments involving the deletion of this insert sequence affect DNA supercoiling and relaxation by ~25 fold with a less severe impact on DNA cleavage. The insert was also shown to be important for DNA binding and DNA-dependent stimulation of ATPase activity. Although the modelling studies do not indicate direct contacts between the insert and DNA, it is proposed that the insert stabilises the DNA gate of gyrase in a conformation that favours G-segment binding and also acts as a relay between the DNA gate and either the ATP- or C-gate to communicate conformational signals. This study has led to further refinement of the strand passage model for DNA gyrase having the insert. Recently there have been several crystal structures of different domains of *M. tuberculosis* DNA gyrase. Crystal structures of GyrA N-terminus (PDB code: 3ILW; 3IFZ), GyrB C-terminus (PDB code: 2ZJT) and Toprim domain (PDB code: 3IGO) are available as shown in the **Figure 1.17**. Functional, biophysical and structural studies of the *M. tuberculosis* catalytic DNA gyrase reaction core (Toprim and the breakage-reunion domains) have also been performed (Piton *et al.*, 2010). The structure of GyrA N-terminal domain (GyrA59) (PDB code: 3ILW) is similar to *E. coli* GyrA59 (PDB code: 1AB4) with 44% sequence identity and 1.27Å rmsd. The difference between the two proteins is in the loop containing helices  $\alpha_3$  and  $\alpha_4$  (Gly88-Ala92). The position of this loop in *M. tuberculosis* GyrA59 (an important region involved in acquiring quinolone-resistance mutation) is different from its location in *E. coli* GyrA NTD (Tretter *et al.*, 2010).

The crystal structure of GyrB C-terminus from 485-714 residues (PDB code: 2ZJT), indicated by GyrB', has a crab-shape organisation and consists of a tail and a Toprim domain (Fu *et al.*, 2009). It is a dimer in the asymmetric unit and shows a pair of negatively charged antenna (R614/K639) on the top and an amphiphilic

surface (R534/R589 and D554/E555) on the bottom, which are conserved in sequence in prokaryotic topo II enzymes. This crystal structure has been helpful to study the possible way of T-segment navigation from the N gate to the DNA gate of DNA gyrase. It has been suggested that GyrB' binds the G-segment of DNA through the two pairs of amphiphilic residues on the bottom and the positively charged antenna interact with DNA duplex (T-segment). Mutational studies have demonstrated that the negatively charged residues on the tail groove are essential for the T-segment transport. A sluice-like model (**Figure: 1.16**) was proposed to explain the T- segment navigation. According to the model, once the T-segment is captured by the N-gate and docked in the opened groove, strong charge-charge repulsion occur between the phosphate groups on the DNA backbone and the negatively charged residues present on the groove bottom (**Figure 1.16**). This repulsive force may generate torsion on the Toprim dimer, which results in the opening of GyrB' dimer. Besides the electrostatic tension, the model also takes into account the energy from ATP hydrolysis to open the GyrB' dimer. It is suggested that the ATP hydrolysis may provide energy for switching GyrB' from a closed to an open state, and electrostatic repulsion may be responsible for the opening of Toprim domain (Fu *et al.*, 2009).



**Figure 1.16: Electrostatic map of the GyrB' dimer and DNA duplex showing the sluice like model for T-segment navigation involving strong charge-charge repulsion (Fu *et al.*, 2009).**

A. *M. tuberculosis* GyrA59 (3ILW)B. *M. tuberculosis* TOPRIM (3IGO)C. *M. tuberculosis* GyrB' (2ZJT)

**Figure 1.17: Crystal structures of different domains of *M. tuberculosis* DNA gyrase.** (A) Crystal structure of *M. tuberculosis* GyrA59 (Tretter et al., 2010), (B) Toprim domain and (C) *M. tuberculosis* GyrB C-terminal domain (GyrB') (Fu et al., 2009). 3ILW and 3IGO were redrawn with PyMOL 1.01.

## 1.5.2 DNA gyrase strand passage mechanism

The DNA gyrase follows the general mechanism of type II topoisomerases for strand passage. A double-stranded break is made in the G segment and the T segment (another duplex) is passed through the G segment, followed by religation of the broken ends of the G segment. Each cycle of strand passage changes the linking number of DNA by two (Brown *et al.*, 1979). A characteristic feature of strand passage in DNA gyrase is the wrapping of approximately 140 bp DNA around the C-terminal domain of the GyrA subunits, presenting the T segment to the ATP-operated clamp (Champoux, 2001).

## 1.5.3 DNA wrapping by DNA gyrase

DNA gyrase can catalyse DNA supercoiling due to its unique capability to wrap a segment of DNA (which contains the G segment) around the enzyme in such a way as to present a T segment to the ATP-operated clamp (Hedde *et al.*, 2004, Reece & Maxwell, 1991, Liu & Wang, 1978a). The wrapping function residues ('GyrA-box' motif) reside in the C-terminal domain of GyrA which has a  $\beta$ -propeller fold (Ruthenburg *et al.*, 2005, Corbett *et al.*, 2004) (**Figure 1.18 A,B**). It has been demonstrated in previous studies that an *E. coli* GyrA C-terminal truncation mutant lacks supercoiling activity while retaining the relaxation activity due to the loss of the DNA-wrapping domain (Kampranis & Maxwell, 1996). The DNA wrapping around the GyrA C-terminal domain is positive in nature (Kampranis *et al.*, 1999a). Similarly, the GyrA C-terminal domain is essential to *M. tuberculosis* DNA gyrase. Site-directed mutagenesis experiments have shown that Y577, R691 and R745 are among the key DNA-binding residues in *M. tuberculosis* GyrA-CTD, and that the third blade of the GyrA-CTD is the main DNA-binding region in *M. tuberculosis* DNA gyrase. The substitutions of Y577A, D669A, R691A, R745A and G729W led to the loss of supercoiling and relaxation activities, with little effect on the drug-dependent DNA cleavage & decatenation activities. There was also no effect on the ATPase activity (Huang *et al.*, 2006).

A recent crystal structure of *Xanthomonas campestris* GyrA C-terminal domain (**Figure 1.18B**) (PDB code: 3L6V) and site-directed mutagenesis experiments have revealed that the conserved  $\beta$ -strand bearing proline contributes directly to gyrase's negative supercoiling activity (Hsieh *et al.*, 2010).

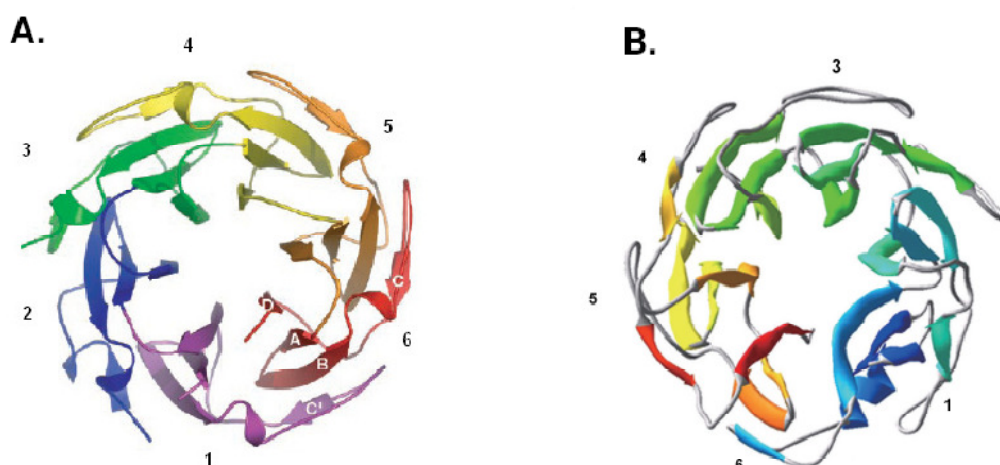


**Figure 1.18: Crystal structures of GyrA C-terminal domain.** (A) Crystal structure of *Borrelia burgdorferi* GyrA C-terminal domain (PDB code: 1SUU) (Corbett *et al.*, 2004) and (B) Crystal structure of *Xanthomonas campestris* GyrA C-terminal domain (PDB code: 3L6V) (Hsieh *et al.*, 2010).

#### 1.5.4 DNA cleavage-religation reaction by DNA gyrase

Studies with *E. coli* DNA gyrase have demonstrated the involvement of both gyrase subunits in the cleavage-religation reaction. In the case of GyrA, the cleavage-religation reaction involves the formation of a 5'-phosphotyrosine intermediate and residues Arg 32, Arg 47, His 78 and His 80 cooperate with the active-site tyrosine residue on the opposite subunit of the GyrA dimer during the cleavage-religation reaction. These residues affect only the DNA cleavage reaction (Hockings & Maxwell, 2002). Glu424, Asp498, Asp500 and Asp 502 in GyrB have been proposed to coordinate  $Mg^{2+}$  for the cleavage-religation reaction. Studies involving the role of GyrB in the cleavage-religation reaction provided evidence to support the idea that cleavage of each DNA strand involves two or more metal ions. The two metal-ion

mechanism for DNA cleavage by DNA gyrase involves polarisation of tyrosine by  $Mg^{2+}$ , which undergoes deprotonation by His 78 or His 80 of GyrA. The tyrosine residue attacks the phosphate group of DNA and forms a negatively charged pentacoordinate phosphate intermediate that is stabilised by two metal ions ( $Mg^{2+}$ ).

The 3'-bridging oxygen atom is stabilised by  $Mg^{2+}$  to make a 3'-oxyanion that results into 3'-hydroxyl group by an unidentified acidic group (**Figure 1.19**) (Noble & Maxwell, 2002). It also has been shown by biophysical and thermal stability experiments that DNA is required for the effective two-site coordination of divalent ions (Sissi *et al.*, 2008).

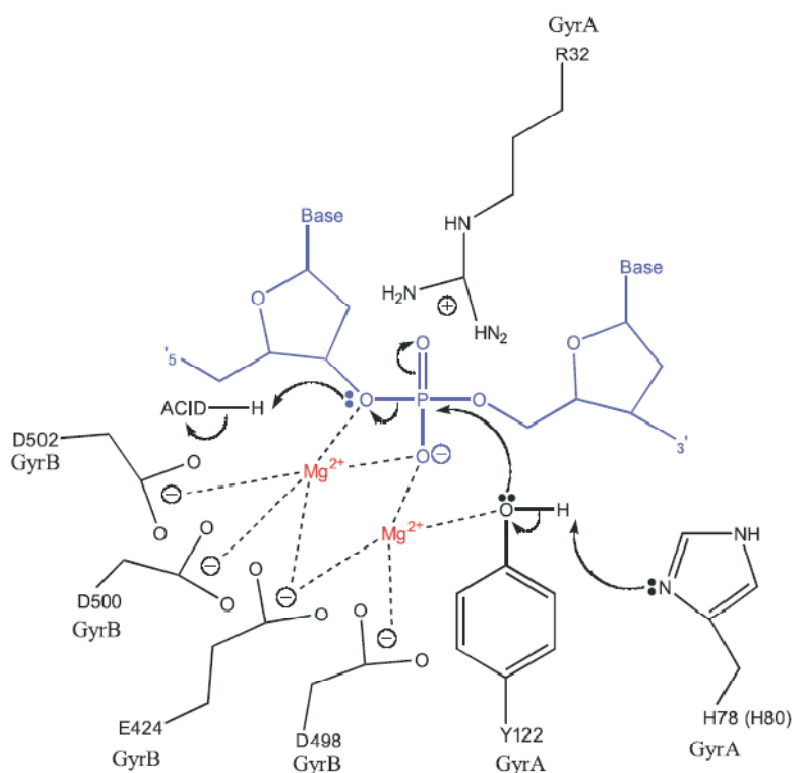


**Figure 1.19: The two-metal ion mechanism for cleavage-religation reaction (Noble & Maxwell, 2002).**

### 1.5.5 ATP hydrolysis by DNA gyrase

Another characteristic feature of DNA gyrase in comparison to other type II topoisomerases is the ATP-dependent DNA supercoiling and ATP-independent relaxation activity. The GyrB subunit has the ATP-binding site and ATP/ADPNP causes the subunits to dimerise. A crystal structure for the 43-kD N-terminal GyrB fragment complexed with ADPNP (PDB code: 1EI1) (Brino *et al.*, 2000, Wigley *et al.*, 1991) shows the dimerisation of the GyrB N-terminal domain. The significance of ATP hydrolysis is clear: DNA gyrase is capable of introducing negative DNA supercoils, which is an energetically unfavourable process.

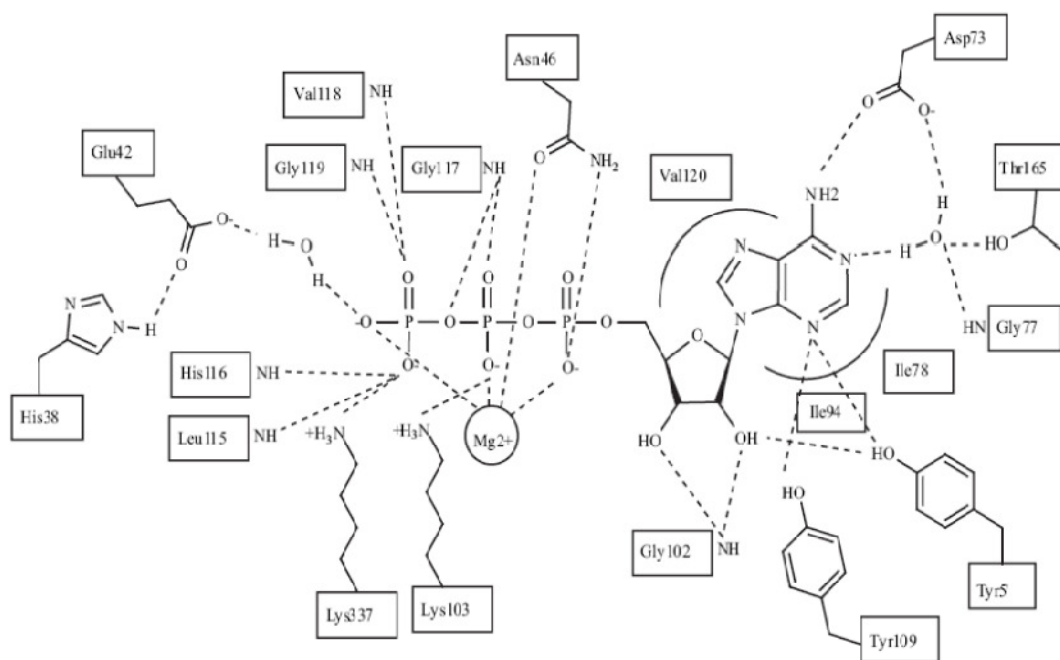


**Figure 1.20: Interaction between GyrB24 and ATP showing hydrogen-bonds with different residues (Oblak *et al.*, 2007).**

The important residues involved in ATP binding (**Figure 1.20**) based on the crystal structure of 43-kDa N-terminal GyrB fragment complex with ADPNP (PDB code: 1EI1) are as follows (Maxwell & Lawson, 2003):

1. Glu42 behaves as a catalytic base and removes a proton from water promoting nucleophilic attack on the  $\gamma$ -phosphate of ATP (Jackson & Maxwell, 1993).
2. His38 stabilises Glu-42 and Lys337 forms hydrogen bonds with the ATP molecule (Jackson & Maxwell, 1993, Smith & Maxwell, 1998).
3. Lys103 forms a salt bridge to the  $\beta$ -phosphate of the ATP molecule (Wigley *et al.*, 1991) and Asn46 forms a hydrogen bond with the ATP molecule and helps coordinate the  $Mg^{2+}$  (Wigley *et al.*, 1991).

Water molecules also play an important role and form a H-bond network with the adenine ring of ATP, and residues Asp73, Gly77 and Thr165. Pro79 and Lys103 have been suggested to be required for coupling of ATP hydrolysis to DNA supercoiling activity (Gross *et al.*, 2003). The crystal structure of the ParE43-ADPNP (PDB code: 1S16) is similar to the crystal structure of GyrB43-ADPNP complex (PDB code: 1EI1) and upon superimposition of the ADPNP structures both the ParE and GyrB ATP-binding sites are nearly identical, as the positions of the majority of essential residues for ATP binding and hydrolysis are conserved. The only difference is presence of Met74 rather than Ile78 found in GyrB. This difference is important in terms of the novobiocin potency for topo IV and DNA gyrase. Novobiocin is a 5-10-fold less potent inhibitor of *E. coli* topo IV compared to *E. coli* DNA gyrase (Bellon *et al.*, 2004). Mutation of Met74 in ParE to Ile increases the potency of novobiocin by 18-fold compared to the wild-type enzyme. Vice-versa in GyrB, resulted in a 22-fold decrease in novobiocin affinity (Oblak *et al.*, 2007).

### 1.5.6 DNA gyrase in eukaryotes

DNA gyrase is also found in eukaryotes such as *Plasmodium falciparum*, *Plasmodium vivax* and *Arabidopsis thaliana*. *Plasmodium falciparum*, has both subunits A (PfGyrA) and B (PfGyrB) that are targeted to the apicoplast (Dar *et al.*, 2007). These subunits are also present in *P. vivax*. Full length PfGyrB shows intrinsic ATPase activity in the absence of PfGyrA or DNA. Heterologous expression of PfGyrA is difficult due to the presence of asparagines and lysine-rich-repeat regions and the unusual codon usage in *Plasmodium* (Dar *et al.*, 2009). In *Arabidopsis thaliana*, four putative gyrase subunit genes were identified, out of which one is homologous to the GyrA subunit and the other three are homologous to the GyrB subunits (Wall *et al.*, 2004). One of the GyrB homologues has been shown recently not to be a gyrase subunit (Evans-Roberts *et al.*, 2010).

## 1.6 Type IIB topoisomerases

Topoisomerase VI belongs to the type IIB topoisomerase family and it was first discovered in *Sulfolobus shibatae* (Bergerat *et al.*, 1997). Type IIB topoisomerases catalyse ATP-dependent relaxation of negatively or positively supercoiled DNA with a preference for decatenation over relaxation (Buhler *et al.*, 2001, Corbett & Berger, 2004). Topo VI, like bacterial topoisomerases consists of two subunits and functions as an A<sub>2</sub>B<sub>2</sub> heterotetramer. Both type IIA and type IIB topoisomerases have descended from a common ancestor (Corbett & Berger, 2003).

Topo VI has no obvious homology to other type II topoisomerase except for the ATPase domain (Bergerat *et al.*, 1997). Sequence alignment has shown that the conserved Toprim fold found in type IA and type IIA topoisomerase is also present in the subunit A of topo VI (Aravind *et al.* 1998). The striking difference between type IIA and IIB topoisomerases is the lack of a cavity for the T-segment and therefore it is likely that the strand passage mechanism is different. The subunit A of topo VI is homologous to the eukaryotic meiotic recombination factor, Spo11, which catalyses double-strand breaks during meiosis (Keeney *et al.*, 1997). However, Spo11 does not rejoin the double-strand breaks and it does not have an equivalent of the B subunit. The B subunit has the characteristic transducer and GHKL domains (Corbett &

Berger, 2003) (**Figure 1.21, A**). A complete structure of topoVI from *Methanosarcina mazei* with 4.0 Å resolution is now available. The structure shows a 220-kDa heterotetramer with ‘twin-gate’ architecture (**Figure 1.21, B**).

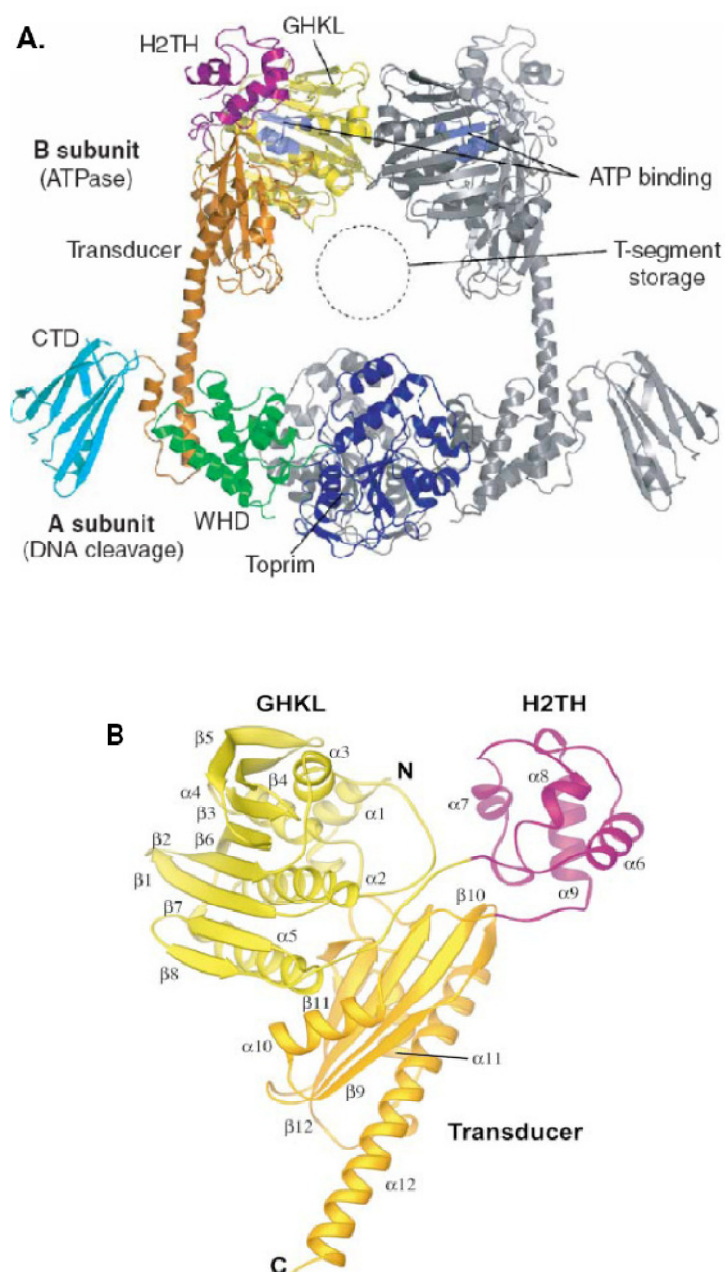


**Figure 1.21: Crystal structure of topo VI.** (A) Structure of complete topo VI (PDB code: 2Q2E) (Corbett et al., 2007) (B) topo VI-B (PDB code: 1MX0) (Corbett & Berger, 2003).

## 1.7 DNA gyrase inhibitors

Since DNA gyrase is the only topoisomerase that can catalyse the introduction of negative supercoils into DNA, it has been exploited as a drug target. It has been possible to develop inhibitors that inactivate gyrase without substantially affecting its human counterpart, topo II (Gatto *et al.*, 1999). DNA gyrase is the target of the fluoroquinolones (eg. ofloxacin, ciprofloxacin, sparfloxacin, moxifloxacin, gatifloxacin), aminocoumarins (novobiocin, clorobiocin), simocyclinones (eg. simocyclinone D8), cyclothialidines, CcdB and microcin B17 (**Figure 1.22**).

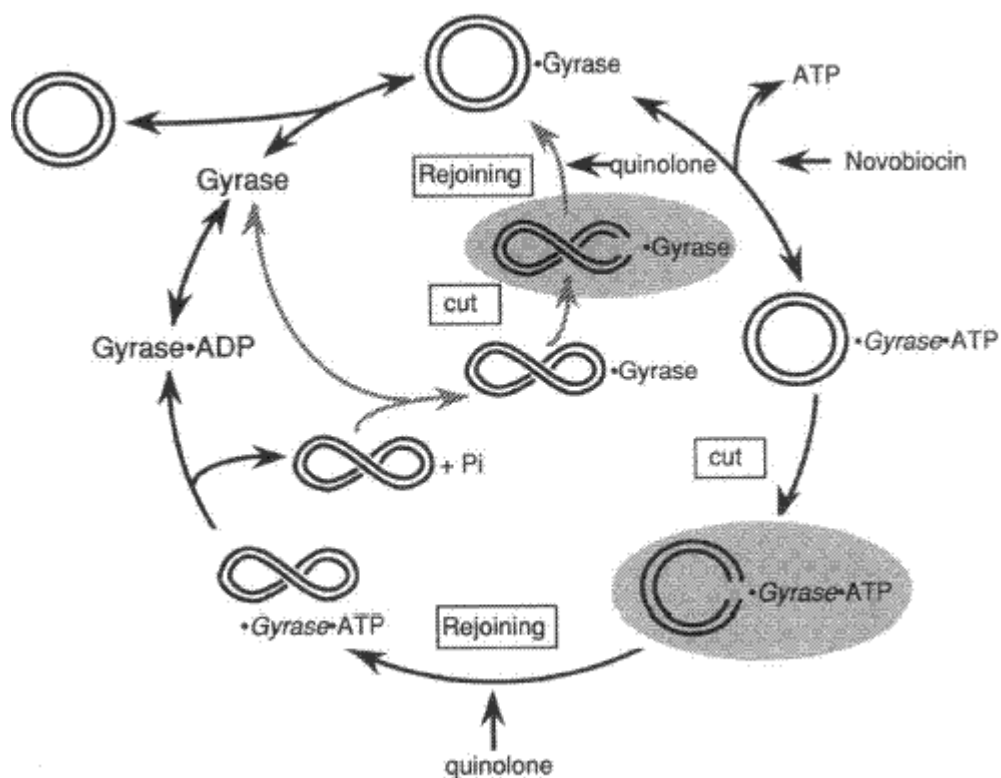


**Figure 1.22:** The DNA gyrase reaction and sites of action of gyrase inhibitors (Nakada *et al.*, 1994).

### 1.7.1 Fluoroquinolones

Fluoroquinolones (7-fluoro-4-oxo-1,4-dihydro-quinoline-3-carboxylic acids) (**Figure 1.23**) have few toxic side effects, good pharmacokinetic properties and potent activity against Gram-positive, Gram-negative and mycobacterial strains. Norfloxacin was the first of a new generation of fluoroquinolone antibacterial. They bind reversibly to the enzyme-DNA complex and stabilize the covalent enzyme tyrosyl-DNA phosphate ester, which is normally a transient intermediate in the topoisomerase reaction. Hydrolysis of this linkage leads to the accumulation of double-stranded DNA fragments and is the bactericidal consequence of fluoroquinolone treatment. Fluoroquinolones are being used in cases of MDR-TB and have a great potential for shortening treatment duration and improving therapy of TB-HIV co-infections. Recently a low-resolution crystal structures (4 Å) of cleavage complexes formed by the *S. pneumoniae* 55-kD ParC breakage-reunion and 30-kD ParE Toprim domains of topoisomerase IV stabilized by moxifloxacin and clinafloxacin (**Figure 1.24**) have provided insights into the fluoroquinolone mechanism of action (Laponogov *et al.*, 2009). The structures reveal that the fluoroquinolones intercalate at the bent gate DNA, stacked against DNA bases and are present in the drug-stabilised cleavage complex as shown in the **Figure 1.25**. They intercalate in the gap between the -1 and +1 nucleotide pairs of the cleaved DNA bound to topo IV.

Studies in the past have identified consensus sequences for fluoroquinolone-mediated DNA cleavage by Gram-negative and Gram-positive type II topoisomerases. Wild type and mutated consensus sequences showed the following features:

- (1) Gn/Cn-rich sequences at and around the cleavage site are hot spots for quinolone-mediated strand breaks.
- (2) Symmetry of the target sequence is important for cleavage.
- (3) In case of *S. pneumoniae*, A and T at position -2 and +6 are cleavage determinants.
- (4) The consensus sequence adopts a heteronomous A/B conformation (Richter *et al.*, 2007).

In the crystal structure the C-7 substituent of the quinolone interacts with DNA base pairs while the 3-carboxyl group contacts S79 (equivalent to positions 83 in *E. coli* GyrA) and is close to S80 (A84 of GyrA). Formation of a  $Mg^{2+}$ -bridge is important for drug binding due to the  $Mg^{2+}$ -dependence of complex formation (Sissi *et al.*, 2001). **Figure 1.25** also shows the residues in ParC (S79, D83) that are responsible for drug resistance upon mutation. Similarly, in the case of ParE, the residues (E474, E475, R456 and D435) responsible for drug-resistance are located within the Toprim domain and are close to the intercalated drug.

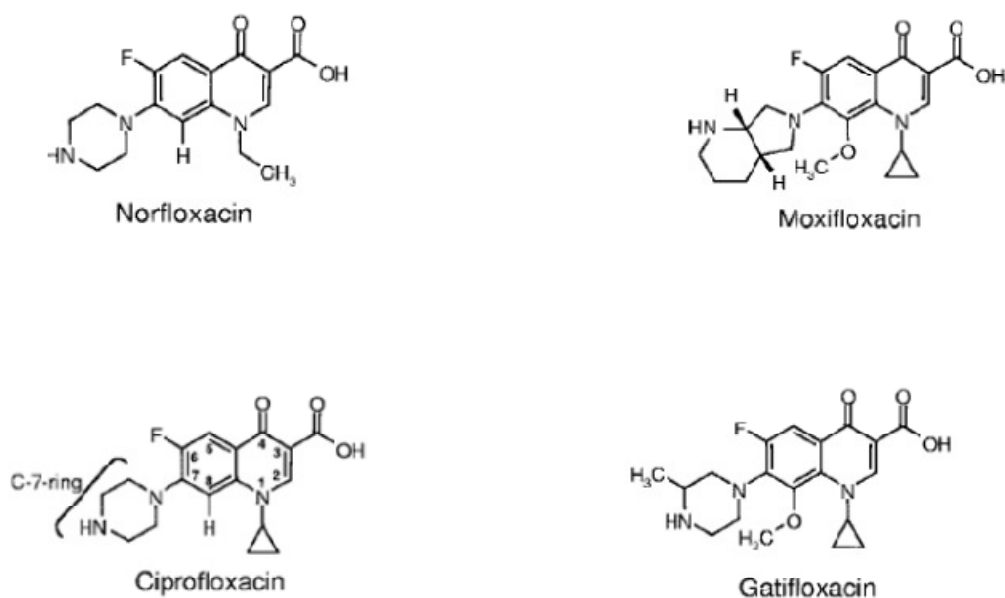


**Figure 1.23: Structures of Flurooquinolones (Drlica *et al.*, 2008).**

However, the existing DNA intercalation model has its limitations. It cannot explain the effects of certain amino acid substitutions and drug structure variations. For example the putative interaction of the C-7 substituent with position 81 as described above and the drugs substituent at position 1 and 8 that alter both the antimicrobial activity and drug-target binding constant (Barnard & Maxwell, 2001). Thus, quinolone binding is a multi-step process that involves at least two steps before and after the DNA cleavage (Critchlow & Maxwell, 1996, Marians & Hiasa, 1997).

A Crystal structure with a resolution of 3.35 Å of *S. aureus* DNA gyrase in complex with fluoroquinolone and DNA is also available (2XCT) (Bax *et al.*, 2010). This structure provides insights into how DNA is cleaved by type IIA topoisomerases and the role of the metal-binding Toprim domains in catalysis (**Figure 1.26**).

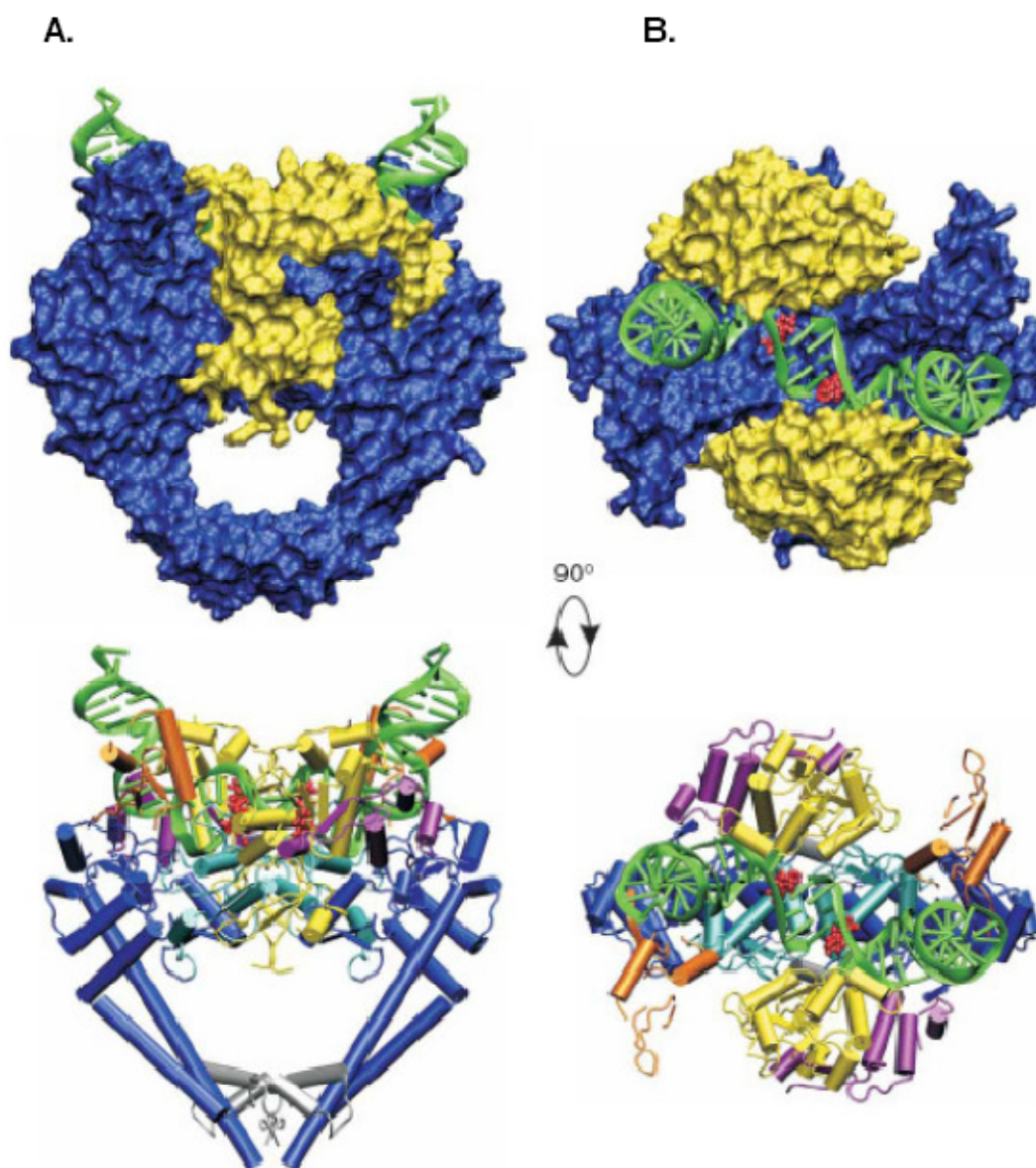


**Figure 1.24: Crystal structure of the topo IV-DNA-moxifloxacin complex.**

*Front (A) and top views (B) of topo IV ParC55 (blue) and ParE30 (yellow) protein complex with the G-segment DNA (green) and moxifloxacin (red) (Laponogov et al., 2009). A & B both are represented in space-filling and ball-and-stick models.*

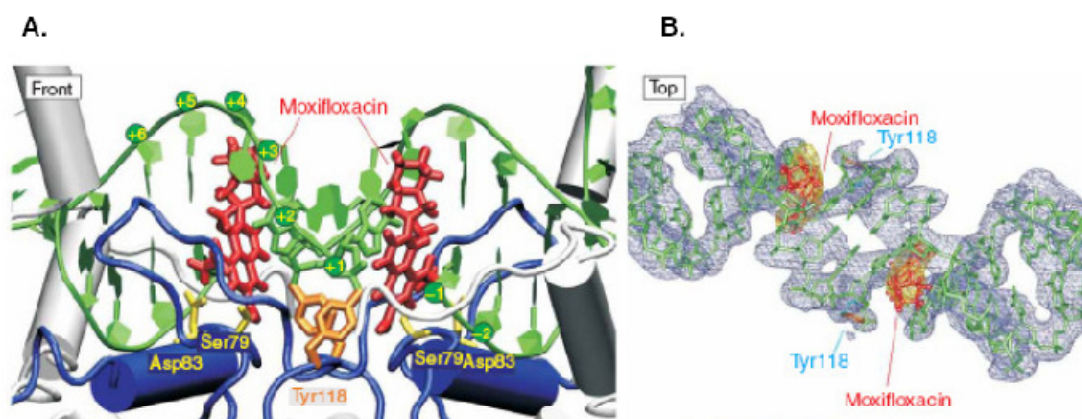


**Figure 1.25: Quinolone-topo IV cleavage complex.**

(A) The DNA G-segment is in green with numbers indicating the backbone position relative to the cleavage point. (B) Top view of the cleaved G-segment DNA molecule (green) attached to the Y118 with intercalated moxifloxacin molecules (red) (Laponogov *et al.*, 2009).

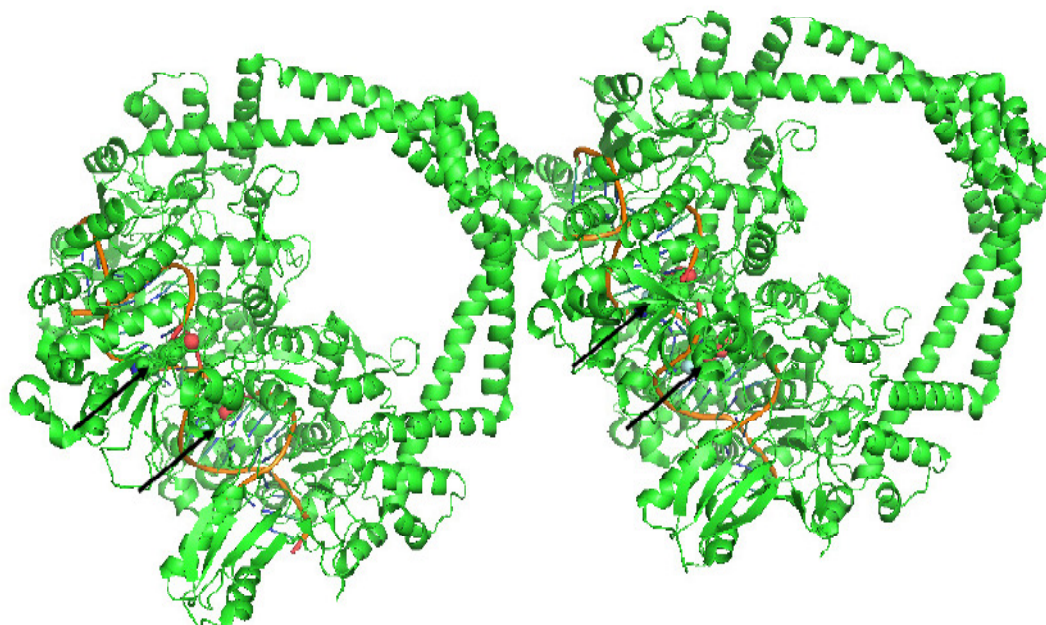


**Figure 1.26: *S. aureus* DNA gyrase in complex with ciprofloxacin and DNA (dimer in an asymmetric unit) (2XCT) (Bax *et al.*, 2010). Arrows point to ciprofloxacin molecules (spheres).**

At the cellular level, it was proposed that the irreversible collision of replication forks with quinolone-mediated complexes is the primary reason for cell death (Khodursky & Cozzarelli, 1998). Reactive oxygen species such as hydroxyl radicals also play an important role in amplification of lethality due to quinolones. The hydroxyl radicals are generated via the Fenton reaction due to iron-misregulation following gyrase poisoning due to quinolones. The iron misregulation occurs due to superoxide-mediated oxidation of iron-sulfur clusters (Dwyer *et al.*, 2007). There is also a difference in the lethality of different generations of quinolones under different conditions. For example, first-generation compounds such as nalidixic acids are not lethal in the presence of chloramphenicol or during anaerobic growth. On the other hand, ciprofloxacin, a third generation compound kills under both conditions but requires higher concentration during anaerobiosis. In the case of *M. tuberculosis*, moxifloxacin is more active when chloramphenicol is added (Malik & Drlica, 2006). Fluoroquinolones are effective in killing bacteria in the presence of chloramphenicol, when the lethal chromosome fragmentation due to quinolones requires on-going protein synthesis. Chloramphenicol blocks the formation of lesions. The connection between cleaved complex destabilisation and chloramphenicol-insensitive killing also provides information about the effects of quinolone structure. For example, the N-1 cyclopropyl group is probably important for cleaved complex destabilisation, since this moiety is the only difference between ciprofloxacin and norfloxacin. Ciprofloxacin kills in the presence of chloramphenicol and norfloxacin does not (Drlica *et al.*, 2008). Besides chloramphenicol, Lon protease may be involved in the repair of lethal lesions due to quinolones. Lon protease has been shown to have a role in chromosome maintenance when studying the survival of bacteria at high quinolone concentration (Crumplin & Smith, 1975).

Despite the lethal actions of fluoroquinolones, resistance to fluoroquinolone is acquired by genetic variations that reduce drug concentration or reduce the affinity of the compounds for its target. The drug concentration plays an important role in determining if non-target or target alleles are selected for mutation. In the case of mycobacteria, mutations in the non-target alleles have been observed due to initial low drug concentrations (Zhou *et al.*, 2000). Thus, the effect of drug concentration on the

mutation has led to the coining of a term called the ‘mutant selection window’ which is a drug concentration range that is above the minimum inhibitory concentration (MIC) but below mutant prevention concentration (MPC) (Drlica, 2003). MIC is the lowest or minimum concentration of drug that blocks the growth of the majority of drug-susceptible cells. MPC (Smith *et al.*, 2003) on the other hand is the drug concentration that blocks the growth of the least susceptible, single-step mutant. Above this concentration, cell growth required the presence of two or more resistance mutations. In other words, MPC is the MIC of the least susceptible single-step mutant (Smith *et al.*, 2003).

QRDR mutations have been the principle factor behind fluoroquinolone resistance. The quinolone-resistance-determining region (QRDR) is the region that contains those amino acids whose mutation leads to quinolone resistance. GyrA amino acids changes that result in resistance to fluoroquinolone are predominantly in the QRDR. The presence of a single mutation in the QRDR usually results in low-level resistance to fluoroquinolone; to obtain high levels of resistance, additional mutations in GyrA are required. The QRDR (Piton *et al.*, 2010) of *M. tuberculosis* is similar to those from other organisms. It is located at the highly conserved N-terminal region of GyrA, and the mutations associated with fluoroquinolone resistance in clinical isolates of *M. tuberculosis* are located in codons equivalent to those in *gyrA* genes from fluoroquinolone-resistant mutants from other bacteria (Goswitz *et al.*, 1992, Hopewell *et al.*, 1990, Yoshida *et al.*, 1990). Laboratory generated quinolone-resistant mutants of *M. tuberculosis* usually have single missense mutations in *gyrA* for low-level resistance, and two mutations in *gyrA*, or one mutation in *gyrA* and one in *gyrB* for high level resistance (Kocagoz *et al.*, 1996). The regions of *gyrB* that encode common mutations that lead to resistance to coumarins and quinolones are also highly conserved between *M. tuberculosis* and other bacteria (Takiff *et al.*, 1994). A study analyzing mutations in both *gyrA* and *gyrB* associated with quinolone resistance identified a novel N510D mutation in *gyrB* that was also associated with quinolone resistance. This study also found that while strains that carry the novel GyrA T80A mutations were slightly resistant to quinolones, several isolates carrying a combination

of GyrA T80A plus A90G mutations were hypersusceptible to quinolones (Aubry *et al.*, 2006b).

Another study investigated the enzymatic efficiency and quinolone sensitivity of *M. tuberculosis* GyrA carrying a mutation at position G88 (Matrat *et al.*, 2006). G88 in *M. tuberculosis* GyrA corresponds to G81 in *E. coli*. The residue is predicted to be involved in the quinolone-binding site. This study clearly established that GyrA G88C and G88A mutations conferred resistance to fluoroquinolones in *M. tuberculosis* by decreasing gyrase inhibition. This study further found that quinolones that do not have an R7 ring or fluorine in R6, minimum inhibitory concentrations (MICs) were similar for the G88A mutants and the H37Rv strain. IC<sub>50</sub>s for the mutant enzymes with both the G88C and G88A were also similar to the IC<sub>50</sub> for the wild-type enzyme. *M. tuberculosis* GyrA protein contains an alanine at the position homologous to serine 83 in the *E. coli* enzyme. Substitution at this position to a hydrophobic residue leads to drug resistance as in case of S83W (Guillemin *et al.*, 1998, Guillemin *et al.*, 1999). However, the most common mutations in fluoroquinolone resistant *M. tuberculosis* clinical isolates are still due to substitutions at codons 90 and 94 of *gyrA*, whose *E. coli* equivalents are also resistance determinants. A list of mutations in DNA gyrase subunits conferring resistance to fluoroquinolone in *E. coli* and *M. tuberculosis* are summarised in **Table 1.2**.

Besides spontaneous mutation in the target gene, three forms of plasmid-mediated quinolone resistance have also been identified. These are Qnr (Martinez-Martinez *et al.*, 1998), Aac(6')-Ib-cr (Robicsek *et al.*, 2006b) and QepA (Yamane *et al.*, 2008). Of the three, Qnr appears to have the most activity, followed by QepA and Aac(6')-Ib-cr. Qnr increases MIC up to 250- fold, while QepA and Aac(6')-Ib-cr increase MIC by 10-fold (Perichon *et al.*, 2007) and 4-fold respectively (Robicsek *et al.*, 2006b). Qnr will be discussed in brief here.

DNA gyrase subunits	<i>E. coli</i>	<i>M. tuberculosis</i>
GyrA	Ser-83→Leu; Ser-83→Trp; Asp-87→Asn; Gly-81→Cys; Ala-84→Pro; Ala-67→Ser; Gln-106→His.	Thr-80→Ala; Gly-88→Cys; Asp-89→Asn; Ala-90→Val; Ser-91→Pro; Asp-94→Ala Asp-94→Asn, Asp-94→His, Asp-94→Gly, Asp-94→Tyr.
GyrB	Asp-426→Asn; Lys-447→Glu.	Asn-533→Thr; Asn-510→Asp.

**Table 1.2: Mutations in the DNA gyrase subunit conferring resistance to fluoroquinolone (Takiff *et al.*, 1994, Von Groll *et al.*, 2009, Yoshida *et al.*, 1990, Kocagoz *et al.*, 1996, Yoshida *et al.*, 1991).**

Qnr was discovered in a strain of *K. pneumoniae* exhibiting resistance to fluoroquinolone and 13 other agents (Martinez-Martinez *et al.*, 1998). QnrA is a 218 amino acid protein that belongs to a large family characterised by pentapeptide repeats. A Qnr homologue, MfpA found in mycobacteria has provided insights into how gyrase is protected from quinolones (Hegde *et al.*, 2005, Montero *et al.*, 2001). The three-dimensional structure of MfpA revealed that it is a dimer and appears to be a DNA mimic (**Figure 1.27**). It has size, shape and electrostatic similarity to B-form DNA (Hegde *et al.*, 2005).

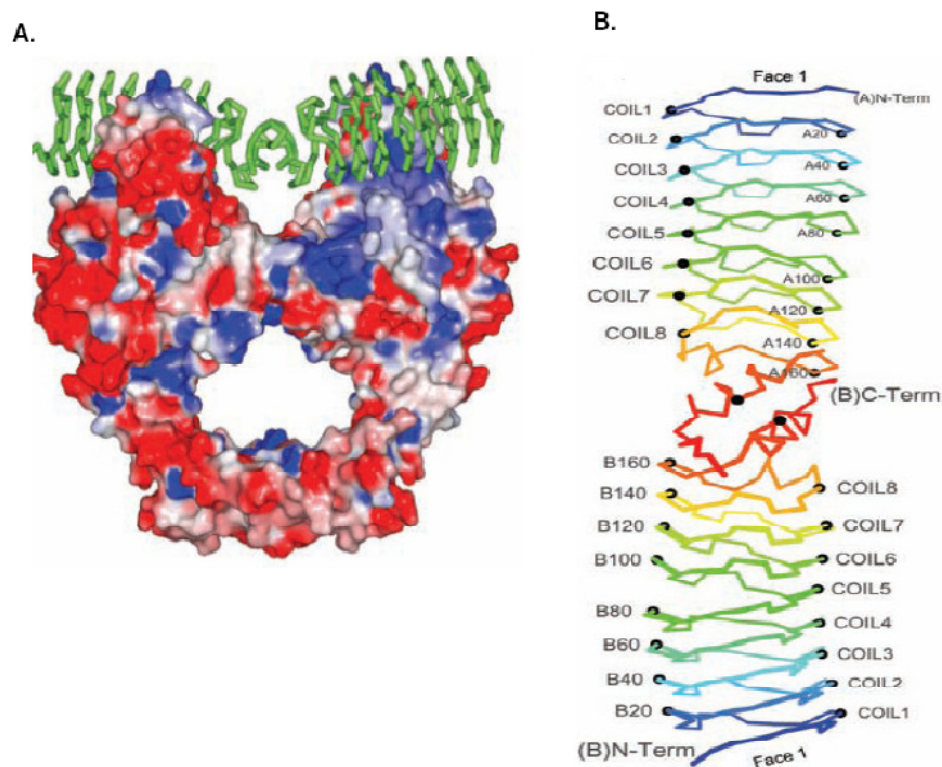


**Figure 1.27: MfpA, Qnr homologue found in *M. tuberculosis*.** (A) Molecular model of MfpA bound to *E. coli* GyrA59. (B) MfpA dimer showing its similarity to B-DNA (Hegde *et al.*, 2005).

In general, Qnr proteins lower quinolone binding to DNA complexes formed with gyrase or topo IV (Tran *et al.*, 2005b) and reverse quinolone-mediated inhibition of the gyrase supercoiling activity (Tran *et al.*, 2005a). It is likely that Qnr acts by altering the DNA-binding properties of gyrase rather than by competitive binding to a quinolone interaction site (Tran *et al.*, 2005a). *qnr* is expected to cause a serious resistance problem due to following two reasons:

1. Firstly, often plasmids having a QnrA determinant also carry genes that provide resistance to other anti-bacterials such as chloramphenicol and sulphonamides (Nordmann & Poirel, 2005).
2. Qnr-expressing plasmids are widely distributed (Nordmann & Poirel, 2005).

QepA and Aac(6')-Ib-cr has not been extensively studied in comparisons to Qnr. Aac(6')-Ib-cr adds an acetyl substituent on the nitrogen atom of the C-7 piperazinyl ring (Robicsek *et al.*, 2006b), but it has no effect on quinolones such as levofloxacin and gemifloxacin lacking piperazinyl nitrogen (Robicsek *et al.*, 2006a). The QepA efflux pump was found in a clinical isolated of *E. coli* in 2006. QepA increases the MIC for fluoroquinolones such as ciprofloxacin by 10-fold (Perichon *et al.*, 2007).

Thus, although quinolones continue to be an important class of antimicrobial agent, bacterial resistance is increasing (Boyd *et al.*, 2008).

### 1.7.2 Aminocoumarins

Aminocoumarin are naturally occurring products of *Streptomyces* species that share common structural features: a 3-amino-4, 7-dihydroxycoumarin structure, an L-noviosyl sugar and an aromatic acyl component attached to the amino group of the aminocoumarin moiety. Novobiocin, coumermycin A<sub>1</sub> and clorobiocin are the three naturally-occurring aminocoumarins produced by *S. spheroides*, *S. rishiriensis* and *S. roseochromogenes*, respectively (Pojer *et al.*, 2002). The difference in clorobiocin and novobiocin is the substitution of the methyl group at the 8' position of the coumarin ring with chlorine atom and a 5-methyl-pyrrole-2-carboxyl group substitutes the carbamoyl group at the 3' position of the noviose. Coumermycin A<sub>1</sub> has coumarin rings attached to the either side of a pyrrole group; a substituted sugar is attached to each of the coumarin rings, and a pyrrole group is attached to each noviose sugar (Figure 1.28).

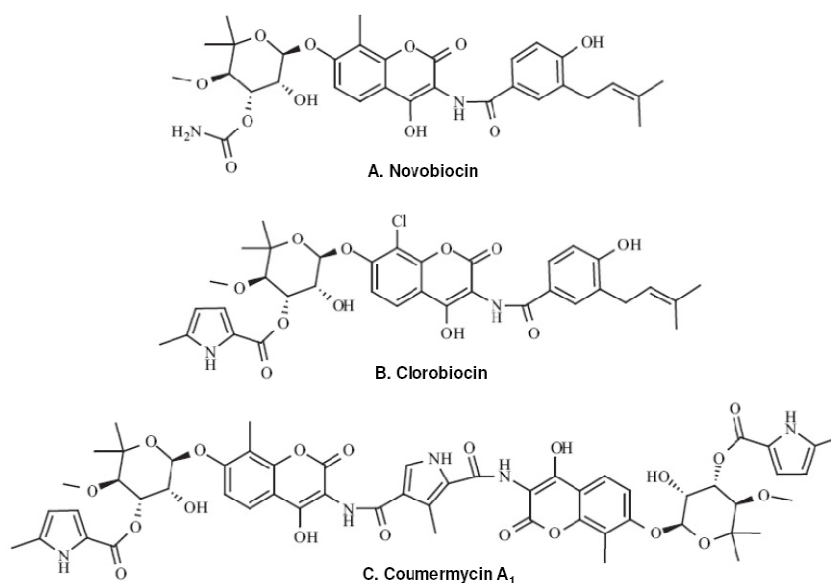


**Figure 1.28: The three main naturally-occurring aminocoumarins: Novobiocin, clorobiocin, and coumermycin A<sub>1</sub> (Oblak *et al.*, 2007).**

Aminocoumarin drugs act by competitively inhibiting the ATPase activity of GyrB (Gormley *et al.*, 1996, Maxwell, 1997). The interactions of aminocoumarin with *E. coli* DNA gyrase is extremely well characterised. Crystal structures of novobiocin and clorobiocin (PDB code: 1KZN) in complex with the GyrB N-terminus (GyrB24) (Holdgate *et al.*, 1997, Lafitte *et al.*, 2002, Maxwell & Lawson, 2003, Lewis *et al.*, 1996) and *Thermus thermophilus* GyrB43 complexed with novobiocin (PDB code: 1KIJ) (Lamour *et al.*, 2002) are available. The crystal structures clearly show an overlap in the binding site of ATP and the aminocoumarin. In the case of novobiocin the binding site of the noviose sugar and the adenine ring of the ATP/ADPNP molecule overlap (**Figure 1.29**).

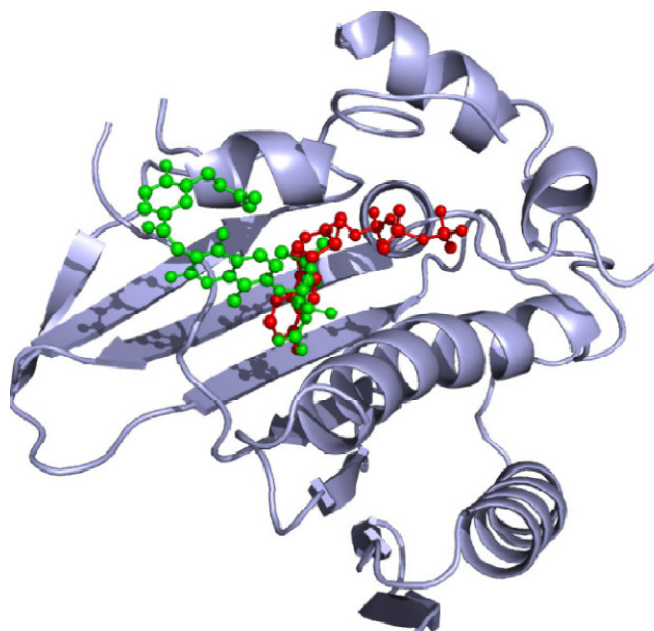


**Figure 1.29: Overlap of the novobiocin (green) and ADPNP (red) binding site at *E. coli* GyrB N-terminus (GyrB24).**

Novobiocin is licensed for the treatment of infections by some Gram-positive organisms and has been shown to be able to enhance the cytotoxic activities of the anti-tumour drugs etoposide and teniposide (Maxwell & Lawson, 2003). Despite the fact that aminocoumarins are potent inhibitors of DNA gyrase, due to their poor solubility, high toxicity and ineffectiveness against Gram-negative bacteria they have limited potential as drugs. The aminocoumarins are ineffective against Gram-negative due to the problem with antibiotic uptake across the bacterial outer membrane (Chusri *et al.*, 2009). Novobiocins under the trade name albamycin and cathomycin have been withdrawn.

### 1.7.3 Simocyclinones

Simocyclinones are a class of new antibiotics that were isolated from *Streptomyces antibioticus* Tü 6040 (Holzenkampfer *et al.*, 2002, Theobald *et al.*, 2000, Schimana *et al.*, 2000). Simocyclinone has an aminocoumarin ring but in contrast to other aminocoumarin antibiotics, it does not contain an L-noviosyl sugar at the 7-OH of the aminocoumarin ring; another sugar, D-olivose, is attached to the acyl moiety (which is a tetraene dicarboxylic acid) by an ester bond. This D-olivose is glycosidically linked to an angucyclic polyketide. The main simocyclinone produced by *Streptomyces antibioticus* Tü 6040 is simocyclinone D8 (**Figure 1.30, B**). In addition to simocyclinone D8, 13 other polyketide containing compounds have been isolated from *Streptomyces antibioticus* Tü 6040 (Theobald *et al.*, 2000). These simocyclinones can be grouped into four classes (A-D) depending upon their structure. These classes are defined by the presence of different functional groups in polyketide (R1), D-olivose (R2), coumarin (R3) parts. The production of different proportions of simocyclinones can be affected by the media composition and fermentation conditions (Schimana *et al.*, 2001) (Theobald *et al.*, 2000). Characterisation and cloning of the simocyclinone D8 biosynthetic gene cluster has revealed 49 open reading frames that code for genes responsible for the synthesis of the four distinct parts of simocyclinone D8 (Trefzer *et al.*, 2002).

Simocyclinone D8 has weak inhibitory activity only against Gram-positive bacteria (Schimana *et al.*, 2000). Wild-type *E. coli* and other Gram-negative bacteria are resistant to simocyclinones because the compounds cannot penetrate the outer membrane (Schimana *et al.*, 2000). In a recent study (Edwards *et al.*, 2009), *E. coli* strain (NR698) was used to isolate simocyclinone-resistant mutants because it carries an in-frame deletion in the *imp* (increased membrane permeability) gene (Ruiz *et al.*, 2005) and is sensitive to simocyclinone. It has also been suggested that efflux pumps such as the AcrB multidrug efflux pump may be responsible for the ineffectiveness of simocyclinones against Gram-negative bacteria (Oppegard *et al.*, 2009). In the producing organism, it is suggested that regulation at the level of TetR repressor SimR and a proton dependent transporter SimX may be responsible for the resistance mechanism and thus preventing suicide of the producer (Le *et al.*, 2009).

Simocyclinone D8 can also inhibit human topoisomerase II with an  $IC_{50}$  of 100  $\mu\text{M}$ , more potent than etoposide with an  $IC_{50}$  of 400  $\mu\text{M}$  (Sadiq *et al.*, 2010).

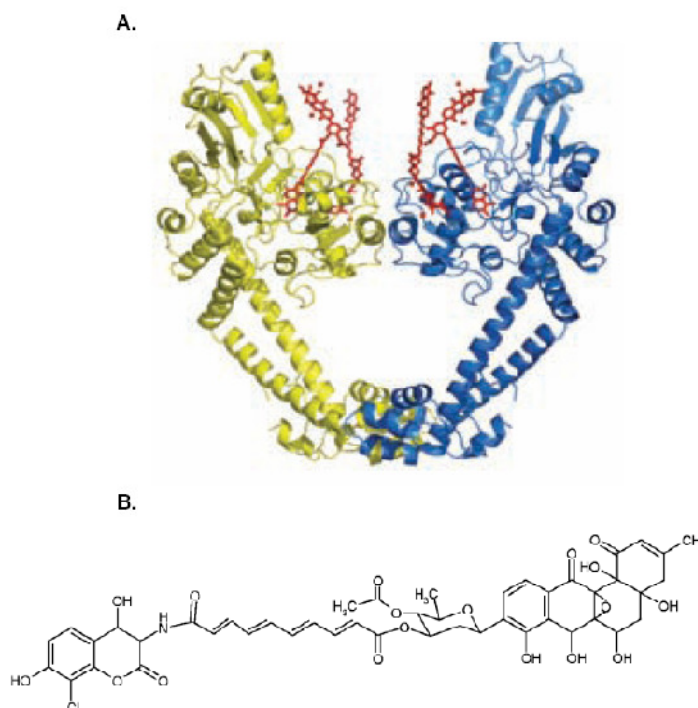


**Figure 1.30: Simocyclinone D8 binds to GyrA59.** Crystal structure (PDB code: 2WL2) of Simocyclinone D8-GyrA59 complex (A: top panel). Structure of Simocyclinone D8 showing the polyketide and coumarin moieties (B: bottom panel) (Edwards *et al.*, 2009).

Studies in the past involving simocyclinone D8 with *E. coli* DNA gyrase suggested that simocyclinones inhibit an early stage of the gyrase catalytic cycle by interacting with the N-terminal domain of GyrA and preventing binding of the enzyme to DNA (Flatman *et al.*, 2005). The recent crystal structure of the complex between the N-terminal domain of *E. coli* GyrA (GyrA59) and simocyclinone D8 identified the binding site for the molecule and provides information about the mechanism of action (Edwards *et al.*, 2009). The structure revealed two distinct binding sites for simocyclinone D8 within each GyrA59 monomer, one for the aminocoumarin moiety and one for the polyketide moiety. In the crystal structure (**Figure 1.30, A**), two GyrA59 dimer are non-covalently crosslinked by four simocyclinone D8 molecules. Each drug molecule binds the aminocoumarin-binding

site of a GyrA59 monomer of one dimer and the polyketide-binding site of a GyrA59 monomer of another dimer.

Analysis of the GyrA59-simocyclinone D8 complex revealed that the distance between the aminocoumarin- and polyketide-binding sites is equal to the length of the tetraene chain which links the aminocoumarin and polyketide moieties of simocyclinone D8. This has led to the proposal that simocyclinone D8 is able to adopt an alternative configuration where it stretches between the two sites within the same GyrA monomer. Nano-ESI MS data has revealed that simocyclinone D8 binds GyrA59 in a cooperative manner, with the binding of one molecule promoting the binding of a second (Edwards, 2009). Both ends of the simocyclinone D8 molecule are required for the positive cooperative binding. The simocyclinone D8 fragments, MGD8N2A (lacks the polyketide moiety) and simocyclinone C4 (lacks the aminocoumarin moiety) do not display positive cooperativity.

Besides the N-terminal domain of the GyrA subunit, a binding site for the drug has also been identified in the C-terminal domain of GyrB (GyrB47) (Sissi *et al.*, 2010). It is suggested that these two distinct sites in both the subunits could cooperate in the reconstituted enzyme. The exact location for the binding of drug within GyrB47 is not known, but it is likely that interaction could be at the protein-protein interface.

#### 1.7.4 Cyclothialidine

Cyclothialidine (**Figure 1.31, A**) contains a unique 12-member lactone ring that is partly integrated into a pentapeptide chain. Cyclothialidine was isolated from *Streptomyces filipinensis* NR0484 and acts by competitively inhibiting the ATPase activity of the GyrB subunit (Nakada *et al.*, 1993, Nakada *et al.*, 1994). The compound was also active against DNA gyrase resistant to novobiocin, suggesting that its precise site of action might be different from that of novobiocin. However, cyclothialidine does not show any growth inhibitory activity against bacterial cells. It may be due to permeability problems across the cytoplasmic membrane (Goetschi *et al.*, 1993) Investigation involving the identification of active structural components have directed the synthesis of a number of new inhibitors that have shown in vitro

activity against gram-positive pathogens (Angehrn *et al.*, 2004, Goetschi *et al.*, 1993).

The crystal structure of GyrB24 complexed with a cyclothialidine (GR122222X) has been determined to 2.0-Å resolution (Lewis *et al.*, 1996) (**Figure 1.31, B**). The majority of the protein-ligand interactions are between the resorcinol ring of cyclothialidine and GyrB24. The drug lies in a hydrophobic pocket and makes a number of hydrogen bonds with the amino acids such as Asn46, Asp73 and Thr165. The drug binding-site does not lie in the ATP-binding pocket of GyrB but partially overlaps with that of ATP. The resorcinol ring occupies a position that prevents binding of the adenine ring.

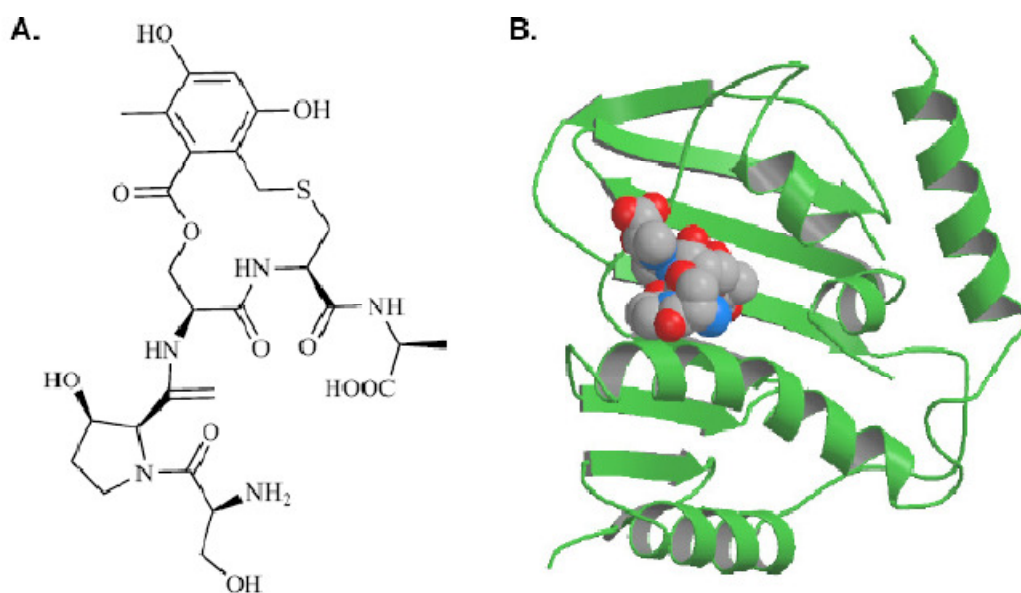


**Figure 1.31: Cyclothialidine inhibits the ATPase activity of the GyrB subunit.** (A) Chemical structure of cyclothialidine (Tse-Dinh, 2007). (B) Crystal structure of GyrB24 complexed with a cyclothialidine (GR122222X) (Lewis *et al.*, 1996).

### 1.7.5 GSK299423

In a recent publication (Bax *et al.*, 2010), GlaxoSmithKline reported the 2.1 Å crystal structure (**Figure 1.32, A**) of a novel inhibitor GSK299423 (**Figure 1.32, B**) in a pre-cleavage complex with *S. aureus* DNA gyrase and a 20-bp DNA duplex (PDB code: 2XCS). GSK299423 is 2,000 times more potent than ciprofloxacin for inhibition of *S. aureus* DNA gyrase supercoiling. It has been suggested that the compound does not stabilise the cleavage complex rather it generated single-strand breaks. These single-strand breaks seem to be associated with covalent phosphotyrosyl-protein–DNA complex formation. However, the gel-based assays do not provide any evidence for the formation of single-stranded breaks.

The binding site of the drug is distinct from but close to the fluoroquinolone binding site. GSK299423 binds midway between the two active sites, with the quinoline-carbonitrile group sitting in between the two central base pairs of the stretched DNA and the oxathiole-pyridine group occupying the non-catalytic pocket that opens up between the two GyrA subunits. The pocket between the two GyrA subunits occupied by the oxathiole-pyridine group is largely hydrophobic, with residues Ala 68, Gly 72, Met 75 and Met 121 making van der Waals interactions with the compound. The crystal structure also provides structural evidence of a second metal-binding site involved in the Toprim domain nucleotidyl phosphotransferase.

The publication also reported a 3.35 Å structure complex with ciprofloxacin, providing detailed structural insight into how DNA is cleaved by type IIA topoisomerases. Comparison of these two structures indicates that for DNA cleavage, the correct positioning of the catalytic tyrosine on the CAP domain with respect to the Toprim domain seems to be achieved by a rigid body-domain movement. The GyrB Asp 512–GyrA Arg A33 ion pair was also proposed to act as a conformational switch to help communicate information about the state of cleavage of the DNA from the active sites to the rest of the protein.

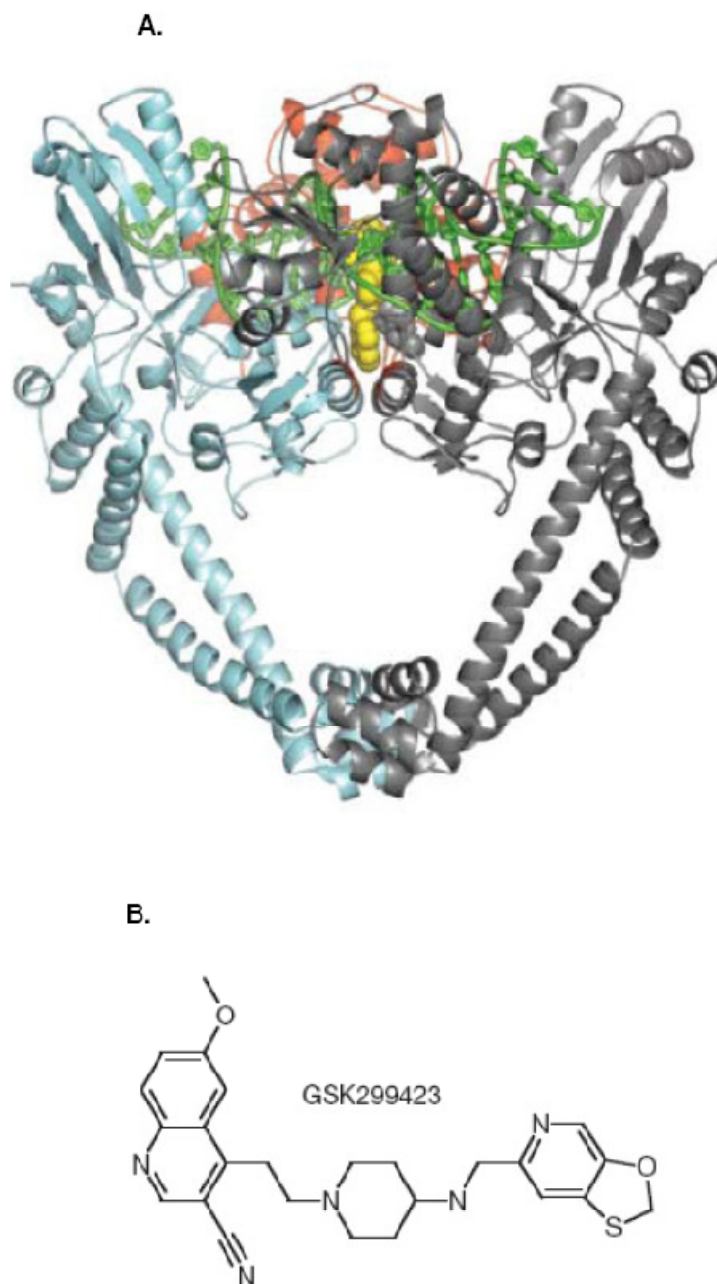


**Figure 1.32: GSK299423 a novel DNA gyrase inhibitor.** (A) *Crystal structure of GyrB27-A56 fusion protein in complex with DNA and GSK299423. GSK299423 is shown in yellow and DNA in green colour.* (B) *Structure of GSK299423 (Bax et al., 2010).*

### 1.7.6 CcdB

CcdB is component of the *ccd* toxin-antitoxin (TA) module encoded by the F plasmid. CcdB is the toxin and CcdA is the antitoxin (Bahassi *et al.*, 1999). CcdB inhibits the catalytic reactions of gyrase by stabilization of the cleavage complex (Bernard *et al.*, 1993). The GyrA C-terminal DNA-wrapping domain and the GyrB N-terminal ATPase domains are dispensable for CcdB's action. Based on the structure of CcdB (PDB code: 3vub) (Loris *et al.*, 1999) and its complex with the N-terminal domain of GyrA (PDB code: 1x75) (Dao-Thi *et al.*, 2005) a model for CcdB action was proposed. The model suggested that a dimeric CcdB binds within the cavity formed by the GyrA dimer, but only when the DNA gate is open. This places the three C-terminal residues of CcdB (Trp99, Gly100 and Ile101) which are critical to its toxicity (Bahassi *et al.*, 1995), in close proximity to the GyrA Arg462 residue. When this residue is mutated, it confers resistance to CcdB (Bernard & Couturier, 1992, Bernard *et al.*, 1993). The structure of CcdB with a fragment of GyrA (GyrA14; PDB code: 1x75) shows a symmetric complex, with an asymmetric centre where the GyrA Arg462 residue stacks between the Trp99 residues of the CcdB monomers.

While CcdB poisons gyrase, CcdA actively dissociates CcdB-gyrase complexes by a process called rejuvenation. The CcdA:CcdB ratio modulates autorepression of the *ccd* operon. Recent crystal structures of CcdB with fragments of CcdA (PDB code: 3HPW & 3G7Z) have provided insights into the mechanism behind rejuvenation and regulation of expression (**Figure 1.33**). This mechanism is complex and autoregulatory (De Jonge *et al.*, 2009).

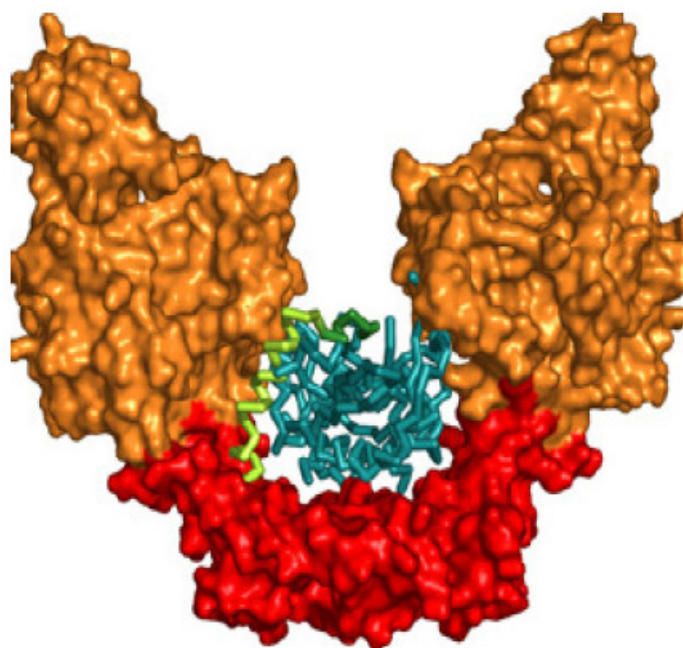


**Figure 1.33: CcdB with multiple interacting partners: CcdA and DNA gyrase.** Representation of  $CcdB_2:CcdA^{37-72}$  and  $GyrA59_2:CcdB_2$  complexes.  $GyrA59_2$  is shown in orange surface representation and  $GyrA14_2$  in red.  $CcdB_2:CcdA^{37-72}$  complex is represented as Ca traces inside the cavity of  $GyrA59$  (De Jonge *et al.*, 2009).

### 1.7.7 Microcin B17

Microcins are antibacterial peptides encoded by genes located on plasmids, or on the chromosome, along with their self-immunity factors, secretion proteins and the post-translational modification enzymes. They have molecular masses below 10-kD and are produced mainly by enterobacteria. They are ribosomally synthesised as precursors and further modified enzymatically. They are secreted under conditions of nutrient depletion. Fourteen microcins have been reported so far, among which only seven have been characterised and Microcin B17 is among the well characterised microcins (Duquesne *et al.*, 2007).

Microcin B17 (MccB17) is a post-translationally-modified 43-amino acid peptide produced by strains of *E. coli* containing the plasmid-borne *mccB17* operon. MccB17 results from the 69 amino acid McbA precursor that is modified by the *mcbB*, *C* and *D* gene products (Mcc synthetase). The genes *mcbE* and *mcbF* encode

two proteins involved in MccB17 secretion and self-immunity while the product of *mcbG* offers complete self-immunity (Garrido *et al.*, 1988) (**Figure 1.34, A**). Serine and cysteine residues react with the carbonyl group of the preceding glycines to produce thiazole or oxazole rings. Thus MccB17 contains four oxazole and four thiazole rings; two thiazole and oxazole rings are in tandem as bis-heterocycles (**Figure 1.34, B**). The effect of MccB17 on bacteria is to arrest DNA replication and to induce the SOS response (Herrero & Moreno, 1986). It has been shown to target bacterial DNA gyrase by the isolation of a resistant mutant in the *gyrB* gene (Vizan *et al.*, 1991). MccB17 has been reported to display potent bactericidal activity against a wide range of gram-negative bacteria including *Escherichia*, *Klebsiella*, *Salmonella*, *Shigella* and *Pseudomonas* (Duquesne *et al.*, 2007).

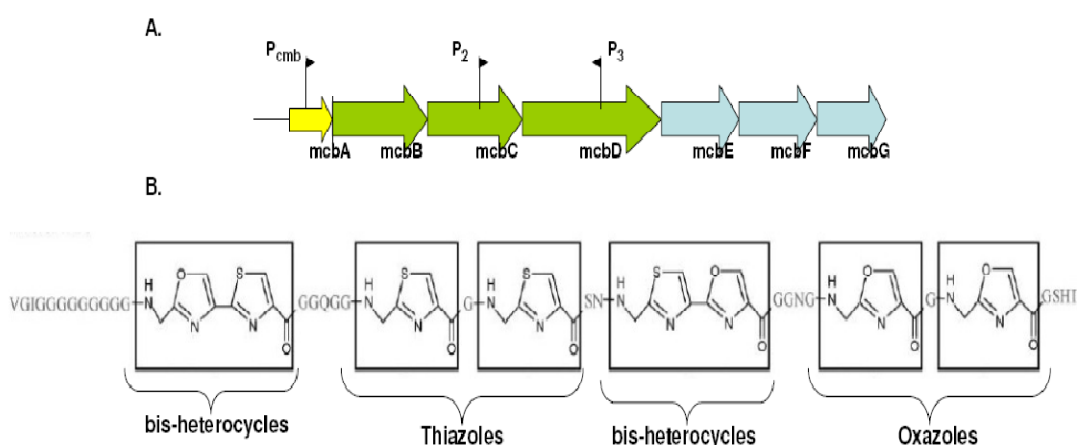


**Figure 1.34: MccB17 chemical structure and gene cluster.** (A) Different genes involved in MccB17 synthesis, modification and self-immunity in the gene cluster. (B) Structure of mature MccB17 having thiazole, oxazoles and bis-heterocycles (Duquesne *et al.*, 2007).

MccB17 stabilises the gyrase-DNA covalent complex and this is responsible for its toxicity (Heddle *et al.*, 2001). It slows down both the DNA supercoiling and relaxation reactions of gyrase and can stabilise the covalent complex between the enzyme and DNA with and without ATP (Pierrat & Maxwell, 2003). With relaxed DNA as a substrate, MccB17 can stabilise a cleavage complex weakly in the absence of ATP but more efficiently in the presence of nucleotide. The peptide can stabilise a cleavage complex more efficiently in the absence of ATP if the DNA substrate is negatively supercoiled; this suggests that it is acting at an enzyme conformation, which arises either when ATP is being hydrolysed during the supercoiling cycle or during the ATP-dependent relaxation of supercoiled DNA. Inhibition of supercoiling and relaxation by MccB17 is due to the reduction of the rate of strand-passage by MccB17 (Pierrat & Maxwell, 2003). MccB17 interacts with the N-terminal domain of GyrA, the C-terminal domain of GyrB and/or DNA, exploiting an enzyme conformation that occurs during the topoisomerase cycle. Thus MccB17 has potential to guide the design of effective antibacterial by identify the active components of this peptide and using them as templates.

## 1.8 Other proteinaceous inhibitors

Other DNA gyrase inhibitors that have been discovered are either enzymes or proteins such MurI and YacG or small molecules like QPT-1. Glutamate racemase (MurI) catalyses the conversion of L-glutamate to D-glutamate. D-glutamate is an important component of the bacterial cell wall. It has been found that besides the catalytic activity of *E. coli* MurI, it also inhibits DNA gyrase in the presence of the peptidoglycan precursor. The requirement of the peptidoglycan precursor is not obligatory for the inhibitory activity of MurI, as out of two MurI in *B. subtilis* one inhibits DNA gyrase in absence of the precursor and *M. tuberculosis* MurI inhibits in the absence of the precursor. *M. tuberculosis* has a single gene for MurI and it inhibits DNA gyrase activity. The inhibitory activity of MurI is not species-specific rather it is enzyme-specific as topo I is not inhibited by it. MurI inhibitory activity is due to its selective binding to the GyrA subunit, which affects DNA binding. Although MurI inhibits DNA gyrase activity, Mur I protects *M. smegmatis* against

the action of ciprofloxacin. This indicates that MurI may be a survival strategy used by the cell to safeguard DNA gyrase. It can also have physiological role of preventing excessive supercoiling (Sengupta & Nagaraja, 2008a, Sengupta *et al.*, 2008, Sengupta *et al.*, 2006).

Similarly, other endogenous proteins in *E. coli* such as YacG and GyrI have DNA gyrase inhibitory activity. The GyrI protein was the first identified chromosomally nucleotide-encoded regulatory factor of *E. coli* DNA gyrase. It inhibits the supercoiling activity of DNA gyrase and overexpression and antisense expression of the *gyrI* gene-induced filamentous cell growth and suppressed cell proliferation (Nakanishi *et al.*, 1998). GyrI binds to the gyrase holoenzyme with higher affinity than to either GyrA or GyrB alone (Nakanishi *et al.*, 2002). Besides its inhibitory activity, it has also been shown to provide limited protection against the quinolones (Chatterji *et al.*, 2003).

YacG is encoded by *E. coli* and has a zinc-finger motif. It inhibits all the activities of DNA gyrase by preventing DNA binding. It binds to the carboxy-terminal domain of GyrB. Topo I and topo IV are not inhibited by YacG (Sengupta & Nagaraja, 2008b).

There are certain pentapeptide repeat proteins such as MfpA and QnrB4, which inhibit DNA gyrase activity. MfpA as described previously is present in *M. tuberculosis* (Hegde *et al.*, 2005), while QnrB4 is encoded by a plasmid borne in enterobacteria. MfpA is more effective in inhibiting *M. tuberculosis* DNA gyrase activity in comparison to the inhibitory activity of QnrB4 against *E. coli* DNA gyrase. Both the proteins are involved in resistance to fluoroquinolone, but the QnrB4 activity is species specific (Merens *et al.*, 2009).

Besides the endogenous DNA gyrase inhibitors, the conventional high-throughput screening of chemical libraries has discovered inhibitors such as QPT-1 (Miller *et al.*, 2008), which has activity against a broad spectrum of pathogenic and antibiotic-resistant bacteria. The molecule was non-toxic and targeted the  $\beta$  subunit of bacterial type II topoisomerase. An introduction to the novel DNA gyrase inhibitors discovered in this project is given in Chapter 4.

## 1.9 Aim of the project

The aim of this Ph.D. project was to establish a fundamental understanding of *M. tuberculosis* DNA gyrase and explore it as a target for novel inhibitors. Bioinformatics analysis revealed some interesting features about the enzyme such as the presence of a putative Ca<sup>2+</sup>- binding site, which was investigated by biochemical and biophysical techniques. Further investigation of the enzyme lead to the discovery of naphthoquinones, aaptamines and quinolines as new classes of DNA gyrase inhibitors.

## Chapter 2: Materials & Methods

### 2.1 Bacteriology

Different strains of *Escherichia coli* (*E. coli*), *Mycobacterium smegmatis* (*M. smegmatis*), growth medium and plasmids were used for microbiology and molecular biology experiments.

#### 2.1.1 *E. coli* and *M. smegmatis* strains

The following *E. coli* and *M. smegmatis* strains listed in **Table 2.1** were used in this study.

Strain	Genotype
BL21 <i>E. coli</i>	F <sup>-</sup> <i>ompT hsdS<sub>B</sub>(r<sub>B</sub><sup>-</sup> m<sub>B</sub><sup>-</sup>) gal dcm</i>
BL21 (DE3) pLysS <i>E. coli</i>	F <sup>-</sup> <i>ompT hsdS<sub>B</sub>(r<sub>B</sub><sup>-</sup> m<sub>B</sub><sup>-</sup>) gal dcm (DE3) pLysS (Cam<sup>R</sup>)</i>
Top 10 chemically competent <i>E. coli</i>	F <sup>-</sup> <i>mcrA Δ(mrr-hsdRMS-mcrBC) φ80lacZΔM15 ΔlacX74 recA1 araD139 Δ(ara-leu)7697 galU galK rpsL (Str<sup>R</sup>) endA1 nupG λ-</i>
DH5α chemically competent <i>E. coli</i>	F <sup>-</sup> <i>φ80lacZΔM15 Δ(lacZYA-argF)U169 deoR recA1 endA1 hsdR17(rk<sup>-</sup>, mk<sup>+</sup>) phoA supE44 thi-1 gyrA96 relA1 λ-</i>
<i>M. smegmatis</i> mc <sup>2</sup> 155	wild-type

**Table 2.1: The list of *E. coli* and *M. smegmatis* strains used in the study.**

### 2.1.2 Media and antibiotics

#### *E. coli* and *M. smegmatis* growth medium

Luria-Bertani (LB) medium was used for the growth of different strains of *E. coli* in liquid media. The liquid media was used for growing transformed colonies for plasmid propagation and for protein expression. The autoclaved liquid medium after preparation was stored at room temperature. The recipe for the medium is as follows:

<b>Luria-Bertani (LB) medium:</b>	Tryptone (OXOID)	10 g
	Yeast extract (OXOID)	5 g
	NaCl	10g
	Water	1L

The solid medium was prepared by adding 15 gm of agar (OXOID) to the LB medium before autoclaving it.

**7H9-Tw medium** was used for the growth of pure cultures of mycobacteria.

<b>7H9-Tw medium:</b>	BD Middlebrook 7H9 broth base	4.7 g
	Glycerol	2 ml
	20% (v/v) Tween 80 (final concentration of 0.05% v/v)	5 ml
	BD oleic albumin dextrose catalase (OADC) enrichment	100 ml
	Water	900 ml

Note: Mix well and filter sterilize the medium before adding Tween 80 and ODAC.

**7H10 agar plates** were used for mycobacteria by including appropriate antibiotics in the medium. The media was prepared as follows:

<b>7H10 agar plates:</b>	Middlebrook 7H10 medium	19 g
	60% glycerol (v/v)	8.4 ml
	OADC enrichment media	100 ml
	Water	900 ml

Note: Autoclave after adding 60% glycerol (v/v). On cooling media to ~50°C, add ODAC.

**SuperBroth** was used for growing cells for large-scale preparation of pBR322.

<b>SuperBroth:</b>	Tryptone	4.8 g
	Yeast Extract	9.6 g
	Glycerol	2.0 ml
	Phosphate Buffer	40 ml
	Water	360 ml

A stock solution of 100 mg/ml of Ampicillin in water was prepared in milli-Q water and added to solid/liquid medium to a final concentration of 100 µg/ml. Chloramphenicol at 30 mg/ml was prepared in 100% ethanol and added to solid/liquid medium to a final concentration of 30 µg/ml. 50 mg/ml Streptomycin was prepared in Milli-Q water and added to solid medium to a final concentration of 20 µg/ml.

### 2.1.3 Preparation of electrocompetent *M. smegmatis* cells

A starting culture of *M. smegmatis* was grown overnight in 7H9-Tw liquid medium overnight at 37°C with shaking at 100 rpm. 1 ml from the overnight cultures was used as seed inoculums for 100 ml cultures. This culture was grown for nearly 24 hr until the OD at 600 nm is between 0.8 -1.0. The grown cells were incubated on ice for 90 min before centrifuging at 2700 g for 10 min at 4°C. The pellets were resuspended in a volume of 10% (w/v) glycerol and washed with successive smaller amounts of 20 ml, 10 ml and 5 ml. Finally, the pellets were suspended in 1 ml of 10% (w/v) glycerol and stored at -80°C in 200 µl aliquots.

### 2.1.4 Preparation of chemically competent *E. coli* cells

In order to prepare chemically competent *E. coli* cells, a single colony was used to inoculate 5 ml LB containing the required antibiotics from a LB agar plate streaked from a glycerol stock and incubated overnight at 37°C. 1 ml of the overnight culture was used to inoculate 100 ml LB containing the required antibiotics. The culture was incubated at 37°C, shaking at 220 rpm, until an OD<sub>600</sub> = 0.6 was achieved. The cells were then incubated on ice for 10 min before being harvested by centrifugation at 3,500 × g. The pellets after centrifugation were resuspended in 20 ml of 100 mM calcium chloride (4°C) and incubated on ice for 20 min. Finally, the cells were centrifuged at 3,500 × g, harvested and resuspended in 2.4 ml 100 mM calcium chloride with 20% glycerol. The cells were frozen with liquid nitrogen and stored at - 80°C in aliquots of 50 µl.

### 2.1.5 Transformation

#### Transformation of chemically competent *E. coli*

2 µl of plasmid (~100 ng/µl) was added to 50 µl of competent cells and incubated on ice for 30 min followed by heat shock at 42°C for 30 sec. After heat shock the transformed cells were again incubated on ice for 2 min. 250 µl of LB was added and incubated at 37°C for 1 hr before plating them on the solid medium.

#### Electroporation of *M. smegmatis*

Electrocompetent *M. smegmatis* cells were thawed on ice and 1 µg of plasmid was added. The transformed cells were incubated on ice for 10 min. After the incubation, 200 µl of transformed cells were transferred to a chilled electroporation cuvette. Electroporation was carried out at 1000 Ω resistance, 2.5 kV voltage, and 25 µF capacitance followed by incubation on ice for 10 min. The cells were then transferred to 5 ml 7H9-Tw medium in a sterile universal tube and recovered at 37°C for at least 2 hours. After the incubation, the cells were spun down by centrifugation for 10 min. The sedimented cells were re-suspended in 100 µl 7H9-Tw medium and serially diluted up to 10<sup>-6</sup>. Finally 100 µl of each dilution was plated on 7H10 agar plates and incubated at 37°C for two days.

## 2.2 Molecular biology methods

### 2.2.1 Oligonucleotides

Vector	Forward Primer	Reverse Primer
pET-20gyrB NΔ40	5'ATCGTGCATATGGCTGCCAGAAA AAGAAGG3'	5'AAGCTTCTCGAGGACATCCAGGAA CCGAACATC3'
pSM-128gyrBval	5'AGTACTCAC GTCGATCGGC CCAGAACAAGGCGC3'	5'CCCGGGCACGATCCGAATACTCTC CTCAGGG3'
pSM-128gyrBmeth	5'AGTACTCAC GTCGATCGGC CCAGAACAAGGCGC3'	5'CCCGGGCATCTAACCGCGCCGTGC3 ,

**Table 2.2: PCR primers for generating PCR products that were cloned into vectors.** *Oligonucleotides for gene cloning and for site-directed mutagenesis were supplied by Sigma-genosys.*

Mutant	Forward Primer	Reverse Primer
GyrA-D504A	5' GGCCGACGGAGCCGTCAGCGACG 3'	5' CGTCGCTGACGGCTCCGTCGGCC 3'
GyrA-E514A	5' TTGATCGCCCGCGCGGACGTCGTTGTC 3'	5' GACAACGACGTCCGCGCGGGCGATCAA 3'
GyrA- E508AD509A	5'- GACGTCAGCGACGCGGCTTTGATCGCCCGC-3'	5'- GCGGGCGATCAAAGCCGCGTCGCTGACGTC-3'

**Table 0.1: Oligonucleotides designed in order to introduce mutations into expression plasmid pET20-gyrA (Huang *et al.*, 2006).**

Primers	Sequence
Forward primer (F-1.1)	5' CACGGCGCGGTTAGATGGGTAA3'
Forward primer (F-1.2)	5'TGGGTAAAAACGAGGCCAGAAGATC3'
Forward primer (F-2)	5'CGACTCAACCGCATGCACGCA3'
Forward primer (F-3)	5'CCAGAAAAAGAAGGCCCAAG3'
Reverse primer (R)	5'ATAACCGGCCATCGCCTCGT3'

**Table 2.4: Oligonucleotide for RT-PCR (reverse transcription-polymerase chain reaction).**

### 2.2.2 Preparation of supercoiled and relaxed pBR322\*

Supercoiled and relaxed pBR322\* were used as substrates in the DNA relaxation and supercoiling assays. pBR322\* has a point mutation to increase its copy number. The nucleotide change is G→T point mutation at bp 3074 (Boros *et al.*, 1984). A brief protocol (Sambrook *et al.*, 1989) for the large scale preparation of supercoiled pBR322\* is as follows:

1. 6 × 400 ml super broth cultures containing 50-100 µg/ml ampicillin grown for up to 2 days were centrifuged at 6000 rpm for 10 min in Beckman polycarbonate pots.
2. Pellets from two pots were pooled and resuspended in 48 ml of 1× SOLUTION I (10 × 500 mM glucose, 250 mM Tris pH 7.5, 100 mM EDTA) followed by addition of 12 ml of 10 mg/ml lysozyme.
3. 120 ml of SOLUTION II (0.2 M NaOH, 1% SDS) was added and stirred well after incubation for 10 min at room temperature.
4. The pellets suspended in SOLUTION II were incubated on ice for 10 min and then chilled SOLUTION III was added and stirred well.
5. The pellets suspended in SOLUTION III (0.24 gm/ml sodium acetate, 0.11 gm/ml acetic acid) were incubated on ice for 25 min and then centrifuged at 6000 rpm for 5 min at 4°C.
6. The supernatant was collected in fresh Beckman pots and 150 ml of isopropanol was added. After isopropanol addition, the solution was again centrifuged at 8000 rpm for 5-10 min at 20 °C.
7. The pellets (total 6 pellets) were redissolved in 28 ml TE (10 mM Tris-HCl, pH 7.5 1 mM EDTA) in a pre-weighed 50 ml falcon tube. 1.019 gm of CsCl and 0.11 ml of 10 mg/ml ethidium bromide solution were added per gram of sample. The mixture was pipetted into Sorvall Ultra Crimp tubes up to the neck.
8. The sealed tubes were centrifuged in a StepSaver rotor in a Sorvall Ultra centrifuge overnight at 45000 rpm.

9. Next day, the lower band was taken out with a wide bore needle and was centrifuged overnight in the presence of CsCl and ethidium bromide at 45,000 rpm.
10. Next day, the band was removed and extracted 3-5 times with 25 ml of water-saturated butanol until all ethidium bromide was removed.
11. An equal volume of water and 2 volumes of isopropanol were added and left at room temperature for DNA to precipitate for a minimum of 2 hrs in Corex tubes.
12. The Corex tubes were centrifuged at 7500 rpm for 30 min and ethanol precipitated overnight at - 20°C. Finally the pellet was resuspended in TE and quantitated.

Relaxed pBR was prepared by relaxing the supercoiled DNA using chicken erythrocyte topoisomerase I followed by phenol extraction and ethanol precipitation (Trask & Muller, 1983).

### **2.2.3 Plasmid DNA purification**

Plasmid DNA was purified using the Qiaprep spin miniprep kit (Qiagen) following the manufacturer's recommended protocol.

### **2.2.4 DNA concentration determination**

DNA concentration was determined using a BioPhotometer (Eppendorf) by measuring the  $A_{260}$  of a sample diluted in milli-Q water (1  $\mu$ l sample + 49  $\mu$ l milli-Q water).

## 2.2.5 PCR and cloning

### pET20-gyrBN40Δ cloning

A typical 50 μl PCR reaction mixture to amplify *gyrB40NΔ* consisted of:

Forward primer 10 μM	1.0 μl
Reverse primer 10 μM	1.0 μl
pET20-gyrB (68 ng/μl)	0.5 μl
dNTP ( 1.25 mM)	8.0 μl
Promega Pfu10× buffer	5.0 μl
Promega Pfu (2–3u/μl)	1.0 μl
DMSO (100%)	2.5 μl
Water	31 μl

The details of the oligonucleotide used in the PCR are provided in **section 2.2.1**.

**Table 2.5** shows the thermocycler program used.

The amplified *gyrBN40Δ* was cloned (blunt-end cloning) into TOPO® cloning vector by following the protocol recommended for Invitrogen TOPO® cloning kit. The clone was verified by sequencing and then restriction digested with NdeI and XhoI (New England Biolabs) for cloning the digested *gyrB40NΔ* insert into the NdeI and XhoI digested pET20. The final stage of cloning into pET20 was performed using the Clonable™ Ligation kit (Novagen).

### pSM128-gyrBmeth & pSM128-gyrBval cloning

A typical 20 μl PCR reaction mixture to amplify *gyrB40NΔ* consisted of:

Forward primer 10 μM	1 μl
Reverse primer 10 μM	1 μl
pET20-gyrB (68 ng/μl)	1 μl
dNTP ( 1.25 mM)	3.2 μl
Promega Pfu10× buffer	2.0 μl
Promega Pfu (2–3u/μl)	0.1 μl
DMSO (100%)	2.0 μl
Water	9.7 μl

The details of the oligonucleotide used in the PCR are provided in **section 2.2.1**. **Table 2.5** shows the thermocycler program used.

Step	Temperature (°C)	Time (min)	Description
1	94	2	Denaturation
2	94	1	Denaturation
3	55	1	Primer annealing
4	72	0.25	Extension
5	-	-	Loop to step 2 ( 35 times)
6	72	10	Ensure complete extension

**Table 2.5: Typical thermocycler program used for amplifying sequences for promoter analysis.** *Reactions were carried out using a PTC-200 thermal cycler (MJ Research).*

The PCR amplified products were cloned (blunt-end cloning) into pGMT<sup>®</sup>-Teasy vector (Promega) with primers containing the ScaI sites. Finally the pGMT<sup>®</sup>-Teasy clones containing the inserts were digested with ScaI (New England Biolabs) and sub-cloned into pSM128 vector to generate pSM128-gyrBmeth & pSM128-gyrBval.

### 2.2.6 Site-directed mutagenesis

PCR was used to introduce mutations into DNA through site-directed mutagenesis. The Stratagene QuickChange<sup>®</sup> Lightning kit was used for site-directed mutagenesis. A typical 50 µl reaction contained:

Forward primer 14 $\mu$ M	1 $\mu$ l
Reverse primer 14 $\mu$ M	1 $\mu$ l
pET20-gyrA (185 ng/ $\mu$ l)	0.5 $\mu$ l
dNTP	1 $\mu$ l
10 $\times$ reaction buffer	5.0 $\mu$ l
Quick Solution reagent	1.5 $\mu$ l
Water	40 $\mu$ l

Finally 1  $\mu$ l QuickChange Lightning Enzyme was added to the PCR mix. **Table 2.6** shows a typical thermocycler program used.

Step	Temperature ( $^{\circ}$ C)	Time (min)	Description
1	95	2	Denaturation
2	95	0.3	Denaturation
3	60	0.16	Primer annealing
4	68	0.5 /kb	Extension
5	-	-	Loop to step 2 ( 18 times)
6	68	5	Ensure complete extension

**Table 2.6: Typical thermocycler program used for side-directed mutagenesis.**  
*Reactions were carried out using a PTC-200 thermal cycler (MJ Research).*

Following the PCR, 2  $\mu$ l DpnI provided in the kit was added to the reaction. The reaction was incubated at 37 $^{\circ}$ C for 5 min followed by transformation into *E. coli* TOP 10 cells. The transformed cells were plated out on LB media containing the required antibiotics. Plasmid DNA was isolated from minipreps that were set up from a single colony and were verified by DNA sequencing.

### 2.2.7 RT-PCR (reverse-transcriptase)

The master mix for the PCR included Promega GoTaq PCR master mix and 10% DMSO. The typical thermocycler program that was used for RT-PCR is shown in **Table 2.7**:

Step	Temperature (°C)	Time (min)	Description
1.	94	2	Denaturation
2.	94	0.5	Denaturation
3.	56	0.5	Primer annealing
4.	72	1	Extension
5.	-	-	Loop to step 2 ( 25 times)

**Table 2.7: Typical thermocycler program used for RT-PCR.**

### 2.2.8 Agarose gel electrophoresis

Agarose gel electrophoresis is a routine technique employed in the project for the detection and topological separation of DNA. In most of the cases 1% agarose gels were prepared by dissolving agarose (SIGMA-ALDRICH) in TAE (40 mM Tris-acetate (pH 7.5), 20 mM sodium acetate, 2 mM EDTA) and heating in a microwave. The dissolved agarose was allowed to cool to lukewarm and then poured into a gel mould with an inserted comb. The gel was allowed to set followed by submerging it in a horizontal electrophoresis tank filled with TAE buffer. The DNA samples were prepared by mixing them with an equal volume of 2×STEB (40% sucrose, 100 mM Tris- HCl (pH 8), 1 mM EDTA, and 0.5 µg/ml bromophenol blue). Gels were run at 20-85 V and stained by soaking in TAE buffer containing 2 µg/ml of ethidium bromide (200 µg/ml) for 10 minutes. Destaining was performed for 10 min in TAE buffer containing no ethidium bromide. Processed gels were visualized by ultraviolet transilluminator and photographed using the GeneGenius Bio-imaging system (Syngene).

### 2.2.9 DNA sequencing

DNA sequencing reactions were carried out using the BigDye v3.1 kit (Applied Biosciences). A typical 10  $\mu$ l reaction consisted of:

Sequencing primer (2 $\mu$ M)	1 $\mu$ l
Big dye buffer	1.5 $\mu$ l
Big dye v3.1	1 $\mu$ l
Template DNA (100 ng/ $\mu$ l)	1-2 $\mu$ l
Total	10 $\mu$ l

**Table 2.8** shows a typical thermocycler program used.

Step	Temperature ( $^{\circ}$ C)	Time (min)	Description
1	96	1	Denaturation
2	96	0.5	Denaturation
3	45	0.25	Primer annealing
4	60	4	Extension
5	-	-	Loop to step 2 ( 29 times)

**Table 2.8: Typical thermocycler program used DNA sequencing.**

*Reactions were carried out using a PTC-200 thermal cycler (MJ Research).*

Once the DNA sequencing reaction had been performed, the samples were submitted to the John Innes Genome Laboratory for analysis. Results were generated in the form of text files and .abi chromatogram trace files. Vector NTI was used to analyse the sequencing data.

## 2.3 Protein Methods

### 2.3.1 Purification of *M. tuberculosis* DNA gyrase and mutants

*M. tuberculosis* GyrA and the double (GyrA E508A, D509A) and quadruple mutants (GyrA D504A, E508A, D509A, E514A) were expressed and purified according to the previously published protocol with slight modifications (Huang *et al.*, 2006). The expression plasmids were transformed into *E. coli* BL21 (DE3) pLysS and a 12 ml overnight culture of the cells was used to inoculate each 1 L culture of LB, containing 100 µg/ml ampicillin and 30 µg/ml chloramphenicol. The cells were grown at 37°C to an OD<sub>600</sub> = 0.4 -0.6.

Once the culture had reached the required cell density, protein expression was induced by the addition of isopropyl β-D-1-thiogalactopyranoside (IPTG) to a final concentrations of 0.4 mM and the culture was left shaking for 4 hr at 37°C. The cells were harvested by centrifugation at 7000 rpm for 15 min using a SLC-6000 rotor (Sorvall). The harvested cells were resuspended in Binding Buffer (20 mM Tris-HCl pH 7.9, 500 mM NaCl and 5 mM imidazole).

The cells were lysed by French press and a complete EDTA-free protease-inhibitor cocktail tablet (Roche) was added before thawing the cells. The cell debris was removed by centrifugation at 84,000× g for 60 min. The supernatant was then purified using a HisTrap HP IMAC 5 ml column (Amersham Bioscience, USA) equilibrated with the Binding Buffer. The column was washed initially with Washing Buffer (20 mM Tris-HCl pH 7.9, 500 mM NaCl and 60 mM imidazole). The his-tagged protein was eluted with Elution Buffer (20 mM Tris-HCl pH 7.9, 500 mM NaCl and 500 mM imidazole) with an imidazole gradient from 60 mM to 500 mM. The peak fractions were pooled based on their purity, analysed using SDS-PAGE and then dialysed in Storing Buffer (50 mM Tris-HCl pH 7.9, 30% glycerol and 5 mM dithiothreitol). The protein were concentrated in Amicon Ultra-4 (< 5 ml) columns and then stored at -20°C.

The same protocol was used for purifying GyrB and GyrB N40Δ, except the final concentration of IPTG was 1 mM IPTG during induction.

### 2.3.2 SDS-PAGE

Sodium dodecyl sulphate polyacrylamide gel electrophoresis (SDS-PAGE) was used to separate, identify and check the quality of proteins of different molecular mass. A 12.5% polyacrylamide resolving gel with a 4% polyacrylamide stacking gel was used. The composition of the gel is shown in **Table 2.9**.

Component	Resolving gel	Stacking gel
Polyacrylamide (37.5:1 acrylamide : bis) (Severn Biotech Ltd.)	12.5 %	4.0%
SDS (W/V)	0.1%	0.1%
Tris.HCl (pH 8.8)	375 mM	-
Tris.HCl (pH 6.8)	-	125 mM
(N,N,N',N'-tetramethylethylenediamine (Sigma)	0.1%	0.1%
Ammonium persulphate (Sigma)	0.1%	0.1%

**Table 2.9: Composition of resolving and stacking gels of a 12.5 % SDS-PAGE.**

Samples for SDS-PAGE analysis were prepared by the addition of an equal volume of SAB (0.125 M Tris-HCl pH 6.8, 4% SDS, 20% glycerol, 10%  $\beta$ -mercaptoethanol and 0.002% bromophenol blue) and boiling for 5 min. Then gels were loaded with the samples along with a suitable molecular weight ladder. Gels were run partially submerged in running buffer (25 mM Tris-HCl, 192 mM glycine and 0.1% SDS) at constant voltage of 90 V through the stacking gel and 150 V through the resolving gel. Gels were run using a Mini-Protean II electrophoresis system (Bio-Rad) and stained by soaking in Instant Blue Coomassie stain (Expedeon) for 30 min. Gels were visualised using a GeneGenius Bio-Imaging system (Syngene).

### 2.3.3 Dialysis

Dialysis was carried out overnight in a large volume of buffer (2 L) at 4°C. The use of dialysis equipment varied depending upon the volume of the protein solution:

**10- 500 µl Slide-A-Lyzer MINI Dialysis Units, 10K MWCO (Thermo Scientific)**

**>3 ml SnakeSkin Dialysis Tubing, 10K MWCO (Thermo Scientific)**

Purified proteins were dialysed in Storing Buffer (50 mM Tris-HCl pH 7.9, 30% glycerol and 5 mM dithiothreitol). Where experiments involved EGTA dialysis, protein was dialysed in Storing Buffer containing 1 mM EGTA.

Similarly, for protein refolding experiments, protein was first dialysed in Buffer A (50 mM Tris-HCl pH 7.5, 100 mM KCl, 2 mM DTT, 8 M Guanidine hydrochloride, 1 mM EDTA) at 37°C for 3 hrs. Then the protein was dialysed in Buffer B (50 mM Tris-HCl pH 7.5, 100 mM KCl, 2 mM DTT, 8 M Urea, 1 mM EDTA, 10% glycerol) at 4°C overnight. The next day the protein sample was dialysed in EB buffer (50 mM Tris-HCl pH 7.5, 100 mM KCl, 2 mM DTT, 1 mM EDTA, 10% glycerol) to remove the denaturing agents and for protein refolding. In Chapter 3 where protein samples were refolded in the presence of EGTA, all the three buffers (A, B, EB) had 1 mM EGTA. For this experiment, a big pool of protein was split into two parts, which was then refolded in the presence and absence of 1 mM EGTA as outlined below in the flowchart (**Figure 2.1**). This protocol was a modified version of the protein refolding protocol that was used for recombining DNA gyrase subunits for transactivation experiment (Hockings & Maxwell, 2002).

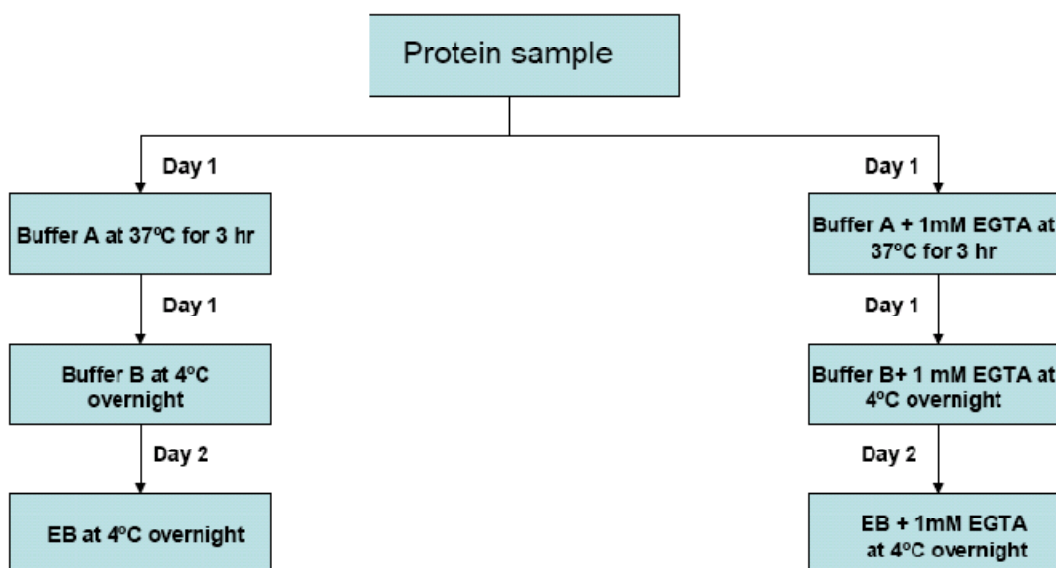


**Figure 2.1: Flowchart for the protein refolding experiment.**

### 2.3.4 Protein concentration

Protein samples were concentrated in Amicon Ultra-4 (< 5 ml) columns with 10-kDa molecular weight cut offs. The protein solution to be concentrated was applied to the reservoir of the concentrator and then centrifuged at 4000 rpm at 4°C until the protein solution had reached the desired volume. In the case of protein samples with a small volume, the samples were concentrated with 10-kDa molecular weight centrifugal concentrators.

### 2.3.5 Protein concentration determination

The protein concentration was determined using the Bradford method (Bradford, 1976). Bradford reagent was prepared by adding 100 mg of Coomassie Brilliant Blue G to 50 ml of 95% (v/v) ethanol plus 100 ml of 85% (v/v) phosphoric acid and made up to one litre with milli-Q water. The reagent was filtered before storing it in a brown bottle covered with a foil. For protein estimation, 2 µl of protein sample was diluted to 100 µl with milli-Q water followed by the addition of 900 µl Bradford reagent. Sample was then incubated at room temperature for 5 min before

taking the absorbance at 595 nm on a BioPhotometer (Eppendorf). The blank solution consisted of 100  $\mu$ l milli-Q water with 900  $\mu$ l Bradford reagent. The protein concentration was determined through a comparison of the absorbance of the protein sample against a calibration curve constructed from BSA standards.

### **2.3.6 Limited Proteolysis**

Limited proteolysis experiments were performed to study the effect of ligands ( $\text{Ca}^{2+}$ , diospyrin) on the digestion profile of DNA gyrase. These experiments reflected conformational changes in the protein induced by the ligand.

6  $\mu$ M GyrA was incubated with 3 mM  $\text{Ca}^{2+}$  at 25°C for 1 hr before incubating it with 1.8  $\mu$ g/ml of trypsin at 37°C in a total reaction mixture of 55  $\mu$ l. 5  $\mu$ l aliquots were collected at different time points (1, 2, 5, 10, 30, 60 and 120 min) and the digestion was stopped by boiling the samples in sample application buffer (SAB). The samples were run on a 12% SDS-PAGE gel to visualise the difference in the digestion profile.

4  $\mu$ M gyrase subunits were incubated with 100  $\mu$ M diospyrin at 25°C for 60 min before incubating it with trypsin at 37°C in a total reaction mixture of 55  $\mu$ l. 5  $\mu$ l aliquots were collected at different time points and the digestion was stopped by boiling the samples in sample application buffer (SAB). The samples were run on a 12% SDS-PAGE gel.

### **2.3.7 Electroblothing & Edman sequencing**

100- 200 pmol of each protein sample was run in triplicates on a NuPAGE 10% Bis-Tris Gels (Invitrogen) and then blotted onto a PVDF membrane using CAPS buffer (10 mM CAPS, pH 11 with or without the inclusion of 10% methanol).

For electroblothing, PVDF membrane was prepared by immersion in HPLC grade methanol for 20 sec followed by equilibration in transfer buffer for 10 min. A gel/ PVDF/ blotting paper sandwich as for Western blotting is prepared and semi-dry blot under 1-3 mA/cm<sup>2</sup> for 45 min-1.5 hr was performed. After blotting, the PVDF membrane was immediately washed with water twice with 10 min shaking. The membrane was stained with 0.1% Coomassie Blue R250 in 50% methanol for 5 min and destained with several changes, 2-5 min each of 30-50% methanol. Finally, the membrane was washed in water and air-dried and stored at -20°C before sending it

for Edman sequencing. The Edman sequencing was done in collaboration with Dr. Mike. A. Weldon at PNAC facility, Dept. of Biochemistry, Cambridge.

N-terminal protein sequencing is achieved by Edman reactions. In this process, the N-terminal amino acid reacts with PITC (phenylisothiocyanate) to form a phenylthiocarbamyl (PTC) protein. The PTC protein is then cleaved with trifluoroacetic acid, resulting in the formation of an intermediate anilinothiazolinone (ATZ). This intermediate is converted to the more stable phenylthiohydantoin (PTH) amino acid derivative and subsequently separated by HPLC. The HPLC fractions are compared against a standard, and identified by the sequencer software.

An essential requirement of this technique is that the protein should be at least 80% pure. It is also important the N-termini of the protein is not blocked. Many proteins may be blocked at the N-terminus by modification during manipulation and purification. Modifications include formyl groups, acetyl groups, and pyroglutamic acid residues acquired during handling steps and exposure to poor quality grade reagents. Depending upon the nature of the modification, some N-terminal blocking groups can be removed with mild acid treatment. Failing this "quick fix" the standard solution is to carry out chemical or enzymatic cleavages followed by HPLC purification.

### **2.3.8 Peptide mass fingerprinting by Orbitrap mass spectrometer**

Peptide mass fingerprinting was performed on a LTQ-Orbitrap<sup>TM</sup> mass spectrometer (Thermo Fisher Scientific Inc) in collaboration with John Innes Centre Proteomics Shared facility.

The sample was in-gel digested with trypsin (Promega) according to the standard procedures and the peptides were extracted with 5% formic acid. Aliquots of the extract were loaded onto a Trap column (C18 PepMap<sup>TM</sup>, Dionex) which was then switched in-line to an analytical column (BEH C18, 1.7  $\mu\text{m}$ , Waters, 75  $\mu\text{m} \times 120 \text{ mm}$ , self-packed). Peptides were separated and eluted with a gradient of 5-40% acetonitrile in water/ 0.1% formic acid at a rate of 1%  $\text{min}^{-1}$ .

The mass spectrometer was operated in positive ion mode at a capillary temperature of 200°C. The source voltage and focusing voltages were tuned for the transmission of MRFA peptide ( $m/z$  524) (Sigma-Aldrich, St. Louis, MO). Data-

dependent analysis was carried out in orbitrap-IT parallel mode using CID fragmentation on the five most abundant ions in each cycle. The collision energy was 35%, an isolation width of 2 was used, and for phosphopeptide analysis multistage activation was enabled. The orbitrap was run with a resolution of 30,000 over the MS range from  $m/z$  350 to  $m/z$  2000 and an MS target of 106 and 1 s maximum scan time. The MS2 was triggered by a minimal signal of 2000 with an AGC target of  $3 \times 10^4$  ions and 150 ms scan time. For selection of 2+ and 3+ charged precursors, charge state and monoisotopic precursor selection was used. Dynamic exclusion was set to 1 count and 30 s exclusion time with an exclusion mass window of  $\pm 20$  ppm. MS scans were saved in profile mode while MSMS scans were saved in centroid mode.

Peaklists from tandem mass spectra were extracted by BioWorks version 3.3.1 (Thermo Fisher Scientific Inc). The resulting peaklist file was used for a database search using Mascot Server 2.2 (Matrix Science, London, UK, in-house) on all bacterial sequences of the SPTrEMBL database (June 2008). Searches were performed with a parent ion mass tolerance of 5.0 ppm and a fragment ion mass tolerance of 0.60 Da. Iodoacetamide derivative of cysteine was specified as a fixed modification, and oxidation of methionine was specified as a variable modification. Trypsin was designated as the protease and up to three missed cleavages were allowed.

### 2.3.9 Circular dichroism

Circular dichroism experiments were carried out in collaboration with Mrs. Fiona Husband (Institute of Food Research, Norwich, UK.).

Circular dichroism is a useful technique for rapid determination of the secondary structure and folding properties of proteins. **Figure 2.2** displays the circular dichroism spectra of different secondary structure elements of protein. The most widely used application of protein CD spectra is to determine whether an expressed, purified protein is folded, or if a mutation has affected its conformation or stability (Greenfield, 2006b). For example in my research project, circular dichroism was used to confirm that the mutations in the putative  $\text{Ca}^{2+}$ -binding site have not misfolded GyrA. The technique relies upon the differential absorption of left-handed

and right-handed circularly polarised light by secondary structure elements (i.e.  $\alpha$ -helix/ $\beta$ -sheet/ $\beta$ -turn). CD has the advantage that measurements can be taken for multiple samples containing  $\leq 20$   $\mu\text{g}$  of proteins in physiological buffers. The limitation of the technique is that it does not provide the residue-specific information that can only be obtained by X-ray crystallography or NMR.

Protein was dialysed in 20 mM HEPES buffer pH 7.5. Far-UV (180-260 nm) CD spectra were recorded at 20°C using a J-715, Rev. 1.00 spectropolarimeter (JASCO Corp.) using a 0.1 mm path length cell. Spectra were the average of 3 accumulations at 100 nm. min<sup>-1</sup> and 0.5 nm resolution.

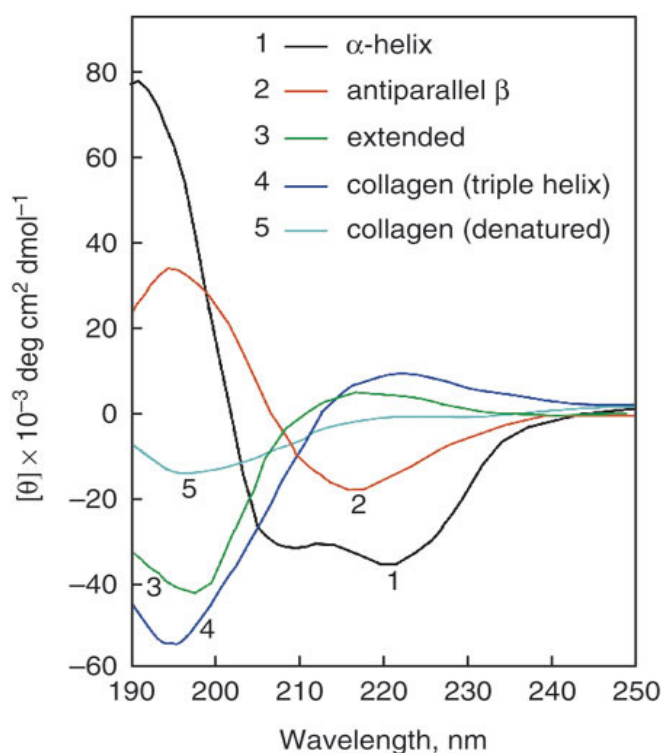


**Figure 2.2: CD spectra of poly-L-lysine at pH 11.1 and placental collagen.** Poly-L-lysine:  $\alpha$ -helical (black), antiparallel  $\beta$ -sheet (red) conformations, extended conformation at pH 5.7 (green). Placental collagen in its native triple-helical (blue) and its denatured form (cyan) (Greenfield, 2006a).

## 2.4 Enzyme assays

### 2.4.1 DNA supercoiling, relaxation, and decatenation assays

A typical supercoiling assay (30  $\mu$ l) containing a range of gyrase concentrations and 0.5  $\mu$ g of relaxed pBR322 in Supercoiling Assay Buffer (40 mM Tris-HCl pH 7.9, 25 mM KCl, 4 mM DTT, 0.1 mg/ml tRNA, 100 mM potassium glutamate, 0.36 mg/ml BSA, 6 mM magnesium acetate, 2 mM spermidine and 1 mM ATP). Reactions were incubated at 37°C for 60 min in a waterbath. After the incubation time, DNA was prepared for electrophoresis by addition of an equal volume of chloroform-isoamylalcohol mixture (24:1), brief vortexing, centrifugation (13,000 rpm for 5 min) and addition of 30  $\mu$ l STEB (40% sucrose, 100 mM Tris-HCl (pH 8), 1 mM EDTA, and 0.5  $\mu$ g/ml bromophenol blue). The products were analysed on a 1% (W/V) agarose gels running at 20 V overnight. The gels were stained with an ethidium bromide solution (2  $\mu$ g/ml).

DNA relaxation assays were performed in a similar way, except they were performed in the absence of ATP and spermidine. The substrate for this reaction was supercoiled pBR322.

A typical decatenation assay (30  $\mu$ l) containing a range of gyrase concentrations and 200 ng kDNA in Decatenation Assay Buffer (40 mM Tris-HCl pH 7.9, 25 mM KCl, 4 mM DTT, 100 mM potassium glutamate, 0.36 mg/ml BSA, 6 mM magnesium acetate and 1 mM ATP). Reactions were incubated at 37°C for 60 min in a water bath, and the DNA was analysed as described above.

### 2.4.2 DNA wrapping assay

For DNA wrapping experiments, the DNA relaxation assay was scaled up to 60  $\mu$ l. After incubation at 37°C for 60 min, the reaction was divided into two halves. The reaction was stopped in one-half with 2  $\times$  STEB and the other half of the reaction was incubated with 2  $\mu$ l of wheat germ topo I (2–10 u/ $\mu$ l) at 37°C for 30 min. The reaction was stopped with 3  $\mu$ l 2% SDS, 0.2  $\mu$ l proteinase K (20 mg/ml) and 2  $\times$  STEB. The DNA was extracted with chloroform: isoamyl alcohol (24:1). The products were analysed on a 1% (W/V) gels running at 20 V overnight and stained with ethidium bromide solution (2  $\mu$ g/ml).

### 2.4.3 Promoter activity assay ( $\beta$ -galactosidase activity assay)

This assay was performed to verify if there are any promoter elements in the region, which code for an additional 40 amino acids at the GyrB N-terminus. This assay provides an advantage for studying mycobacterial promoters as mycobacteria do not naturally produce  $\beta$ -galactosidase and therefore no background enzyme activity is present. The assay is based on the conversion of ortho-nitrophenyl- $\beta$ -D-galactopyranoside (ONPG) to ortho-nitrophenol (ONP) by  $\beta$ -galactosidase, which is only expressed in the presence of an active promoter.

In this method, cell extracts were prepared and the protein concentration was determined. The cell free extracts were prepared by centrifuging liquid cultures at 2500- 3000 $\times$ g for 10 min at room temperature. The pelleted cells were washed with the original culture volume of 10 mM Tris-HCl pH 8 and resuspended in 1 ml of 10 mM Tris-HCl pH 8. The resuspended cells were transferred to a lysing Matrix B tube (Q-BIOGENE) and transferred to a FastPrep™ (Q-BIOGENE). The cells were lysed at a speed 6.0 for 30 sec and centrifuged at 1600 $\times$ g for 5 min. The cell-free extracts were then transferred to a sterile 1.5 ml tube.

For the assay, three Falcon 2054 polystyrene tubes containing 900  $\mu$ l of Z-buffer (60 mM Na<sub>2</sub>HPO<sub>4</sub>, 40 mM Na<sub>2</sub>PO<sub>4</sub>, 10 mM KCl and 1 mM MgSO<sub>4</sub>) were taken. As a negative control 100  $\mu$ l sterile distilled water was added to one of the tubes and to the other two tubes 100  $\mu$ l of two different cell-free extracts were added. The tubes were then incubated for 5 min at 37°C followed by addition of 200  $\mu$ l of ONPG solution to start the reaction. The reaction was then incubated for up to 90 min at 37°C. Finally, 500  $\mu$ l of 1 M NaHCO<sub>3</sub> was added to each tube to stop the reaction. The contents of the tube were emptied into a cuvette and the optical density was measured at 420 nm. Z-buffer was used as blank. The  $\beta$ -galactosidase activity was calculated using the following formula and reported in Miller units:

$$(\text{OD}_{420} \times 1.7) / (t \times v \times p \times 0.0045)$$

Where t = reaction time (min), v = volume of cell free extract (ml) and p = total protein concentration (mg/ml).

## 2.5 Biophysical techniques

### 2.5.1 ICP-AES

ICP-AES (Inductively coupled plasma atomic emission spectroscopy) was used to determine the concentration of divalent ions ( $\text{Mg}^{2+}$  &  $\text{Ca}^{2+}$ ) in the protein sample. ICP-AES experiments were performed in collaboration with Mr. Graham Chilvers (University of East Anglia, UK).

ICP-AES is an analytical technique used for the detection of metals or cations in food, environmental or biological samples. It is a type of emission spectroscopy that uses the inductively coupled plasma to produce excited atoms and ions that emit electromagnetic radiation at wavelengths characteristic of a particular element. The intensity of this emission is indicative of the element within the sample.

The basic principle of the instrument is that when an aerosol of an analyte is passed through argon gas plasma, the matrix is broken down and elements in that plasma are excited. The electrons will jump to higher energy states in order to preserve the equilibrium. As the elements move to a cooler part of the plasma, the electrons will relax back to the ground state, giving off a photon, which is uniquely related to its parent element. There are two types of electron emission used in ICP emission spectroscopy: atomic and ionic emissions. Atomic emissions are electrons that have been excited from the ground state, to relax and emit a photon of characteristic wavelength. Ionic emissions are caused by electrons that have been excited from the atomic orbits into such a higher energy state they are no longer part of that atom and therefore the atom is ionised. Alkaline earth elements (Ca, Mg etc) are easily ionized, so ionic emission wavelengths are most intense, and for non-metals (S, P etc) and metalloids (As, Se, etc) atomic emission wavelengths are the most intense.

The instrument consists of the sample introduction system that transports the analytes of interest to the argon plasma that causes the sample to undergo desolvation and excitation resulting in emission of characteristic radiation. The spectrometer separates the radiation of interest and the detection system measures the intensity of the selected radiation and compares it to the known intensity of analyte standards for quantitative determination (**Figure 2.3**).

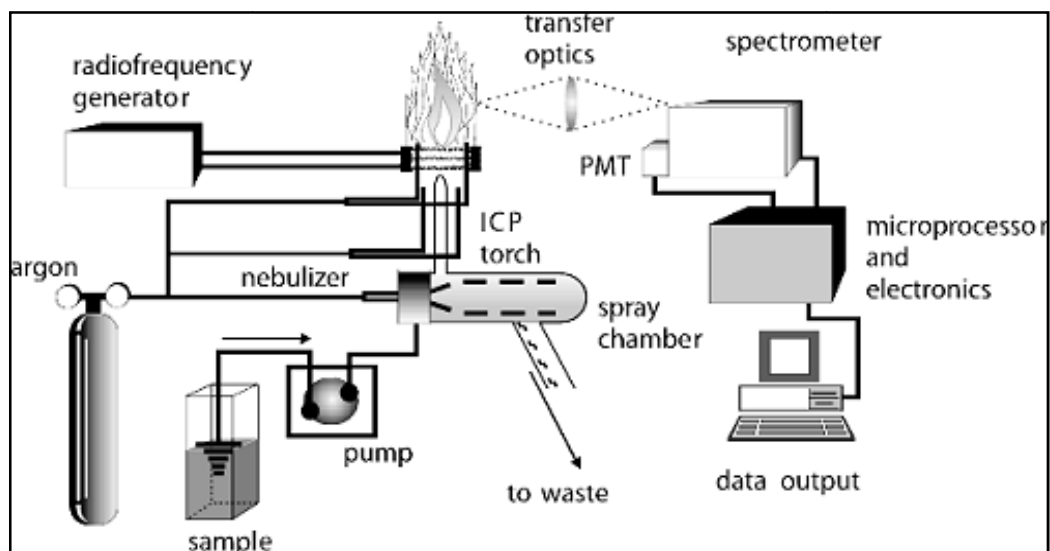


**Figure 2.3: Illustration of ICP-AES for the detection of metals or cations.**  
 (Ref: [http://www.balticuniv.uu.se/environmentalscience/ch12/chapter12\\_g.htm](http://www.balticuniv.uu.se/environmentalscience/ch12/chapter12_g.htm))

The protein samples in the storing buffer with appropriate buffer controls were analysed on Varian Vista Pro ICP-Atomic emission Spectrometer under following settings listed in **Table 2.10**:

<b>Power</b>	<b>1.2 KW</b>
<b>Plasma flow</b>	<b>15.0 L/min</b>
<b>Auxiliary flow</b>	<b>1.5 L/min</b>
<b>Nebulizer flow</b>	<b>1.05 L/min</b>
<b>Reading time</b>	<b>5 sec</b>
<b>Number of replicates</b>	<b>6</b>
<b>Ca<sup>2+</sup>-emission lines</b>	<b>315 and 317 nm</b>
<b>Mg<sup>2+</sup>-emission lines</b>	<b>279 and 280 nm</b>

**Table 2.10: Instrument setting for ICP-AES.**

### 2.5.2 Nano-ESI MS

In our experiments to study diospyrin interactions with different DNA gyrase subunits, nano-ESI MS (nanoflow electrospray ionization mass spectrometry) was used. These experiments were performed in collaboration with Dr. Adam McKay (University College London, UK.).

There is an advantage in using nano-ESI MS over conventional electrospray ionization mass spectrometry (ESI-MS). Conventional ESI-MS is not suitable for studying large non-covalent protein complexes, which can be disrupted due to high curtain gas flow rates and spray heating which are required for the evaporation of the sample droplets. Nanoflow electrospray ionization was initially developed to overcome the limitation of low salt tolerance and large sample volume associated with ESI. The main development of this technique was the use of gold-coated borosilicated capillaries, with tip orifice diameters of around 1-4  $\mu\text{M}$ . This allowed lower flow rates of 20 nl/min for the production of smaller droplets with a diameter of <200 nm, in comparison to standard electrospray ionization which requires flow rates of 1- 10  $\mu\text{l}/\text{min}$  and produces droplets of 10  $\mu\text{m}$  diameter. Due to smaller droplet size high curtain gas flow rates and heating is no longer required for evaporation and this helps to maintain non-covalent complexes. **Figure 2.4** shows a schematic representation of the Electrospray ionisation process.

In this study protein (*M. tuberculosis* GyrA, *M. tuberculosis* GyrB, *E. coli* GyrB43, *E. coli* GyrB47) were buffer exchanged into 250 mM ammonium acetate at pH 7.5 using mini gel filtration columns (Bio-Rad). A 13 mM stock solution of diospyrin was prepared in 100% DMSO. All the drug dilutions were prepared from this stock and added to the protein solution to give a final DMSO concentration of not more than 10%. Gold-coated borosilicate capillaries were used to load 2-3  $\mu\text{l}$  of the protein-drug samples. Ions were generated by nanoflow electrospray ionisation with a capillary voltage of 1.2-1.6 V. Spectra were recorded on a Synapt™ High Definition Mass Spectrometry™ (HDMS™) Q-TOF mass spectrometer (Waters, Manchester, UK) modified for high mass operation. Spectra were externally calibrated using 33 mg/ml cesium iodide.

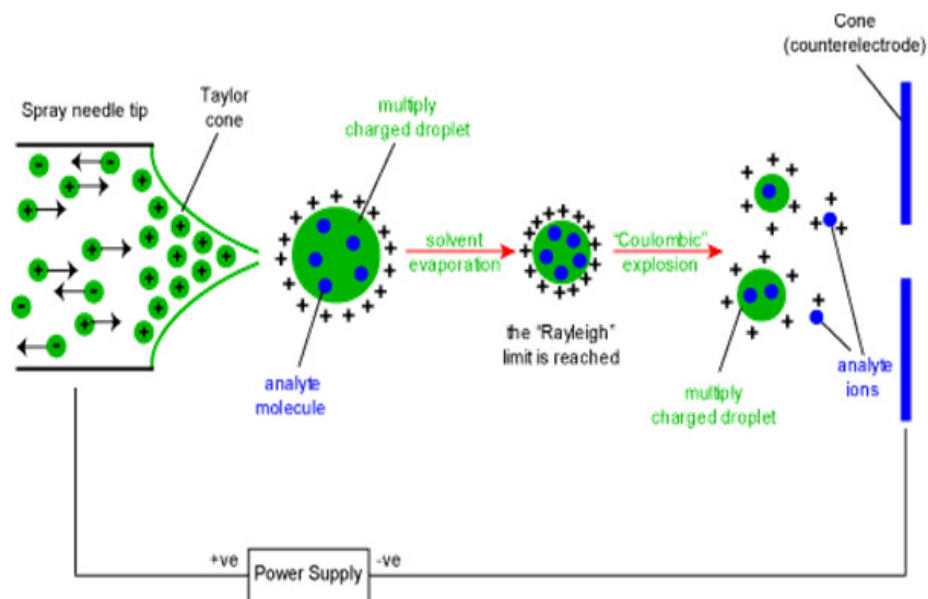


**Figure 2.4: Electro spray ionisation process.**

*An electric field is applied between the capillary and the counter-electrode. The protein solutions emerge from the capillary forming a Taylor cone, which give rise to charged droplets. The charged droplets move along the electric field towards the mass spectrometer and solvent evaporates from the droplets, which leads to fission of charged droplets into naked charge ions, which enter the mass spectrometer. (Ref: <http://www.chm.bris.ac.uk/ms/theory/esi-ionisation.html>).*

### 2.5.3 BIAcore

Surface plasmon resonance (SPR) allows molecular interactions (e.g. protein–protein, protein–small molecule interactions) to be monitored in real-time. The technique involves sample injection over a sensor surface, onto which a potential interacting partner has been immobilised. The interaction between the injected sample and immobilised partner on the sensor chip changes the mass at the surface. This in turn alters the refractive index at the interface between the sensor surface and the solution. The sensogram recorded during these interactions trace the association and dissociation of complexes. This data can also provide kinetic information about the system. SPR was used to analyse the binding of diospyrin to gyrase subunits.

Surface plasmon resonance experiments were performed using a Biacore T100 instrument (Biacore AB, Uppsala, Sweden) at 25°C. Protein was immobilised on a CM5 sensor chip (BIAcore) via amine coupling in immobilisation buffer (10 mM HEPES pH 7.4, 150 mM NaCl, 3.4 mM EDTA and 0.05% P20 surfactant). The immobilisation process included activation of the surface carboxyl groups by injecting 1:1 mixture of N-hydroxysuccinimide (0.1 M) and 1-ethyl-3-(3-dimethylaminopropyl) carbodiimide (0.4 M) across the surface of the chip at 5-10  $\mu$ l/min. Protein dialysed and diluted in 10 mM sodium acetate (pH 4.5) was injected across the surface of the chip until a response of 4000 to 6000 response unit was reached. The active esters were deactivated by injection of 1 M ethanolamine/ HCl pH 8.0.

Kinetic experiments were performed at 25°C in Running Buffer (35 mM Tris-HCl pH 7.5, 24 mM KCl, 4 mM MgCl<sub>2</sub>, 5 mM DTT, 6.5 % glycerol and 0.02% P20 surfactant). The flow rate was set at 30  $\mu$ l/min. Various concentrations of diospyrin prepared in the Running Buffer were injected over the immobilised proteins, and the association phase was observed for 210 s. After the end of the injection, the flow was switched back to drug-free buffer and the dissociation phase was observed for 240 s. At the end of the dissociation phase, the surface was regenerated. Several conditions recommended by the manufacturers were tried. The conditions were either ineffective or they affected the chip surface. The best regeneration condition that could be achieved was with 40 mM NaOH and 0.5% P20 but this affected the chip surface to a certain extent. The data was analysed by BIAevaluation software.

### **2.5.4 Protein crystallography**

Crystallisation trials were carried out by vapour diffusion in a sitting-drop format with 96-well MRC plates (Molecular Dimensions) using a variety of screens such as Hampton Research, Molecular Dimension and Qiagen. A Tecan robot and a nanodrop robot were used to set up crystallisation screens. Drops consisted of 1  $\mu$ l protein solution (with and without drug) and 1  $\mu$ l precipitant solution. Crystallisation screens were usually set up with a protein concentration of 5-10 mg/ml. Screens were stored at 20 °C.

Any hits obtained from the screens were optimised by hanging drop vapour diffusion in a 24 well VDX plates (Molecular Dimensions). Different ratios of protein solution (with and without drug) and reservoir solutions were placed on a plastic coverslip which was then suspended and sealed with vacuum grease over a well containing 1 ml of reservoir solution.

*E. coli* GyrB24 + 1 mM Novobiocin + 1 mM Diospyrin crystals soaked in the cryoprotectant (450  $\mu$ l PEG550 MME (50%) + 100  $\mu$ l 1M MME pH 6.5) were mounted for X-ray data collection using Cryoloops (Hampton Research). X-ray data was collected in-house by mounting crystals on the goniostat and flashcooled to 100 K in a stream of gaseous nitrogen produced by an X-Stream cryocooler (Rigaku-MSD). Diffraction data were collected using a Mar 345 image-plate detector (MarResearch). Initial diffraction images were taken at 0° and 90° to assess the quality of the diffraction and estimate resolution. The diffraction data was processed using software such as MOSFLM (Leslie, 2006), PHRASER (McCoy *et al.*, 2007) and COOT (Emsley & Cowtan, 2004) to check the presence of diospyrin in the diffraction data.

## 2.6 Bioinformatics software

### 2.6.1 Clustal W and MUSCLE

Clustal W is a general purpose multiple sequence alignment program for DNA or proteins. It calculates the best match for the selected sequences, and aligns them so that the identities, similarities and differences between the sequences can be seen. It also generates cladograms or phylograms, which are useful for studying evolutionary relationship between sequences. This information is very useful in designing experiments to test and modify the function of specific proteins and in identifying new members of protein families. Clustal W2 (Larkin *et al.*, 2007) is available from the EBI website.

MUSCLE (Edgar, 2004a, Edgar, 2004b) is another program for creating multiple sequence alignment of amino acids or nucleotide sequences. It is predicted to be faster and more accurate than ClustalW. The algorithm of this tool works by first generating a tree by a method called as *k*-mer clustering based on the number of sub-sequences that two sequences have in common. In the second step, the tree is

used to construct progressive alignment. From the multiple alignments, a pair-wise identity of each pair of sequences is computed. This gives a new distance matrix from which a new tree is estimated and thus it leads to improvement of multiple sequence alignment. The tool uses several iterations of tree and sequence alignment refinement.

### **2.6.2 PSIPRED**

PSIPRED (Jones, 1999) is a protein structure prediction server developed by the Bioinformatics group at UCL Department of Computer Science. It is a server that aggregates several structure prediction methods into one location. Several prediction methods such as PSIPRED v3.0, MEMSAT3 & MEMSAT-SVM, pGenTHREADER and pDOMTHREADER are available as choice for the user. The input single letter amino acid code is submitted via the server and the results are sent via email.

### **2.6.3 PROSITE**

PROSITE (Gasteiger *et al.*, 2003) is a web-based tool available from the ExPASy Proteomics Server. The tool identifies and predicts structural and functional patterns for a protein sequence. These predictions are based on the patterns and profiles specific for more than a thousand protein families and domains stored in the database. Each of these signatures comes with documentation providing background information on the structure and function of these proteins. PROSITE is complemented by ProRule. ProRule is a collection of rules based on profiles and patterns, which provides additional information about functionally and structurally critical amino acids.

### **2.6.4 Phyre and BioInfoBank MetaServer**

Phyre (Kelley & Sternberg, 2009) is a protein homology/analogy recognition server maintained by the bioinformatics group at Imperial College London. Phyre generates models that are produced based on finding a sequence alignment to a known structure, copying the coordinates and relabeling the residues according to the sequence provided by the user. The tool uses profiles generated by PSI-Blast for both the sequence provided by the user and the sequences of the known structures. This enables the tool to detect remotely homologous structures. Phyre performs a profile-profile matching algorithm together with predicted secondary structure matching.

While modelling insertions or deletions, Phyre makes changes to the backbone of the known structure / template.

BioInfoBank MetaServer (Ginalski *et al.*, 2003) is a structure prediction server that provides access to various fold recognition, function prediction and local structure prediction methods. Amino acids are deposited to the sever with a reference name for the job and an e-mail address. All results of fold recognition server are translated into uniform formats and they can be viewed on the web page. The information extracted from the raw output of the servers includes the PDB codes of the hits, the alignment and the similarity scores specific for every server. The Meta Server is coupled to consensus servers that provide jury predictions based on the results collected from other services.

### **2.6.5 Insight II**

Insight II is a comprehensive graphic molecular modelling program from Accelrys. With the aid of other programs such as CHARMM, Insight II can be used to virtually build or manipulate any class of molecule or molecular system. It has several applications such as molecular docking, superimposition, molecular orbital calculations, conformational search using molecular mechanics and dynamics and dynamic simulation. Insight II was used to model *M. tuberculosis* GyrA.

### **2.6.6 AutoDock Vina 1.0.2**

AutoDock Vina is a new open-source program for drug discovery, molecular docking and virtual screening. It has been designed and implemented by Dr. Oleg Trott at The Scripps Research Institute. For its input and output, Vina uses the PDBQT molecular structure file format. PDBQT files can be generated and viewed using MGLTools. It can be run as standalone software on Windows XP, Linux, and Mac operating systems. Several auxiliary software programs such as MGL Tools, PyMOL can be useful in docking and virtual screening with AutoDock Vina. AutoDock Vina was used for virtually screening at the putative Ca<sup>2+</sup>-binding site in GyrA.

### **2.6.7 Discovery Studio 2.5.5**

Discovery Studio is a life science modelling and simulation suite of applications focused on optimizing the drug discovery process from Accelrys. It can be used to investigate and test hypothesis in silico prior to experimental implementation using its life science modelling and simulation tools. The system requirement for the software is Windows 2003 and higher versions, Red Hat<sup>®</sup> Enterprise Linux<sup>®</sup> 4.0 and SUSE<sup>®</sup> Linux Enterprise 10. LibDock protocol is available in Discovery Studio 2.5.5 for virtual docking experiments. The protocol uses protein site features referred to as HotSpots. HotSpots consist of two types: polar and apolar. A polar hotspot is preferred by a polar ligand atom (hydrogen bond donor or acceptor). An apolar atom (a carbon atom) prefers an apolar HotSpot. The receptor HotSpot file is calculated prior to the docking procedure. The rigid ligand poses are placed into the active site and HotSpots are matched as triplets. The poses are pruned and a final optimization step is performed before the poses are scored. Libdock was used for the in-silico docking of diospyrin onto the *M. tuberculosis* GyrB43 model.

## Chapter 3: Unique features of *M. tuberculosis*

### DNA gyrase

Bacterial DNA gyrase is one of the proven targets for antibacterial chemotherapy (Maxwell, 1997). It is a type II DNA topoisomerase found in all bacteria. Most of our current information is related to the enzyme from *E. coli*, a Gram-negative bacterium, with limited information about the DNA gyrase from *Mycobacterium tuberculosis*, a Gram-positive bacterium. Although there is similarity between the DNA gyrase from these two bacteria, there are also key differences, which can be exploited for identifying new drug molecules for tuberculosis. Keeping this in mind, bioinformatics analysis was performed which led to the identification of unique features of *M. tuberculosis* DNA gyrase:

- A. Prediction of the presence of 40 additional amino acids at the GyrB N-terminus.
- B. The presence of a predicted putative Ca<sup>2+</sup>-binding site in *M. tuberculosis* GyrA subunit.

### 3.1 Purification of *M. tuberculosis* DNA gyrase

*Mycobacterium tuberculosis* GyrA and GyrB subunit were over-expressed and purified using the expression plasmids pET20-gyrA and pET20-gyrB (Huang *et al.*, 2006) respectively transformed in BL21 (DE3) pLysS cells as described in the **Materials and Methods** section. On average, 1 mg of purified protein was obtained from a 1 L culture. The molecular weights of purified GyrA and GyrB subunits with C-terminal histidine tags are 93-kDa and 79-kDa respectively. The quality of the purified enzyme was assessed by SDS-PAGE (**Figure 3.1**) and assays were performed to test the enzyme activity. The purified GyrA and GyrB subunits exhibited DNA supercoiling, relaxation and decatenation activity (**Figure 3.2**). The protocol for the expression and purification of the wild-type protein was also used for the expression and purification of GyrB40N $\Delta$  and GyrA proteins with mutation in the Ca<sup>2+</sup>-binding site.

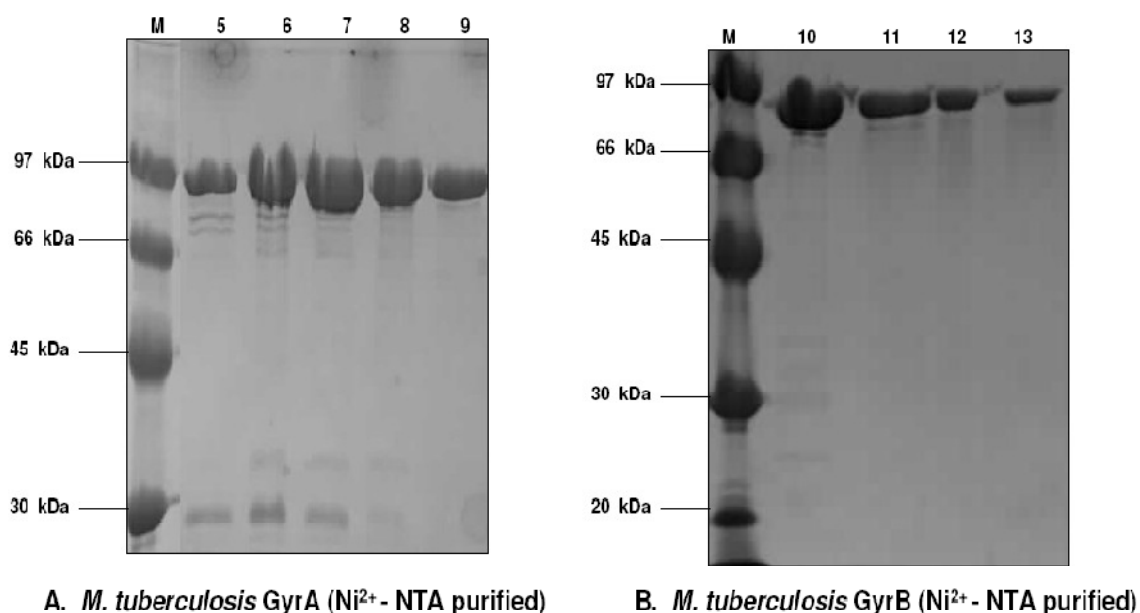


**Figure 3.1:** SDS-PAGE (12%) of DNA gyrase subunits purified by affinity chromatography. The left panel (A) shows different fractions (represented by numbers) of GyrA and the right panel (B) shows different fractions of GyrB purified from a His Trap HP IMAC 5 ml column.

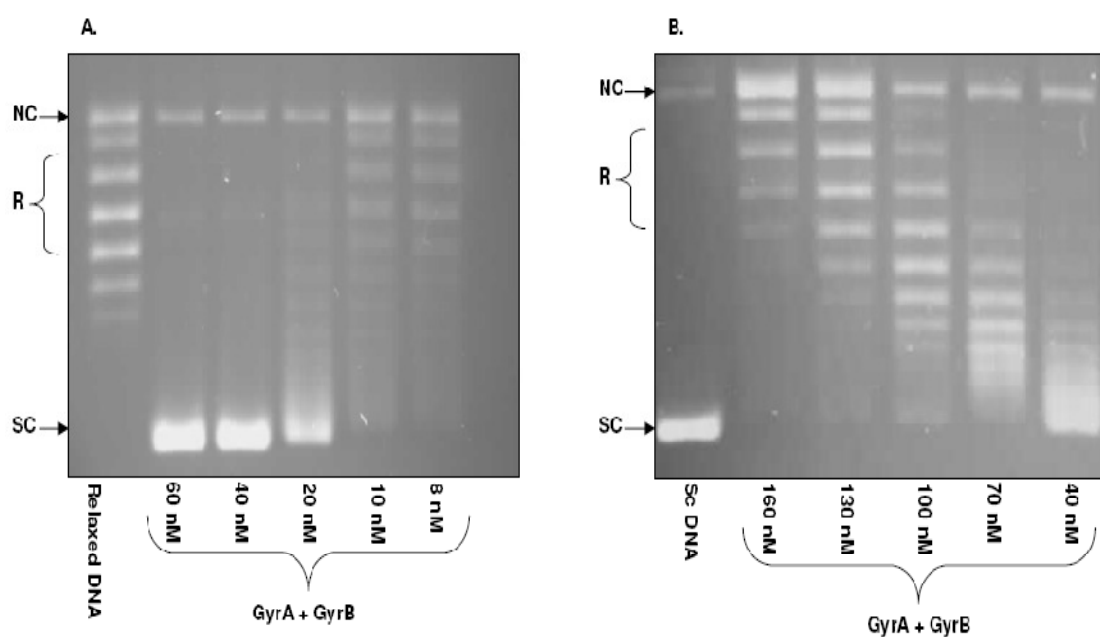


**Figure 3.2: Enzyme activity of purified *M. tuberculosis* DNA gyrase.** The left panel (A) shows the supercoiling activity and the right panel (B) shows the relaxation activity of purified DNA gyrase subunits mixed in equimolar concentration. A range of concentrations of  $A_2B_2$  were incubated with  $0.5 \mu\text{g}$  relaxed pBR322 in the presence of ATP & spermidine for the supercoiling assay (A) and  $0.5 \mu\text{g}$  supercoiled pBR322 in the absence of ATP and spermidine for the relaxation assay. NC: nicked circular DNA, R: relaxed topoisomers, SC: supercoiled DNA.

## 3.2 Bioinformatics analysis of *M. tuberculosis*

### DNA gyrase

Bioinformatics analysis was performed for both the subunits of *M. tuberculosis* DNA gyrase to identify any unique structural features of the enzyme in comparison to other well-studied bacterial DNA gyrase such as *E. coli* DNA gyrase. The first stage of the analysis involved multiple sequence alignment using ClustalW 1.83 followed by advance homology modelling and docking studies.

### 3.3 *M. tuberculosis* GyrB promoter analysis

There are structural differences between the *M. tuberculosis* GyrB and *E. coli* GyrB subunits and these have been investigated. For example, *E. coli* GyrB has a large insertion closer to the carboxy-terminus which is absent in *M. tuberculosis* GyrB (Schoeffler *et al.*, 2010, Madhusudan & Nagaraja, 1995). In order to identify other structural differences, multiple sequence alignment was performed between the *M. tuberculosis* GyrB and other bacterial GyrB sequences using ClustalW 1.83.

The multiple sequence alignment indicated the presence of 40 amino acids at the N-terminus of GyrB subunit as shown in **Figure 3.3**.

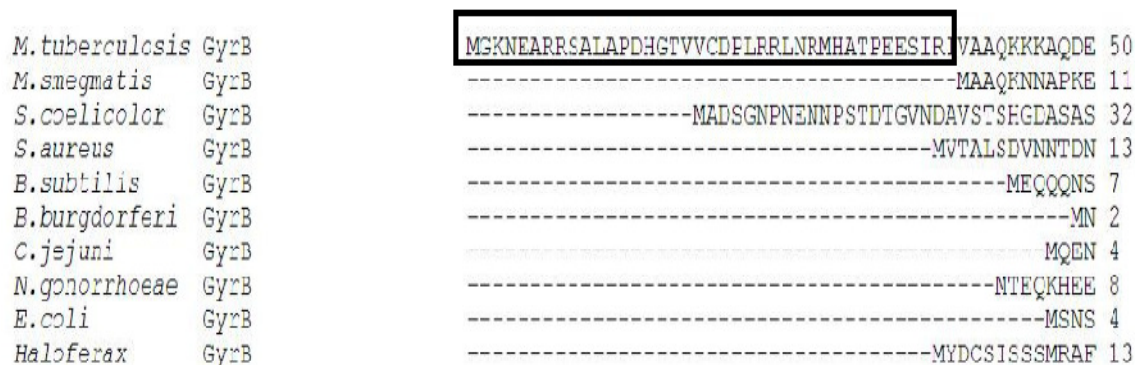


**Figure 3.3: Multiple sequence alignment of bacterial GyrB using ClustalW 1.83 (Larkin *et al.*, 2007).** The 40 additional amino acids at the N-terminus of *M. tuberculosis* GyrB is enclosed in a rectangle.

The N-terminus of GyrB is involved in ATP binding and hydrolysis (Ali *et al.*, 1993). Therefore, it was important to investigate if there is any effect of these additional 40 additional amino acids on the DNA gyrase activity.

Besides this, there is also a discrepancy between the *M. tuberculosis* GyrB sequences retrieved from different databases. For example, in the case of NCBI code CAB02426 for *M. tuberculosis* H37Rv GyrB, the 40 additional amino acids are present in the sequence starting with amino acids *MGKNEARRSA*. While the same protein cross-referenced in UniProtKB/Swiss-Prot as P0C5C5, lacks these additional amino acids and the sequence starts with *MAAQKKKAQD*. But for other *M. tuberculosis* strains, such as *M. tuberculosis* T92 in UniProtKB/Swiss-Prot, the

GyrB sequence (UniProtKB/Swiss-Prot: D5XPA3) has 40 additional amino acids and starts with *MGKNEARRSA*. Similarly, in case of *M. bovis* AF2122/97 both the NCBI (CAD92867) and UniProtKB/Swiss-Prot (Q7U312) indicates the presence of an additional 40 amino acids at the GyrB N-terminus.

Due to these discrepancies in the exact start of GyrB between different sequences and databases, it was important to determine the exact start site of GyrB and if there is any significance of these additional 40 amino acids on the activity of the enzyme. As we know from previous work (Unniraman *et al.*, 2002) on *M. tuberculosis* gyrase, the genes encoding the two subunits are present next to each other in the genome, with *gyrB* upstream of *gyrA*. As a result, the primary transcript is dicistronic and in addition to the principle promoter, there are multiple weaker promoters that appear to fine-tune transcription. Thus in this study it will also be interesting to investigate if there are any promoter elements within these 40 amino acids of *M. tuberculosis* GyrB. The investigation was done at the level of promoter, RNA and protein by promoter analysis, RT-PCR (reverse transcriptase-PCR) and mutation studies respectively. The work on promoter analysis and RT-PCR was done in collaboration with Dr. Amanda Brown and Prof. Tanya Parish (Barts & the London, Queen Mary's School of Medicine and Dentistry, London).

### 3.3.1 RT-PCR for *M. tuberculosis* GyrB transcript

The first stage of the study involved RT-PCR to determine if the transcript includes the sequence corresponding to the additional 40 amino acids on the GyrB N-terminus. Based on the *M. tuberculosis* codon usage (Andersson & Sharp, 1996) and the Shine-Dalgarno consensus sequence (Agarwal *et al.*, 2006), the putative ribosome-binding site (RBS) is probably present in the sequence corresponding to the addition 40 amino acids as shown in the sequence below.

```
.> Intergenomic sequence: 4997- 5243
cac gtcgatcggc ccagaacaag gcgctccggc cccggcctga gagcctcgag gacgaagcgg
atccgatgc cggacgtcgg gacgcaccag gaagaaagat gtccgacgca cggcgcgggt agatg
ggtaa aaacgaggcc agaagatcgg ccctggcgcc cgatcacggt acagtgtgtg gegacccct
gcggcgactc aaccgatgc acgcaacccc tgaggagagt attcggatcg tg
//
```

The putative ribosome-binding site (RBS) is underlined and boldfaced. The promoter elements are only in bold.

The following sets of nested primers were designed for RT-PCR as shown in the **Figure 3.4**:

1. Forward primer (F-1.1): upstream near the start of the region corresponding to the additional 40 amino acids at position 5109 bp.
2. Forward primer (F-1.2): at the start of the region corresponding to the additional 40 amino acids at position 5123 bp.
3. Forward primer (F-2): in the middle of the region corresponding to the 40 amino acids at position 5195 bp.
4. Forward primer (F-3): 5 bp after at the end of 40 amino acids at position 5247 bp.
5. Reverse primer (R): at position 5433 bp.

The sequence of the primers and the RT-PCR conditions are described in the **Materials and Methods** section. Before performing RT-PCR, RNA prepared from the crude extract of *M. tuberculosis* cells was divided into two batches for making cDNA. In one of the batch reaction mixture 1  $\mu$ l of Superscript II reverse transcriptase was added (cDNA+RT). The other batch included all of the components apart from reverse transcriptase (cDNA-RT). cDNA-RT acts as a control to show that the product amplified in the cDNA+RT is due to RNA reverse transcribed from cDNA rather than genomic DNA contamination. Another control without the template was included to show that there is no DNA contamination and a control to show that the PCR is working.

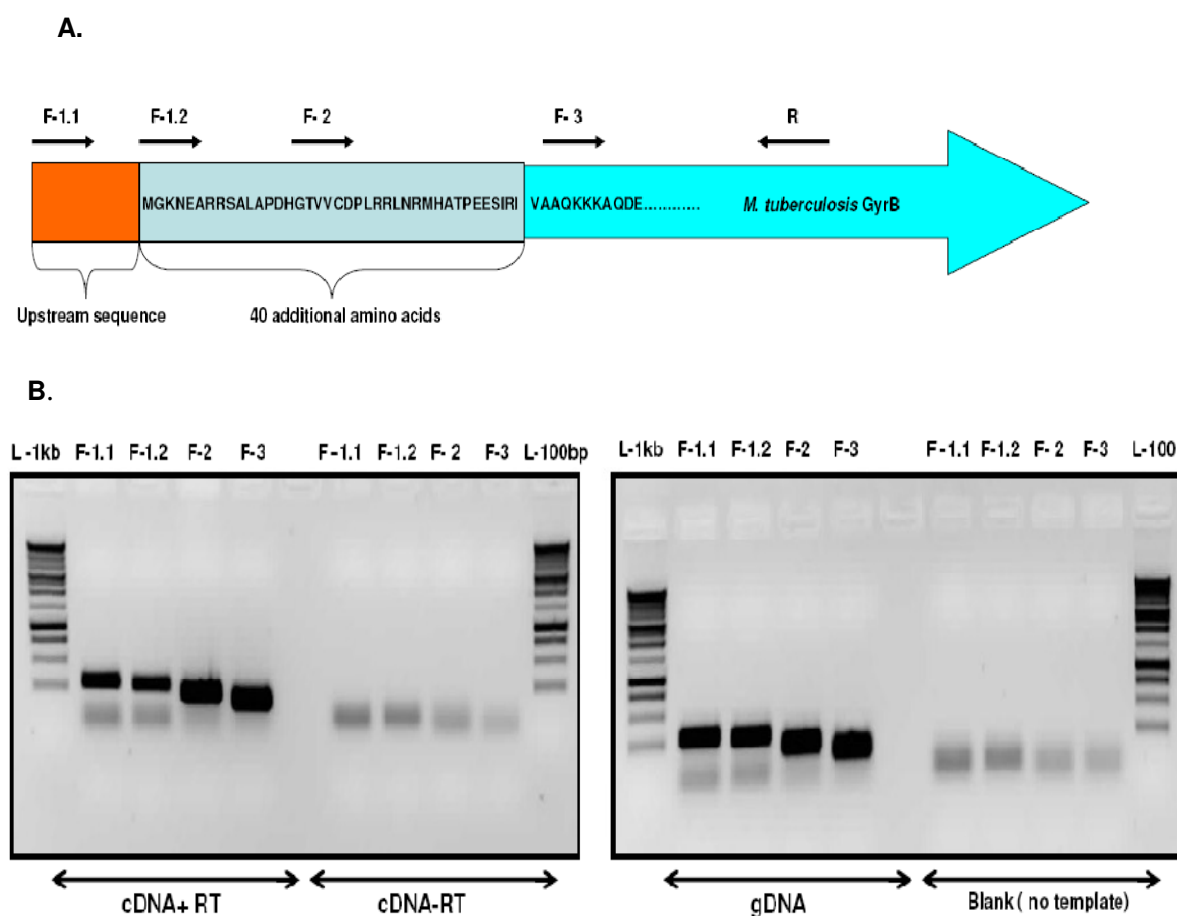


**Figure 3.4: RT- PCR for *M. tuberculosis* GyrB transcripts.** (A)Cartoon representation of the position of RT-PCR primers. (B)The RT-PCR products obtained with different primers (F-1.1, F-1.2, F-2, F-3, and R). cDNA+RT are the test samples with the template cDNA and reverse transcriptase. cDNA-RT lacks reverse transcriptase; gDNA (genomic DNA) is a positive control; blank contains all the ingredients except template to show that there is no DNA contamination. L-1 kb: Promega- cat # G5711 DNA ladder.

As shown in the **Figure 3.4**, PCR products are obtained with all the primers (F-1.1, F-1.2, F-2, F-3) both including and excluding the 40 bp region; although the bands obtained with F-1.1, F-1.2 are weaker than the bands due to the other two primers. No PCR products are present in the cDNA-RT control, which shows that the bands in cDNA+RT are due to PCR products of cDNA. The gDNA control clearly demonstrates that the PCR conditions were optimal and the blank control shows that

there is no DNA contamination in the starting material. The bands in the blank and cDNA-RT may be due to primer-dimer.

This RT-PCR experiment clearly demonstrates that the region corresponding to the 40 amino acids is also expressed in the transcripts (F-1.2, F-2). This was also verified by sequencing the RT-PCR products.

### 3.3.2 Mass spectrometric analysis

After verifying that there are some species of transcript that code for the additional 40 amino acids, the next step of the investigation was to identify if these additional amino acids are present in the protein. Due to safety, issues and the amount of protein required for N-terminal sequencing it was not possible to isolate or over-express native GyrB from the crude extract of *M. tuberculosis* cells. However, it was feasible to verify if these 40 amino acids are present in heterologous expression of the protein in *E. coli* before generating a deletion mutant. The deletion mutant was generated to see if there is any effect of this mutation on the enzyme activity.

The GyrB band from an SDS-PAGE was submitted to the John Innes Proteomics facility for Orbitrap analysis. As shown in the **Figure 3.5**, the mass spectrometric analysis indicates that the 40 additional amino acids are present in the *M. tuberculosis* GyrB over-expressed in *E. coli*. We expect the presence of 40 additional amino acids in the over-expressed *M. tuberculosis* GyrB because the pET20 vector has its own ribosomal-binding site (RBS). This experiment only confirmed the expression of 40 additional amino acids.

```

1  MGKNEARRSA LAPDHGTVVC DPLRRLNRMH ATPEESIRIV AAQKKAQDE
51  YGAASITILE GLEAVRKRPG MYIGSTGERG LHHLIWEVVD NAVDEAMAGY
101 ATTVNVVLE DGGVEVADDG RGIPVATHAS GIPTVDVVMT QLHAGGKFDG
151 DAYAISGLH GVGVSVVAL STRLEVEIKR DGYEWSQVYE KSEPLGLKQG
201 APTKKTGSTV RFWADPAVFE TTEYDFETVA RRLQEMAFIN KGLTINLTDE
251 RVTQDEVVDE VVSDVAEAPK SASERAAEST APHKVKSRTF HYPGGLVDFV
301 KHINRTKNAI HSSIVDFSGK GTGHEVEIAM QWNAGYSESV HTFANTINTH
351 EGGTHEEGFR SALTSVVNKY AKDRKLLKDK DPNLGTGDDIR EGLAAVISVK
401 VSEPQFEGQT KTKLGNTEVK SFVQKVCNEQ LTHWFEANPT DSKVVVNKAV
451 SSAQARIAAR KARELVRRKS ATDIGGLPGK LADCRSTDPR KSELYVVEGD
501 SAGGSAKSGR DSMFQAILPL RGKIINVEKA RIDRVLKNTQ VQAIITALGT
551 GIHDEFDIGK LRYHKIVLMA DADVDGQHIS TLLLTLLFRF MRPLIENGHV
601 FLAQPPLYKL KWQRSDPEFA YSDRERDGLL EAGLKAGKKI NKEDGIQRYK
651 GLGEMDAKEL WETTMDFSVR VLRQVTLDDA AAADLFSIL MGEDVDARRS
701 FITRNAKDVR FLDV

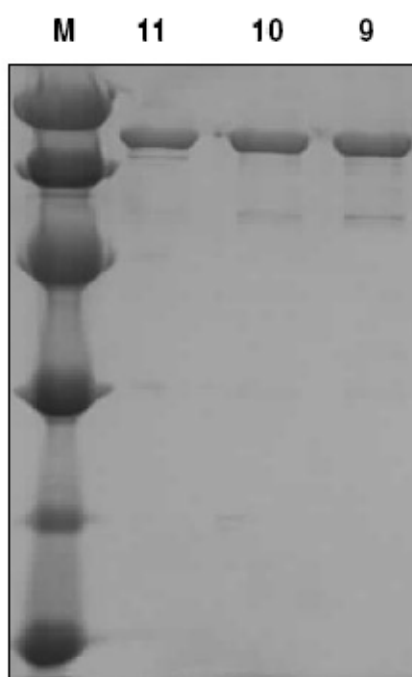
```

Start - End	Observed	Mr (expt)	Mr (calc)	ppm	Miss	Sequence
9 - 24	854.43	1706.84	1706.84	0	0	R.SALAPDHGTVVCDPLR.R ( <a href="#">Ions score 79</a> )
9 - 24	569.95	1706.84	1706.84	1	0	R.SALAPDHGTVVCDPLR.R ( <a href="#">Ions score 39</a> )
9 - 25	621.99	1862.94	1862.94	-1	1	R.SALAPDHGTVVCDPLR.L ( <a href="#">Ions score 23</a> )
29 - 38	585.78	1169.55	1169.55	1	0	R.MHATPEESIR.I ( <a href="#">Ions score 16</a> )
29 - 38	585.78	1169.55	1169.55	1	0	R.MHATPEESIR.I ( <a href="#">Ions score 15</a> )
39 - 44	315.20	628.39	628.39	1	0	R.IVAAQK.K ( <a href="#">Ions score 6</a> )

**Figure 3.5: Orbitrap analysis of *M. tuberculosis* GyrB over-expressed in *E. coli* BL21 indicates the presence of 40 additional amino acids (enclosed in the rectangle). Observed peptides are indicated in red.**

### 3.3.3 GyrB N40 $\Delta$ deletion mutant

The GyrB N40 $\Delta$  deletion mutant was constructed using PCR by amplifying the GyrB sequence excluding the region coding for the additional 40 amino acids, and the amplified PCR product was cloned into pET-20 as described in the **Materials and Methods** section. The plasmid referred as pET-20- GyrB N40 $\Delta$  was verified by big dye sequencing and the deletion mutant was expressed in *E. coli* BL21 (DE3) pLysS. Since the protein was his-tagged, it was purified by affinity chromatography (HisTrap HP IMAC 5 ml columns). The protein was also further purified by gel filtration (Superdex 200 pg; 16/60) for setting up crystallisation screens as shown in **Figure 3.6**.



```

GyrBN40Δ (1)  -----GCTGCCAGAAAAAGAAGG'
Sequence data (51) TACATATG GCTGCCAGAAAAAGAAGG'

```

**Figure 3.6:** Different fractions of GyrBN40 $\Delta$  deletion mutant purified by HisTrap HP IMAC 5 ml and Superdex 200 pg; 16/60 column. The alignment of sequencing data from the start of the sequence in pET-20-GyrBN40 $\Delta$  (bottom) and GyrBN40 $\Delta$  sequence (top) is shown. The sequence does not start with the codon ATG as in pET-20- GyrB. The unshaded part of the sequence data is the vector sequence.

The supercoiling, relaxation and decatenation activity of the purified GyrB N40 $\Delta$  deletion mutant was compared with GyrB WT. As shown in the **Figure 3.7** & **Figure 3.8**, there was no effect of the deletion on the activity of the enzyme. This demonstrates that the presence or absence of 40 amino acids at the N-terminus of *M. tuberculosis* GyrB has no effect on the enzyme activity.

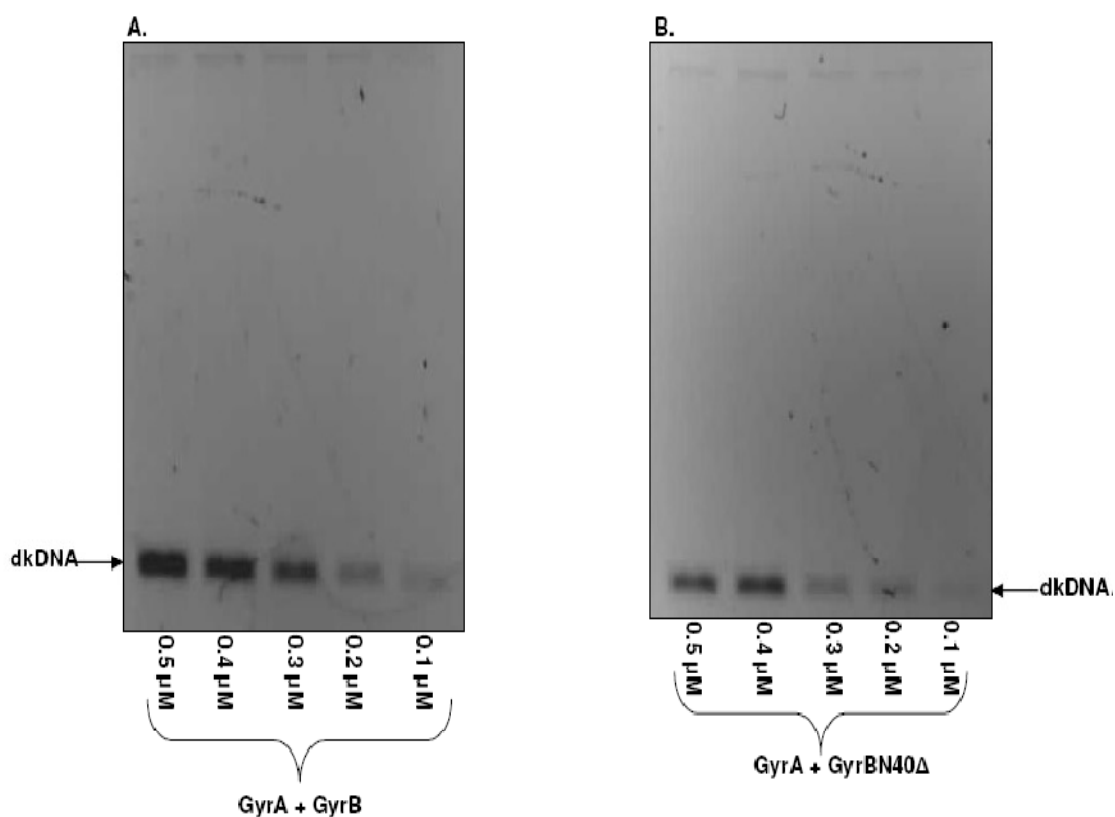


**Figure 3.7: Effect of GyrBN40 $\Delta$  on the decatenation activity of *M. tuberculosis* DNA gyrase.** *There is no difference between the decatenation activity of the GyrB WT (A) and GyrB N40 $\Delta$  mutant (B). The assay was done at a range of concentrations of DNA gyrase. kDNA is trapped in the gel well, while dkDNA (decatenated minicircles) migrates faster than kDNA as indicated by the bands in the picture.*

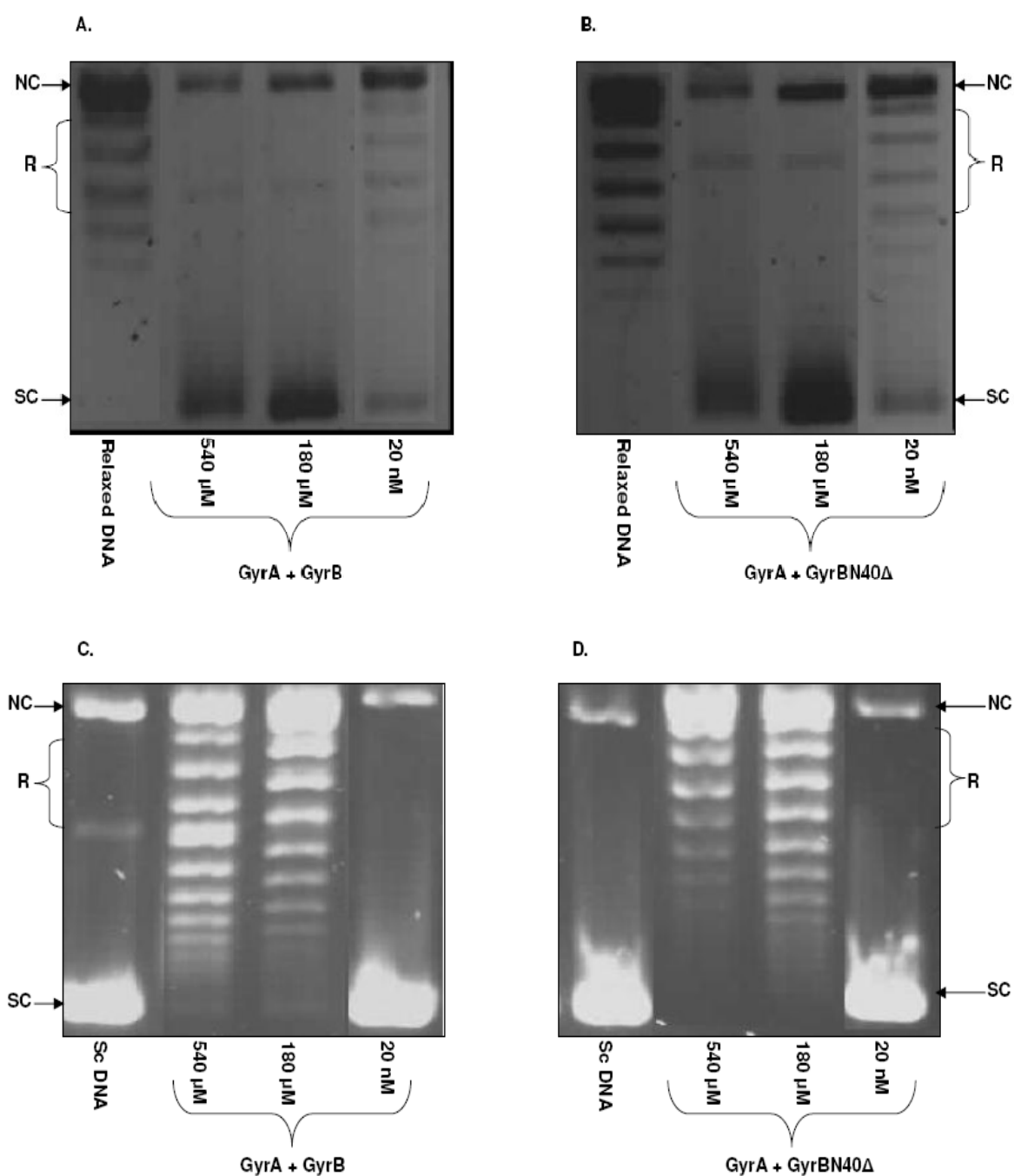


**Figure 3.8: Effect of GyrB N40A on the supercoiling and relaxation activity of *M. tuberculosis* DNA gyrase.** There is little or no difference between the supercoiling (A & B) and relaxation activity (C & D) of the GyrB WT and GyrB N40Δ mutant. NC: nicked circular DNA, R: relaxed topoisomers, SC: supercoiled DNA.

### 3.3.4 Promoter analysis

Based on the above observations, it seems that there is no functional significance to the 40 amino acids at the N-terminus of GyrB, but at the transcriptome level two RNA species with and without the region expressing the 40 amino acids are found. Due to experimental limitations, investigation into the native GyrB from *M. tuberculosis* was not possible. The question therefore still exists what is the significance of the sequence encoding these additional amino acids and should they be included in the sequence for GyrB? In previous work (Unniraman *et al.*, 2002) on *M. tuberculosis* DNA gyrase promoters, putative promoter elements referred to as  $P_{B1}$  are predicted to be located upstream of the *gyrB* gene in addition to several other promoters that appear to fine-tune transcription. Interestingly these promoter elements were predicted to lie in the same region as that coding for the additional 40 amino acids, as shown in the **Figure 3.9**.

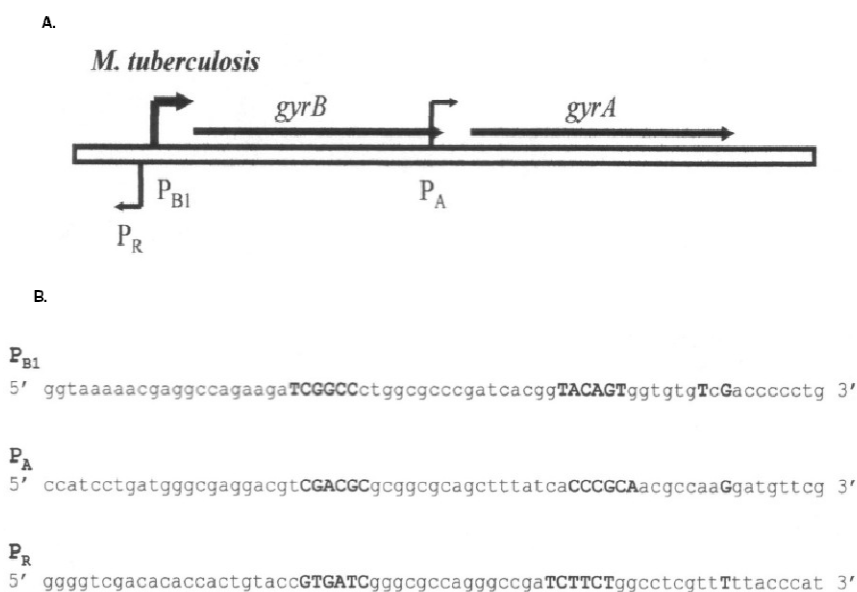


**Figure 3.9: Promoters of *M. tuberculosis* DNA gyrase.** (A) The relative position of different promoters with respect to *gyrB* and *gyrA* genes.  $P_{B1}$  is predicted to be the primary *gyr* promoter, while  $P_A$  and  $P_R$  are weak promoter elements and have been predicted to be regulatory in function. (B) Sequence of the putative promoter elements. Promoter elements of  $P_{B1}$  that are present in the region coding 40 amino acids at the N-terminus are indicated in bold (Unniraman *et al.*, 2002).

$P_{B1}$  shows extensive conservation with  $P_{gyr}$ , the promoter driving the *gyr* genes of *M. smegmatis*, indicating that they are evolutionarily related. The other promoters are weak and may have a regulatory role; for example  $P_A$ , located upstream of *gyrA* gene is weaker than  $P_{B1}$ .  $P_R$  overlaps  $P_{B1}$  and its function is also regulatory. When this sequence was analysed by Artemis software (Rutherford *et al.*, 2000), *TCGGCC* and *TACAGT* were identified as the -35 and -10 sequences as shown in **Figure 3.10**. The result was the same as predicted before (Unniraman *et al.*, 2002).

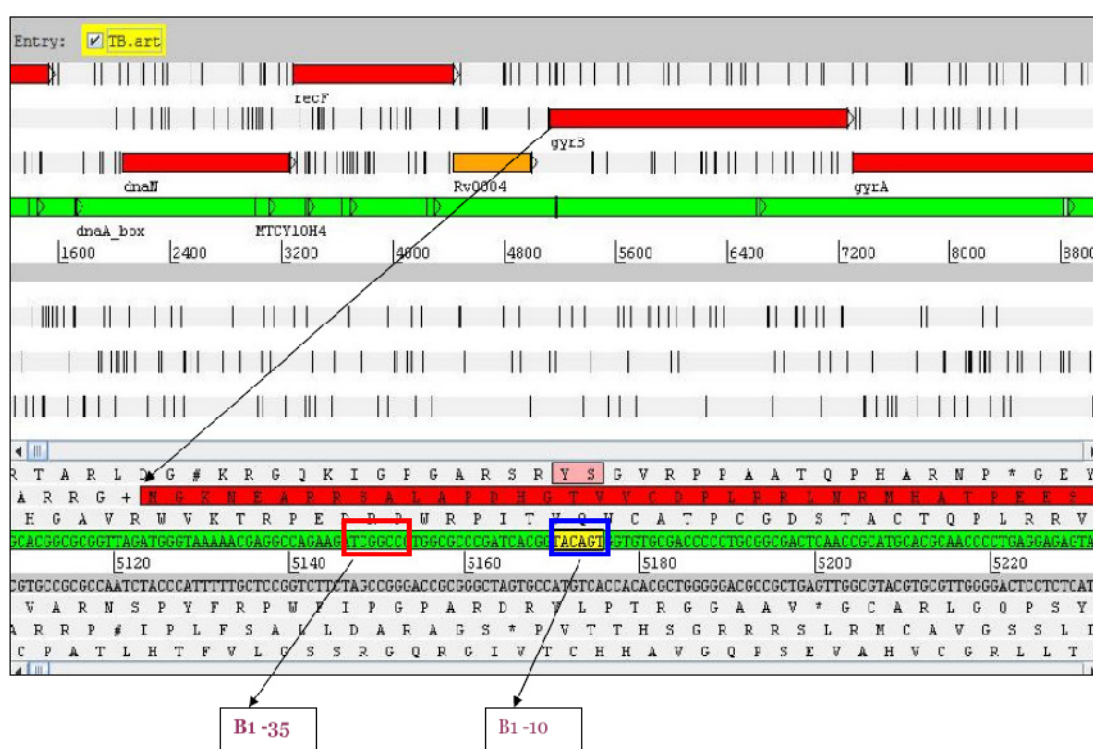


**Figure 3.10:** Screen capture of Artemis analysis of *gyr* promoter elements (-35 and -10) (<http://www.sanger.ac.uk/resources/software/artemis/>). As indicated by arrows the promoter elements are present in the region encoding the predicted 40 amino acids at the N-terminus of GyrB.

Therefore, it was decided to do promoter analysis using the vector pSM128. pSM128 is a promoter-less lacZ fusion vector that is routinely used for the analysis of mycobacterial promoters (Jain *et al.*, 2005, Haydel *et al.*, 2002, Parish *et al.*, 2001) and also been used to conduct rapid antimycobacterial drug screening (Srivastava *et*

*al.*, 1997) and screen for potential vaccine strains (Kumar *et al.*, 1998). Any sequences that are predicted to have promoter elements can be cloned into pSM128 and analysed for promoter activity. This system provides an advantage for studying mycobacterial promoters as mycobacterium do not naturally produce  $\beta$ -galactosidase and therefore no background enzyme activity is present.

The following two plasmids were generated for the analysis:

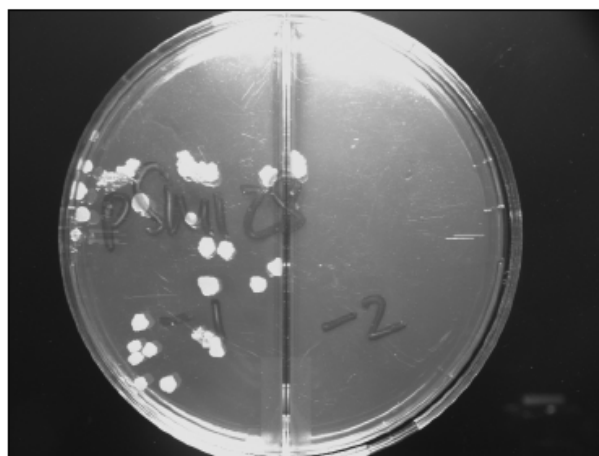
1. pSM-128-Met: cloning 125 bp upstream of the predicted start site (4997-5125 bp; Met (**atg**) into pSM128. The sequence cloned into the plasmid is as follows:

```
> Met: 4997-5125 bp
cac gtcgatcggc ccagaacaag gcgctccggt cccggcctga gagcctcgag gacgaagcgg
atccgatgc cggacgtcgg gacgcaccag gaagaaagat gtccgacgca cggcgcgggt ag atg
//
```

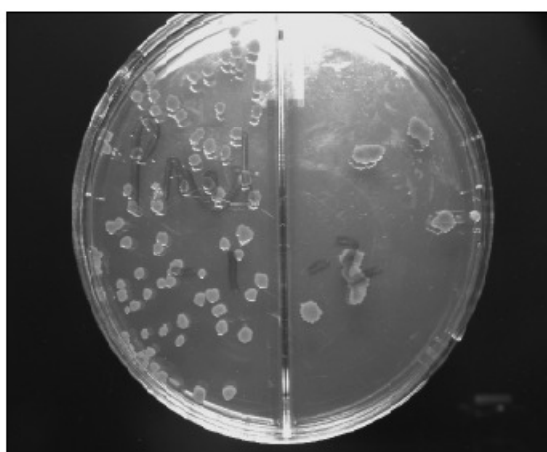
2. pSM-128-Val: cloning the region from pSM-128-Met till the end of 40 amino acids ending with Val (**gtg**) into pSM128. The sequence cloned into the plasmid is as follows:

```
.> Intergenomic sequence Val: 4997- 5243
cac gtcgatcggc ccagaacaag gcgctccggt cccggcctga gagcctcgag gacgaagcgg
atccgatgc cggacgtcgg gacgcaccag gaagaaagat gtccgacgca cggcgcgggt agatg
ggtaa aaacgaggcc agaagatcgg ccctggcgcc cgtcacggt acagtgggtg gcgaccctt
gcggcgactc aaccgcatgc acgcaacccc tgaggagagt attcggatcg tg
//
```

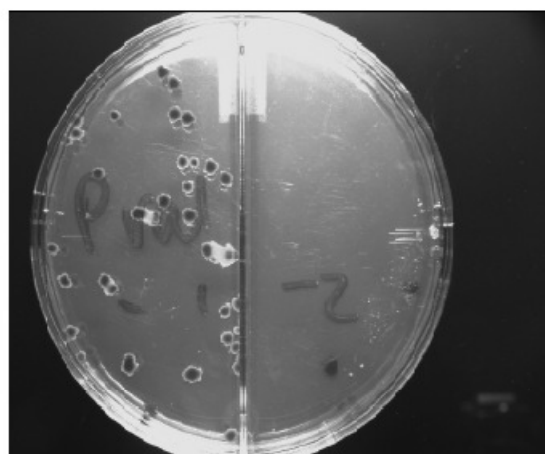
These plasmids were then transformed into *M. smegmatis* mc<sup>2</sup>-155 by electroporation. The crude extract of the transformed cells was used to assay the promoter activity by recording the formation a soluble yellow product at 410 nm. This product is formed by conversion of the substrate nitrophenyl- $\beta$ -D-galactopyranoside (ONPG) to o-nitrophenol (ONP) by  $\beta$ -galactosidase. The detailed procedure for the assay is provided in the **Materials and Methods**.



A. *M. smegmatis* transformed with pSM128



B. *M. smegmatis* transformed with pSM128-Met



C. *M. smegmatis* transformed with pSM128-Val

**Figure 3.11:** Colonies of *M. smegmatis* mc<sup>2</sup>-155 obtained by transformation of the cells with pSM-128, pSM-128-Met and pSM-128-Val plasmids. The colonies transformed with pSM-128 (A), with pSM-128-Met (B) and and pSM-128-Val (C) are colourless, light blue and dark blue respectively.

*M. smegmatis* mc<sup>2</sup>-155 containing pSM-128-Val gave blue colonies in comparison to colonies transformed with pSM-128-Met, as shown in the **Figure 3.11**. This indicated the possibility of promoter activity with pSM-128-Val. The crude extract from the transformed cells were assayed for active promoter activity by recording the formation a soluble yellow product, o-nitrophenol (ONP) at 410 nm. As expected, the results (**Figure 3.12**) of the assay using cell crude extracts showed at least 10 times more  $\beta$ -galactosidase activity with pSM-128-Val in comparison to pSM-128-Met. The background activity in the crude extract of pSM-128 transformants was low in comparison to pSM-128-Met transformants.

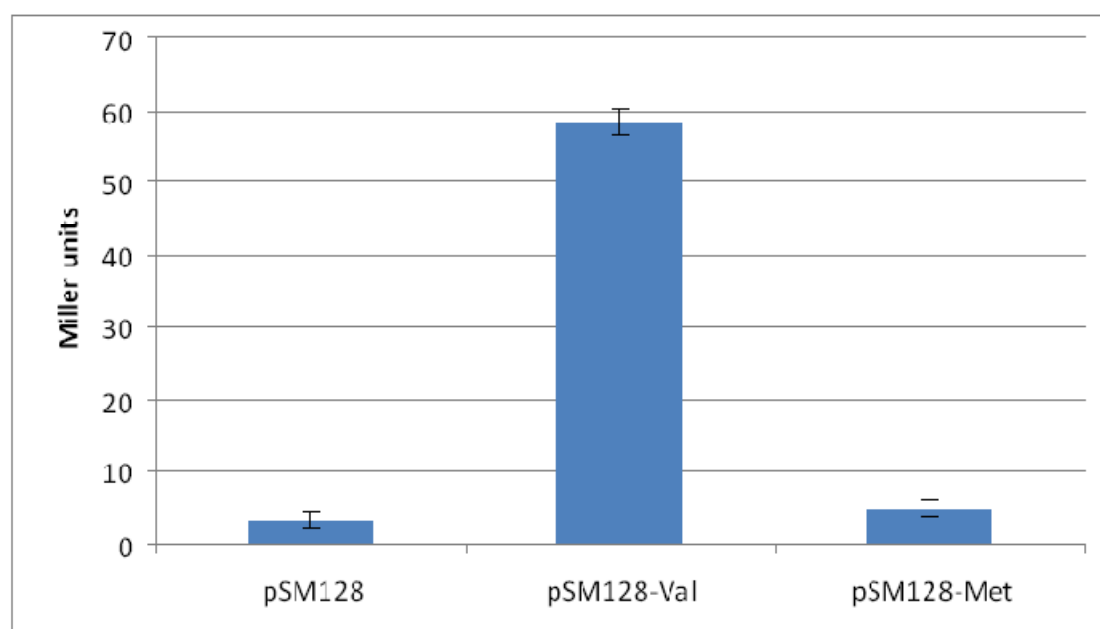


**Figure 3.12:**  $\beta$ -galactosidase activity recorded from the crude extract of *M. smegmatis* mc<sup>2</sup>-155 cells transformed with pSM-128, pSM-128-Val and pSM-128-Met respectively.  $\beta$ -galactosidase activity will only be observed in the crude extracts of the cells transformed with pSM-128 plasmid having active promoter elements.  $\beta$ -galactosidase expression regulated by the active promoter leads to formation of a soluble yellow product o-nitrophenol (ONP) from nitrophenyl- $\beta$ -D-galactopyranoside (ONPG). The activity was recorded on a spectrometer at 410 nm.

Thus, these experiments further confirm the prediction of the presence of promoter elements in the region corresponding to the predicted 40 amino acids at the GyrB N-terminus. The data indicate that the real start codon for *M. tuberculosis* GyrB is GTG (Val). This is the first report that demonstrates that the additional 40 amino acids at the GyrB N-terminus, recorded by several databases such as NCBI and UniProtKB/Swiss-Prot does not have a functional significance and it may be an annotation discrepancy. At present, I have not been able to identify the reason for the existence of two transcript species. Future work in identifying the regulation and coordination of multiple promoters and primary promoter may provide clue. At present, we are limited by the little information we have about the transcription and translation of *M. tuberculosis* DNA gyrase gene in-vivo. These studies in future will be helpful for answering basic questions about mycobacterial growth and metabolism that will have impact on designing effective drugs for TB.

### 3.4 A putative Ca<sup>2+</sup>-binding site in DNA gyrase

*M. tuberculosis* is very different in its physiology and lifestyle from the well-studied model organism *E. coli*. These differences also exist in terms of their topoisomerases. Topo IV (a type II topoisomerase) is absent in *M. tuberculosis* unlike *E. coli* (Aubry *et al.*, 2004). *M. tuberculosis* DNA gyrase is also efficient in relaxation and decatenation activity in comparison to *E. coli* gyrase. It is logical to attribute the efficient relaxation and decatenation of *M. tuberculosis* DNA gyrase to the absence of topo IV (**Figure 3.13**). This led to the investigation of differences between *M. tuberculosis* DNA gyrase and other bacterial DNA gyrase at the sequence level.

Multiple sequence alignment was performed for *M. tuberculosis* GyrA and other bacterial GyrA using ClustalW 1.83 default parameters (Larkin *et al.*, 2007). As shown in the multiple sequence alignment (**Figure 3.14**), there is a characteristic Ca<sup>2+</sup>-binding sequence in *M. tuberculosis* GyrA: 504DVSDEDIAREDV516.

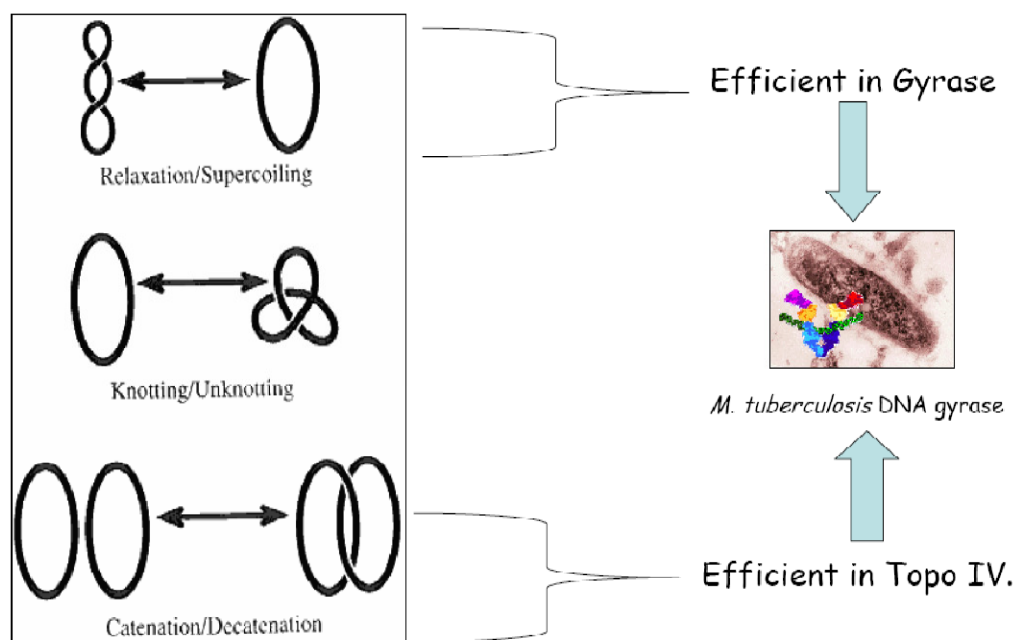


**Figure 3.13: DNA gyrase is the only type II topoisomerase in *M. tuberculosis*, and is efficient in supercoiling, relaxation and decatenation.**

<u><i>M. tuberculosis</i> GyrA</u>	AKIEAEIADLEDILAKPERQRGIVRDELAEIVDRHGDDRTRTRIIAAD-GD 504
<u><i>M. smegmatis</i> GyrA</u>	AKIEAEIADLEDILAKPERQRGIVRDELKEIVDKHGDARTRTRIVPAD-GE 505
<u><i>S. coelicolor</i> GyrA</u>	DELQAKITEYNEILASPVRQRGIVSEELTALVEKYGDDRRTKLIPIYE-GD 501
<u><i>N. gonorrhoeae</i> GyrA</u>	KNLMGKIIDFVDILSKPERITQIIRDELEEEIKTNYGDERRSEINPFG-GD 536
<u><i>E. coli</i> GyrA</u>	KELLDQIAELLRILGSADRLMEVIRELELVREQFGDKRRTEITANS-AD 527
<u><i>S. aureus</i> GyrA</u>	NELNLYISELEAILADEEVLQLVRDELTEIRDRFGDERRTEIQLGGFED 495
<u><i>B. subtilis</i> GyrA</u>	OSLVKLI AELKDILANEYKVL E I IREELTEIKERFNDERRTEIVTSGLET 494
<u><i>B. burgdorferi</i> GyrA</u>	NILLSLIKDYEDILLNPVRIINI IREETINLGLKFGDERRTKIYDE-EV 494
<u><i>C. jejuni</i> GyrA</u>	AELMKEIARLEEILKSETLLENLIRDELKEIRSKFDVPRITQIEDDY-DD 494
<u><i>Haloferax</i> GyrA</u>	EDVQATIERLETILGQSELD A VIESELLDIKDEYADDRRTSFVANT-GE 511
<u><i>Haloferax</i> HypoA</u>	RGAHPPQVRARIYLAAGEARGLPEPRPLGVRTVHRGGRLRGRVQAG-- 299
	*
<u><i>M. tuberculosis</i> GyrA</u>	VSD--EDLIAREDVVVTITETGYAKRTKTDLYRSQKRGKGVQAGLQKD 552
<u><i>M. smegmatis</i> GyrA</u>	VSD--EDLIAREDVVVTITETGYAKRTKTDLYRSQKRGKGVQAGLQKD 553
<u><i>S. coelicolor</i> GyrA</u>	MSI--EDLIAEEDIVVTIVTRGGYIKRTKTDYRAQKRGKGVGRTKTKLED 549
<u><i>N. gonorrhoeae</i> GyrA</u>	IAD--EDLIPQREMIVTLTHGGYIKTQPTTDYQ&QRRGGKQA&AATKDE 586
<u><i>E. coli</i> GyrA</u>	INL--EDLITQEDVVVTLSHQGYVYQPLSEYEAQRRGGKGSAAARIKEE 575
<u><i>S. aureus</i> GyrA</u>	LED--EDLIPEEQIVITLSHNNYIKRLPVSTYRAONRGGKGVQGMNTLEE 543
<u><i>B. subtilis</i> GyrA</u>	IED--EDLIERENIVVTLTHNGYVKRLPASTYRSQKRGKGVQGMNTNED 542
<u><i>B. burgdorferi</i> GyrA</u>	LKTSMSDLMQENIVVMLTKRGLKRLSQNEYKLGCTGGKGLSSFDLNDG 544
<u><i>C. jejuni</i> GyrA</u>	ID--IEDLIPNENIVVTITHRGYIKRVPSKQYEQKRGKGLAVTTYDD 542
<u><i>Haloferax</i> GyrA</u>	VTR--ADLIPEEDVVVVSDDYIKRMPVSRFRAQHRGGKGIIGTDLKEG 559
<u><i>Haloferax</i> HypoA</u>	-----PRQVPGDFAPQGEDSERRETPPRPHSRKRR----- 330
	:     :: . : :     : . .     . :     :

**Figure 3.14: Multiple sequence alignment of bacterial GyrA using ClustalW 1.83 (Larkin *et al.*, 2007). The characteristic  $Ca^{2+}$ -binding sequence present in *M. tuberculosis* DNA GyrA aligned with other bacterial GyrA is enclosed in the rectangle. The putative  $Ca^{2+}$ -binding sequence fits with loop and PS00018 pattern.**

Further analysis of *M. tuberculosis* GyrA by PROSITE at EXPASY (Gasteiger *et al.*, 2003); indicated that the sequence ‘504 DVSDLEDLIAREDV 516’ is a potential EF-hand-like calcium binding domain.

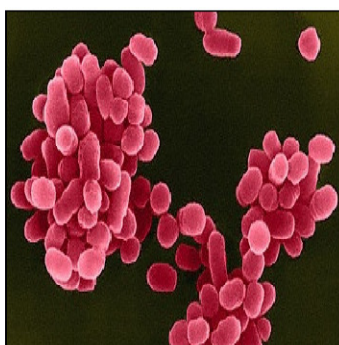
Based on the sequence alignment (**Figure 3.15**), sequences homologous to the putative  $\text{Ca}^{2+}$ - binding site are also found in the closely related *Mycobacterium bovis*, *Brucella melitensis* and *Corynebacterium diphtheriae*. Interestingly *B. melitensis* and *C. diphtheriae* are human pathogens, and *C. diphtheriae* lacks topo IV. This indicates that the presence of the  $\text{Ca}^{2+}$ - binding site in GyrA may have some correlation with the dual role that DNA gyrase has to play in the absence of topo IV. The significance of gyrase in the absence of topo IV is also evident from the fact that in the absence of topo IV, mutations in *gyrA* gene confer quinolone resistance (Payot *et al.*, 2002, Sierra *et al.*, 2005).

```

GyrA_M.tub (475) QRGIVRDELAIEIVDRHGDDRRTRI IAAADGDVSDLEDLIAREDVVVTITETG
GyrA_B.meli (493) VMNIVKEEMIAVRDEFATPRRTEIGFGGAE MDDLEDLIAREDMVVTVSHAG
GyrA_C.dep (473) QRAIVRDELAIEIVDKYGD RRRTQIIAATGDVTEEDLIARENVVVTITSTG
Consensus (501) QRAIVRDELAIEIVDKHGDDRRRT IIAA GDVSDLEDLIAREDVVVTIT TG

GyrA_M.tub (525) YAKRKTDL YRSQKRGGKGVQAGLQDDIVAHFFVCSTHDLILFFTTQG
GyrA_B.meli (543) YIKRVPLTTYRAQRGGKGRSGMATKEEDFVTRLFVANHTHPVLFSSRG
GyrA_C.dep (523) YAKRKTVDAYKSQRGGKGVRCGAELKQDDVVRHFFVSTH DWILFFTNFG
Consensus (551) YAKRKTLD YRSQKRGGKGV GAALKQDDIV HFFVASTHD ILFFTS G

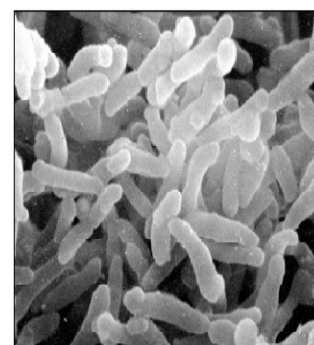
```



A. *Brucella melitensis* causes brucellosis



B. *Mycobacterium tuberculosis* causes tuberculosis in humans



C. *Corynebacterium diphtheriae* causes Diphtheria.

**Figure 3.15:** Multiples sequence alignment for GyrA from *B. melitensis*, *M. tuberculosis* and *C. diphtheriae*. The sequence of the putative  $\text{Ca}^{2+}$ - binding site is enclosed in a square.

### 3.4.1 EF-hand $\text{Ca}^{2+}$ - binding domain

The EF-hand proteins have a characteristic helix-loop-helix  $\text{Ca}^{2+}$ -binding motif and they constitute one of the largest protein families involved in numerous biological processes. There are now 66 subfamilies for this protein (Kawasaki *et al.*, 1998, Kretsinger & Nockolds, 1973, Ravasi *et al.*, 2004). EF-hands are divided into two major groups: the canonical EF-hand (calmodulin and prokaryotic calerythrin) (**Figure 3.16**) and the pseudo EF-hands, exclusively found in the N-termini of S100 and S100-like proteins (**Figure 3.16**). The major difference between the two groups lies in the  $\text{Ca}^{2+}$ -binding loop: the 12-residue canonical EF-hand loop binds  $\text{Ca}^{2+}$  mainly via side chain carboxylates or carbonyls, which are denoted by loop sequence position: 1, 3, 5, 12; whereas the pseudo EF-hand loop is 14-residues with positions 1, 4, 5 and 9 coordinating the  $\text{Ca}^{2+}$  (**Figure 3.18**). Water molecules may also be involved in coordinating  $\text{Ca}^{2+}$ . Among all the structures reported for  $\text{Ca}^{2+}$  - binding proteins, the majority of EF-hand motifs are paired; proteins with odd numbers of EF-hands are coupled through homo- or heterodimerization (Hunter & Chazin, 1998, Grabarek, 2006, Ravulapalli *et al.*, 2005). The situation is similar in the case of *M. tuberculosis* GyrA, the single EF-hand-like  $\text{Ca}^{2+}$ -binding site is paired as *M. tuberculosis* GyrA59 (N-terminal) exists as a dimer (Tretter *et al.*, 2010). Although the crystal structure (PDB code: 3ILW) does not include the putative  $\text{Ca}^{2+}$  -binding site. This pairing enables communication and many EF-hands show positive cooperativity.

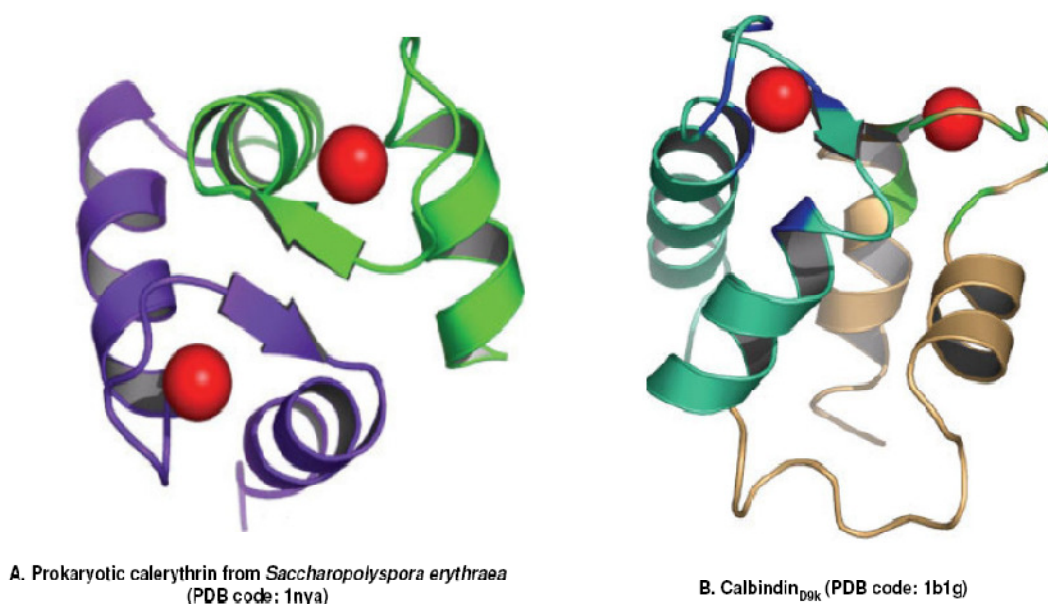


**Figure 3.16: The two major groups of EF-hands: (A) Canonical EF-hand domain from *Saccharopolyspora erythraea* (PDB code: 1nya) and (B) Pseudo-canonical EF-hand from Calbindin<sub>D9K</sub> (PDB code: 1b1g). The protein has both the N-terminal pseudo EF-hand  $\text{Ca}^{2+}$ -binding ligand (blue) and the C-terminal canonical EF-hand (green) (Zhou *et al.*, 2006). The red spheres represent the  $\text{Ca}^{2+}$  atoms.**

Secondary structure prediction of *M. tuberculosis* GyrA by PSIPRED (Jones, 1999) indicated that the predicted  $\text{Ca}^{2+}$ -binding site is loop-helix-loop-strand as shown in **Figure 3.17**. This secondary structure prediction does not follow the textbook definition of an EF-hand (Gifford *et al.*, 2007). There are examples of other bacterial proteins, which have different EF-hand secondary structure patterns. The best examples of this are the periplasmic galactose-binding protein (*Salmonella typhimurium*; PDB code: 1gcg) (Vyas *et al.*, 1987) and alginate-binding protein (*Sphingomonas* sp.; PDB code: 1kwh) (Mishima *et al.*, 2003) (**Figure 3.17**).

Prokaryotic EF-hand-like proteins are involved in  $\text{Ca}^{2+}$  signalling and homeostasis in bacteria (Michiels *et al.*, 2002, Rigden *et al.*, 2003, Rigden & Galperin, 2004, Yang, 2001). They contain flexible lengths of  $\text{Ca}^{2+}$ -binding loops that differ from the EF-hand motifs but their coordination properties resemble those of classical EF-hand motifs.

A recent publication (Zhou *et al.*, 2006) on an improved pattern search method for the identification of EF-hand and EF-like Ca<sup>2+</sup>-binding proteins predicted a Ca<sup>2+</sup>- binding site in a closely related species *M. bovis*. The signature sequence predicted to be a Ca<sup>2+</sup>- binding site in *M. bovis* GyrA (NCBI code: CAD92868) is also found in *M. tuberculosis* GyrA (NCBI code: CAB02427). This is an interesting fact as *M. bovis* has been reported to be a causative agent of tuberculosis in humans like *M. tuberculosis* (Jou *et al.*, 2008).

This method (Zhou *et al.*, 2006) is based on a series of patterns that were generated from the metal-binding properties of currently available EF-hand proteins and the helical structural context around the Ca<sup>2+</sup>-binding loop. The pattern PS00018 for predicting the canonical EF-hand sites (<http://us.expasy.org/cgi-bin/nicesite.pl?PS00018>) were modified by allowing more choices (Glu, Gln and Ser) at position 1 (axis X) and adding constraints at the flanking helical regions. A modified pattern for the prediction of pseudo EF-hand sites was also generated by loosening the constraints at the C-terminal canonical EF-hand and including reserved residues in the N-terminal pseudo EF-hand, which were called eloopf, eloop, loopf, and loop. This new pattern in comparison to PS00303, significantly improved the predictive accuracy and sensitivity. Based on the sequence, the putative Ca<sup>2+</sup>-binding site in GyrA fits with the loop and PS00018 pattern (Zhou *et al.*, 2006).

The loop pattern sequence is:

```
[DNS]-x-[DNS]-{FLIVWY}-[DNESTG]-[DNQGHRK]-{GP}-[LIVMC]-
[DENQSTAGC]-x (2)-[ED].
```

The PS00018 sequence is:

```
D-x-[DNS]-{ILVIFYW}-[DENSTG]-[DNQGHRK]-{GP}-[LIVMC]
[DENQSTAGC]-x (2) - [DE]-[LIVMFYW].
```

The pattern is represented by PROSITE PAttern. In this format, amino acids are represented by IUPAC one-letter codes, x for any amino acid, [ ] represents accepted amino acids, { } represents the amino acids that are not accepted, '-' separates the pattern element, and x (n) represents the n times repetition of an element.

Thus, there is supporting bioinformatic evidence for the presence of EF-hand like Ca<sup>2+</sup> - binding domain in *M. tuberculosis* GyrA.



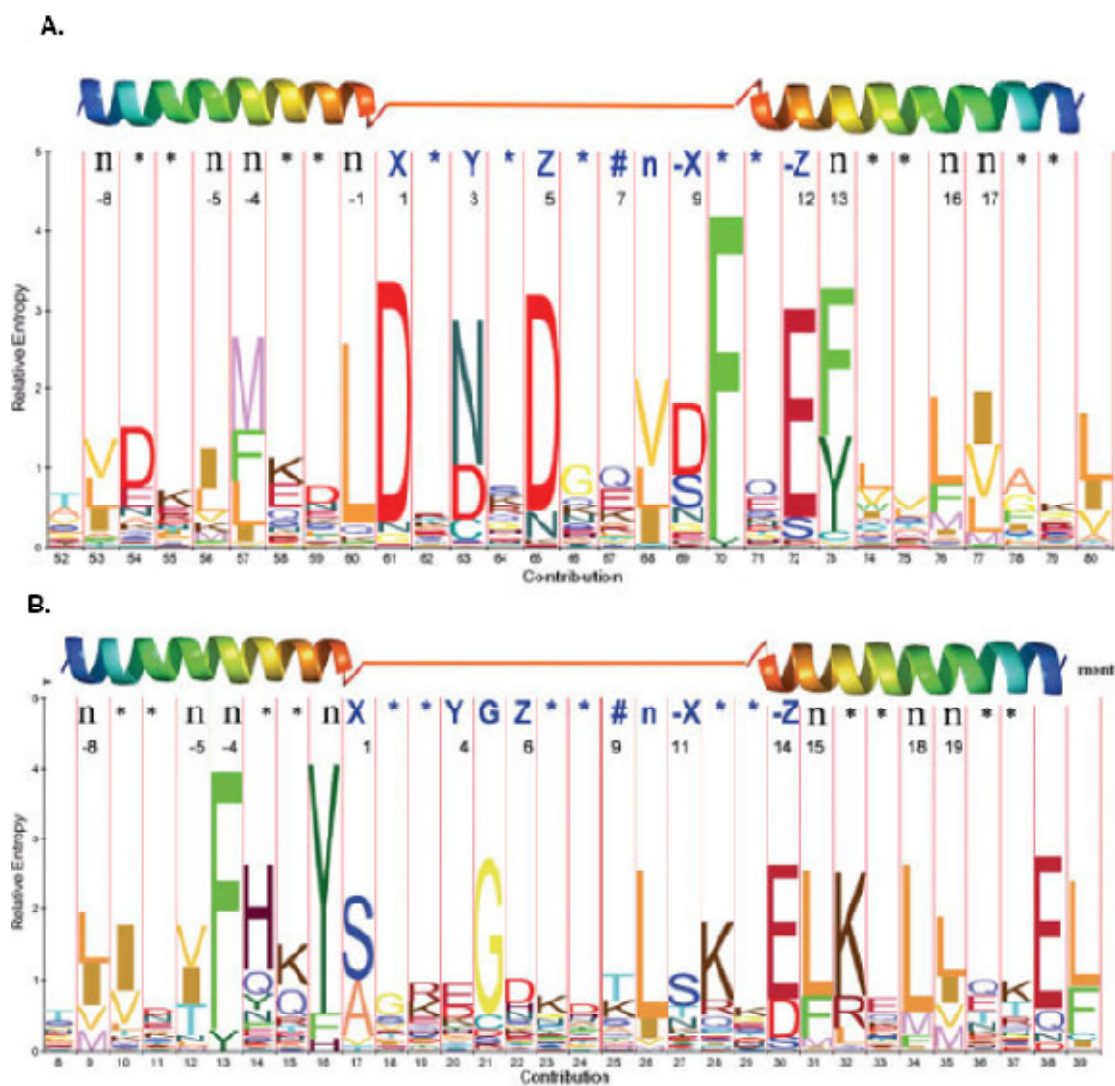


**Figure 3.18: Illustration of differences between canonical and pseudo-EF hand.** Consensus sequence of canonical EF-hand (A) and pseudo EF-hand (B) domains based on the prediction method. *n*: the hydrophobic residues within the flanking helices, #: the potential  $\text{Ca}^{2+}$  - binding ligands involving the main chain carbonyl groups (Zhou et al., 2006).

### 3.4.2 Model for the Ca<sup>2+</sup> - binding site

Recently crystal structures for the N-terminal (PDB codes: 3ILW & 3IFZ) (Tretter *et al.*, 2010) and C-terminal domains (PDB code : 2ZJT) (Fu *et al.*, 2009) of *M. tuberculosis* GyrA subunit has been solved. However, both the structures lack the putative Ca<sup>2+</sup>-binding site and there is no crystal structure for the complete *M. tuberculosis* GyrA subunit. In the absence of the crystal structures containing the putative Ca<sup>2+</sup>- binding site, molecular homology modelling was done using the package Insight II (Accelrys). This protein modelling work was done in collaboration with Dr Faridoon Yousafzai (Computational and Systems Biology, John Innes Centre).

To build a 3-D homology model of the *M. tuberculosis* GyrA subunit, suitable templates were searched for by using tools such as the Protein Homology/ Analogy Recognition Engine (Phyre) (Kelley & Sternberg, 2009) and the BioInfoBank Metaserver (Ginalski *et al.*, 2003). The *M. tuberculosis* GyrA complete sequence was submitted to these search engines and *E. coli* ParC subunit (PDB code: 1ZVU) (Corbett *et al.*, 2005) was identified as the top hit from both the servers. The N-terminal domain of *E. coli* Par C subunit (PDB code: 1ZVU) and the C-terminal domain of *Borrelia burgdorferi* GyrA subunit (PDB code: 1SUU) (Corbett *et al.*, 2004) were used as templates to model respectively the N- and C-terminal domains of *M. tuberculosis* GyrA. Sequence alignment between the template and *M. tuberculosis* GyrA was performed. The alignment between the N-terminus of *M. tuberculosis* GyrA and the N-terminal domain of ParC subunit (PDB code: 1ZVU) was kept the same as that generated by Phyre (**Figure 3.19**). The alignment between C-terminal domain of *M. tuberculosis* GyrA and the C-terminal domain of *Borrelia burgdorferi* (PDB code: 1SUU) was generated by MUSCLE (Edgar, 2004b, Edgar, 2004a) as shown in **Figure 3.19**. For modelling the Ca<sup>2+</sup>- binding site, PDB search and sequence search tools such as BLAST were used to identify suitable templates.

**A.**

```

      *      20      *      40      *      60      *      80      *      1
1zvu : MDRALPFIQDGLKPVQRRIVYAMSELGLNASAKFKKSARTVGDVLGKYHPHGDSACYEMVLMQAQFFSYRYPLVDGGGNWGPDDPKSFAAMRYTESR : 98
MTGyr_A : -GRALPEVRDGLKPVHRRVLYAMFDGFRPDRSHAKSARSVAETMGNYPHPGDSASYDSLVRMAQFWSLRYPLVDGGGNFSGPNDPP-AAMRYTEAR : 96

      00      *      120      *      140      *      160      *      180      *
1zvu : LSKYSELLSELQCGIADWVPNFDGTLQEFKMLPARLPNILLNGTTGIAVGMATDIPPHNLREVAQAAIALIDQPKT---TLDQLLDIVQCFDYPTTE : 192
MTGyr_A : LTPLAMEMLRIDEETVDFIPNYDGRVQEFTVLPSTRFPNLLANGSGGIAGVMATNIPPHNLRELACAVFWALENHDADEEETLAAVMGRVKGFDFPTA : 194

      200      *      220      *      240      *      260      *      280      *
1zvu : AEIITSRAEIRKIYENGRGSVVRMRAVWKKE----DGAVVISALPHQVSGARVLEQIAAQMRNKKLPMVDDLEDESDHENPTRLVIVPRSNRVDMDCV : 285
MTGyr_A : G-LIVGSGQTADAYKTGRGSIRMGRVVEVEDSRGRTSLVITELPQVNHDFNFTSIAEQVRDGKLAGISNIEDQSSDRVGLRIVIEIKRD-AVAKVV : 290

      300      *      320      *      340      *      360      *      380      *
1zvu : MNHLEFATDLEKSYRINLNMIGLDGRPAVKNNLEILSEWLVFRDTRVRRRLNRYLEKVLKRLHILEGLLVAFPLNIDEVIEIIRNEDE---PKPALMSR : 380
MTGyr_A : INNLYKHTQLQTSFGANMLAI-VDGVPTLRDQLIRIYVDHQLDVIVRRTTYRIRKANERAHILEGLVKALDADLDEVIALLIRASETVDIARAGLIEL : 387

      400      *      420      *      440      *      460      *      480
1zvu : FGLTETQAEAILKLPRLAKLEEMKIRGEQSELEKERDQLQGLASERKMNLLKKELOADAQAYGDDRRSPLOQEREKAMSEHDMLEPS : 471
MTGyr_A : LDIDHIQAQAILDMLRRLAALERQRIIDDLAKIEAIEADLEDILAKPERQRGIVRDELAEIVDRHGDDRRTRIIAADG--DVSDEDIAR : 476

```

**B.**

```

      *      20      *      40      *      60      *      80      *      100
1SUU : MSDLMQKENIVVMLTKKGLKRLSQNEYKLGQTGGKGLSSFDLNDGDEIVIALCVNTHDYLFMISNEGKLYLINAYEIKDSSRASKGQNISELINLGDQE
MTGyr_A : -----EDVVVTITETGYAKRKTDLYRSQKRGKGVQAGLQDDIVAHFPVCSTHDLILFFTTQGRVYRAKAYDLPEASRTARGQHVANLLAFQPEE

      *      120      *      140      *      160      *      180      *      200
1SUU : EILTIKNSKDLTDDAYLLLTASGKIARFESTDFKAVKSRGVIVIKLNDKDFVTSAEIVFKDEKVICLSKKGSAFIFNSRD--VRLTNRGTQGVCGMKLK
MTGyr_A : RIAQVIQIRGYTDAPYLVLATRNGLVKKSKLTFDSDNRSGGIVAVNLRDNDDELVGAVLCSAGDLLLLVSANGSIRFSATDEALRPMGRATSGVQGMRFN

      *      220      *      240      *      260      *      280      *      300
1SUU : EGDLFVKVLSVKNENPYLLIVSENGYKRLNMSKISELKRATGYTSYKSDKKAGSVVDAIAVSEDEIILLVSKRSKALRTVAGKVSQGGKDARGIQVLF
MTGyr_A : IDDRLLSLNVVREGTYLLVATSGGYAKRTAIEEYPVQGRGGKGLVLT-MYDRRGRGLVGALIVDDSELYAVTSGGGVIRTAARQVRKAGRQTKGVRIMN

      *      320      *
1SUU : L-DNDSLVSVKFIK-----
MTGyr_A : LGEEDTLLAIARNABESGDDNAVDANGADQTGN

```

**Figure 3.19: Sequence alignment for *M. tuberculosis* GyrA.** Alignment between the N- terminus of *M. tuberculosis* GyrA and the N-terminal domain of Par C subunit (A) generated by Phyre has 39% identity, 61% similarity and 3% gaps. The alignment between the *M. tuberculosis* GyrA C- terminus and the C-terminal domain of *Borrelia burgdorferi* (B) has 25% identity, 51% similarity and 8% gaps.

After generating the sequence alignment, the coordinates were transferred from the template proteins to the modelling protein and other structural entities such as loops were built using the programme Insight II (Accelrys). The final refined model was generated by removing bumps, resolving chirality, bond length and dihedral angles ( $\Omega$  values).

As discussed before, the predicted putative  $\text{Ca}^{2+}$ -binding site in *M. tuberculosis* GyrA does not follow the standard helix-loop-helix definition. There are several other prokaryotic proteins having the  $\text{Ca}^{2+}$ -binding sites that do not follow the canonical EF-hand motif pattern. From the PDB search two such proteins were identified: psychrophilic metalloprotease from *Pseudoalteromonas* (PDB code: 1H71) (Aghajari *et al.*, 2003) and metallo-protease from *Pseudomonas aeruginosa* (PDB id: 1KAP) (Baumann *et al.*, 1993); both have sequences similar to the EF-hand  $\text{Ca}^{2+}$ -binding site in a loop-loop-strand and a strand-loop-strand structural motifs. Initially 1H71 was used as a template to build the putative  $\text{Ca}^{2+}$ -binding site in *M. tuberculosis* GyrA.

The  $\text{Ca}^{2+}$ -binding sites in the homology model and in 1H71 is shown in **Figure 3.20**. The sequence from D504-V516 was forced to adopt the same fold as that of the  $\text{Ca}^{2+}$ -binding site in 1H71. Although the  $\text{Ca}^{2+}$ -binding site for *M. tuberculosis* GyrA was developed, the structure failed to optimise due to the presence of un-resolved bumps in the structure. An alternative strategy was used to fit the  $\text{Ca}^{2+}$ -binding site. While optimising the model including the  $\text{Ca}^{2+}$ -binding site (modelled based on the template 1H71), the entire model was restrained except for the five residues on the each side of the D504-V516 sequence to allow the N- and C-terminal domains to adopt suitable orientations relative to each other. This strategy was successful and the model was developed, which will be hereafter referred to as MtGyrA-1H71. In this model, the  $\text{Ca}^{2+}$  coordinated to 6 residues: D504 (side-chain-O), S506 (side-chain-O), E508 (side-chain-O), L510 (backbone-O), A512 (backbone-O) and E514 (side-chain-O) in an octahedral geometry. Although, the  $\text{Ca}^{2+}$ -binding fold is the same as that of template protein, the coordination sphere of  $\text{Ca}^{2+}$  is different. In the template protein 1H71, alternate residues D49, N51, D53, V55 and N57 are bonded to  $\text{Ca}^{2+}$ , except the last residue N114 that is 56 amino acids

away from N57. The  $\text{Ca}^{2+}$  is coordinated by side chain atoms except V55 where the backbone oxygen is bonded to  $\text{Ca}^{2+}$ . In the case of *M. tuberculosis* GyrA model, the  $\text{Ca}^{2+}$ -binding site is composed of six alternating residues, four out of which provide side-chains while the other two L510 and A512; provide backbone oxygen atoms for  $\text{Ca}^{2+}$ .



**Figure 3.20: Homology model of the *M. tuberculosis* GyrA  $\text{Ca}^{2+}$ -binding site (MtGyrA-1H71) based on the psychrophilic metalloprotease from *Pseudomonas* sp. (PDB code: 1H71). The cartoon shows the  $\text{Ca}^{2+}$ -binding site in 1H71 above the GyrA  $\text{Ca}^{2+}$ -binding site for comparison.**

Another protein *Staphylococcus aureus* metalloproteinase (PDB id: 1BQB) (Banbula *et al.*, 1998) having a  $\text{Ca}^{2+}$ -binding site, was found to have the best sequence identity and similarity with the predicted  $\text{Ca}^{2+}$ -binding site in *M. tuberculosis* DNA gyrase. This template was identified by searching PDB for structures having  $\text{Ca}^{2+}$  as a ligand (~4000 hits), followed by sequence searching D504-V516, which gave 790 hits. The combination of both these techniques along with the removal of sequences  $\geq 90\%$  identity, found 21 unique chains which were

individually examined for the best fit to the predicted  $\text{Ca}^{2+}$ -binding sequence D504-V516 in terms of sequence identity and similarity. Using the *Staphylococcus aureus* metalloproteinase (PDB id: 1BQB) as a template another model was generated and referred to as MtGyrA-1BQB (**Figure 3.21**). The template structure had 2  $\text{Ca}^{2+}$  atoms in the loop corresponding to the predicted  $\text{Ca}^{2+}$  -binding loop of *M. tuberculosis* GyrA. Based on the template, 2  $\text{Ca}^{2+}$  atoms were modelled in MtGyrA-1BQB.

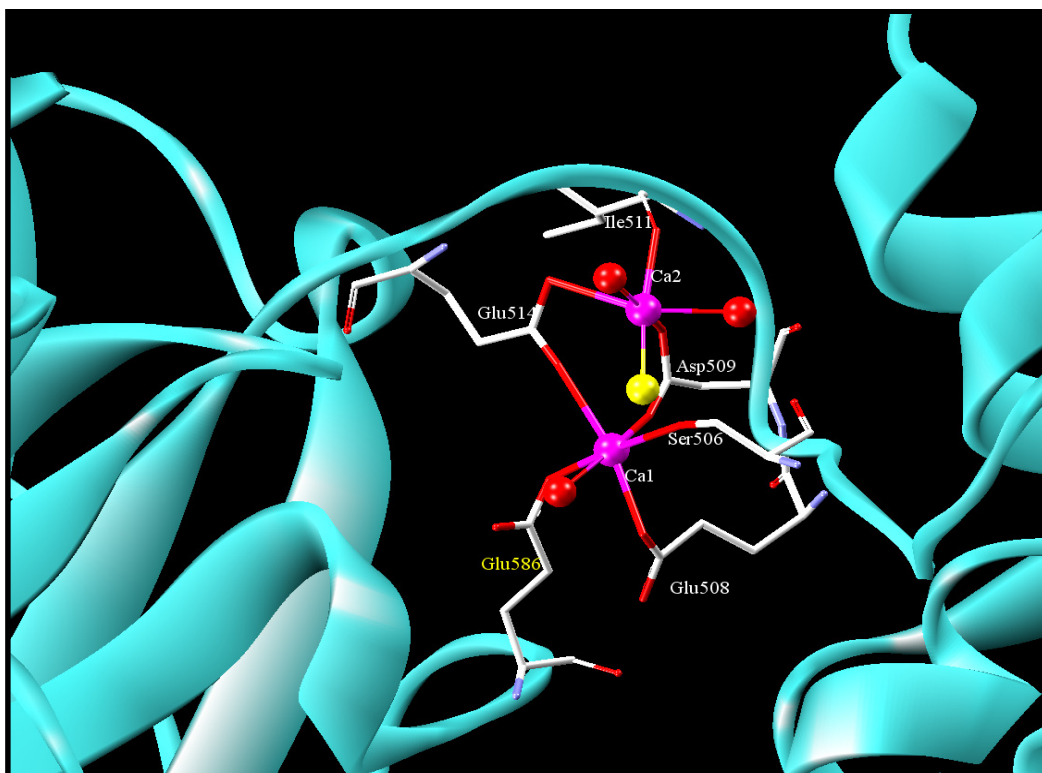


**Figure 3.21:** Homology model of *M. tuberculosis* GyrA  $\text{Ca}^{2+}$ -binding site (MtGyrA-1BQB) based on *Staphylococcus aureus* metalloproteinase (PDB code: 1BQB). One water molecule coordinates  $\text{Ca}^{2+}$ -1 and three water molecules coordinate  $\text{Ca}^{2+}$ -2 as represented by yellow and red balls.

Although there is 57% similarity and 71% sequence identity between the Ca<sup>2+</sup>-binding loops of 1BQB and *M. tuberculosis* GyrA, there are differences in the 3-D environment of the Ca<sup>2+</sup> atoms. The first difference is that in the case of *M. tuberculosis* GyrA, one of the Ca<sup>2+</sup>-coordinating residues is S506 but the corresponding residue in 1BQB is D179 that coordinates the two Ca<sup>2+</sup> atoms. Second, in 1BQB, one of the calciums (referred as Ca<sup>2+</sup>-1) is attached to two water molecules, while in the case of MtGyrA-1BQB; it is attached to only one water molecule. This is due to E586 coordination in MtGyrA-1BQB, the corresponding residue D140 in 1BQB is at a different place and coordinates the other Ca<sup>2+</sup> atom (referred as Ca<sup>2+</sup>-2). The Ca<sup>2+</sup>-2 atom in the case of 1BQB is coordinated to only one water molecule, while in case of MtGyrA-1BQB it needs 3 water molecules for an octahedral coordination (**Figure 3.22**).

The overall electrostatics of the Ca<sup>2+</sup>-binding site is also different in both the proteins. 1BQB has six negatively charged (five Ca<sup>2+</sup>-coordinated and one non-coordinated acidic residues) and no positively charged residue. On the other hand *M. tuberculosis* GyrA, has five negatively charged (four Ca<sup>2+</sup> coordinated and one non-coordinated acidic residues) and one positively charged residue.

Due to the unique nature of the predicted Ca<sup>2+</sup>-binding site in *M. tuberculosis* GyrA, two models namely MtGyrA-1H71 and MtGyrA-1BQB were generated based on the metalloprotease from *Pseudoalteromonas* (PDB code: 1H71) and *Staphylococcus aureus* metalloproteinase (PDB id: 1BQB) respectively. In the absence of a complete crystal structure for *M. tuberculosis* GyrA it is difficult to predict which of the models is correct. Mutation studies in the Ca<sup>2+</sup>-binding site were designed to mutate acidic amino acids that have significant importance in coordinating Ca<sup>2+</sup>. For example the quadruple mutant (GyrA D504A, E508A, D509A, E514A) described in later sections involves mutation of two acidic residues (D504 and E508) from MtGyrA-1H71 and two acidic residues (E509, E514A) from MtGyrA-1BQB. E508 is an important acidic residue shown to coordinate Ca<sup>2+</sup> in both the models.

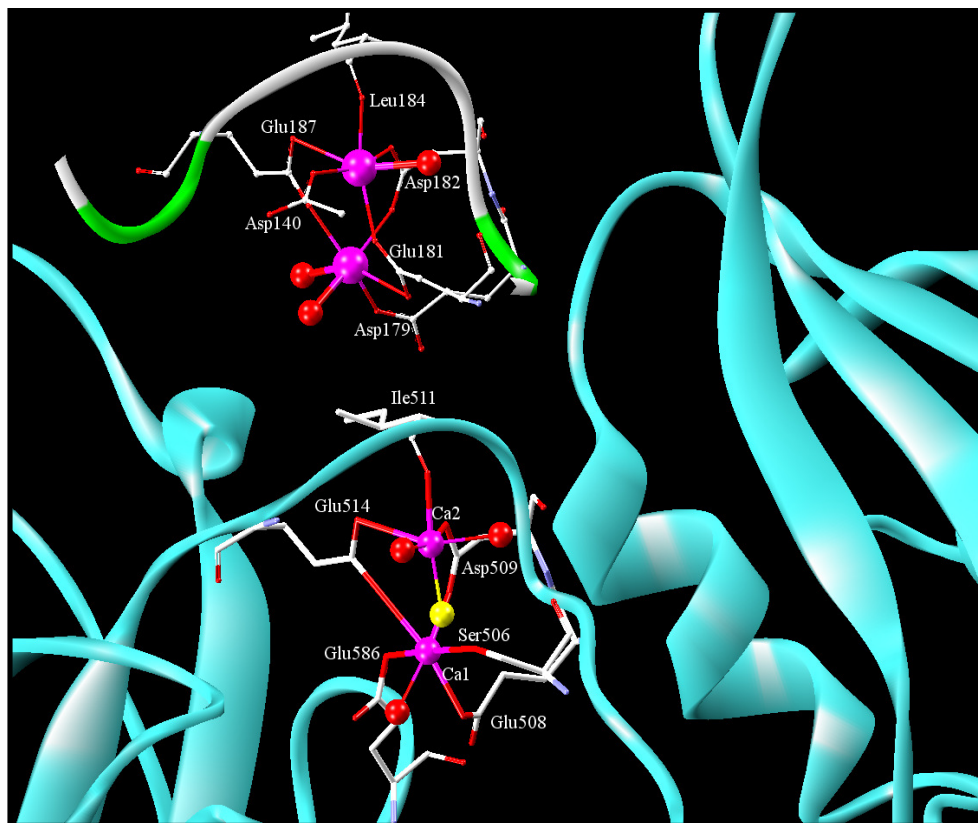


**Figure 3.22:** Difference between the 3-D environments of the GyrA  $\text{Ca}^{2+}$  - binding site and the *Staphylococcus aureus* metalloproteinase (PDB id: 1BQB) template. The cartoon shows the  $\text{Ca}^{2+}$ -binding site in 1BQB above the GyrA  $\text{Ca}^{2+}$ -binding site for comparison. One water molecule coordinates  $\text{Ca}^{2+}$ -1 and three water molecules coordinate  $\text{Ca}^{2+}$ -2 as represented yellow and red balls.

### 3.5 Conclusion

DNA gyrase is a type II topoisomerase present in all prokaryotes and plants. The enzyme has been well studied and characterised in *E. coli*, a Gram-negative bacteria, with limited information about the enzyme from pathogenic bacteria such as *M. tuberculosis*. Most of the studies done on *M. tuberculosis* DNA gyrase have been related to inhibitors such as fluoroquinolones (Aubry *et al.*, 2004). Although the aim of my project is to identify novel inhibitors for *M. tuberculosis* DNA gyrase, it was also important to explore the unique characteristic of this enzyme.

Bioinformatics analysis was performed to compare *M. tuberculosis* DNA gyrase with other bacterial gyrases. Based on multiple sequence alignment of bacterial DNA gyrase, the following two unique features were identified in the *M. tuberculosis* DNA gyrase:

1. Prediction of the presence of an additional 40 amino acids at the *M. tuberculosis* GyrB N-terminus.
2. Prediction of a unique EF-hand like  $\text{Ca}^{2+}$  - binding site in *M. tuberculosis* GyrA.

Bioinformatics analysis predicted the presence of 40 additional amino acids on the N-terminus of *M. tuberculosis* GyrB in comparison to GyrB from other bacteria. Since the ATP-binding site is present at the N-terminus of GyrB, investigation about the function of these additional amino acids was important. There are also differences in the GyrB sequences retrieved from different databases. For example *M. tuberculosis H37Rv* GyrB sequence (NCBI code CAB02426) from NCBI has 40 additional amino acids at the GyrB N-terminus, which are absent from the same sequence cross-referenced in UniProtKB/Swiss-Prot (P0C5C5).

The first stage of analysis involved nested RT-PCR with primers designed at different positions within and flanking the region encoding the 40 amino acids. The RT-PCR results indicated the presence of both the transcript species with and without the region encoding the 40 additional amino acids. Due to the inability to over-express the protein in *M. tuberculosis*, it was not possible to confirm the presence of these additional 40 amino acids on the N-terminus of native GyrB from *M. tuberculosis*. However, the presence of these amino acids was confirmed by mass fingerprinting of protein expressed in *E. coli*. In future *C. glutamicum* can also be used to express *M. tuberculosis* proteins.

A deletion mutant, GyrB N40 $\Delta$ , was generated which had no effect on supercoiling, relaxation and decatenation activity of DNA gyrase. There was also no effect of the deletion mutation on the novobiocin-sensitivity of the enzyme. This indicates that there is no functional significance of these additional 40 amino acids on the GyrB N-terminus. Promoter analysis using pSM-128-Val (pSM-128 cloned with the sequence encoding the 40 additional amino acids) showed promoter activity

with the  $\beta$ -galactosidase assay. These experiments further confirmed the previous finding (Unniraman *et al.*, 2002) that the promoter elements are present in the sequence encoding the 40 additional amino acids. Therefore, this work has identified the starting coding for *M. tuberculosis* GyrB, which is Val41 instead of Met1. In future work it will be interesting to investigate the presence of two transcript species.

An EF-hand like  $\text{Ca}^{2+}$ -binding site has never been reported in other DNA topoisomerases. A few publications based on the bioinformatics analysis have predicted the possibility of the presence of a  $\text{Ca}^{2+}$ -binding site in DNA gyrase (Michiels *et al.*, 2002, Zhou *et al.*, 2006), but there has been no experimental evidence in support of the observation. In one publication (Zhou *et al.*, 2006), a  $\text{Ca}^{2+}$ -binding site was predicted to be present in the *M. bovis* GyrA subunit. *M. bovis* is a closely-related species to *M. tuberculosis* and forms the part of *M. tuberculosis* complex (Frothingham, 1995). Interestingly the sequence that was predicted to be a  $\text{Ca}^{2+}$ -binding site in *M. bovis* is also present in *M. tuberculosis* DNA gyrase '504 DVSDLEDLIAREDV- 516'. Further characterisation of the *M. tuberculosis* GyrA by PROSITE at EXPASY also identified an EF-hand like  $\text{Ca}^{2+}$ -binding site. Another interesting fact is that a similar sequence is also found in the GyrA subunit of the Gram-positive bacterium *Corynebacterium diphtheriae*, which lacks topo IV, also absent in *M. tuberculosis*. Topo IV is another type II topoisomerase efficient in DNA relaxation and decatenation (Zechiedrich *et al.*, 1997). Along with DNA gyrase, topo IV is present in most bacteria, like *E. coli*, and is the primary decatenase.

Since there is no crystal structure for the complete *M. tuberculosis* GyrA, the first stage of the investigation involved homology modelling of GyrA. Two homology models were generated referred to as MtGyrA-1H71, based on the template metalloprotease from *Pseudoalteromonas* (PDB code: 1H71) and MtGyrA-1BQB based on *Staphylococcus aureus* metalloproteinase (PDB id: 1BQB). The  $\text{Ca}^{2+}$ -binding site is present at the junction of N- and C-terminus domains of GyrA as shown in the **Figure 3.23**. Although the predicted  $\text{Ca}^{2+}$ -binding site in GyrA is an EF-hand like binding site, it does not follow the standard helix-loop-helix pattern rather a loop-helix-loop-strand, there are examples of similar bacterial proteins that do not follow the standard helix-loop-helix pattern. For example periplasmic

galactose-binding protein from *Salmonella typhimurium* (PDB code: 1gcg) has a helix-loop-strand pattern (Mishima *et al.*, 2003, Zhou *et al.*, 2006). The  $\text{Ca}^{2+}$ -binding site seems to follow the loop and PS00018 patterns. These patterns have been used for bioinformatics prediction of canonical EF-hand  $\text{Ca}^{2+}$ -binding sites (Zhou *et al.*, 2006).

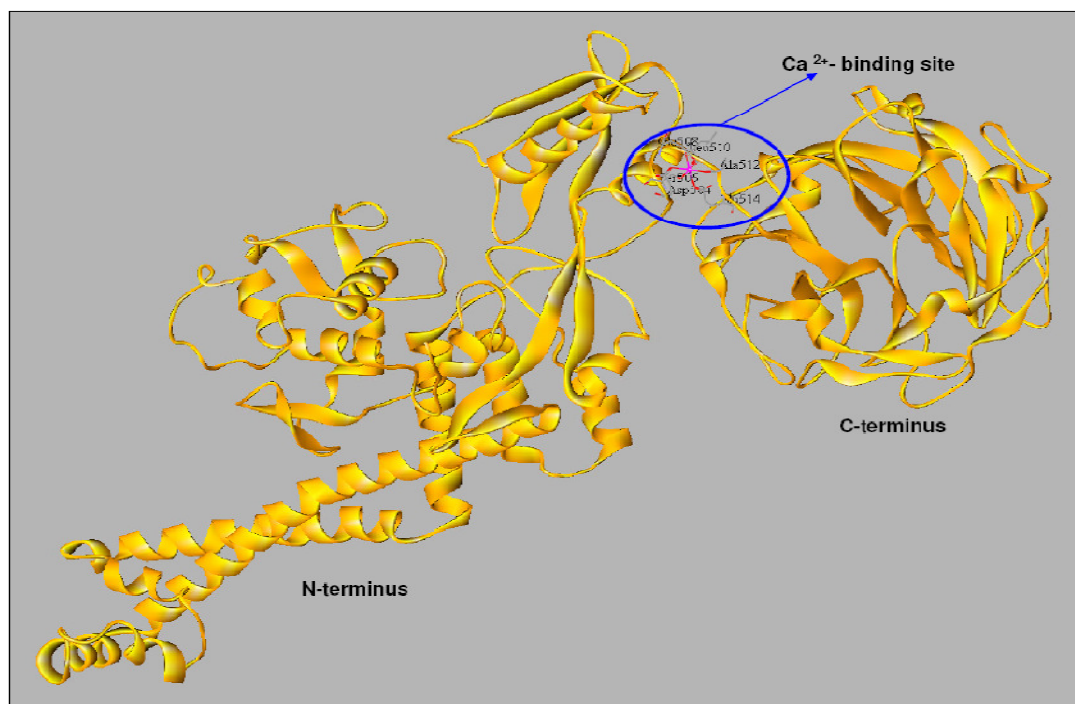


**Figure 3.23:** The predicted  $\text{Ca}^{2+}$ -binding site in between the N- and C-terminal domains of *M. tuberculosis* DNA gyrase.

## Chapter 4: Investigation of a putative Ca<sup>2+</sup>-binding site in *M. tuberculosis* GyrA

Bioinformatics analysis of *M. tuberculosis* GyrA (Chapter 3) revealed the presence of a unique putative Ca<sup>2+</sup>-binding site. Biochemical analysis to study the relevance of Ca<sup>2+</sup> and site-directed mutagenesis experiments in support of the models (MtGyrA-1H71 and MtGyrA-1BQB) were performed. The biochemical analysis involved protein dialysis, protein refolding and limited proteolysis experiments. Weak relaxation activity was observed when GyrA was dialysed in 1 mM EGTA, which then could be regained by the addition of Ca<sup>2+</sup>. This effect was intense when GyrA was refolded in the presence of 1 mM EGTA, leading to the complete loss of relaxation activity with weak supercoiling activity. Limited proteolysis experiments done in the presence of Ca<sup>2+</sup>, demonstrated conformational change in the protein, which resulted in disappearance of a 47-kDa band.

Mutations (D504A, E508A, D509A, E514A) in the putative Ca<sup>2+</sup>-binding site affected the supercoiling activity of the enzyme which led to incomplete supercoiling. Thus, these experiments demonstrate the significance of the Ca<sup>2+</sup> and its binding site in GyrA. Due to the significance of the Ca<sup>2+</sup>-binding site, virtual screening was performed at this site to explore it further as a target site for novel inhibitors.

## 4.1 Bacterial DNA gyrase $\text{Ca}^{2+}$ selectivity

According to the bioinformatics analysis, the putative  $\text{Ca}^{2+}$ - binding site is present in *M. tuberculosis* DNA gyrase but not in *E. coli* gyrase. This suggests that  $\text{Ca}^{2+}$  may have a specific role in the activity of *M. tuberculosis* DNA gyrase. From previous studies, we know that *E. coli* DNA gyrase can supercoil relaxed DNA when  $\text{Ca}^{2+}$  ion is substituted for  $\text{Mg}^{2+}$ .  $\text{Ca}^{2+}$  also induces the formation of the cleavage complex in case of *E. coli* DNA gyrase (Reece & Maxwell, 1989). On the contrary, although *M. tuberculosis* DNA gyrase has the putative  $\text{Ca}^{2+}$ - binding site, it shows little or no supercoiling in the presence of  $\text{Ca}^{2+}$  alone (**Figure 4.1**). Earlier characterisation studies done on this enzyme confirm this finding and also indicate the inability of the enzyme to relax supercoil DNA and induce cleavage formation in the presence of  $\text{Ca}^{2+}$  alone (Aubry *et al.*, 2006a).

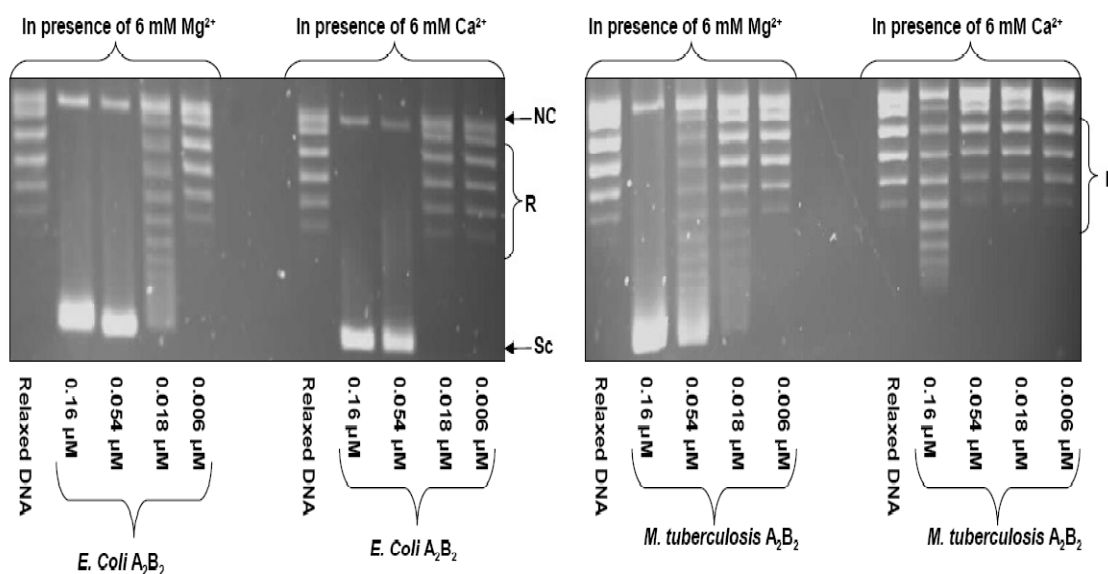


**Figure 4.1:** *E. coli* and *M. tuberculosis* DNA gyrase supercoiling assay in the presence of 6 mM  $\text{Mg}^{2+}$  and  $\text{Ca}^{2+}$ . NC: nicked Circular DNA, R: relaxed topoisomers, SC: supercoiled DNA.

An interesting observation was made when subunits of *M. tuberculosis* and *E. coli* DNA gyrase were mixed. *M. tuberculosis* GyrA when mixed with equimolar concentration of *E. coli* GyrB exhibited DNA supercoiling activity in the presence of 6 mM Mg<sup>2+</sup>, whereas only weak supercoiling was observed in the case of vice versa (*E. coli* GyrA mixed with equimolar concentration of *M. tuberculosis* GyrB). The assay with equimolar concentration of *M. tuberculosis* GyrA and *E. coli* GyrB was repeated in the presence of 6 mM Ca<sup>2+</sup>. In the presence of 6 mM Ca<sup>2+</sup>, no supercoiling activity was observed (Figure 4.2). This indicates that the ability of the Ca<sup>2+</sup> to support DNA supercoiling depends on the presence of *E. coli* GyrA and *M. tuberculosis* GyrA cannot substitute it.

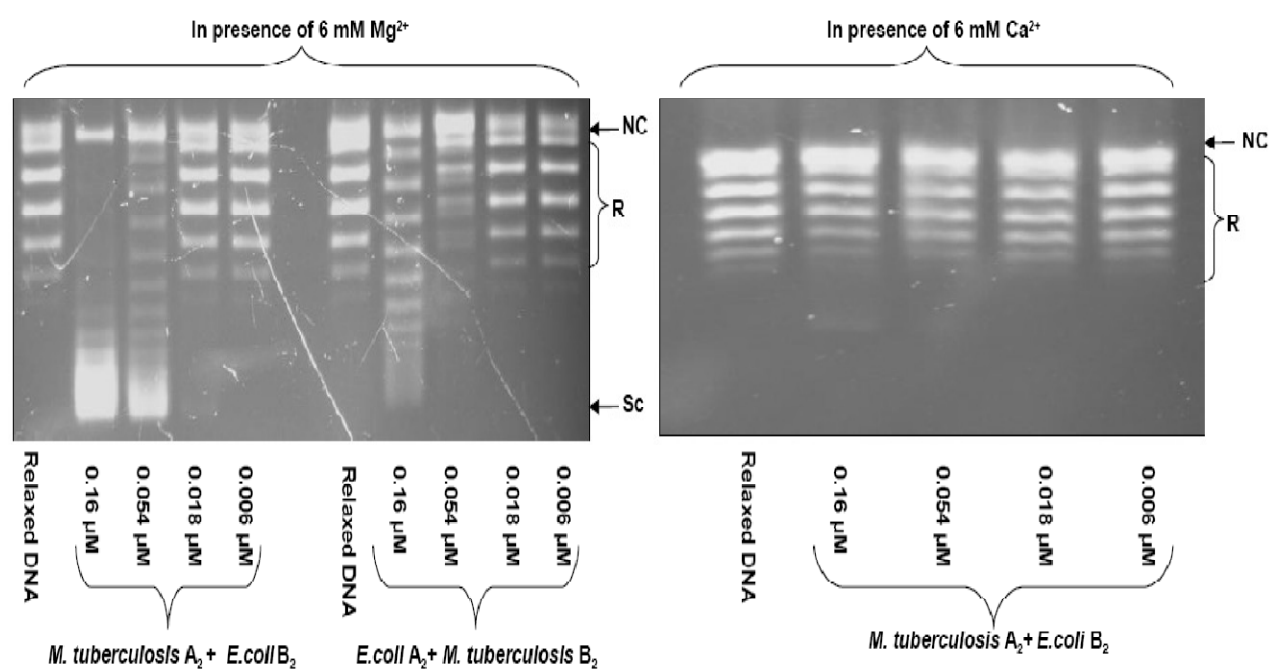


**Figure 4.2: Supercoiling assay of *M. tuberculosis* and *E. coli* hybrid enzyme in the presence of 6 mM Mg<sup>2+</sup> and 6 mM Ca<sup>2+</sup>. NC: nicked Circular DNA, R: relaxed topoisomers, SC: supercoiled DNA.**

The results of the experiment can be summarised as follows (**Table 4.1**):

GyrA	GyrB	Mg <sup>2+</sup>	Ca <sup>2+</sup>
<i>E. coli</i>	<i>E. coli</i>	+	+
<i>M. tuberculosis</i>	<i>M. tuberculosis</i>	+	-
<i>E. coli</i>	<i>M. tuberculosis</i>	-	NT
<i>M. tuberculosis</i>	<i>E. coli</i>	+	-

**Table 4.1: Summary of supercoiling activity of wild-type and hybrid enzymes in the presence Mg<sup>2+</sup> and Ca<sup>2+</sup>. +: activity observed; -: no activity; NT: not tested.**

Studies involving the use of hybrid enzymes have been performed in the past for *X. albilineans* (Hashimi *et al.*, 2008), *P. falciparum* (Dar *et al.*, 2007, Dar *et al.*, 2009) and *B. subtilis* (Orr & Staudenbauer, 1982) DNA gyrase subunits in combination with *E. coli* DNA gyrase subunits. These studies have provided important information about activity of enzyme. In the case of *X. albilineans* (Xa), DNA gyrase shows 20- to 25-fold higher resistance than *E. coli* DNA (Ec) gyrase to albicidin. In order to test the hypothesis that the GyrA subunit confers albicidin resistance, hybrid enzyme (XaA+EcB) was reconstituted. The reconstituted hybrid enzyme (XaA+EcB) showed the same level of resistance as the native *X. albilineans* DNA gyrase (XaAB). Thus it implies that the GyrA subunit is the albicidin target. Similarly it was shown using the hybrid enzyme (XaA+EcB) that *X. albilineans* GyrA subunit is associated with an inability to relax supercoiled DNA (Hashimi *et al.*, 2008). In the case of *P. falciparum*, hybrid enzyme studies were carried out to investigate the importance of a 45-amino-acid residue insertion in the Toprim domain of *P. falciparum* GyrB (Pf GyrB) which is not present in prokaryotic DNA gyrase. No DNA cleavage and supercoiling activity was observed with the 45 amino acid deletion mutant (Pf GyrB $\Delta$ 45) and *E. coli* GyrA indicating that the 45 amino acid residues in the Toprim domain of PfGyrB has a role in DNA binding and cleavage (Dar *et al.*, 2009).

Similarly when the *B. subtilis* DNA gyrase subunits were purified for the first time, their activities were verified by reconstituting hybrid enzymes with *E. coli* DNA gyrase subunits (Orr & Staudenbauer, 1982). All these observations are summarised in **Table 4.2**.

Supercoiling and relaxation assays were also performed for *M. tuberculosis* DNA gyrase in the presence of 4 mM Mg<sup>2+</sup> and 1 mM Ca<sup>2+</sup>. The enzyme activity in the presence of this divalent mixture was similar to that in the presence of 4 mM Mg<sup>2+</sup> alone.

GyrA	GyrB	Enzyme Activity / Effect
<i>X. albilineans</i>	<i>E. coli</i>	Albicidin resistance similar to native <i>X. albilineans</i> DNA gyrase .
<i>X. albilineans</i>	<i>E. coli</i>	No relaxation activity
<i>E. coli</i>	<i>X. albilineans</i>	No supercoiling activity but relaxation activity observed.
<i>E. coli</i>	<i>P. falciparum</i> GyrB $\Delta$ 45	No DNA cleavage or supercoiling activity.
<i>E. coli</i>	<i>B. subtilis</i>	Supercoiling activity observed.
<i>B. subtilis</i>	<i>E. coli</i>	No supercoiling activity observed.
<i>M. tuberculosis</i>	<i>E. coli</i>	Supercoiling activity observed.
<i>E. coli</i>	<i>M. tuberculosis</i>	No supercoiling activity observed.

**Table 4.2: Summary of the activity of hybrid enzymes from different sources.**

## 4.2 Ca<sup>2+</sup>-assisted Mg<sup>2+</sup>-dependent enzyme

According to the model MtGyrA-1BQB (**Figure 3.22**), there is the possibility of the presence of two Ca<sup>2+</sup> in the predicted binding site. It was decided to see if there is any effect of Ca<sup>2+</sup> chelation on the activity of the enzyme. Since EGTA is a specific chelator of Ca<sup>2+</sup>, it was decided to dialyse the *M. tuberculosis* GyrA subunit in the presence of 1 mM EGTA as described in **Material and Methods**. There was little effect of EGTA dialysis on the supercoiling and decatenation activity of the enzyme (**Figure 4.3**). EGTA dialysis affected the relaxation activity of the enzyme.

The relaxation activity of the EGTA-dialysed sample was ~2-3 fold weaker than the relaxation activity of enzyme dialysed in the absence of EGTA (**Figure 4.4, A&C**). Interestingly, this weak relaxation activity due to EGTA dialysis was regained by the addition of 1 mM Ca<sup>2+</sup> to the assay and it was similar to the relaxation activity of *M. tuberculosis* GyrA prior to EGTA dialysis (**Figure 4.4, A&D**). The final Ca<sup>2+</sup> concentration in the assay was 1 mM and the EGTA concentration was 200  $\mu$ M.

Time-course experiments were performed to analyse the loss in relaxation activity due to the EGTA dialysis of GyrA wild-type. As shown in the **Figure 4.5**, weaker relaxation activity is observed for GyrA dialysed in EGTA at different time points in comparison to GyrA dialysed without EGTA. At 125 min and 180 min, we observe a ladder of topoisomers for the GyrA dialysed without EGTA; these topoisomers may be positive supercoiled and are not observed in GyrA dialysed in EGTA. The apparent difference in the rate of the relaxation reaction in the presence or absence of EGTA is ~2-3 folds, consistent with the results in **Figure 4.4**.

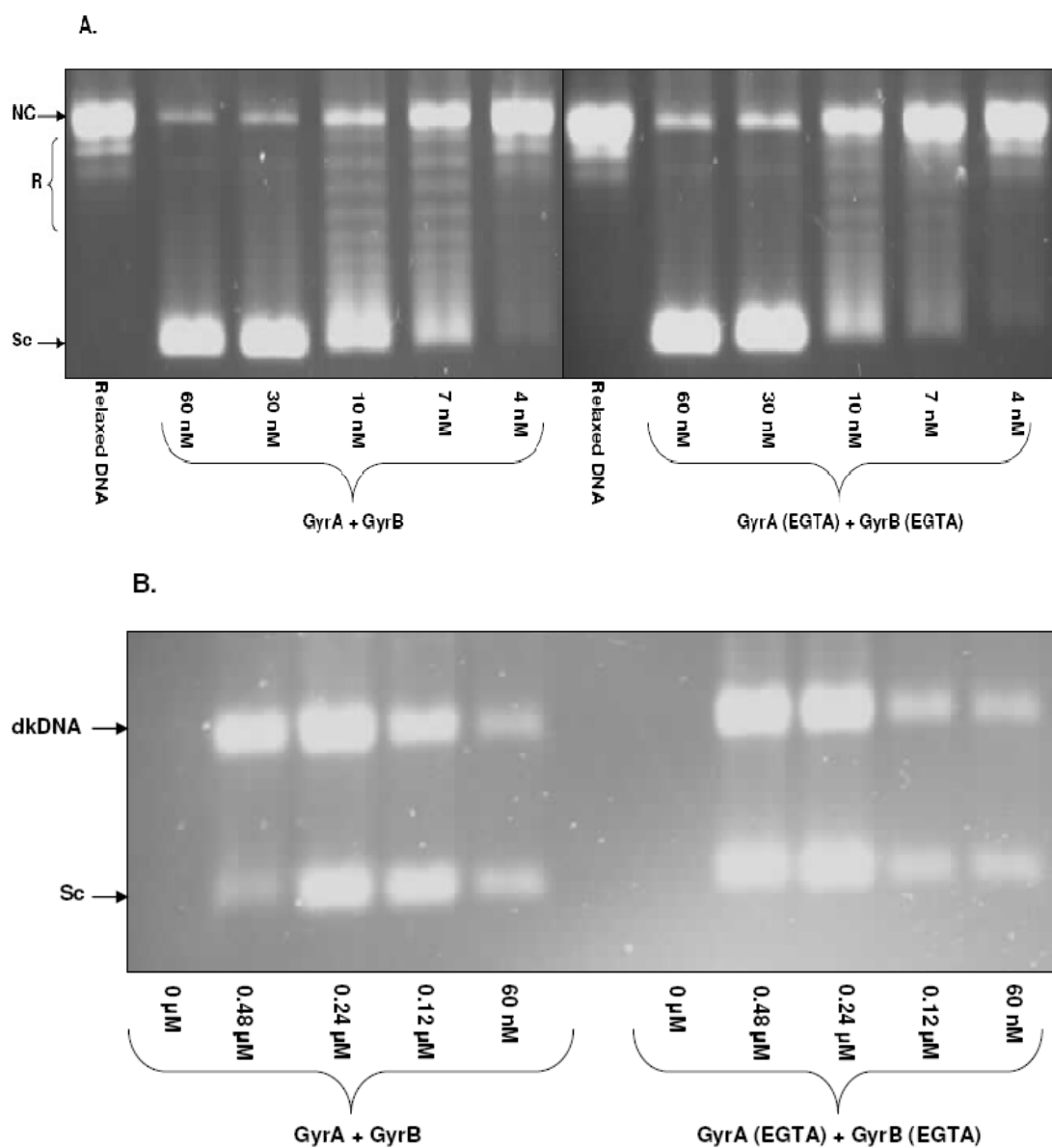


**Figure 4.3: Effect of EGTA dialysis on the supercoiling and decatenation activity of *M. tuberculosis* DNA gyrase.** The little effect of EGTA dialysis on the supercoiling activity (A) can be seen at 10 & 7 nM; while the effect on decatenation activity (B) can be seen at 0.12  $\mu$ M and 60 nM. NC: nicked Circular DNA, R: relaxed topoisomers, SC: supercoiled DNA, dkDNA: decatenated DNA.

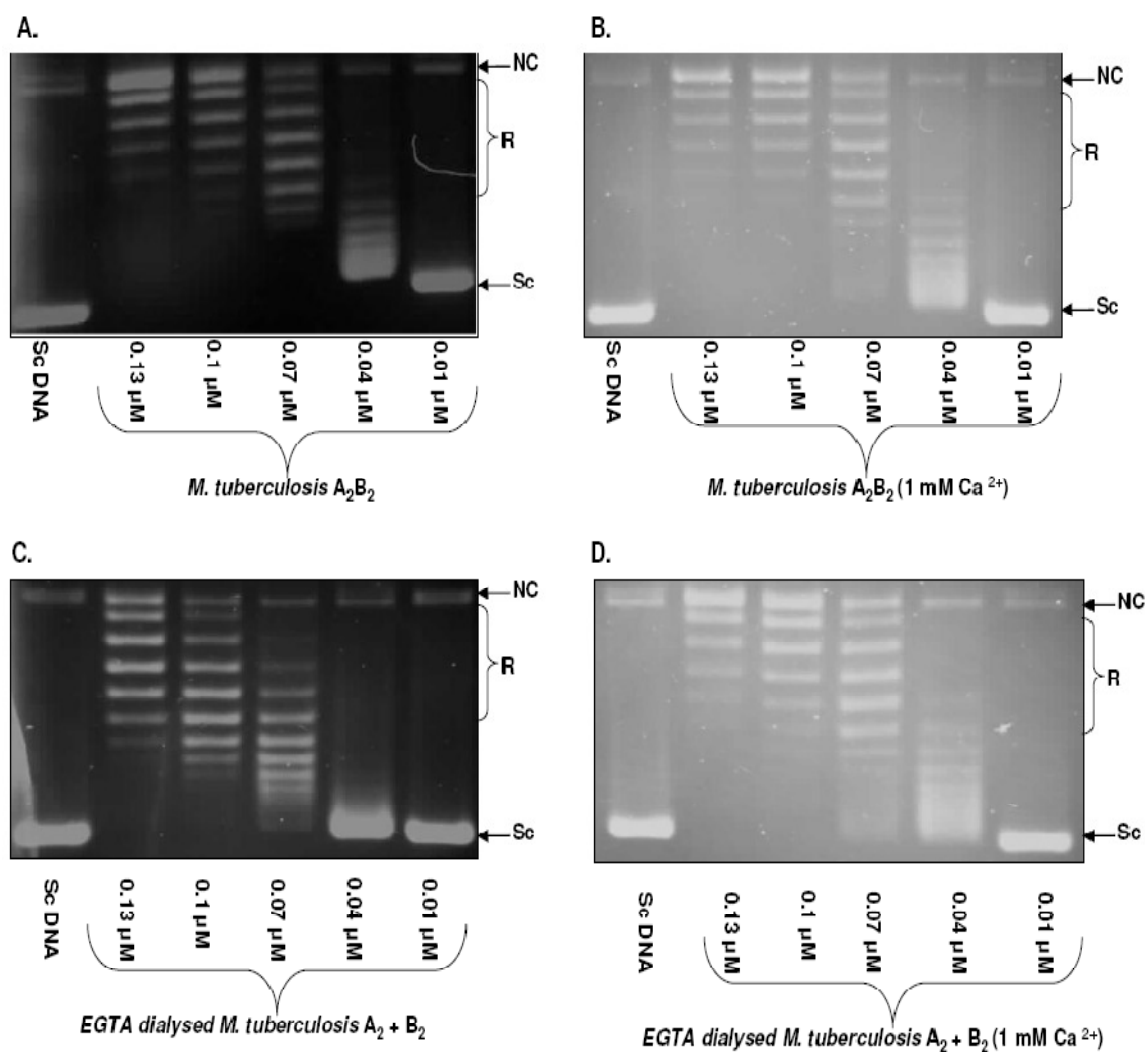


**Figure 4.4: DNA relaxation assay in the presence and absence of 1 mM  $\text{Ca}^{2+}$ .** *M. tuberculosis* gyrase in the presence and absence of 1 mM  $\text{Ca}^{2+}$  (A, B); EGTA dialysed *M. tuberculosis* GyrA + GyrB in the presence and absence of 1 mM  $\text{Ca}^{2+}$  (C, D). Reduced relaxation activity due to EGTA dialysis (C) is regained by inclusion of 1 mM  $\text{Ca}^{2+}$  in the assay (D); as indicated by a similar topoisomerase pattern as seen in (A) & (B). NC: nicked Circular DNA, R: relaxed topoisomers, SC: supercoiled DNA.

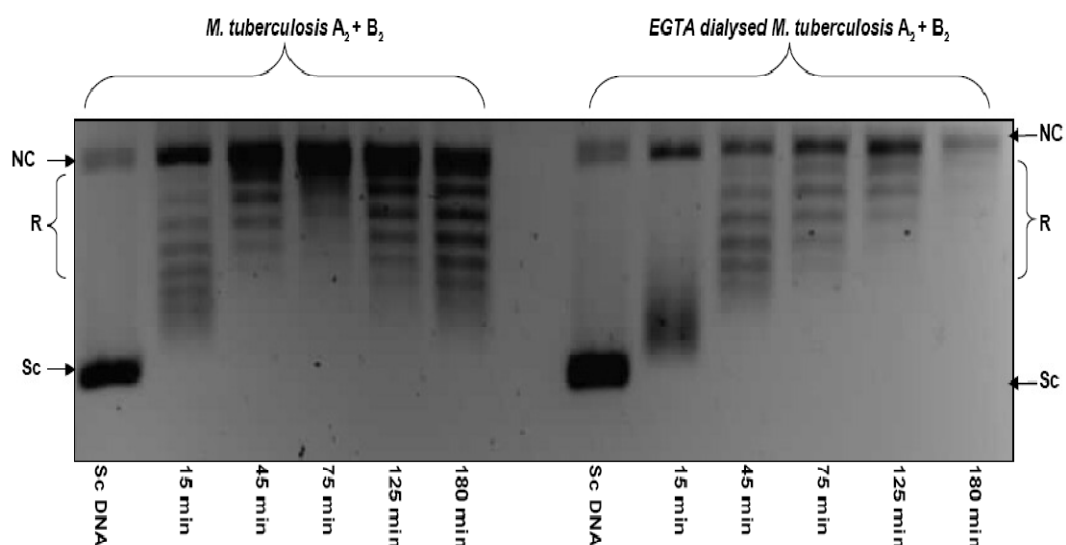


**Figure 4.5:** Time-course experiment to demonstrate the difference in the relaxation activity of GyrA dialysed in the absence and presence of EGTA. The weaker relaxation activity of GyrA dialysed in EGTA is demonstrated by the topoisomer distribution. NC: nicked Circular DNA, R: relaxed topoisomers, SC: supercoiled DNA.

The observed effects on the relaxation activity of *M. tuberculosis* DNA gyrase enzyme due to EGTA dialysis prompted protein-refolding experiments in the presence of EGTA. This method is a harsh treatment for the protein to make sure that any tightly bound  $\text{Ca}^{2+}$  is removed during protein refolding in the presence of EGTA. In short, the purified *M. tuberculosis* GyrA pool was divided into two main fractions based on their dialysis in 1 mM EGTA. Each of these fractions was further divided into two fractions. One fraction was denatured with guanidine hydrochloride/urea and refolded, while the other fraction was not refolded. The details of the protein refolding are described in detail in **Material and Methods** section.

In order to ensure that  $\text{Ca}^{2+}$  contamination is not carried over from *M. tuberculosis* GyrB in the assay, the purified pool of *M. tuberculosis* GyrB was divided into two fractions. Each of the fractions was dialysed in the presence or absence of 1 mM EGTA; *M. tuberculosis* GyrB was not denatured and refolded unlike *M. tuberculosis* GyrA (**Figure 4.6**).

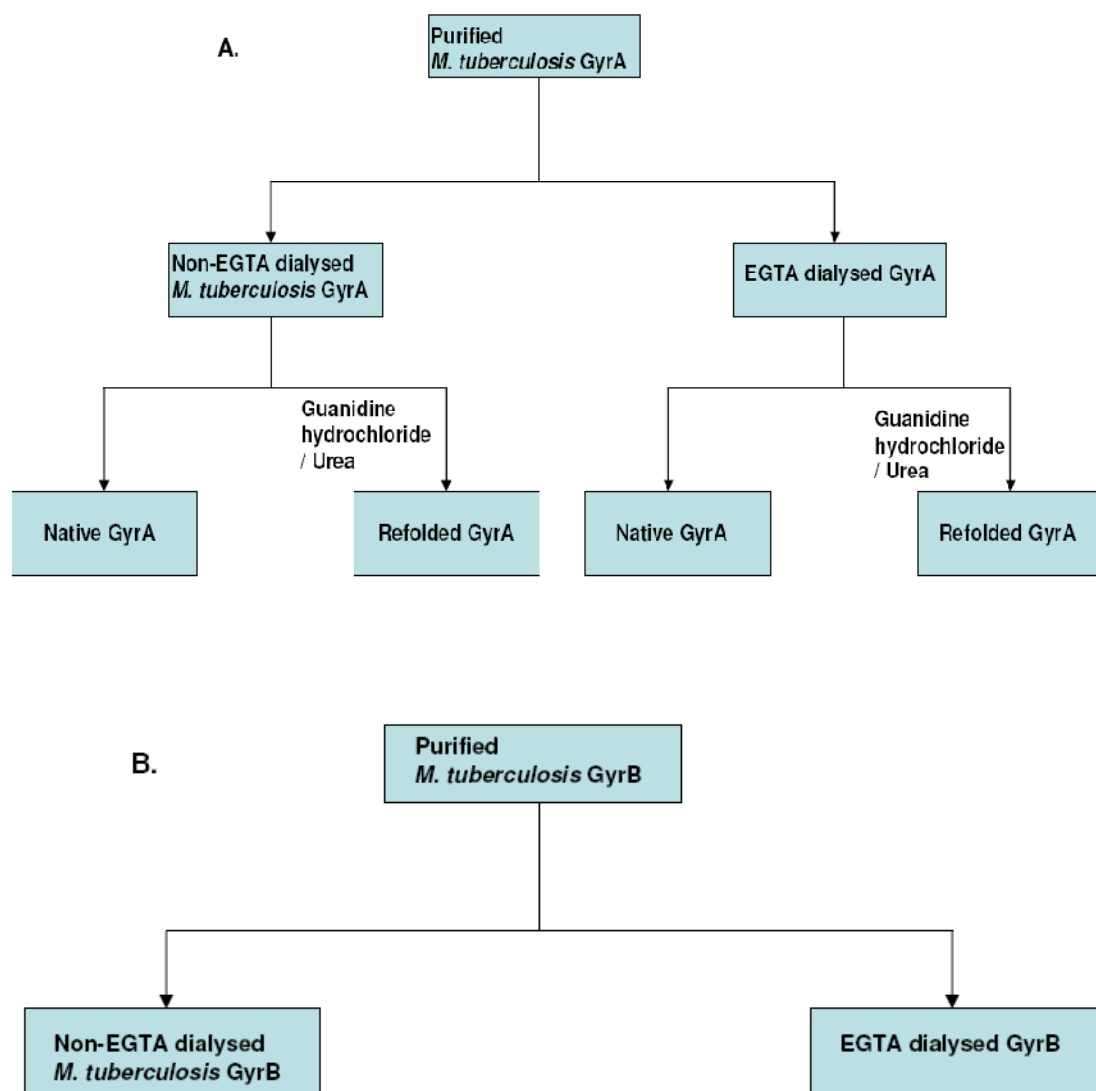


**Figure 4.6: Experimental plan for protein refolding experiment.**

(A) Flow chart for *M. tuberculosis* GyrA refolding experiment. (B) Flow chart for *M. tuberculosis* GyrB EGTA dialysis.

The *M. tuberculosis* GyrA samples from the refolding experiment were analysed for  $\text{Ca}^{2+}$  and  $\text{Mg}^{2+}$  concentration by ICP-AES (Inductively coupled plasma atomic emission spectroscopy). The details of this ICP-AES technique are described in detail in the Materials and Method section. This method is useful for determining the concentration of trace elements like  $\text{Ca}^{2+}$  and  $\text{Mg}^{2+}$  (**Table 4.3**, **Table 4.4**). Although this technique is sensitive for detecting trace elements, it has its limitations. It is important to consider these limitations for experimental design and data analysis. ICP-AES estimates the total concentration of divalent ions like  $\text{Ca}^{2+}$  and  $\text{Mg}^{2+}$  in the sample, but it does not provide any information about the amount of divalent ions bound to the protein sample alone. Data inconsistency can also be a problem due to external contamination. These can be common contaminants such as  $\text{Ca}^{2+}$  from glassware and plastic ware. For example, the apparent  $\text{Ca}^{2+}$  concentration in the two buffers (B) as shown by asterisk is very different. This illustrates the potential difficulties with this method and it means that small differences in  $\text{Ca}^{2+}$  concentration are unreliable.

Based on the **Table 4.3**, 50  $\mu\text{M}$  of  $\text{Ca}^{2+}$  is associated with the native *M. tuberculosis* GyrA and the protein concentration is 10  $\mu\text{M}$  per dimer. Therefore,  $\sim 5$   $\text{Ca}^{2+}$  atoms are associated with the native protein dimer. This is consistent with the MtGyrA-1BQB model in terms of the presence of two  $\text{Ca}^{2+}$  per *M. tuberculosis* GyrA subunit or four  $\text{Ca}^{2+}$  per *M. tuberculosis* GyrA dimer.

The difference in  $\text{Ca}^{2+}$  concentration between the native and refolded protein is  $\sim 20$   $\mu\text{M}$ . Although the amount of  $\text{Mg}^{2+}$  is comparatively less in the samples, there is an increase in its concentration in the refolded sample. This may be due to contamination or that during the refolding process the putative  $\text{Ca}^{2+}$ - binding site binds  $\text{Mg}^{2+}$ , which is available in the buffer environment. This is not surprising as the calcium EF-hand binding sites shows affinity towards  $\text{Mg}^{2+}$  (Gifford *et al.*, 2007).

Protein	Ca <sup>2+</sup> concentration Buffer (B) ng/ml	Ca <sup>2+</sup> concentration Protein (A) ng/ml	A-B ng/ml
1. GyrA native (2 mg/ml) ~10 μM	*453.98	2455.8	2001.82 = 50 μM
2. GyrA refolded (2 mg/ml) ~10 μM	*70.379	1324	1253.621 = 31 μM

Protein	Mg <sup>2+</sup> concentration Buffer (D) ng/ml	Mg <sup>2+</sup> concentration Protein (C) ng/ml	C-D ng/ml
1. GyrA native (2 mg/ml) ~10 μM	7.7415	121.2	113.458 = 4.6 μM
2. GyrA refolded (2 mg/ml) ~10 μM	5.777	321.76	315.983 = 12 μM

**Table 4.3: ICP-AES Estimation of Ca<sup>2+</sup> and Mg<sup>2+</sup> in native and refolded *M. tuberculosis* GyrA. These single measurements were recorded at 317 nm.**

When *M. tuberculosis* GyrA is dialysed and refolded in the presence of EGTA, there is decrease in the amount of Ca<sup>2+</sup>. There is a difference of 26 μM (A-E) between the Ca<sup>2+</sup> concentration of protein dialysed with and without EGTA. This difference is comparatively less in case of protein refolded in the presence and absence of EGTA. It is 6 μM (A-E) which may be due to contamination or it may be the remaining free Ca<sup>2+</sup> in the solution that cannot be further removed by EGTA chelation. Thus, EGTA treatment was effective in reducing the Ca<sup>2+</sup> concentration in the sample.

<b>Protein</b>	<b>Ca<sup>2+</sup> concentration in Buffer (F) ng/ml</b>	<b>Ca<sup>2+</sup> concentration Protein (E) ng/ml</b>	<b>E-F ng/ml</b>
1. GyrA native (2 mg/ml) ~10 $\mu$ M	95.615	1040.3	944.685 =23 $\mu$ M
2. GyrA refolded (1 mg/ml) ~5 $\mu$ M	81.461	1063.2	981.739 =24 $\mu$ M

<b>Protein</b>	<b>Mg<sup>2+</sup> concentration Buffer (H) ng/ml</b>	<b>Mg<sup>2+</sup> concentration Protein (G) ng/ml</b>	<b>G-H ng/ml</b>
1. GyrA native (2 mg/ml) ~10 $\mu$ M	5.8249	35.29	29.4651 = 1.2 $\mu$ M
2. GyrA refolded (1 mg/ml) ~5 $\mu$ M	8.856	94.793	85.937 = 3.5 $\mu$ M

**Table 4.4: ICP-AES Estimation of Ca<sup>2+</sup> and Mg<sup>2+</sup> in *M. tuberculosis* GyrA dialysed or refolded in the presence of 1 mM EGTA. These single measurements were recorded at 317 nm.**

The samples analysed by ICP-AES were used for studying the effect of EGTA and refolding on the enzyme activity of the treated samples. DNA supercoiling, relaxation and decatenation assays were performed. The summary of the results are shown in **Table 4.5**.

<i>M. tuberculosis</i> DNA gyrase	Supercoiling activity	Relaxation activity	Decatenation activity
1. GyrA + GyrB	+++	+++	+++
2. Refolded GyrA + GyrB	+++	+++	+++
3. EGTA- dialysed GyrA + EGTA-dialysed GyrB	++	No activity	++
4. Refolded EGTA- dialysed GyrA+ EGTA -dialysed GyrB	+	No activity	No activity

**Table 4.5: Summary table for the effect of EGTA dialysis and refolding on the enzyme activity.** + represents ~ 3 fold difference in the enzyme activity.

As shown in **Figure 4.7 & Figure 4.8**, there is no effect of refolding alone on the enzyme activity of *M. tuberculosis* GyrA (supercoiling, relaxation and decatenation). This suggests that the refolding procedure does not damage the protein and it acts as a control for the refolding done in the presence of 1 mM EGTA. Although the concentration of  $\text{Ca}^{2+}$  based on ICP-AES analysis is less in the refolded GyrA (31  $\mu\text{M}$ ) in comparison to the native protein (50  $\mu\text{M}$ ), there is no effect of this decrease in the  $\text{Ca}^{2+}$  concentration on the enzyme activity. This may be because in the absence of chelating agent such as EGTA there is an opportunity for the protein to acquire  $\text{Ca}^{2+}$  from the surrounding medium.

In contrast to this, dialysis or refolding *M. tuberculosis* GyrA in the presence of 1 mM EGTA leads to complete loss of relaxation activity and weak supercoiling activity. The supercoiling activity is weakest when *M. tuberculosis* GyrA is refolded in the presence of 1 mM EGTA. This effect of weak supercoiling activity is similar to the effect of mutations in the  $\text{Ca}^{2+}$ -binding site which will be discussed in the next section. Decatenation activity of GyrA dialysed in EGTA is weaker in comparison to GyrA dialysed in the absence of EGTA. While complete loss of decatenation activity is observed when GyrA is refolded in the presence of 1 mM EGTA. This experiment suggests that EGTA is effective in chelating  $\text{Ca}^{2+}$  from the protein, which has significant effect on the enzyme activity. The interesting observation is the complete loss of relaxation and decatenation activity while weak supercoiling activity is

retained. This indicates that the protein is not completely denatured and the observation is due to the specific effect of EGTA on the relaxation / decatenation reactions.

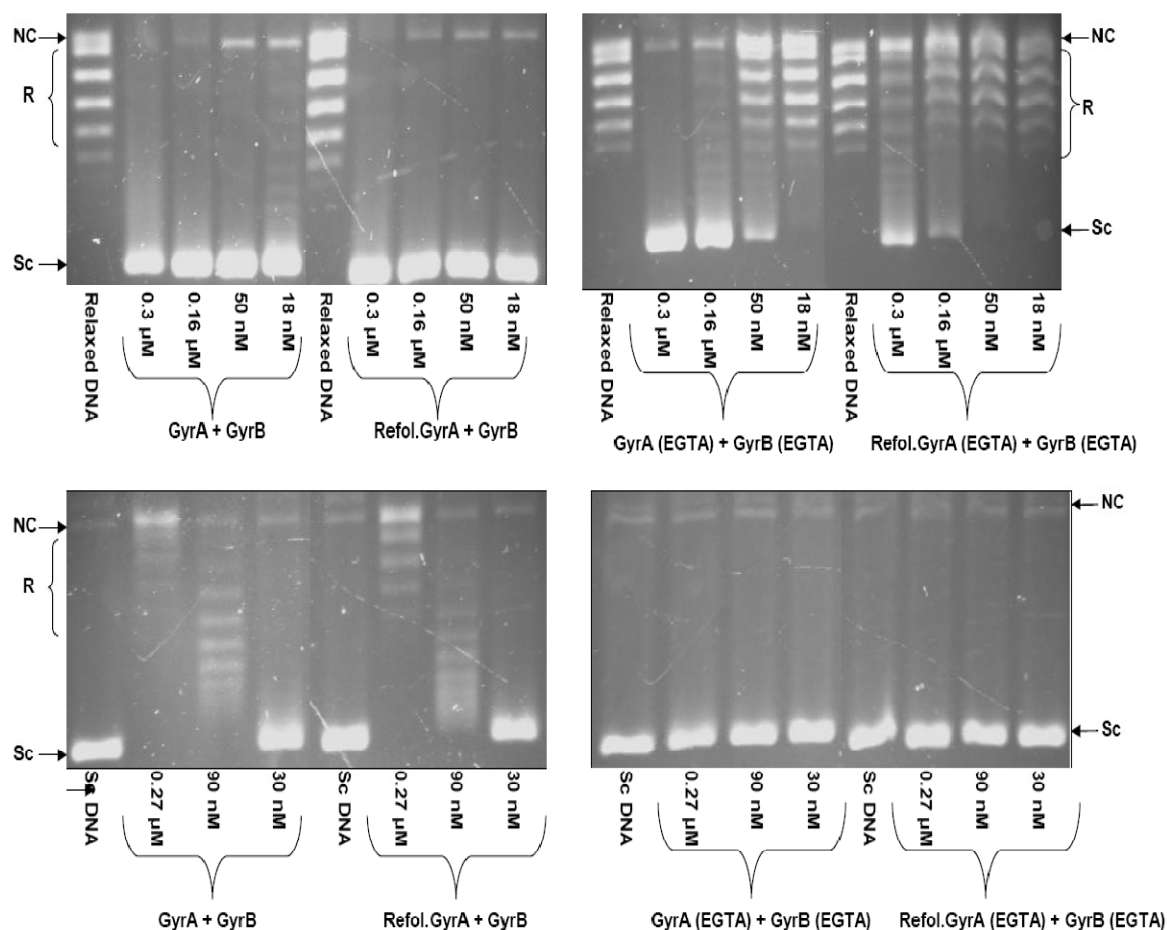


**Figure 4.7: Effect of protein refolding in the presence and absence of EGTA on the supercoiling and relaxation activity of DNA gyrase.** *Weak supercoiling activity (top panel) and loss of relaxation activity (bottom panel) due to dialysis or refolding of M. tuberculosis GyrA in the presence of 1 mM EGTA. NC: nicked Circular DNA, R: relaxed topoisomers, SC: supercoiled DNA.*

The complete loss of relaxation and weak supercoiling activity due to EGTA dialysis in this experiment is different from the weak relaxation activity observed on EGTA dialysis in previous experiment. This may be due to difference is several factors such as protein batch, availability of  $\text{Ca}^{2+}$  for effective chelation by EGTA and external contamination due to  $\text{Ca}^{2+}$ . However, the consistent observation in all the experiments is the effect of EGTA dialysis on the relaxation activity of *M. tuberculosis* DNA gyrase.

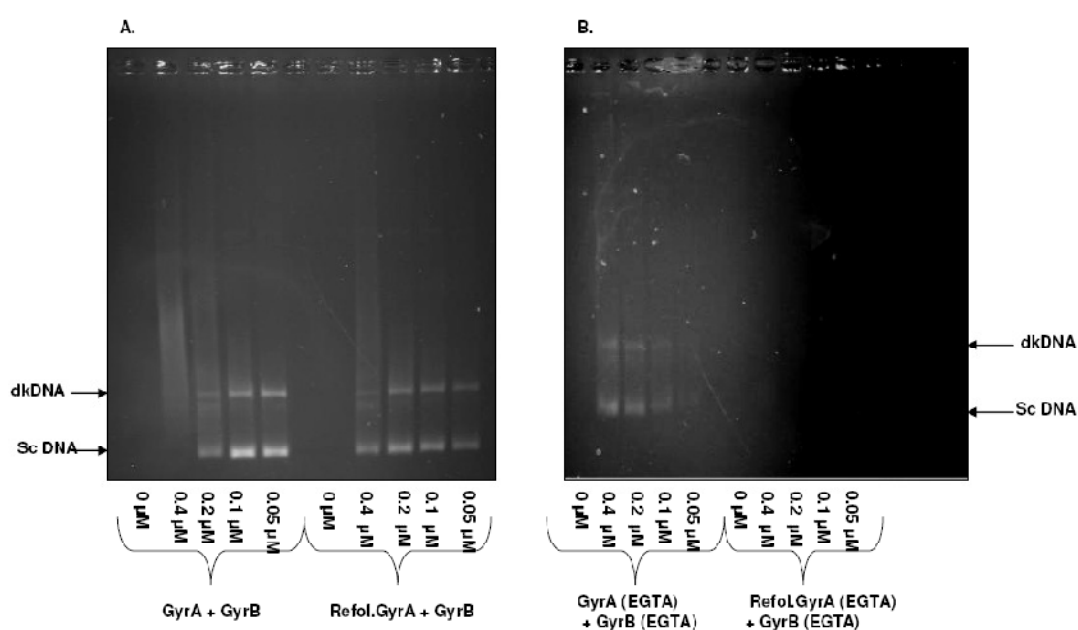


**Figure 4.8: Effect of protein refolding in the presence and absence of EGTA on the decatenation activity of DNA gyrase. dkDNA: decatenated DNA, SC: supercoiled DNA.**

### 4.3 SDM of the $\text{Ca}^{2+}$ -binding site

Based on the *M. tuberculosis* GyrA model described previously, double (E508A, D509A) and quadruple mutants (D504A, E508A, D509A, E514A) were created in the putative  $\text{Ca}^{2+}$ -binding site by site-directed mutagenesis. The acidic amino acids that were proposed to be directly involved in  $\text{Ca}^{2+}$ -binding were mutated by site-directed mutagenesis to alanine as described in **Materials and Methods**. Some of the residues that were mutated are involved in  $\text{Ca}^{2+}$ -binding in both MtGyrA-1H71 and MtGyrA-1BQB model. Residue D509 is involved in coordinating

$\text{Ca}^{2+}$  only in MtGyrA-1BQB model and D504 is involved in coordinating  $\text{Ca}^{2+}$  in MtGyrA-1H71 model. The double mutation as shown in (Figure: 4.9) involved mutation of Glu 508 (GAG) to Ala (GCG) and Asp 509 (GAT) to Ala (GCT). In addition to the double mutation, two more mutations were introduced in the double mutant involving residues Asp 504 (GAC) and Glu 514 (GAG) to Ala (GCT) as shown in the Figure 4.9, Figure 4.10 & Figure 4.11.

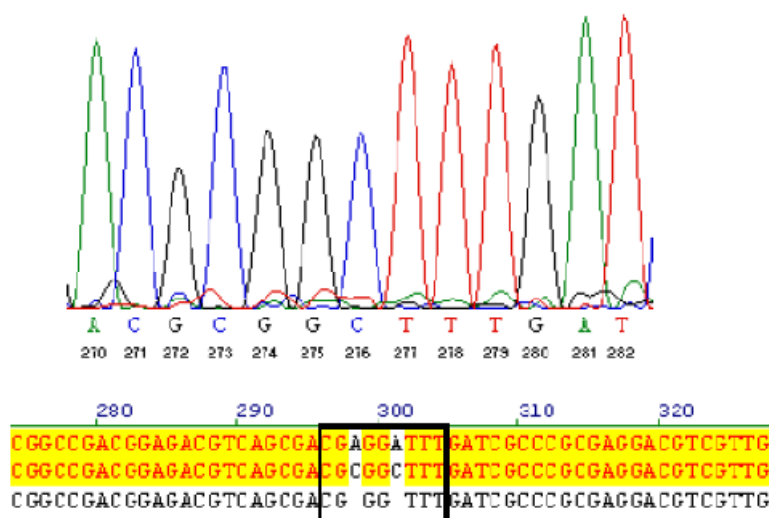


Figure 4.9: Double mutation in the  $\text{Ca}^{2+}$  - binding site: Glu508 to Ala and Asp509 to Ala.

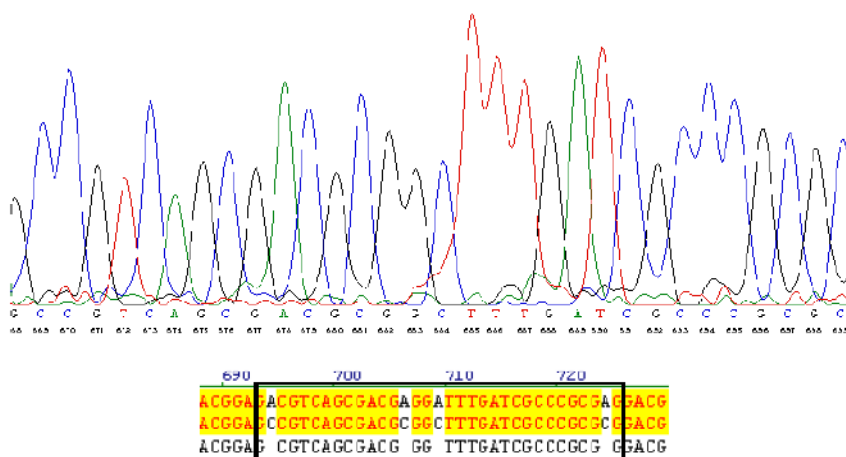
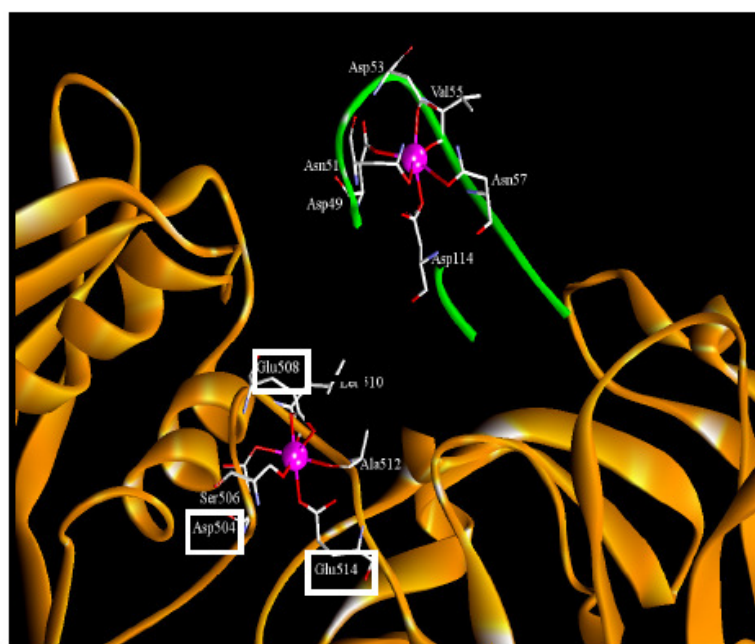
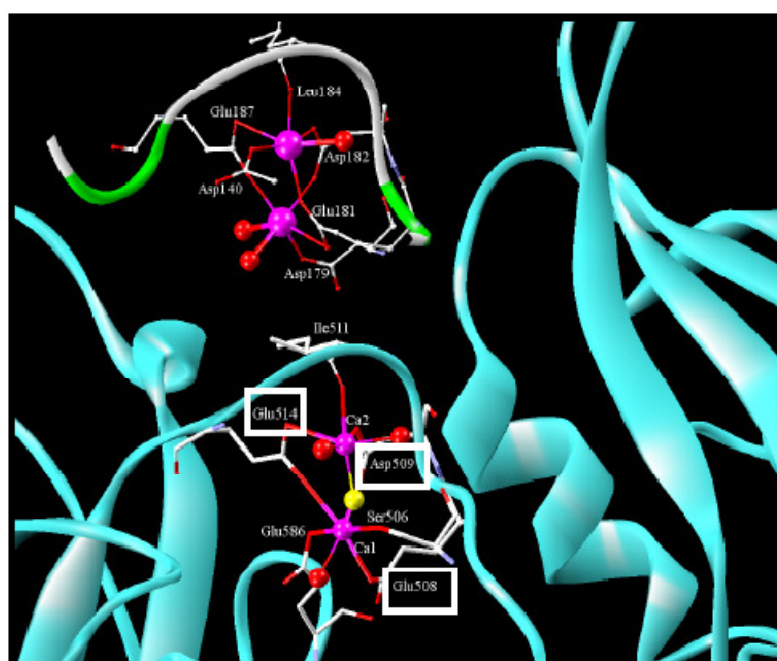


Figure 4.10: Quadruple mutation in the  $\text{Ca}^{2+}$ -binding site: Glu508 to Ala; Asp509 to Ala; Asp 504 to Ala and Glu 514 to Ala.



MtGyrA-1H71



MtGyrA-1BQB

**Figure 4.11: Acidic amino-acids in MtGyrA-1H71 and MtGyrA-1BQB model that were mutated to alanine in side-directed mutagenesis experiments.**

DNA gyrase activity assays (supercoiling, relaxation and decatenation) were performed to study the effect of double (GyrA E508A, D509A) and quadruple mutations (GyrA D504A, E508A, D509A, E514A) on the enzyme activity. There was no significant effect of double mutations (GyrA E508A, D509A) on the supercoiling activity of the enzyme. Weak supercoiling activity observed at 10 nM enzyme concentration in case of double mutant may be due to experimental error (**Figure 4.12**). While in case of the quadruple mutant (GyrA D504A, E508A, D509A, E514A) a significant effect was observed on the supercoiling activity of the enzyme in comparison to the wild-type. This is indicated by incomplete supercoiling as shown in **Figure 4.12**. This effect is even more marked when the supercoiling assay is performed in the buffer having magnesium chloride rather than magnesium acetate and without potassium glutamate as shown in the **Figure 4.13**. Interestingly no effect of the quadruple mutation (GyrA D504A, E508A, D509A, E514A) was observed on the relaxation (**Figure 4.14**) and decatenation activity (**Figure 4.15**) of the enzyme, though previous reports indicate a slight effect on the relaxation activity of the enzyme due to E514A mutations (Huang *et al.*, 2006).

Since there is little or no effect of the quadruple mutation (GyrA D504A, E508A, D509A, and E514A) on the decatenation activity of the enzyme, we assume that there will be no effect of the double mutation (GyrA E508A, D509A) on decatenation. From the assay, the significant observation is that the quadruple mutant (GyrA D504A, E508A, D509A, and E514A) is efficient in decatenation but it is not efficient in supercoiling DNA in comparison to the wild-type. This is evident from the observation that minicircles that are released from the megacircles during the decatenation reaction are supercoiled in case of the wild-type but not in case of quadruple mutant as shown in **Figure 4.15**.

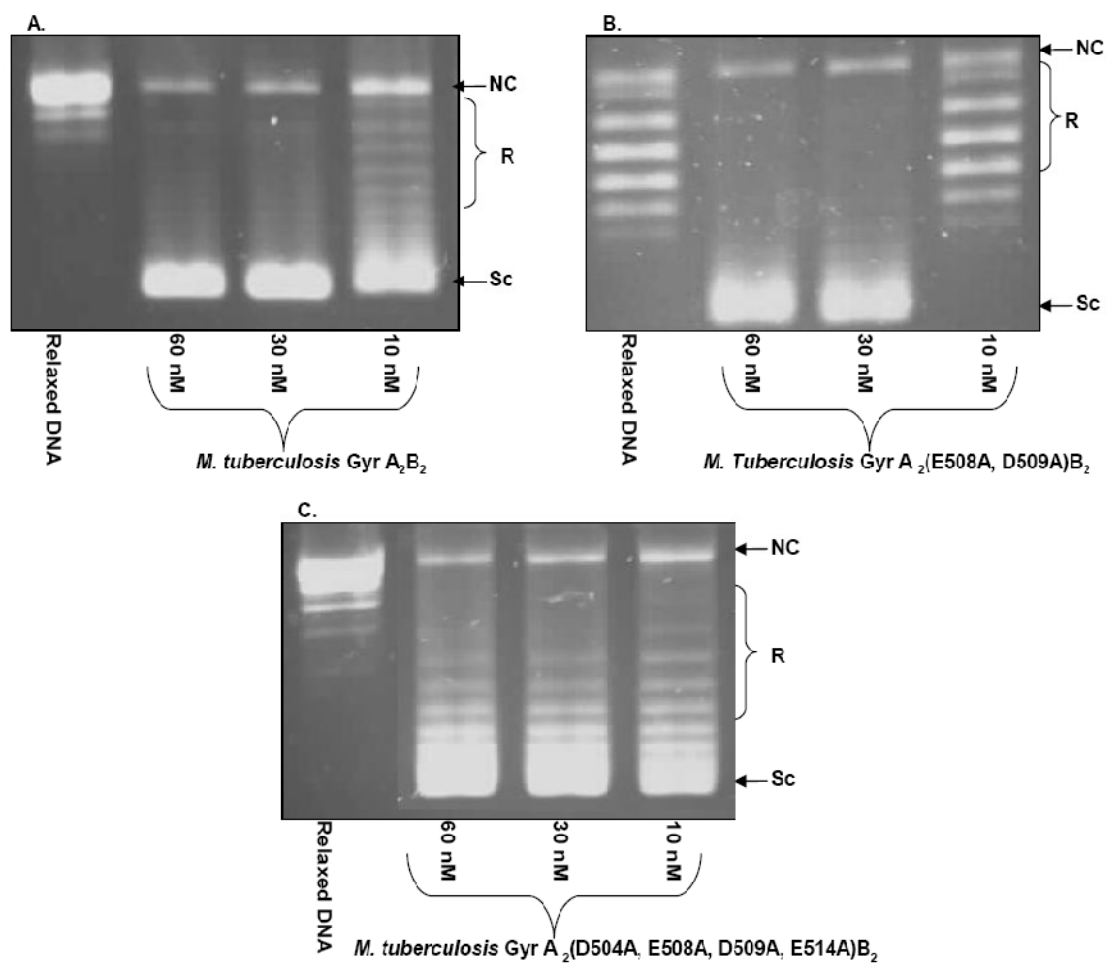


**Figure 4.12: Effect of double (GyrA E508A, D509A) and quadruple mutations (GyrA D504A, E508A, D509A, E514A) on supercoiling activity.** (A) Supercoiling activity of *M. tuberculosis* GyrA<sub>2</sub>B<sub>2</sub>. (B) Supercoiling activity of *M. tuberculosis* GyrA<sup>(E508A, D509A)</sup><sub>2</sub>B<sub>2</sub>. (C) Supercoiling activity of *M. tuberculosis* GyrA<sup>(D504A, E508A, D509A, E514A)</sup><sub>2</sub>B<sub>2</sub>. NC: nicked Circular DNA, R: relaxed topoisomers, SC: supercoiled DNA.

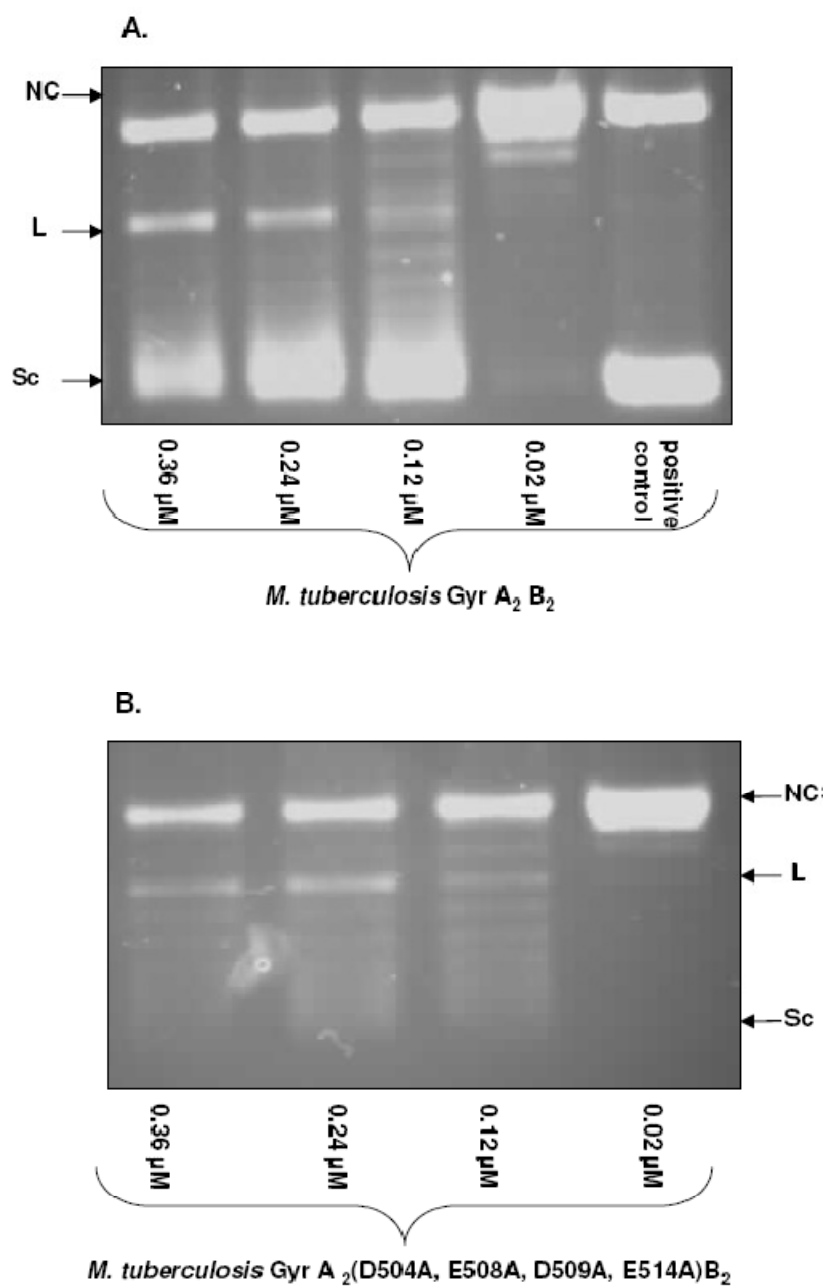


**Figure 4.13: Effect of quadruple mutations (GyrA D504A, E508A, D509A, E514A) on the supercoiling activity under different assay conditions.** *Little or no supercoiling is observed for the quadruple mutant (B) in comparison to the wild-type enzyme (A) in assay buffer having magnesium chloride and no potassium glutamate. The linear DNA is observed due to the sample treatment with SDS and proteinase K. This linear DNA is not observed with E. coli DNA gyrase as a positive control.*

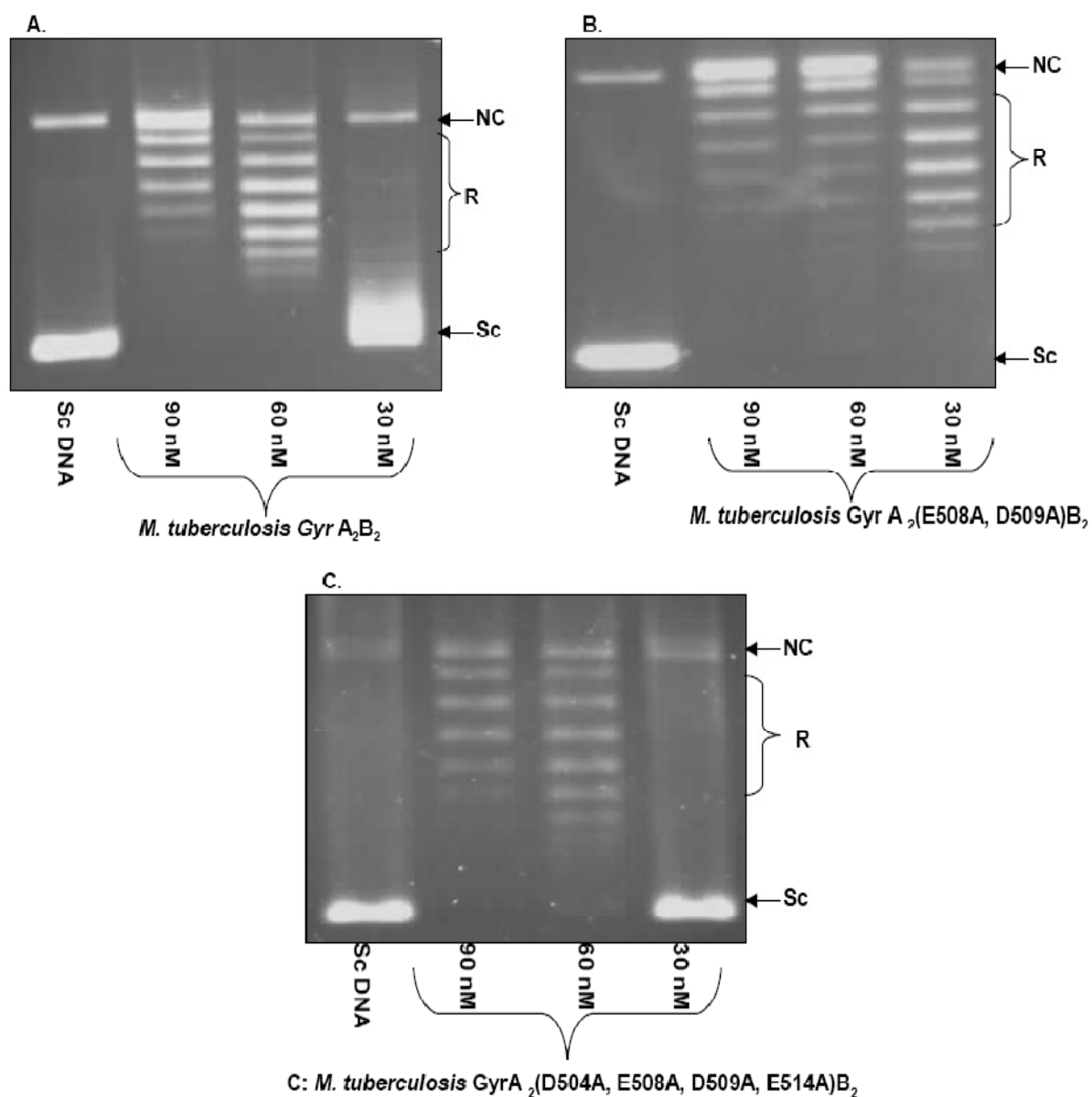


**Figure 4.14: No significant effect of double (GyrA E508A, D509A) and quadruple mutations (GyrA D504A, E508A, D509A, E514A) on the relaxation activity.** (A) Relaxation activity of *M. tuberculosis* GyrA<sub>2</sub>B<sub>2</sub>. (B) Relaxation activity of *M. tuberculosis* GyrA<sup>(E508A, D509A)</sup><sub>2</sub>B<sub>2</sub>. (C) Relaxation activity of *M. tuberculosis* GyrA<sup>(D504A, E508A, D509A, E514A)</sup><sub>2</sub>B<sub>2</sub>. NC: nicked Circular DNA, R: relaxed topoisomers, SC: supercoiled DNA.

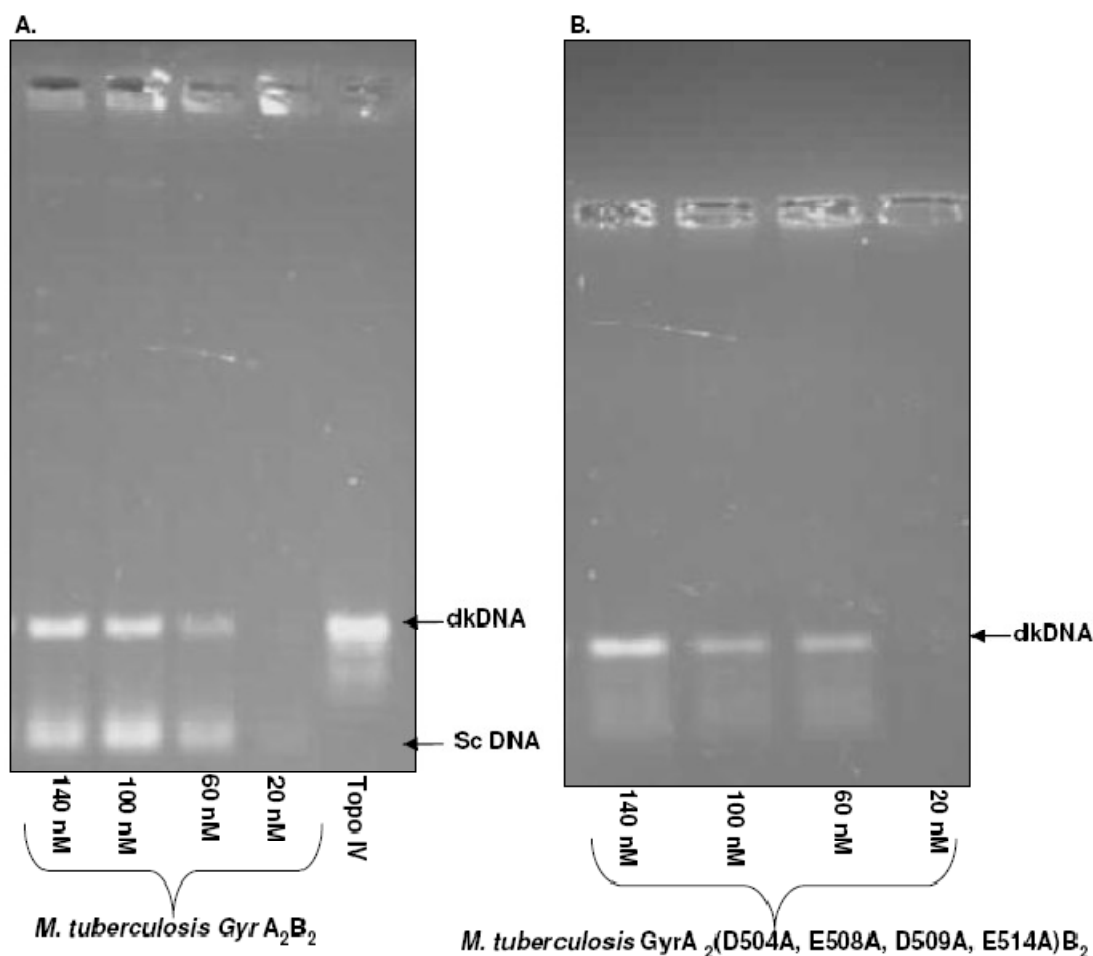


**Figure 4.15: Decatenation activity of the wild-type and quadruple mutant.** Efficient decatenation by (A) *M. tuberculosis* GyrA<sub>2</sub>B<sub>2</sub>; (B) *M. tuberculosis* GyrA<sub>2</sub><sup>(D504A, E508A, D509A, E514A)</sup>B<sub>2</sub>. *E. coli* topo IV decatenation activity is shown as a positive control. SC: supercoiled DNA and dkDNA: decatenated DNA.

Due to the weak supercoiling activity of the quadruple mutant (GyrA D504A, E508A, D509A, E514A), it was important to determine whether this was a specific effect due to the loss of Ca<sup>2+</sup> or it was due to the protein misfolding. Circular dichroism (CD) was employed to verify whether or not the quadruple mutant was folded correctly. Far-UV (180-260 nm) CD spectra was collected for both the GyrA WT and GyrA D504A, E508A, D509A- E514A mutant as shown in **Figure 4.16**.

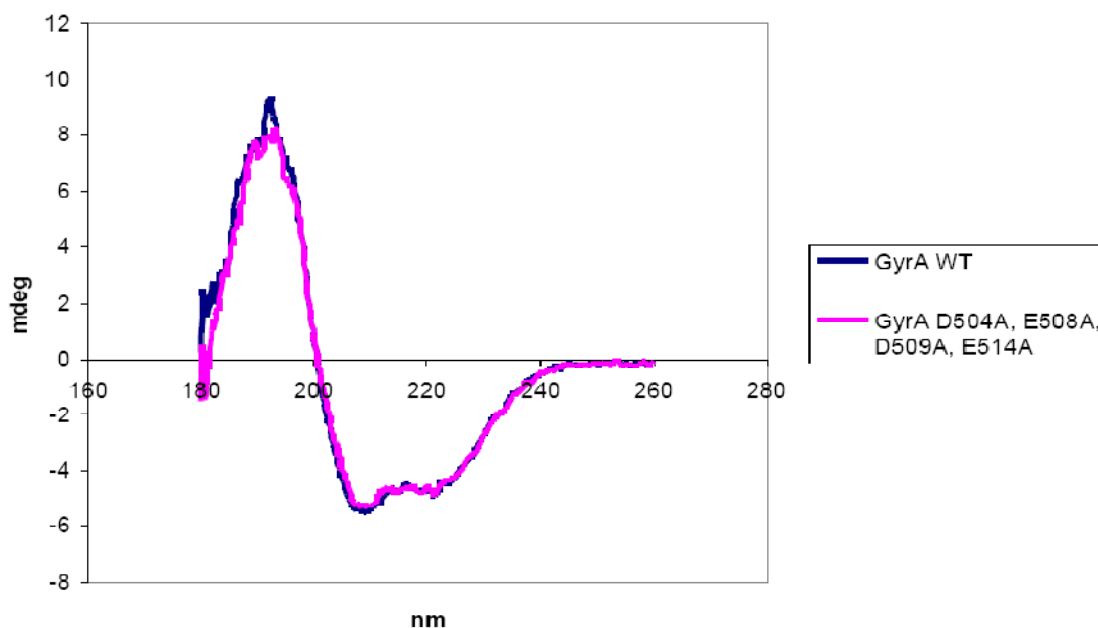


**Figure 4.16: Far-UV (180-260 nm) CD spectra of wild-type GyrA and GyrA D504A, E508A, D509A, E514A.** *The spectra were recorded at 20°C using a J-710 spectropolarimeter (Jasco Ltd.).*

The CD spectra of the wild-type and mutant proteins look similar suggesting that the mutant is not misfolded. Although the CD spectra clearly demonstrates that the four mutations in the quadruple mutant have not drastically affected its folding, but this data cannot rule out the more subtle changes due to the loss of  $\text{Ca}^{2+}$  from the binding site, which may have an effect on the supercoiling activity of the enzyme.

The weak supercoiling activity of the quadruple mutant (GyrAD504A, E508A, D509A, E514A) without any effect on the relaxation activity indicates that the mutation may have affected DNA wrapping. This is because DNA gyrase's unique ability to catalyse DNA supercoiling is thought to derive from the wrapping of G segment around the enzyme in such a way as to present a T segment to the ATP-operated clamp. The wrapping function resides in the C-terminal domain of GyrA.

It has been shown in previous studies that a *E. coli* GyrA C-terminal truncation mutant lacks supercoiling activity while retaining the relaxation activity due to the loss of the DNA-wrapping domain (Kampranis & Maxwell, 1996). The DNA wrapping assay is based on the principle that the DNA wrapping around the

GyrA C-terminal domain is positive in nature (Liu & Wang, 1978b, Kampranis *et al.*, 1999a, Liu & Wang, 1978a) and this can be demonstrated by using topo I. In a typical DNA wrapping assay, the DNA-gyrase complex is relaxed by topo I. Positive superhelical wrapping induces the formation of opposing negative crossovers in unconstrained regions of DNA that can be relaxed with topo I, while the positive supercoiled DNA around the wrapping domain, which is not accessible, cannot be relaxed with topo I. As a result, positively supercoiled DNA is produced after topo I relaxation of gyrase-DNA complexes. Similar experiments have also been performed in the past to investigate the DNA wrapping (Heddle *et al.*, 2004, Williams *et al.*, 2001).

As shown in **Figure 4.17**, positively supercoiled DNA is produced in case of wild-type GyrA after topo I treatment, which is not observed in case of quadruple mutant (D504A, E508A, D509A, E514A) indicating the effect of the mutations on DNA wrapping. This effect on wrapping could be due to the loss of  $\text{Ca}^{2+}$  at the  $\text{Ca}^{2+}$ -binding site due to the mutations. It can be suggested that  $\text{Ca}^{2+}$  may be important for maintaining the structural integrity of the DNA wrapping domain via the  $\text{Ca}^{2+}$ -binding site.

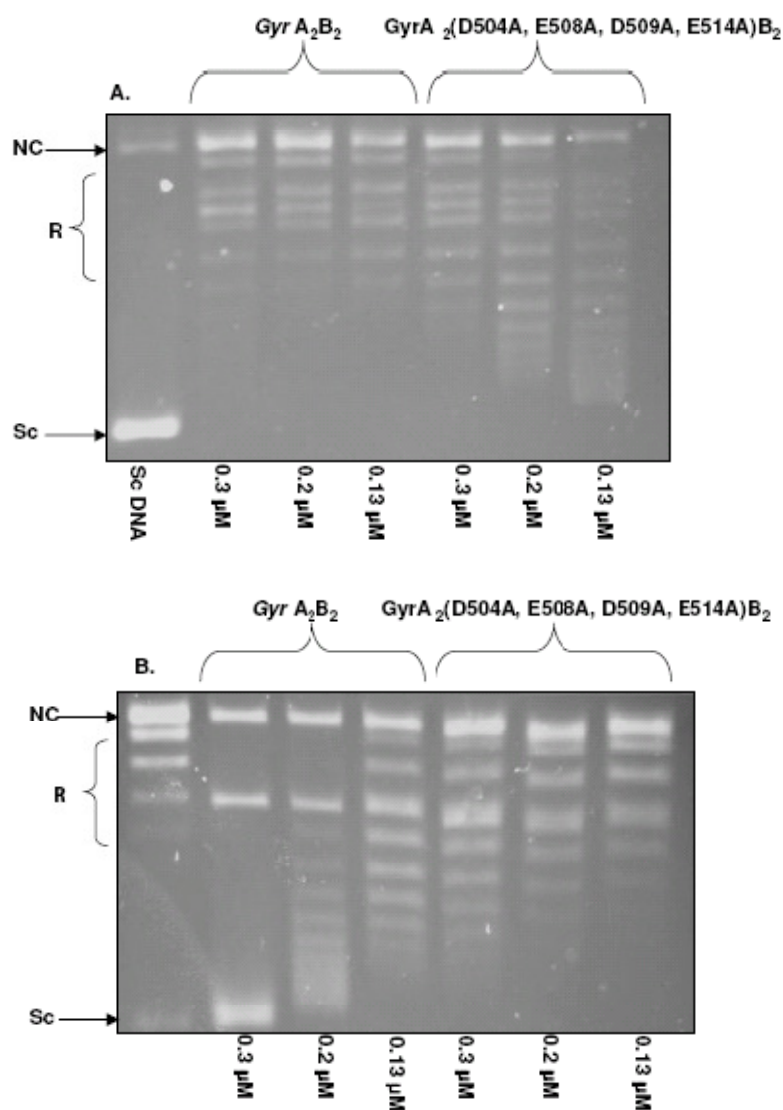


**Figure 4.17:** The effect of quadruple mutation (D504A, E508A, D509A, and E514A) on DNA wrapping around GyrA. (A) The relaxation assay of the GyrA WT and the quadruple mutant (D504A, E508A, D509A, E514A) without relaxing it further with topoisomerase I. (B) The other half of the reaction treated with wheat germ topoisomerase I.

## 4.4 Effect of EGTA on the activity of mutants

The quadruple mutation (GyrA D504A, E508A, D509A, and E514A) in the putative  $\text{Ca}^{2+}$ -binding site affected the supercoiling activity of the enzyme. It was decided to study the effect of EGTA dialysis on the enzyme activity of the mutants.

Little effect was observed on the supercoiling and relaxation activity of the double mutant (GyrA E508A, D509A) and the quadruple mutant (GyrA D504A, E508A, D509A, E514A) when dialysed in the presence of 1 mM EGTA as shown in the **Figure 4.18**.

Far-UV (180-260 nm) CD spectra were collected for both the GyrA WT and GyrA D504A, E508A, D509A, E514A mutant dialysed in 1mM EGTA as shown in the **Figure 4.19**. Although the spectra for the GyrA WT and GyrA D504A, E508A, D509A, E514A mutant do not appear identical, this is due to a protein concentration effect. Scaling the mutant spectra by the average difference to overlay with the spectra for the wild-type protein, we can see that the profiles of the plots are very similar, suggesting that both proteins are folded in the same configuration.

Thus these experiments demonstrate the following observations:

1. Weak supercoiling activity of the GyrA D504A, E508A, D509A, E514A mutant due to the effect of the mutations on DNA wrapping.
2. EGTA dialysis affects the relaxation activity of the wild-type enzyme which can be regained by adding  $\text{Ca}^{2+}$ .
3. Protein refolding in presence of EGTA affects the supercoiling and relaxation activity of the enzyme. The refolded wild-type enzyme is weak in supercoiling with complete loss of relaxation activity.

The observations discussed above clearly indicate the significance of  $\text{Ca}^{2+}$  and the  $\text{Ca}^{2+}$ -binding site.

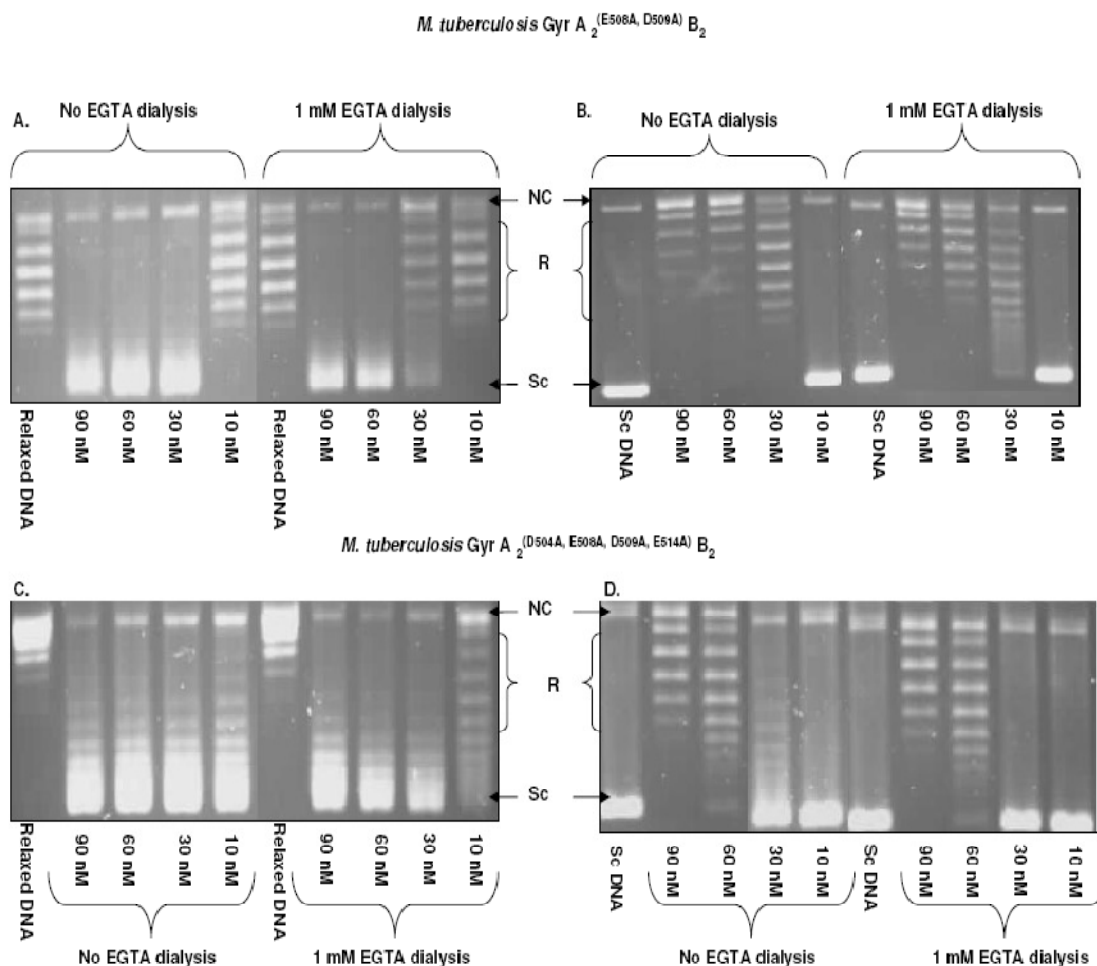


**Figure 4.18: Effect of EGTA on the supercoiling and relaxation activity of the mutants.** (A) Supercoiling activity of GyrA E508A, D509A mutant; (B) relaxation activity of GyrA E508A, D509A mutant; (C) supercoiling activity of GyrA D504A, E508A, D509A, E514A mutant (D) relaxation activity of GyrA D504A, E508A, D509A, E514A.

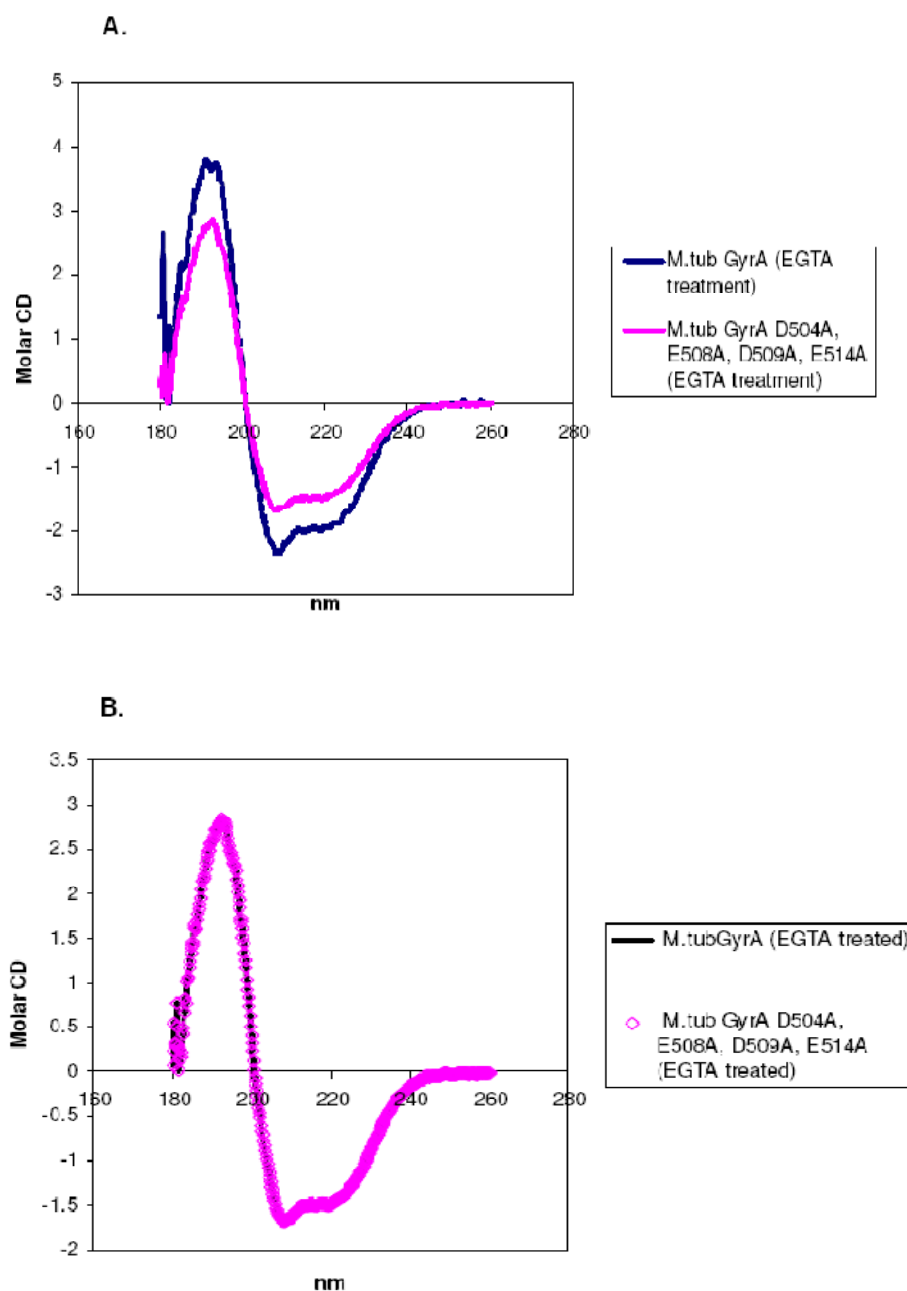


**Figure 4.19: Far-UV (180-260 nm) CD spectra of wild-type GyrA (dialysed in 1 mM EGTA) and GyrA D504A, E508A, D509A, E514A (dialysed in 1 mM EGTA). The spectra were recorded at 20°C using a J-710 spectropolarimeter (Jasco Ltd.). (A) Circular dichroism spectrum for wild-type GyrA (dialysed in EGTA) and (B) GyrA D504A, E508A, D509A, E514A (dialysed in EGTA); scaled to adjust for concentration effects.**

## 4.5 Limited Proteolysis of GyrA

From the site-directed mutagenesis and refolding experiments it is evident that there is an effect of removal of  $\text{Ca}^{2+}$  on the activity of GyrA. This effect indicates that  $\text{Ca}^{2+}$  may have structural and/or functional significance. Limited proteolysis experiments with trypsin were performed for GyrA in the presence and absence of  $\text{Ca}^{2+}$  to investigate protein conformational changes induced by  $\text{Ca}^{2+}$ , as described in the **Materials and Methods** section.

As shown in the **Figure 4.20**, there are differences in the trypsin digestion profile of GyrA in the presence and absence of 3 mM  $\text{Ca}^{2+}$ . One of the characteristic differences is the disappearance of a 47-kDa band in the presence of  $\text{Ca}^{2+}$  indicated by a rectangle in **Figure 4.20**. The same experiment was repeated with *M. tuberculosis* GyrB in the presence and absence of  $\text{Ca}^{2+}$  as a control. As shown in the **Figure 4.21**, little or no difference was observed in the digestion profile of the protein due to  $\text{Ca}^{2+}$ . This indicates that  $\text{Ca}^{2+}$  has a structural significance for GyrA and the disappearance of the 47-kDa band is a specific effect and is not due to changes in the activity of trypsin due to the presence of  $\text{Ca}^{2+}$ .

After observing changes in the trypsin digestion profile of GyrA in the presence of  $\text{Ca}^{2+}$ , the next step was to identify the different bands. This information will be useful for identifying the 47-kDa band and the protein domain that is affected by the presence of  $\text{Ca}^{2+}$ .

Edman sequencing was employed to identify the bands obtained by trypsin digestion of GyrA. The bands were first electroblotted onto a PVDF membrane as described in the **Material and Methods** section. After electroblotting, the bands were cut from the membrane and were sent for sequencing to the Proteomics facility. The Edman sequencing work was done under the guidance of Dr. Mike Naldrett (John Innes Centre). The bands that were electroblotted and sequenced are shown in the **Figure 4.22**. From the Edman sequencing data, the N-terminal sequences for the bands were obtained.

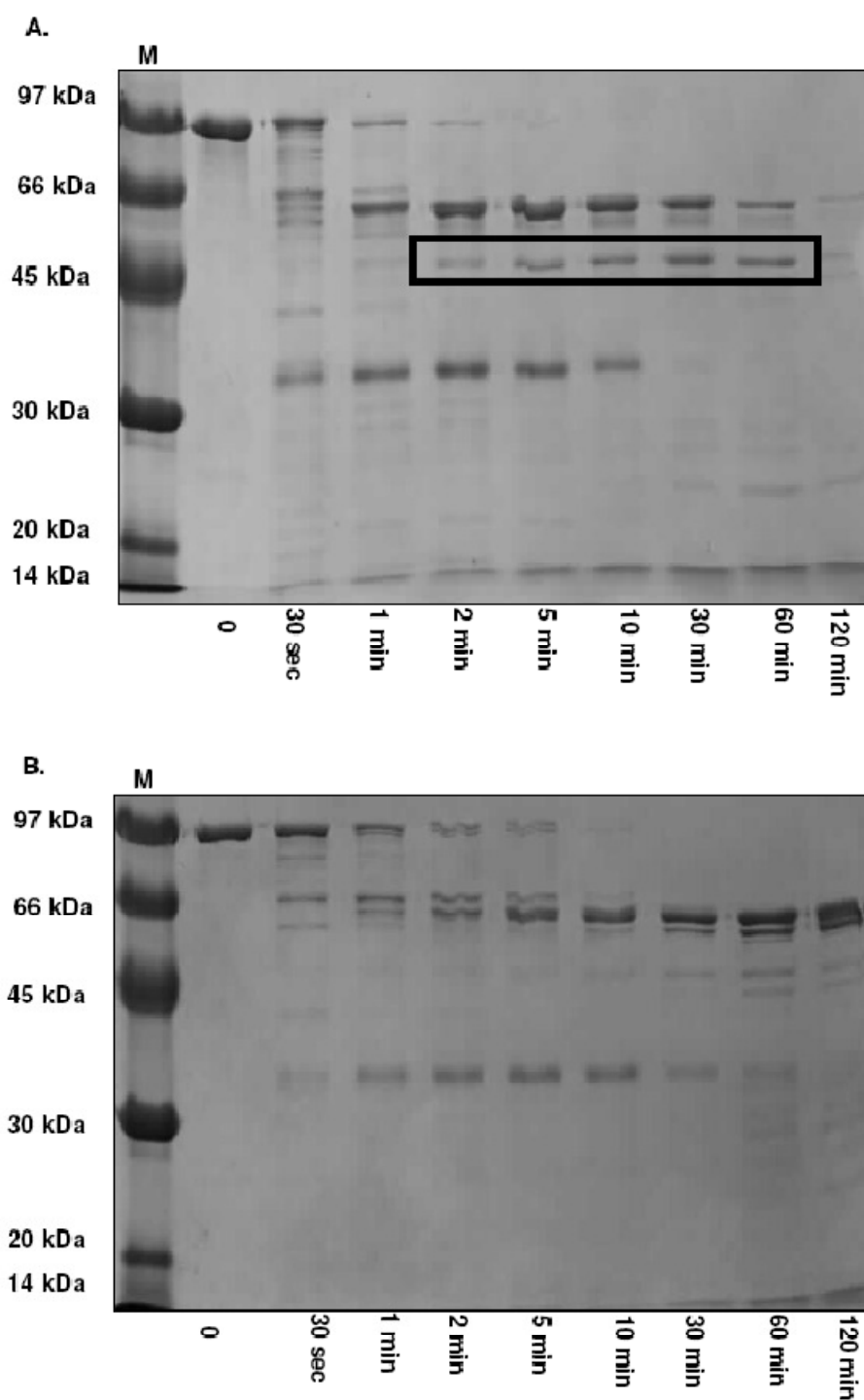


**Figure 4.20:** Tryptic digest of the *M. tuberculosis* GyrA in the absence of  $\text{Ca}^{2+}$  (A) and in the presence of  $\text{Ca}^{2+}$  (B). *M* indicates *GE* low molecular weight marker and the rectangle highlights the 47-kDa band.

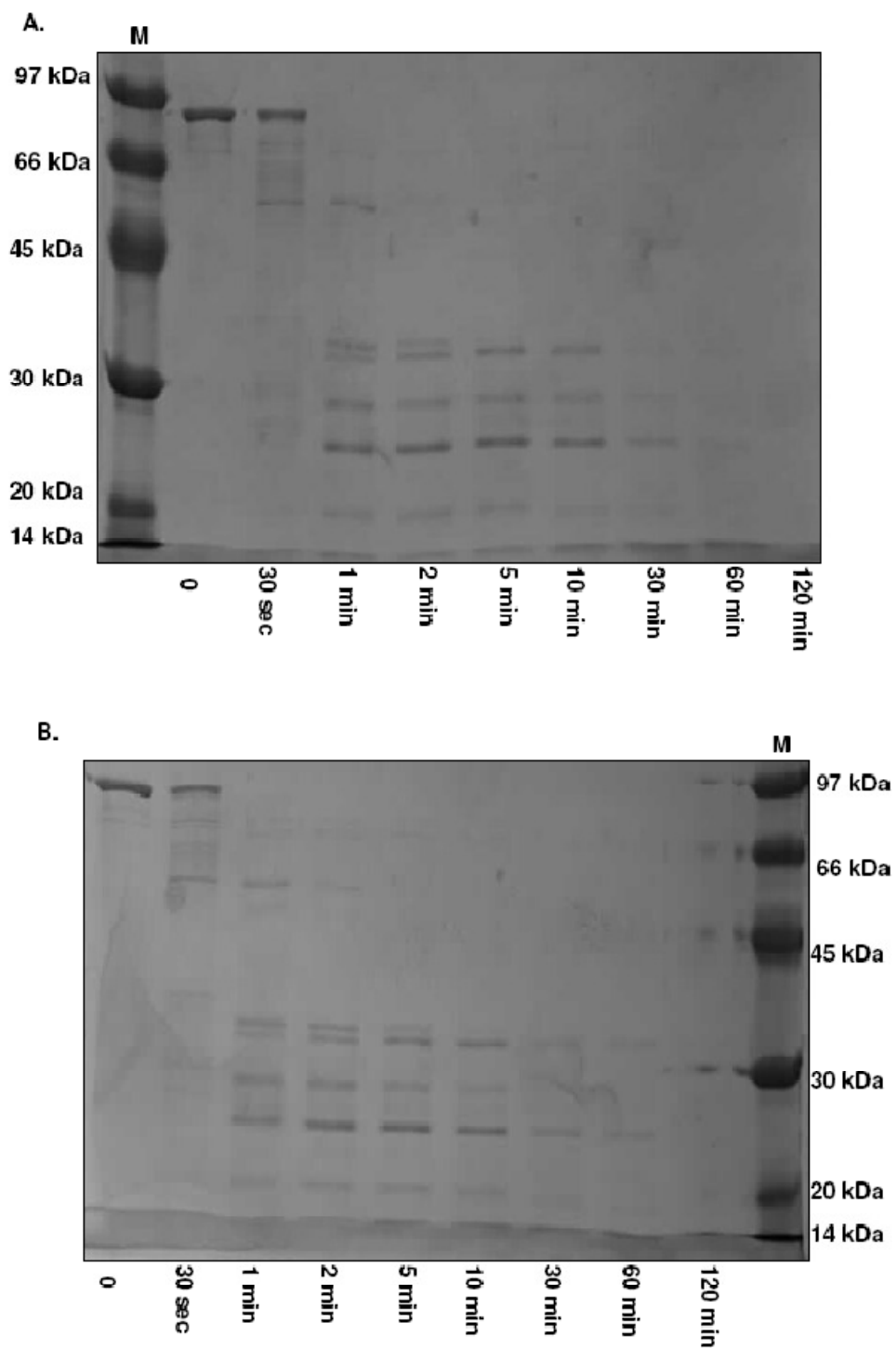


**Figure 4.21:** Tryptic digest of the *M. tuberculosis* GyrB in the absence of Ca<sup>2+</sup> (A) and in the presence of Ca<sup>2+</sup> (B). *M* indicates GE low molecular weight marker and rectangle represents the 47-kDa band.

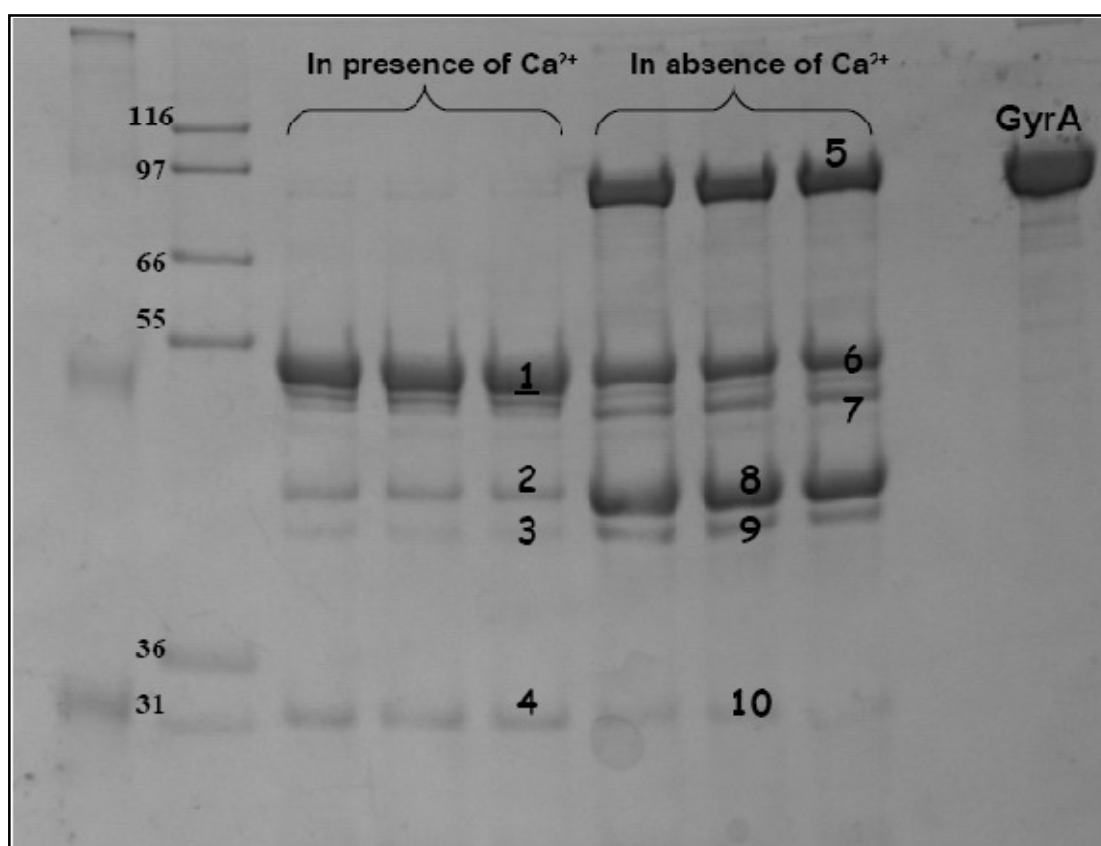


**Figure 4.22:** Trypsin digestion profile of *M. tuberculosis* GyrA in the presence and absence of Ca<sup>2+</sup> at 30 min time point analysed by 10% NuPAGE Novex Bis-Tris gel (Invitrogen). The bands that were sent for Edman sequencing are indicated by numbers.

The molecular weight of the bands was estimated by extrapolating the graph between the molecular weight of the protein ladder and its mobility as shown in the **Figure 4.23**. Based on the molecular weight and the N-terminal sequence of the bands, the sequence coverage of the bands was determined (**Table 4.6**).

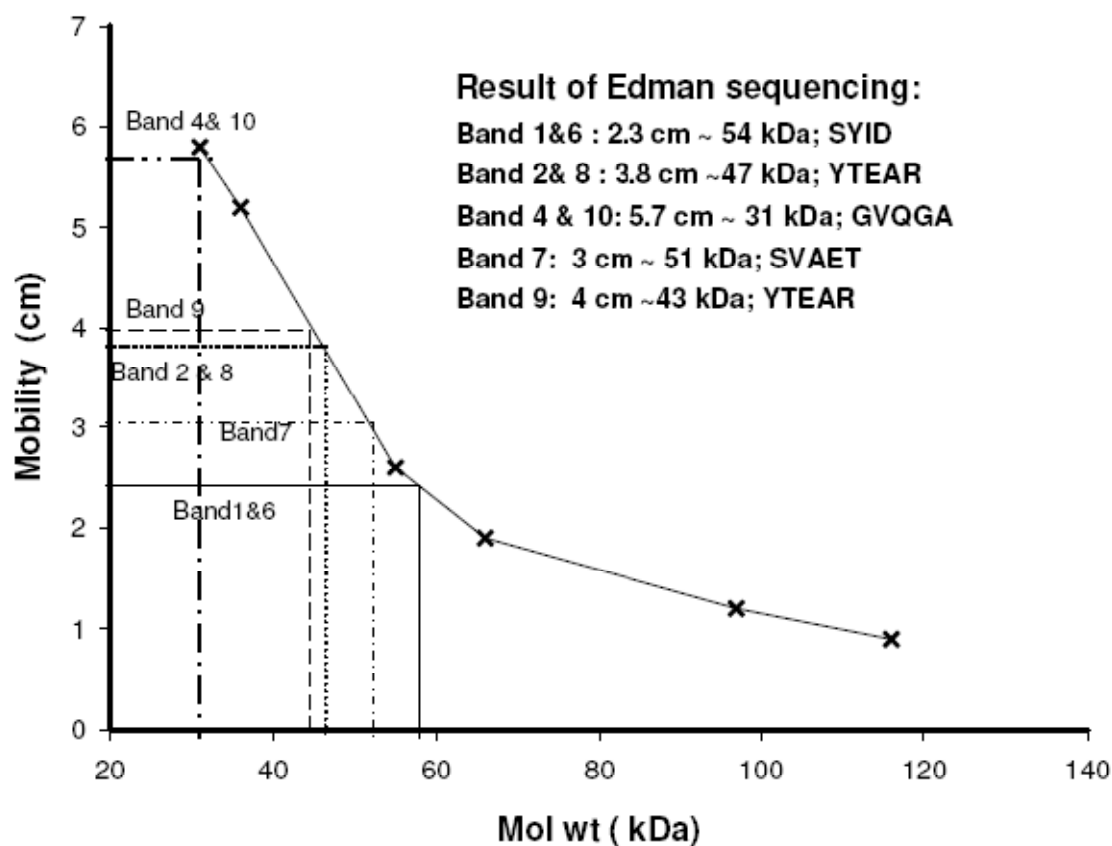


**Figure 4.23: Molecular weight estimation of the bands.** *This was done by extrapolating the mobility of the band against the graph plotted between the mobility of the protein ladder against its molecular weight (kDa).*

Bands	N-terminal sequence (Edman sequencing)	Molecular weight (approx)	Sequence coverage
1 & 6	R26↓SYID	~ 54-kDa	S27- G503
7	R75↓SVAET	~51-kDa	S76 - K542
2 & 8	R128↓YTEAR	~47-kDa	Y129 - K542
9	R128↓YTEAR	~43-kDa	Y129 - G503
4 & 10	K542↓GVQGA	~ 31-kDa	543G -N839

**Table 4.6: Sequence coverage and molecular weights for bands (1- 10).**

```

> M. tuberculosis GyrA
MTDTTLPDDSLDRIEVDIEQEMQRSYIDYAMSVIVGRALPEVRDGLKPVHRRVLYAMFDSGFRPDR
SHAKSARSVAETMGNYHPHGDA SIYDSLVRMAQPWSLRYPLVDGQGNFGSPGNDPPAAMR ↓ YTEARLT
PLAMEMLREIDEETVDFIPNYDGRVQEP TVLP SRFPNLLANGSGGIAVGMATNIPPHNLRELADAVFW
ALENHDADEEETLAAVMGRVKGPDFPTAGLIVGSQGTADAYKTGRGSIRMRGVVEEEDSRGRTSLVI
TELPYQVNHDFNFI TSIAEQVRDGLAGISNIEDQSSDRVGLRIVIEIKRDAVAKVVINNLYKHTQLQT
SFGANMLAIVDGPVPTLRLDQLIRYYVDHQLDVIVRRTTYRLRKANERAHILRGLVKALDALDEVIAL
IRASETVDIARAGLIELLDIDEIQAQA I LDMQLRRLAALERQRI IDDLAKIEAEIADLED I LAKPERQ
RGIVRDELAEIVDRHGDDRRTRIIAAD GDVSD E DLIARE D V VVTITETGYAKR TKTDLYRSQKRGGK ↑
GVQGAGLKQDDIVAHFFVCSTHDLILFFTTQGRVYRAKAYDLPEASRTARGQHVANLLAFQPEERIAQ
VIQIRGYTDAPYLVLATRNLVKKSKLTD FDSNRSGGIVAVNLRDNDDELVGAVLCSAGDDLLLVSANG
QSIRFSATDEALRPMGRATSGVQGMRFNIDDRLLSLNVVREGTYLLVATSGGYAKRTAIEEYPVQGRG
GKGVLTVMYDRRRRLV GALIVDDDSELYAVTSGGGVIRTAARQVRKAGRQTKGVRLMNLGEGDTLLA
IARNAEESGDDNAVDANGADQTGN

```

**Figure 4.24: The sequence coverage of band 2&8 (~ 47-kDa).** Band 2&8 is shown by blue bold font and the  $Ca^{2+}$  - binding site is indicated by red blue bold font.

↓ represent the start and ↑ represent the end of the band 2 &8.

It was possible to obtain sequence information for most of the bands except band 5 and 3. Band 5 corresponds to the intact GyrA subunit and may be as a result of partial digestion by trypsin. It is clear from the **Figure 4.22**, that band 5 is absent in the presence of  $Ca^{2+}$  which signifies the complete digestion of GyrA subunit by trypsin. Band 3 is one of the faintest bands on the gel and this must have affected its recovery from the membrane. Band 3 is similar to band 9, which seems to be a further degradation product of band 8 and therefore band 3 is probably the result of further degradation of band 2.

The interesting observation from this experiment is that out of all the bands; band 7, 2 and 8 includes the putative calcium binding site (504 DVSD E DLIARE DV 516) as shown in the **Figure 4.24**. These are bands that exhibit differences in the presence and absence of  $Ca^{2+}$ . Band 7 disappears in the presence of  $Ca^{2+}$ , while band 8 becomes fainter in the presence of  $Ca^{2+}$  and appears as band 2. This signifies that  $Ca^{2+}$  may be inducing structural changes that are exposing the cleavage site and making it more susceptible to digestion by trypsin. Thus the experiment clearly

demonstrates that  $\text{Ca}^{2+}$  has structural and functional significance for *M. tuberculosis* GyrA.

## 4.6 Virtual screening at the $\text{Ca}^{2+}$ -binding site

### 4.6.1 Introduction

The identification of a unique  $\text{Ca}^{2+}$ -binding site in *M. tuberculosis* GyrA encouraged the investigation of this site as a target for discovery of novel inhibitors. This is the first preliminary attempt to explore the putative  $\text{Ca}^{2+}$ - binding site for identifying novel inhibitors. Virtual screening was used as a tool to help identify inhibitors that can bind to the putative  $\text{Ca}^{2+}$ - binding site. Ligand and structure-based virtual screening has been useful to aid drug discovery in large pharmaceutical companies to scan large chemical libraries, saving time and resources. Virtual screening can filter out compounds, but it does not necessarily pick out the best inhibitor from the library. The method only reduces the number of hits that can be tested in the assays. In this case also, virtual screening was used to filter NCI diversity set II to identify hits that have the potential to bind to the  $\text{Ca}^{2+}$ - binding site and can inhibit the activity of the enzyme. An alternative approach could have been to screen compounds in a high-throughput screening assay and dock those compounds into the  $\text{Ca}^{2+}$  - binding site that have inhibitory activity. This approach would have been resource-intensive. In case of virtual screening, compounds with no information about their activity against DNA gyrase were tested for their binding to the putative  $\text{Ca}^{2+}$  - binding site. There have been success stories with this approach in the past. In a recent publication (Ostrov *et al.*, 2007), novel DNA gyrase inhibitors were identified by high-throughput virtual screening. A chemical ligand database with approximately 140,000 small molecules (molecular weight less than 500 Da) was molecularly docked onto two sites of *E. coli* DNA gyrase. The target sites were (i) a previously unexplored structural pocket formed at the dimer interface of subunit A and (ii) a small region of the ATP- binding pocket on subunit B overlapping the site targeted by coumarin and cyclothialidine drugs. The approach was successful in identifying several small-molecule compounds that inhibited the DNA supercoiling activity of purified *E. coli* DNA gyrase.

### 4.6.2 Docking-based virtual screening

The virtual screening and docking experiments were done in collaboration with Lora Mak (Theoretical Systems Biology, Institute of Food Research Norwich).

The NCI diversity II dataset (The NCI/DTP Open Chemical Repository: <http://dtp.cancer.gov>) downloaded from the ZINC database (Irwin & Shoichet, 2004) was used as the library source for compounds. The ZINC database was used as it is a free database of purchasable molecules available in 3D formats compatible with popular docking programs. The NCI diversity II dataset was selected as the compounds from this dataset are accessible for research. The NCI diversity II dataset is a diversity-derived subset of the NCI/DTP repository of nearly 140000 compounds. The dataset has a contained 1880 compounds with the molecular mass range of 114.1 to 696.12 g/mol. It also includes tautomers and protonation variants near physiological pH (5.7-8.2) which increased the number of docking structures to 2044.

For the virtual screening experiment, AutoDock Vina v1.0.2 (Goodsell *et al.*, 1996) was used. The target protein was a homology model of *M. tuberculosis* GyrA (MtGyrA-1BQB) as described in the previous section. This model without the Ca<sup>2+</sup> is described hereafter as model-1 which was energy minimised using the CHARMM (Brooks *et al.*, 1983) force field within the DiscoveryStudio environment (Accelrys) to produce another model referred to as model-2. In both the models, the Ca<sup>2+</sup> ions were removed. The structural quality of model-2 was validated using PROCHECK v 3.5.4 (Laskowski *et al.*, 1993). The target protein and the ligands were prepared for docking using the MGL Tools v 1.5.4 as per the standard procedure (<http://mgltools.scripps.edu/>). Since AutoDock Vina uses the same PDBQT file format as AutoDock4, AutoDock tools GUI was used to prepare the protein structure for docking. This procedure involved assigning atom type, charge and merging non-polar hydrogens. To convert ligands to the PDBQT file format, the `prepare_ligand4.py` program of the AutoDock tools was used in the batch mode. There were no restrictions to the numbers of bonds selected as rotatable and thus accepting the number of active torsions set by the program. The flexible ligands were

then docked to both the rigid and flexible model-1 and model-2 using the flexible side chains of amino acids having significance in  $\text{Ca}^{2+}$ -binding.

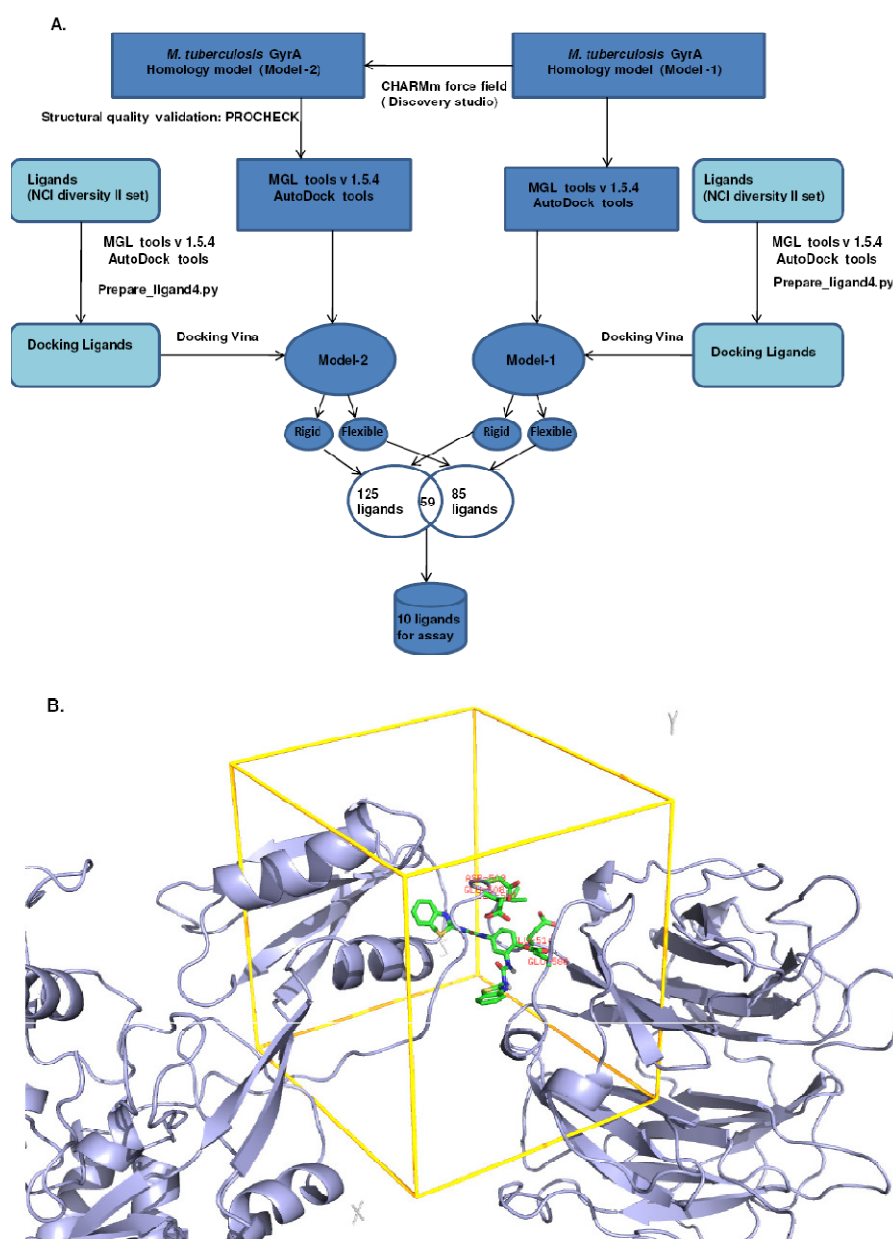


**Figure 4.25: Virtual screening of NCI diversity set II.** (A) Flowchart depicting the applied protocol for virtually screening novel inhibitors for *M. tuberculosis* DNA gyrase and (B) depicting the search area including the N-terminal and C-terminal region of Gyrase flanking the  $\text{Ca}^{2+}$ -binding site docked with ZINC1572309.

The search box was centered on the putative  $\text{Ca}^{2+}$ -binding site with the coordinates -85, 40, -13 including some of the flanking parts of the C- and the N-terminal region. The dimensions of the search box in all the three coordinates (x, y, and z) were 30, 34, 34 Å as shown in the **Figure 4.25**. The exhaustiveness of search was set to 8 and 16, while all other parameters were at default values. The docking was performed on the Norwich Bioscience Institute's Linux cluster.

In-silico docking resulted in the selection of a set of 188 and a set of 144 ligands as potential inhibitors after the rigid and flexible docking to model-1 and model-2 respectively. Three simulations runs per rigid models and four simulations per flexible models were carried out. The intersection between these two ligand subsets yielded 51 compounds that could favorably bind to GyrA  $\text{Ca}^{2+}$ -binding site in all the simulations after removing the different tautomers of the same compounds.

The compounds are shown in **Figure 4.26**.

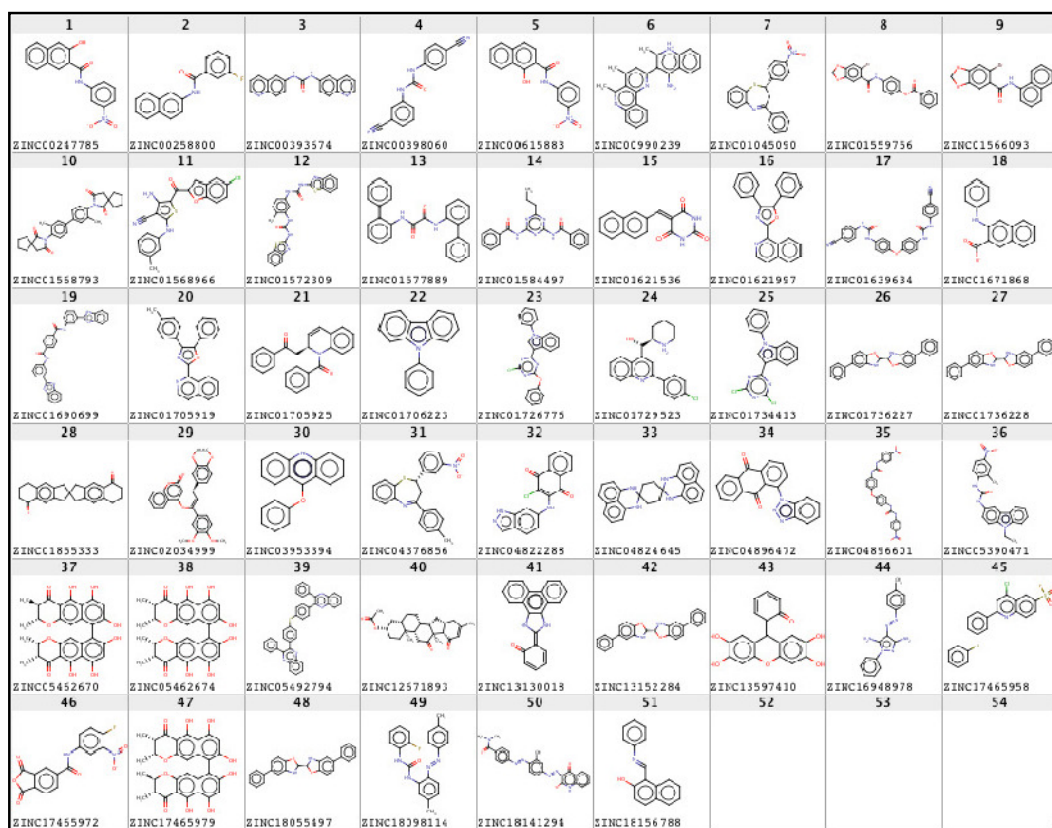


**Figure 4.26:** 51 hit compounds from the virtual screening of NCI diversity set II centered at the  $\text{Ca}^{2+}$ -binding site in *M. tuberculosis* GyrA.

Out of these 51 compounds, 10 compounds (**Figure 4.28**) were selected for assays based on their binding energies. The energy values and pharmacokinetic properties of these compounds are listed in **Table 4.7**. These 10 compounds were initially tested for their activity at 100  $\mu\text{M}$  concentration in a supercoiling assay followed by assay at the same concentration in the relaxation assay. 100  $\mu\text{M}$  is the arbitrary concentration cut off for weak inhibitors. The logic was that any compound that inhibits the enzyme activity at 100  $\mu\text{M}$  will be a potential candidate for further investigation. Some of the compounds (ZINC13130018, ZINC01690699, ZINC01639634, ZINC01736227, and ZINC01572309) showed weak inhibitory activity in the supercoiling assay; whereas many of the compounds showed inhibitory activity in the relaxation assay, except ZINC00393674. Compounds ZINC13130018, ZINC01577889, ZINC05390471 and ZINC01736227 showed more or less complete inhibition at 100  $\mu\text{M}$  as shown in **Figure 4.27**.

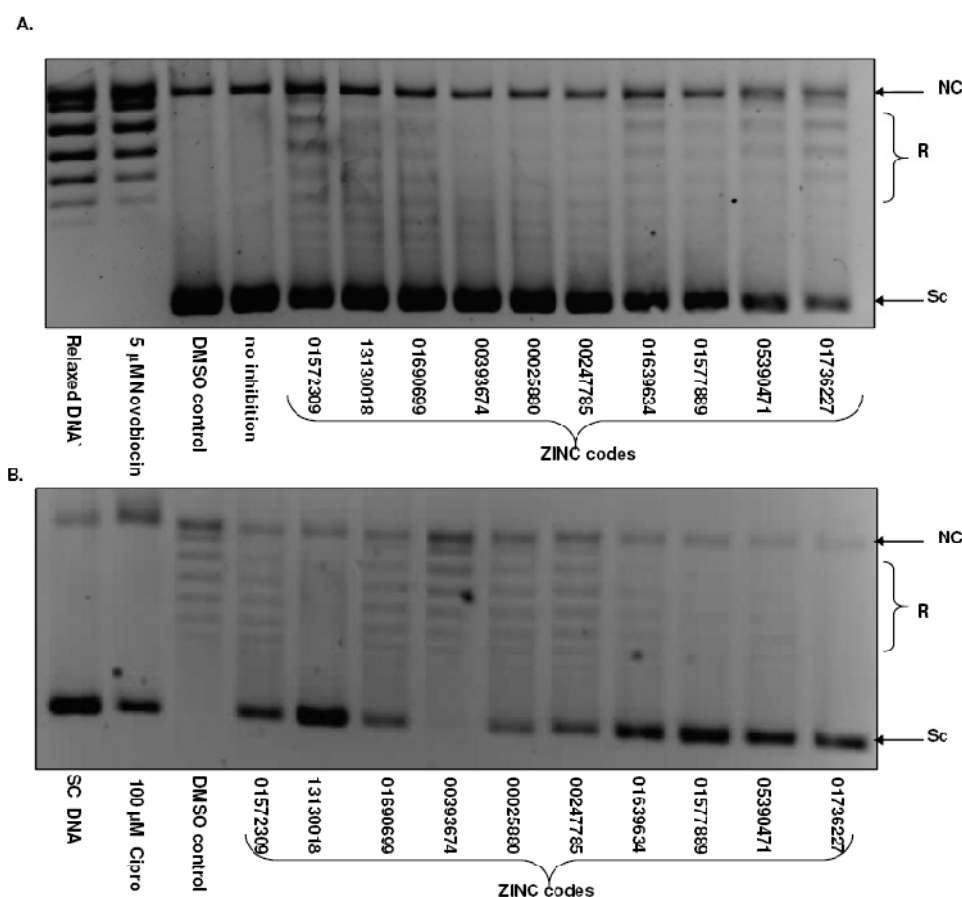


**Figure 4.27: Inhibitory activity of the 10 selected compounds (100  $\mu\text{M}$ ) against the supercoiling (A) and relaxation activity (B) of *M. tuberculosis* DNA gyrase.**

Compounds ZINC01572309, ZINC13130018, ZINC01690699, and ZINC01639634 showed inhibitory activity against both supercoiling and relaxation activity of *M. tuberculosis* DNA gyrase, but these compounds are more efficient in inhibiting relaxation. The H-bonding and hydrophobic interactions for the best predicted binding modes of these compounds in the Ca<sup>2+</sup>-binding site are shown in the **Figure 4.29 & Figure 4.30**. Compounds ZINC01572309, ZINC01690699, ZINC1639634, ZINC13130018 and ZINC01736227 were also tested for the in vitro activity against *M. tuberculosis* and compounds ZINC13130018 & ZINC1639634 showed MIC of ~ 50 µM (Dr. Amanda Brown & Prof. Tanya Parish, Barts and the London School of Medicine and Dentistry).

Thus the above initial results are quite promising as a first attempt to explore the predicted Ca<sup>2+</sup>-binding site in *M. tuberculosis* GyrA. At this point it is important to remember that on EGTA dialysis, the relaxation activity of the dialysed protein is affected. Since these molecules have the same effect they can be further explored as probes to investigate the significance of the Ca<sup>2+</sup>-binding site.

In the absence of a complete crystal structure, a homology model of the GyrA Ca<sup>2+</sup>-binding pocket was used for virtual screening. Homology models have been used successfully in drug discovery studies related to receptors of medical significance such as dopamine D3, muscarinic M1, and vasopressin V1a (Evers & Klebe, 2004a, Neumann *et al.*, 2009, Evers & Klebe, 2004b) for which very few crystal structures are available. In this modelling strategy the small molecules were docked to two models of GyrA differing with backbone RMSD of 1.50 Å. The backbone RMSD between the 12 residues of the Ca<sup>2+</sup>-binding sites of model-1 and model-2 was 1.83 Å (computed using SwissPDBViewer).

As with every method, these are the limitations with this approach which could be resolved in future work.

1. Conformational changes in the predicted  $\text{Ca}^{2+}$ -binding site has not considered when the  $\text{A}_2\text{B}_2$  complex is formed.
2. Exploring the possibility of ligands to bind sites other than the  $\text{Ca}^{2+}$ -binding site.

In future these limitations can be resolved along with characterization of the lead molecules ( $\text{IC}_{50}$  determination; cleavage assay).

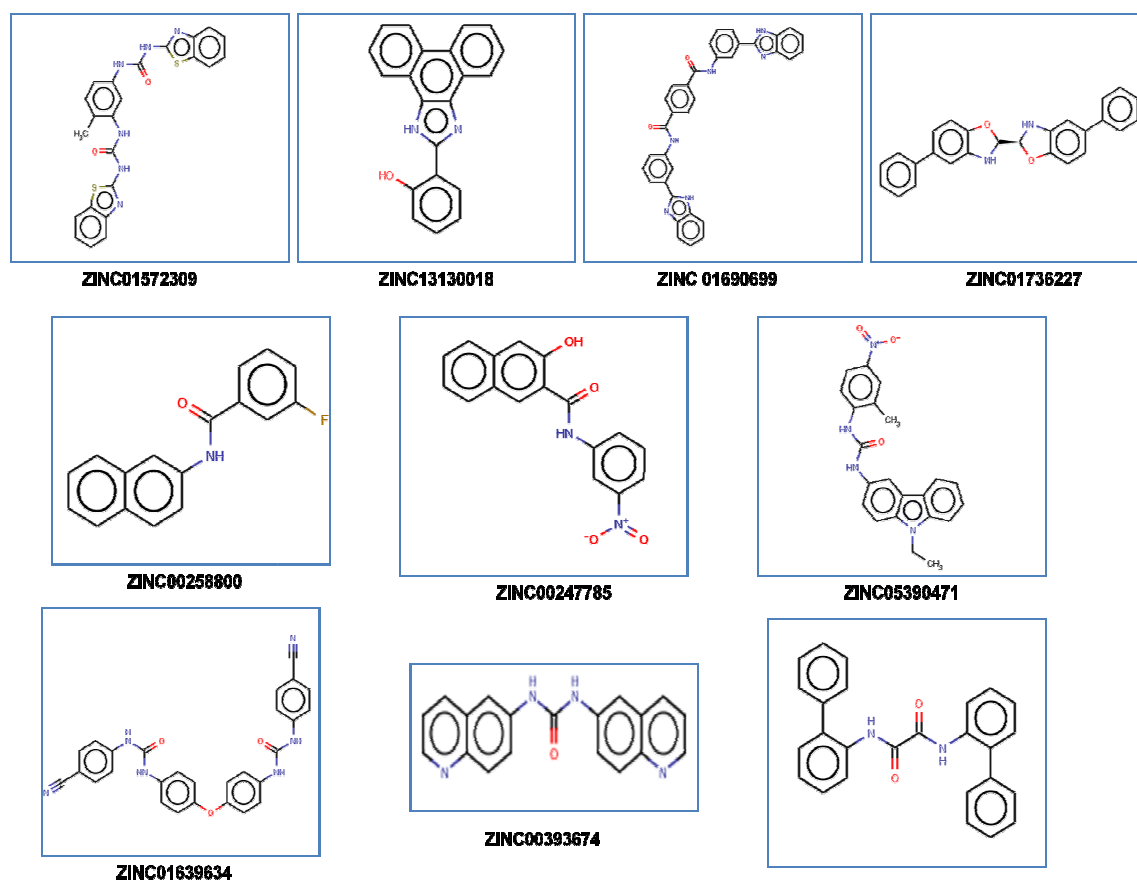


**Figure 4.28:** Chemical structures of 10 selected compounds from the virtual screening that were tested for their inhibitory activity in a standard supercoiling and relaxation assay.

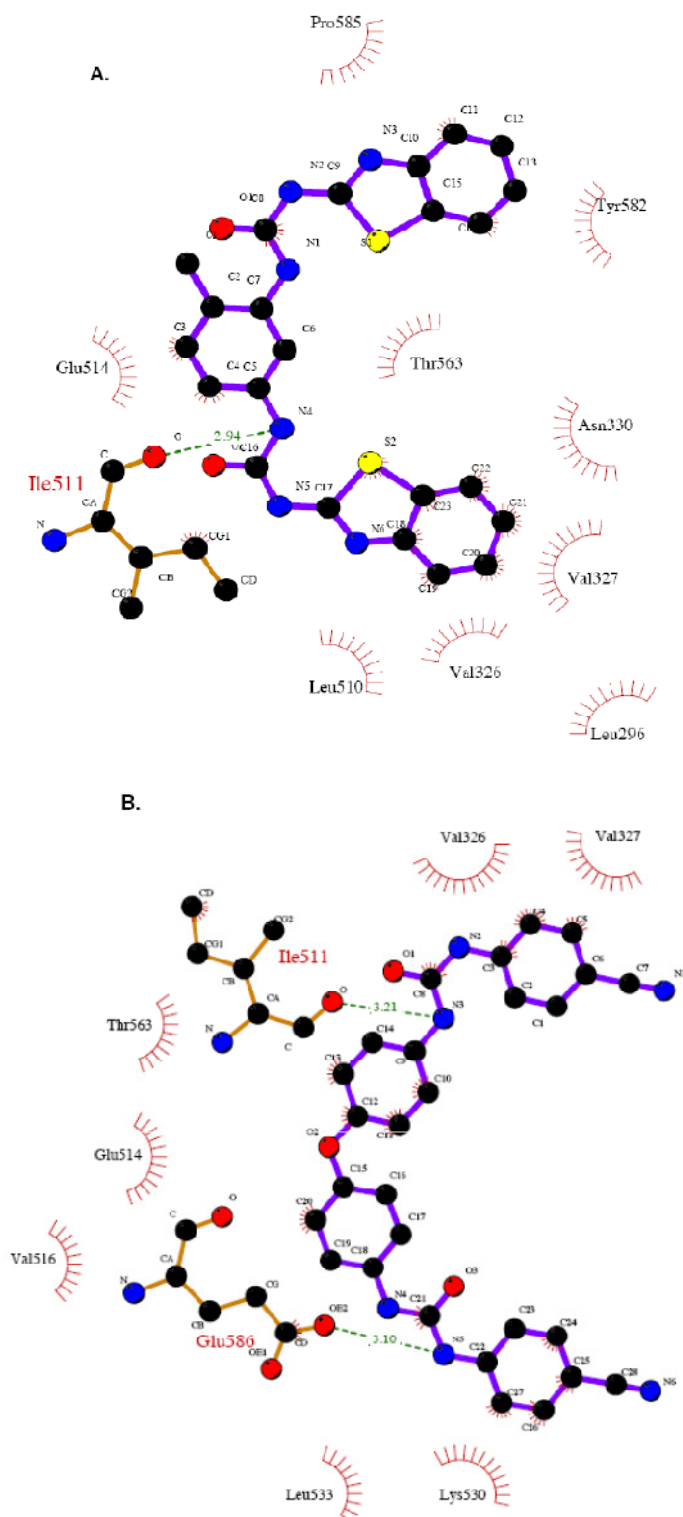


**Figure 4.29: Predicted binding modes for ligands ZINC01572309 (A) and ZINC01639634 (B).** *Hydrogen bonds are depicted by dashed lines and residues involved in van der Waals interactions are shown with red arcs.*

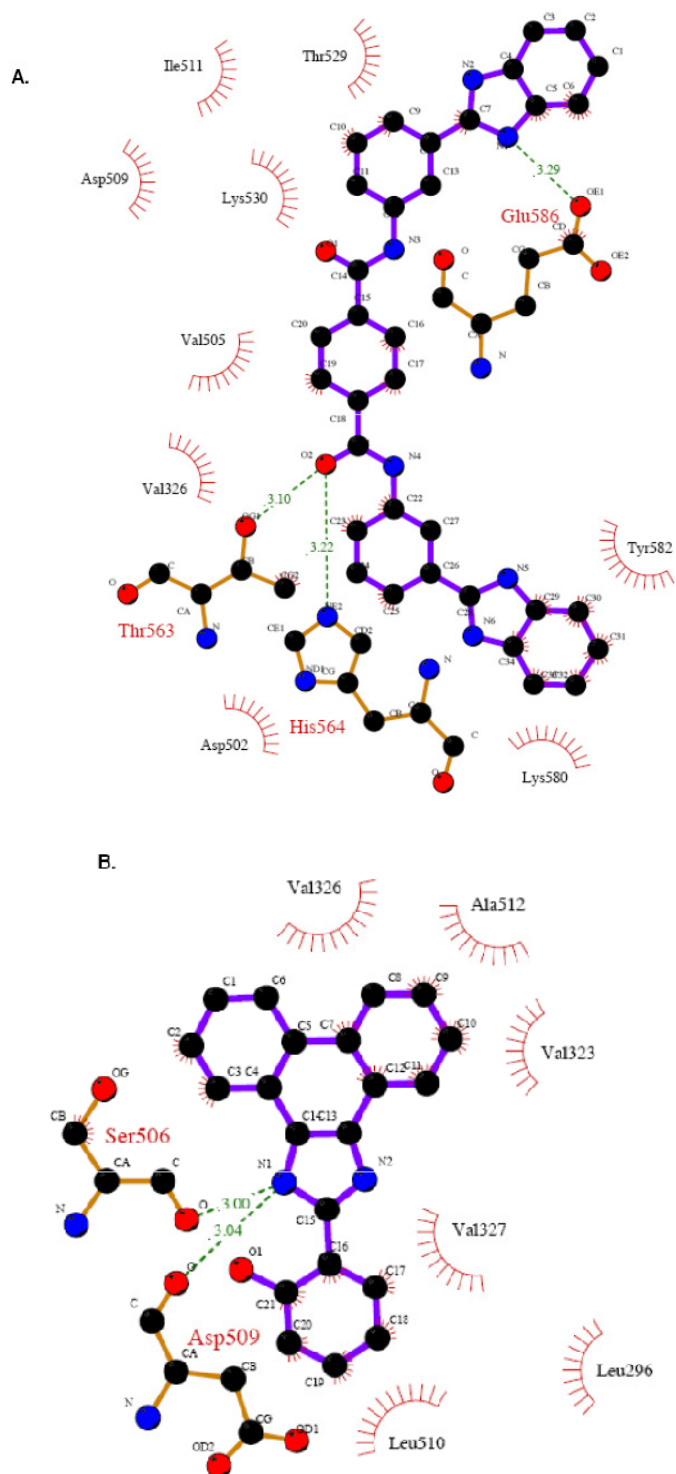


**Figure 4.30:** Predicted binding modes for ligands ZINC01690699 (A) and ZINC13130018 (B). Hydrogen bonds are depicted by dashed lines and residues involved in van der Waals interactions are shown with red arcs.

Compounds	Mol.mass	FEB (kcal/mole)	#RotBonds	XLOGP	TPSA
ZINC01572309	474.56	-11.5	4	5.84	108
ZINC13130018	310.35	-11.7	1	5.55	49
ZINC01690699	548.59	-11.0	6	6.89	115
ZINC01736227	392.45	-10.4	3	6.51	42
ZINC00393674	314.34	-10.2	2	3.1	66
ZINC00247785	308.29	-10.0	3	4.41	95
ZINC05390471	388.42	-9.9	4	5.43	92
ZINC01639634	488.50	-9.8	6	5.61	139
ZINC00258800	265.38	-9.6	2	4.15	29
ZINC01577889	392.45	-9.6	5	5.41	58

**Table 4.7: AutoDock Vina v1.0.2 calculated free energy of binding (FEB), number of rotatable bonds (#RotBonds), calculated hydrophobicity distribution (XLOGP) and molecular topological polar surface area (TPSA).**

## 4.7 Conclusion

Based on the bioinformatics analysis described in **Chapter3**, a putative  $\text{Ca}^{2+}$ -binding site was identified in the *M. tuberculosis* GyrA. In the absence of a crystal structure of the complete subunit, a model was generated to guide biochemical and site-directed mutagenesis studies. The model has also been described in detail in **Chapter 3**.

The initial biochemical studies involved investigation of the effect of  $\text{Ca}^{2+}$  on the enzyme activity. In previous studies it has been shown that *M. tuberculosis* DNA gyrase does not show supercoiling and relaxation activity in the presence of  $\text{Ca}^{2+}$  alone; unlike *E. coli* DNA gyrase where  $\text{Ca}^{2+}$  can substitute for  $\text{Mg}^{2+}$  (Aubry *et al.*, 2006a). In order to test the hypothesis that the inability of  $\text{Ca}^{2+}$  to support supercoiling depends on the presence of *M. tuberculosis* GyrA, individual subunits of *M. tuberculosis* and *E. coli* DNA gyrase were swapped. Supercoiling activity was observed when *M. tuberculosis* GyrA and *E. coli* GyrB were assayed in the presence of 6 mM  $\text{Mg}^{2+}$ , but no supercoiling activity was observed when the same assay was

repeated in the presence of 6 mM  $\text{Ca}^{2+}$  (**Table 4.1**). This indicates that the ability of the  $\text{Ca}^{2+}$  to support DNA supercoiling depends on the presence of *E. coli* GyrA, and *M. tuberculosis* GyrA cannot substitute for it.

In order to study the effect of removal of  $\text{Ca}^{2+}$  bound to GyrA, EGTA dialysis and protein refolding experiments were carried out. When GyrA was dialysed in EGTA, the dialysis affected the relaxation activity of the enzyme; the EGTA-dialysed protein was less active in relaxation assays in comparison to the protein dialysed in the absence of EGTA. This weaker relaxation activity could be restored by adding  $\text{Ca}^{2+}$  to the assay. This difference in the relaxation activity of protein dialysed in the presence and absence of EGTA was also investigated by a time-course experiment. Based on the effect of EGTA on the enzyme activity, refolding experiments were designed to investigate the removal  $\text{Ca}^{2+}$  tightly bound at the  $\text{Ca}^{2+}$ -binding site. Protein refolding was performed in the presence and absence of EGTA assuming that during the refolding process the tightly-bound  $\text{Ca}^{2+}$  is released from the binding site and is available for chelation by EGTA.

ICP-AES was used to estimate the concentration of  $\text{Ca}^{2+}$  and  $\text{Mg}^{2+}$  in the samples. The ICP-AES data indicates that EGTA was effective in reducing the concentration of  $\text{Ca}^{2+}$  in the sample.

The effect of dialysis or dialysis and refolding in the presence of EGTA was the complete loss of relaxation activity with weak supercoiling activity. On the other hand decatenation activity was weak when the protein was dialysed in EGTA, but it was completely lost when GyrA was dialysed and refolded in EGTA. This effect was specifically due to EGTA treatment and not due to protein misfolding as there was little effect on the relaxation, supercoiling and decatenation activity of refolded enzyme. The CD spectra for the EGTA-dialysed protein also indicated that the protein was not misfolded. This indicated that the loss of  $\text{Ca}^{2+}$  significantly affects the relaxation and decatenation activity with little effect on DNA supercoiling.

Based on the homology models MtGyrA-1H71 and MtGyrA-1BQB, mutation studies in the  $\text{Ca}^{2+}$ -binding site were designed to mutate acidic amino acids that have significant importance in coordinating  $\text{Ca}^{2+}$ . For example the quadruple mutant (GyrA D504A, E508A, D509A, E514A) involves mutation of two acidic residues

D504 and E508 from the model MtGyrA-1H71 and two acidic residues E509, E514A from the model MtGyrA-1BQB; E508 is an important acidic residue shown to coordinate  $\text{Ca}^{2+}$  in both models. The quadruple mutation affected the supercoiling activity of the enzyme. A DNA wrapping experiments demonstrated that the weak supercoiling activity of the mutant was due to the effect of the mutations on the wrapping of DNA around gyrase. But the quadruple mutant did not significantly affect the relaxation and decatenation activity of the enzyme. The CD spectra for the quadruple mutant (GyrA D504A, E508A, D509A, E514A) shows that the spectra is not different from the GyrA wild-type indicating that the mutation has not resulted in protein misfolding.

Limited proteolysis experiments were done with trypsin for GyrA and GyrB in the presence and absence of 3 mM  $\text{Ca}^{2+}$ . As expected, a difference was observed in the digestion profile of GyrA but not in case of GyrB. In the case of GyrA, the most striking difference was the disappearance of a 47-kDa band in the presence of 3 mM  $\text{Ca}^{2+}$ . From Edman sequencing it was shown that the 47-kDa band (band 2 & 8) included the  $\text{Ca}^{2+}$ - binding site. This suggests that  $\text{Ca}^{2+}$  induces conformational changes that involve the  $\text{Ca}^{2+}$ - binding site. The position of band 2 & 8 is shown in the **Figure 4.31**.

A model has been described based on the experimental data in **chapter 6**. According to the model,  $\text{Ca}^{2+}$  acts as a regulator that controls the flexibility of the arm/linker connecting the GyrA N- and C-terminal domains.  $\text{Ca}^{2+}$  may help to maintain *M. tuberculosis* DNA gyrase in a state which would favour all the topological reactions. In the absence of topo IV in *M. tuberculosis*, this may be important to keep the enzyme in a state ready for both supercoiling and relaxation/decatenation reaction.

Considering the potential significance of the  $\text{Ca}^{2+}$ -binding site, virtual screening for inhibitors was performed using the NCI diversity set II library from the ZINC database. Compounds ZINC01572309, ZINC13130018, ZINC01690699, and ZINC1639634 showed inhibitory activity against both supercoiling and relaxation activity of *M. tuberculosis* DNA gyrase. Compounds ZINC13130018 & ZINC1639634 have also shown ans MIC of  $\sim 50 \mu\text{M}$  against *M. tuberculosis* in vitro.



**Figure 4.31: Representation of the domains affected during the trypsin digestion in the presence of 3 mM  $\text{Ca}^{2+}$ . Structural region ( $\text{Ca}^{2+}$ - binding site) corresponding to band 2 & 8 are coloured while the rest of the structure is in white.**

In this chapter, I have discussed the identification of a  $\text{Ca}^{2+}$ - binding site in *M. tuberculosis* GyrA. The effect of  $\text{Ca}^{2+}$  on the activity of *M. tuberculosis* DNA gyrase indicates that the  $\text{Ca}^{2+}$ - binding site in *M. tuberculosis* DNA gyrase belongs to the class of  $\text{Ca}^{2+}$  sensors. Functionally, EF-hand proteins can be divided into two general classes: the  $\text{Ca}^{2+}$  sensors and the  $\text{Ca}^{2+}$  buffer (Gifford *et al.*, 2007).  $\text{Ca}^{2+}$  sensors translate the chemical signal of an increased calcium concentration into diverse biochemical response. This involves calcium-induced conformation change. In case of *M. tuberculosis* DNA gyrase,  $\text{Ca}^{2+}$  is behaving as a signaling switch to coordinate its activity as an efficient DNA supercoiling and relaxing enzyme in the absence of topo IV. Due to the significance of this site, it was further explored for identifying inhibitors for virtual screening. In future, radioactive  $\text{Ca}^{45}$  isotope can be used to further characterise the putative  $\text{Ca}^{2+}$ -binding site and its novel inhibitors.

## Chapter 5: Identification and characterisation of novel gyrase inhibitors

Biochemical studies described in Chapter 4 provided the platform for identification of novel DNA gyrase inhibitors targeting the *M. tuberculosis* enzyme. In this chapter, three classes of compound: quinolines, aaptamines and naphthoquinones were selected for investigation of their potential as inhibitors of *M. tuberculosis* DNA gyrase. Aaptamines and naphthoquinones (Mahapatra *et al.*, 2007, Gul *et al.*, 2006) have been shown to have anti-mycobacterial activity. Quinolines have been shown to induce cross-resistance to fluoroquinolones by generating mutations in DNA gyrase and topo IV (Davidson *et al.*, 2008), and also inhibit *M. tuberculosis* DNA gyrase activity. Out of all the three classes of compounds, naphthoquinones were found to be most effective and were studied in detail.

The mechanism behind the inhibitory activity of naphthoquinones was studied using gel-based assays, nano-ESI-MS (collaboration with Dr Adam McKay; University College London, UK), surface plasmon resonance (guidance of Dr. Sandra Grieve; John Innes Centre, Norwich, UK), computational modelling (collaboration with Dr Faridoon Yousafzai; John Innes Centre, Norwich, UK) and limited proteolysis experiments.

## 5.1 Introduction

Traditional target-based drug screening is performed by high-throughput screening of chemical libraries, which may be synthetic/natural products or combinations of both (2009, Janda, 1994). I have used a different approach for identifying potential new gyrase inhibitors. I decided to investigate selected classes of compounds that have published information about their antibacterial activity. These compounds also did not have any information about their possible targets. There were two advantages of this method. The first advantage is that since these compounds are already been shown to have antibacterial activity, I know that they have biological activity and can get into the bacterial cell. The other advantage is that if any of these compounds exhibit inhibitory activity against DNA gyrase, then it is likely that collaborators would be able to perform synthetic chemistry on the selected molecule to design better inhibitors. Although with this method it should be feasible to identify novel DNA gyrase inhibitors, like any other screening procedure a significant hit will not indicate that DNA gyrase is the only target for that particular molecule in-vivo. There may be a possibility of several other targets for the same molecule. Three different families of compounds: quinolines, aaptamines and naphthoquinones were studied for their activity against *M. tuberculosis* gyrase. Aaptamines and naphthoquinones have been shown to have antibacterial activity with no information about their potential targets (Gul *et al.*, 2006), while quinolines have been shown to induce cross-resistance to fluoroquinolones (Davidson *et al.*, 2008). Although representative molecules from each family (chloroquine, 1N, 4N-didodecyl aaptamine, diospyrin) have been identified as potential inhibitors of DNA gyrase, detail studies were done only on naphthoquinones, and specifically on diospyrin, due to its comparatively lower IC<sub>50</sub> in in-vitro DNA gyrase assays.

## 5.2 Quinolines

Quinolines, such as chloroquine, have been used traditionally for the treatment of malaria, arthritis, and lupus for many years, but the precise mechanism of their action remains unclear (Foley & Tilley, 1998). Members from this family of compounds like mefloquine and its analogues also have been reported to have antimycobacterial properties (Bermudez *et al.*, 1999). This fact is not surprising as a compound isolated from the commercial preparation of chloroquine was modified to produce the antibacterial compound, nalidixic acid (Appelbaum & Hunter, 2000). Fluorine was subsequently added to produce the fluoroquinolones, resulting in both an increase in potency and spectrum (Appelbaum & Hunter, 2000). Due to the common origin of fluoroquinolones and chloroquine, their pharmacore is similar (Figure 5.1).

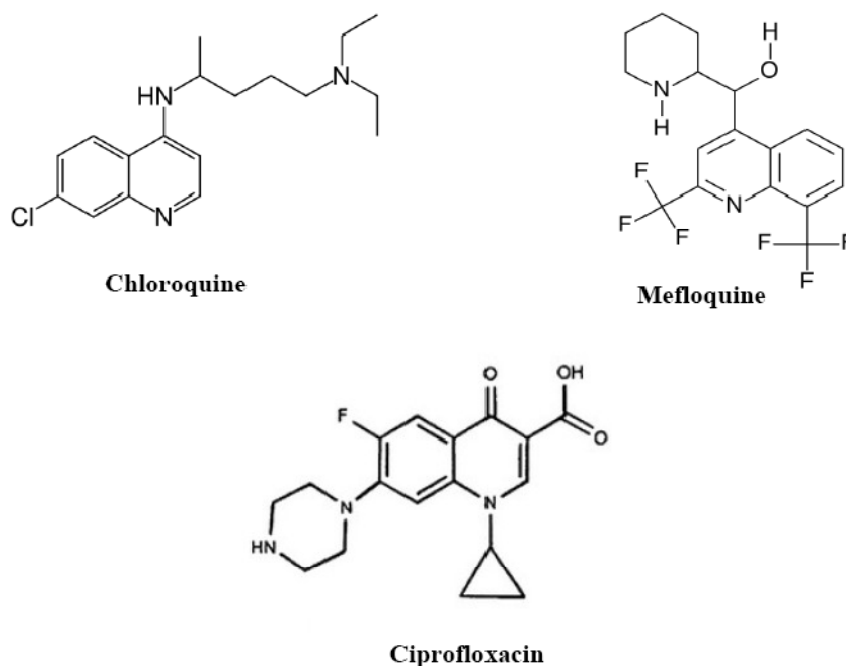


**Figure 5.1: Similar pharmacore of the fluoroquinolones and quinolines.**

The antimycobacterial properties of mefloquine and its relatedness to fluoroquinolones has led to the development of mefloquine-based ligands as potential antituberculosis agents (Jayaprakash *et al.*, 2006). Despite the fact that it has not been possible to identify mutants resistant to mefloquine by both *in vivo* and

in vitro selection, microarray studies indicate the role of genes involved in membrane transport and cellular replication (Danelishvili *et al.*, 2005).

In a recent study (Davidson *et al.*, 2008) it was reported that in a remote village of South America, 4.8% of the village carried cipro-resistant *E. coli* with QRDR mutations. QRDR mutations are mutations in the gyrase and topo IV quinolone-resistance determining regions (Feng-Jui & Hsiu-Jung, 2003 ). The ciprofloxacin-resistant *E. coli* isolates from Guyana had S83L/ D87N mutations in *gyrA*, S80I/ E84G/E84V mutations in *parC* and S458A, L416F, S458T mutations in *parE* (Davidson *et al.*, 2008). The interesting fact about this observation was that the patients had never been exposed to quinolones, but there was an extensive use of chloroquine in the population for malaria treatment and prevention. Similarly, isolates tested for ciprofloxacin resistance after exposure to chloroquine showed D87Y and S80I mutation in *gyrA* and *parC* respectively.

This observation raises the interesting question as to whether quinolines target DNA gyrase in *M. tuberculosis*. This information could be useful for developing the well-known antimalarial quinolines as inhibitors for mycobacterial gyrase. Since malaria is prevalent in the parts of tropical countries, where TB is an epidemic, treatment for two diseases with a single class of drugs could be beneficial.

Standard supercoiling and relaxation assay were performed to study the effect of chloroquine and mefloquine on the activity of *M. tuberculosis* DNA gyrase. Chloroquine was found to be a more potent inhibitor of DNA gyrase in comparison to mefloquine (**Table 5.1; Figure 5.2**).

In our lab it has been shown that in the presence of mefloquine, *E. coli* DNA gyrase forms a cleavage complex. Interestingly similar experiments done with *M. tuberculosis* DNA gyrase demonstrate the formation of cleavage complex only in the presence of chloroquine as shown in **Figure 5.3**.

These experiments demonstrate that quinolines inhibit *M. tuberculosis* DNA gyrase activity and they could be optimised further as potential TB drugs.

Quinolines	Supercoiling Assays IC <sub>50</sub> values (approx)	Relaxation Assay IC <sub>50</sub> values (approx)
Chloroquine	80 $\mu$ M	80 $\mu$ M
Mefloquine	300 $\mu$ M	300 $\mu$ M

**Table 5.1: IC<sub>50</sub> values for Chloroquine and Mefloquine based on supercoiling and relaxation assays.**

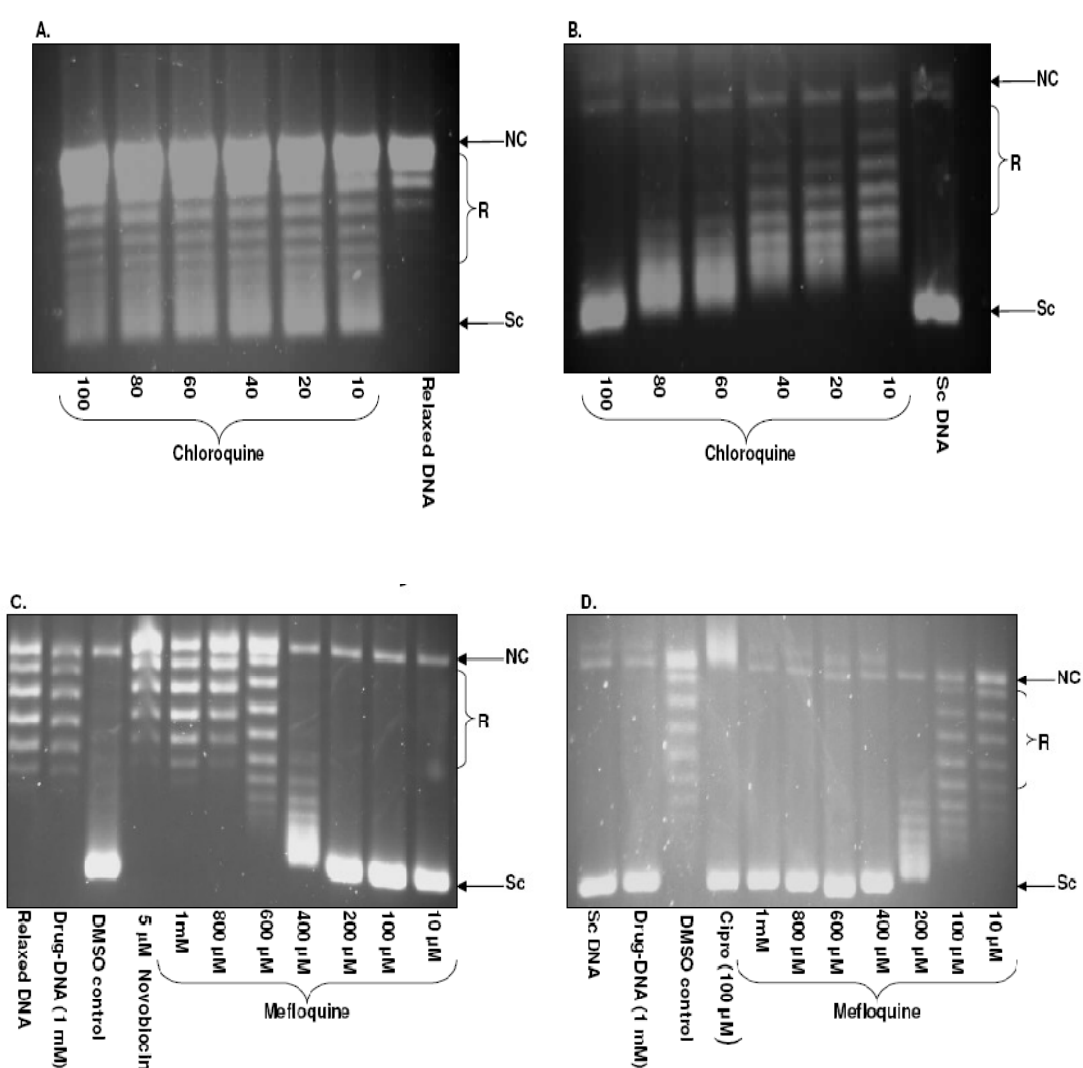


**Figure 5.2: Inhibitory activity of chloroquine and Mefloquine.** Supercoiling inhibition assay (A) and relaxation inhibition assay (B) of chloroquine against *M. tuberculosis* DNA gyrase. Mefloquine inhibition of supercoiling (C) and relaxation activity (D). NC: nicked Circular DNA, R: relaxed topoisomers, SC: supercoiled DNA.

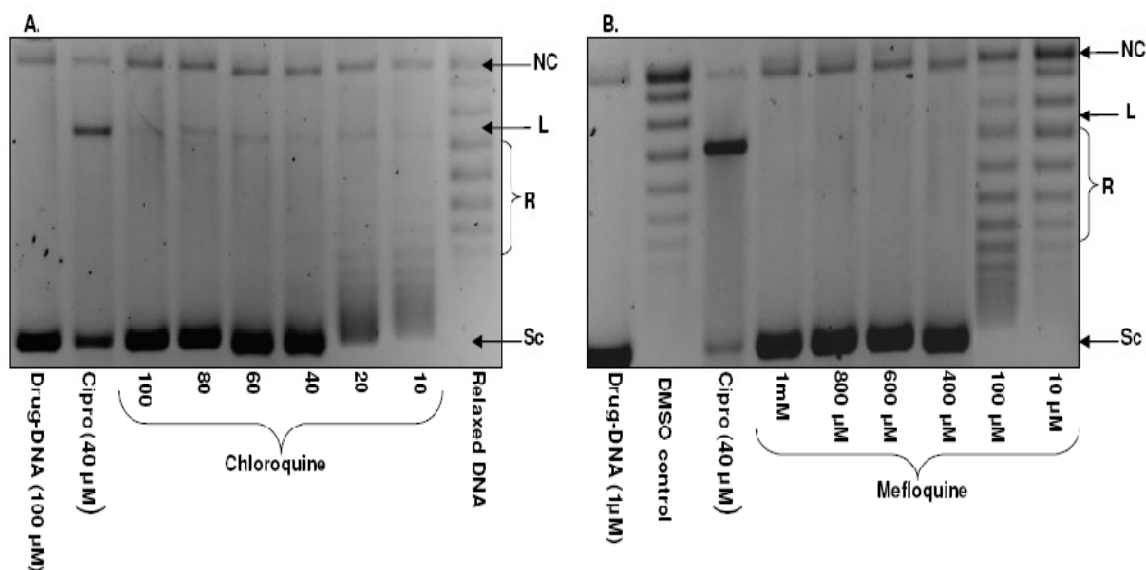


**Figure 5.3: DNA cleavage assay in the presence of chloroquine (A) and mefloquine (B) in the absence of ATP. DNA cleavage is observed in the presence of ciprofloxacin and chloroquine, but no linear DNA is observed with mefloquine. NC: nicked Circular DNA, L: linear DNA, R: relaxed topoisomers, SC: supercoiled DNA.**

### 5.3 Aaptamines and marine extracts

The aaptamine class of compounds is commonly isolated from various species of the marine sponge genus *Aaptos* (Jang *et al.*, 2007). The sponge belongs to the order Hadromerida and family Suberitidae. When the marine product was first isolated (Nakamura *et al.*, 1982), it was reported to have antineoplastic and  $\alpha$ -adrenoreceptor blocking activity. Isoaaptamine (Nakamura *et al.*, 1987), a closely related compound can also be isolated from *Aapto aaptos* (Figure 5.4).



**Figure 5.4: Aptos, a marine sponge and a natural source of Aaptamine.**

Since its original discovery a series of research articles have been published regarding the total synthetic and semi-synthetic derivatives of aaptamines (Ross Kelly & Maguire, 1985, Pelletier & Cava, 1985, Andrew & Raphael, 1987). Although the synthetic yield of aaptamine is low from quinoline and isoquinoline precursors, still it is likely to be the more cost efficient choice for the production of aaptamines (Larghi *et al.*, 2009). Chemically all the aaptamine compounds are alkaloids that contain the benzonaphthyridine core structure (**Figure 5.5**). Isoquinolones, dopamine and quinolines (anti-malarial) share structural similarity with aaptmaine.

Aaptamine has potent toxicity which can be attributed to its ability to intercalate into DNA (Bowling *et al.*, 2008). DNA intercalation is common with compounds like aaptamines; they intercalate between adjacent base pairs of intact DNA through  $\pi$ -bond interactions and in some instances several molecules stack together in the same area between the base pairs (Bowling *et al.*, 2008). It has been suggested that the inhibition of the S-phase of the cell cycle (Pettit *et al.*, 2004), which may lead to cytotoxicity, may be due to interaction with DNA or a topoisomerase. Structure-activity relation studies (Shen *et al.*, 1999) have shown that the C-9 hydroxyl position is important for the cytotoxic activity and acylation at this

position causes a decrease in activity. The closely related bis (naphthalimide) derivative DMP 840 (A) has been reported to be a topoisomerase II inhibitor (Nitiss *et al.*, 1998) and is currently in phase I clinical trials (Thompson *et al.*, 1999).

Aaptamines have anti-cancer (Pettit *et al.*, 2004, Shen *et al.*, 1999), antiviral (Bowling *et al.*, 2008) and antibacterial (Gul *et al.*, 2006) properties that encourage the evaluation of their derivatives for therapeutic potential. Since aaptamines are related to quinolines, possess antimycobacterial activity (Pettit *et al.*, 2004) and are predicted to interact with topoisomerases, I decided to assay seven aaptamine derivatives and marine extracts: iso-aaptamine nonyl dimer, 8-hydroxymanzamine, manzamine, aaptamine, iso-aaptamine, 1N,4N-didodecyl-aaptamine, kaempferol-3-O- $\alpha$ -L-(2,3-di-E-Pcomaroyl)-rhamnoside to study their effect on the activity of *M. tuberculosis* DNA gyrase **Figure 5.5**. The compounds were kindly donated by Prof. Mark T. Hamann (Research Institute of Pharmaceutical Sciences, University of Mississippi). The compounds were tested in standard supercoiling assays.

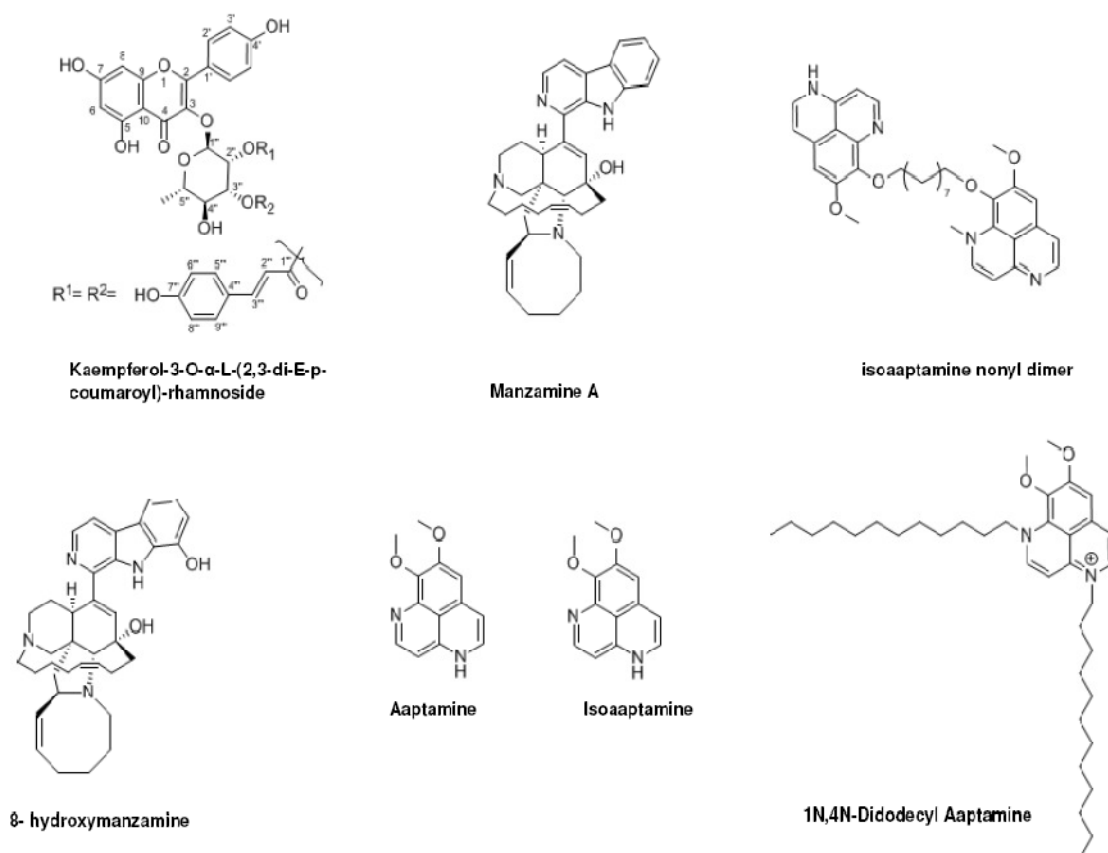


**Figure 5.5:** Aaptamines and marine extracts.

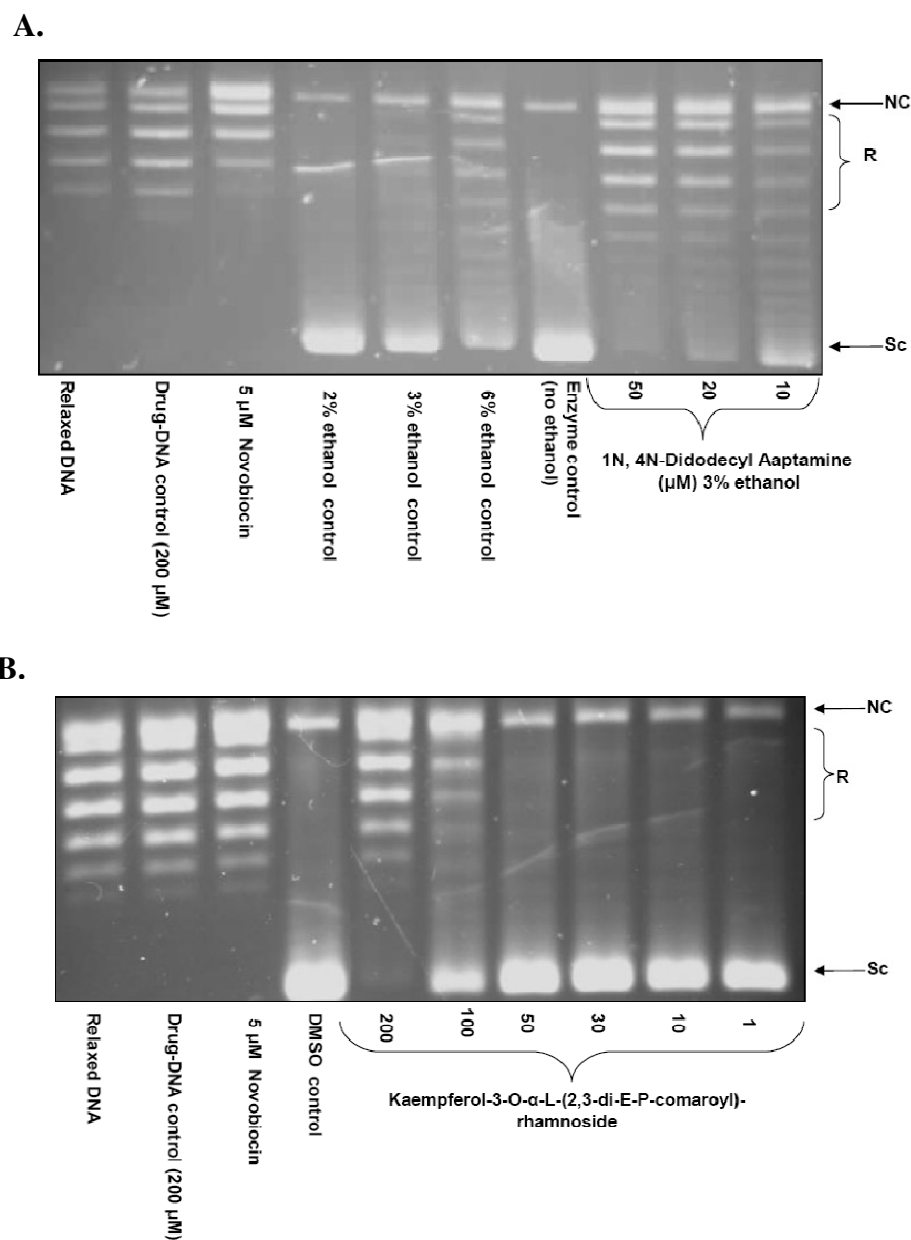


**Figure 5.6: Inhibitory activity of aaptamine and kaempferol. Supercoiling inhibition assay of aaptamine (A) and kaempferol (B) against *M. tuberculosis* DNA gyrase (0.1 mM). The final concentration of ethanol in the assay is 3% in the presence of the aaptamine. Kaempferol is soluble in 100% DMSO and the final concentration of DMSO is 5% in the presence of the drug. NC: nicked Circular DNA, R: relaxed topoisomers, SC: supercoiled DNA.**

Out of all the compounds that were tested, 1N, 4N-Didodecyl Aaptamine (**Figure 5.6**) is potentially a good inhibitor of *M. tuberculosis* DNA gyrase ( $IC_{50}$ ~10-20  $\mu$ M), while Kaempferol-3-O- $\alpha$ -L-(2,3-di-E-P-comaroyl)-rhamnoside (**Figure 5.6**) is a weak inhibitor with an  $IC_{50}$ ~50- 100  $\mu$ M. The rest of the compounds did not have any effect on the activity of the enzyme.

## 5.4 Naphthoquinones

The use of medicinal plants such as *Acacia nilotica*, *Cassine papillosa*, *Cheopodium ambrosioides*, *Combretum molle*, *Euclea natalensis* (**Figure 5.7**) etc. by native South Africans to cure TB has been reported (Pujol, 1990.). The indigenous people of South Africa extensively use *E. natalensis* A.DC. for diseases such as chest complains, bronchitis, pleurisy, chronic asthma, urinary tract infections, venereal diseases and oral health (Van Wyk & Van Wyk, 1997). A significant amount of work has been done on the antimycobacterial activity of *E. natalensis*, which has been shown to exhibit activity against drug-sensitive and drug-resistant strains of *M. tuberculosis* (Lall & Meyer, 2001). It is a tree of the *Ebenaceae* family and is a rich source of a class of compounds known as naphthoquinones.



**Figure 5.7:** *E. natalensis*, a medicinal plant and a natural source of naphthoquinones.

Naphthoquinones can be represented as derivatives of naphthalene with the replacement of two hydrogen atoms by two ketone groups. A well known member of naphthoquinone family is 7-methyljuglone (5-hydroxy-7-methyl-1,4-naphthoquinone). A series of synthetic and plant-derived naphthoquinone derivatives of the 7-methyljuglone scaffold such as diospyrin, menadione, shinalone, neodiospyrin, and isodiospyrin are available (**Figure 5.8**).

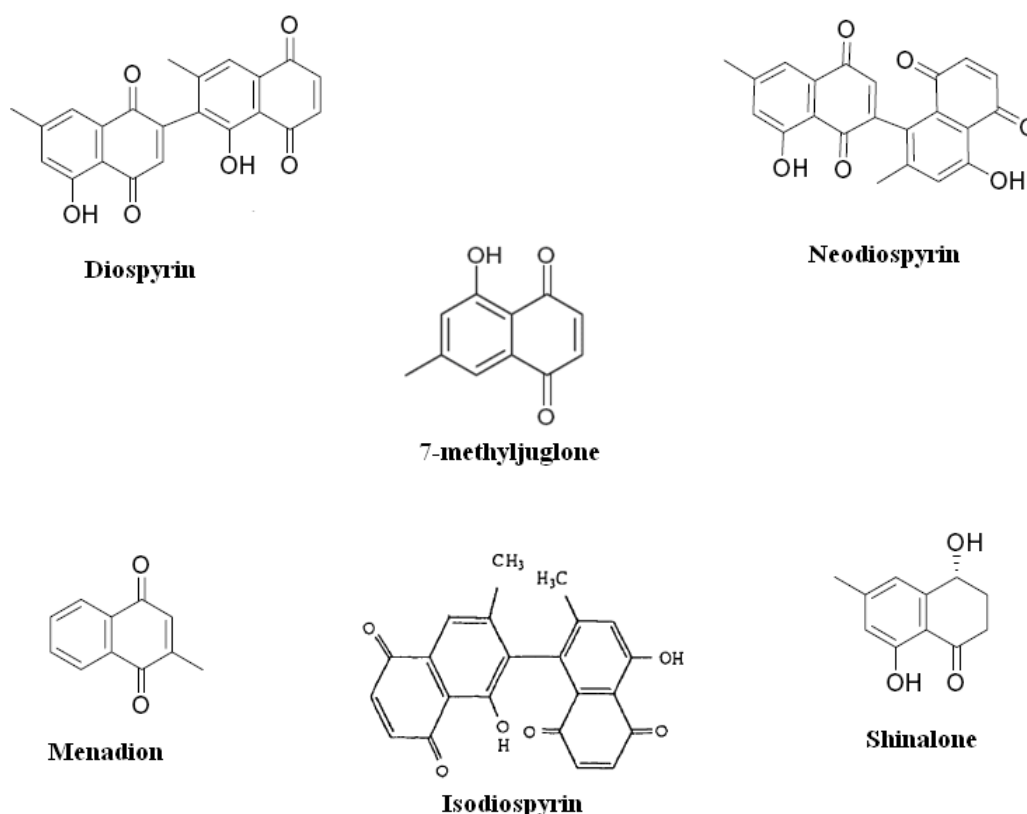


**Figure 5.8: Naphthoquinones studied for their activity against mycobacterial DNA gyrase.**

Naphthoquinones have a broad range of biological activity that can be exploited for the design of new antibacterials (Mahapatra *et al.*, 2007), anti-leishmaniasis (Ray *et al.*, 1998, Yardley *et al.*, 1996) and antitumor compounds (Hazra *et al.*, 1984, Ting *et al.*, 2003). 7-methyljuglone and its derivatives (**Table 5.2**) have been shown to have antimycobacterial activity (Mahapatra *et al.*, 2007). 7-methyljuglone is the most potent in-vivo against *M. tuberculosis* H37Rv. The selectivity index is a ratio between  $IC_{50}$  and MIC ( $IC_{50}/MIC$ ). The bactericidal activities were reported by MICs and the compound cytotoxicity for the Vero cell

line was reported by  $IC_{50}$ . The selectivity index is a ratio between the  $IC_{50}$  and MIC ( $IC_{50}/MIC$ ). It indicates the target specificity of the compound. A compound with higher  $IC_{50}$  and lower MIC will be an effective bactericidal and less toxic. In drug development, compounds with a selectivity index of  $>1,000$  are regarded as promising candidates for clinical development. 7-methyljuglone has a higher selectivity index in comparison to other derivatives. It is suggested that the poor selectivity of the derivatives is possibly due their non-specific activity with other disulfide reductase (e.g. thioredoxin reductase, lipoamide dehydrogenase) which are also found in mammalian cells (Mahapatra *et al.*, 2007). 7-methyljuglone has the ability to enhance the activity of the first-line drugs isoniazid and rifampicin against both extracellular and intracellular *M. tuberculosis* (Bapela *et al.*, 2006). The MIC values of naphthoquinones indicate that the ketone groups on C1 and C4 or aromaticity between the carbon atoms are important for antimycobacterial activity.

Compound	MIC ( $\mu\text{g/ml}$ )	$IC_{50}$ ( $\mu\text{g/ml}$ )	Selectivity index
1. 7-methyljuglone	0.5	15.1	30.22
2. Diospyrin	8.0	17.8	2.2
3. Neodiospyrin	10.0	32.0	3.2
4. Menadione	5.0	6.5	1.30
5. Shinanalone	$> 100$	-	-

**Table 5.2: Antituberculosis activity and cytotoxicity of 7-methyljuglone and its derivatives (Mahapatra *et al.*, 2007).**

Besides the antimycobacterial activity of diospyrin, it also has antitumour (Hazra *et al.*, 1984) anti-leishmaniasis and antiprotozoal activities (Hazra *et al.*, 1995). Diospyrin inhibits the growth of *Leshmania donovani* promastigotes (Yardley *et al.*, 1996), *Trypanosoma cruzi*, *Trypanosoma brucei* (Yardley *et al.*, 1996) and *Plasmodium falciparum* (Hazra *et al.*, 1995) in vitro. Further studies performed on this compound show that diospyrin interacts specifically with topoisomerase I of leishmania but does not inhibit type II topoisomerase of *Leshmania donovani* and requires a much higher concentration to inhibit type I topoisomerase of calf thymus

(Ray *et al.*, 1998). Mechanistically, like camptothecin, diospyrin stabilises the topoisomerase I cleavage complex *in vitro* (Ray *et al.*, 1998).

A related bisnaphthoquinone, isodiospyrin from the plant *Diospyros morrisiana* also inhibits relaxation and kinase activity of human topoisomerase I. But unlike diospyrin it does not stabilise the cleavage complex rather it limits human topoisomerase I access to the DNA substrate by direct binding to human topoisomerase I (Ting *et al.*, 2003). The exact binding site of isodiospyrin on human topoisomerase I is not clear, but it is predicted that cysteine residues in the protein could be isodiospyrin's potential binding site on human topoisomerase I, given that naphthoquinones are well known to interact with sulphhydryl-containing proteins.

## 5.5 Targets for naphthoquinones

Despite the fact that naphthoquinones exhibit antimycobacterial activity, there is no defined target for this class of compounds. It is postulated that due to structural similarities between 7-methyljuglone and menaquinone it is feasible that 7-methyljuglone interacts with the enzymes in the mycobacterial electron transport chain (**Figure 5.9**) (Mahapatra *et al.*, 2007). The electron flow might be slowed or stopped due to the difference in the redox potential of the incorporated 7-methyljuglone (van der Kooy *et al.*, 2006). Menaquinone is a natural redox cyler in *Mycobacterium*, which mediates electron transfer between different membrane-bound enzymes of the respiratory chain (Garbe, 2004). Menaquinone is an attractive drug target because *M. tuberculosis* lacks ubiquinone and makes use of only menaquinone in the electron transport chain. There is also the possibility that 7-methyljuglone binds to the *Men* enzyme responsible for the formation of menaquinone and inhibits the addition of the hydrophobic side-chain, influencing ATP production (van der Kooy *et al.*, 2006).

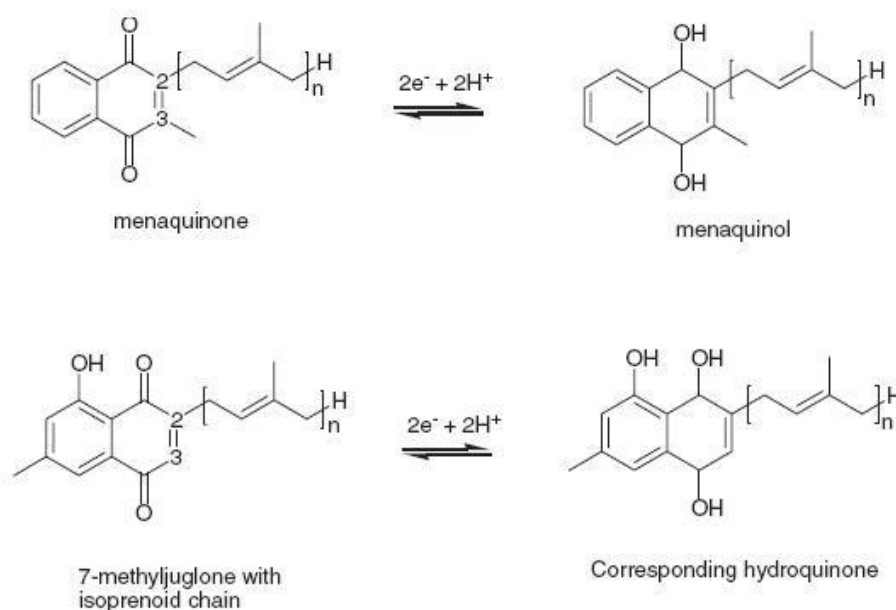


**Figure 5.9: Structural similarities between 7-methyljuglone and menaquinone.**

Due to their structural similarity it is possible that 7-methyljuglone interacts with the enzymes in the mycobacterial electron transport chain (van der Kooy *et al.*, 2006).

Another predicted target for naphthoquinones is Mycothiol disulfide reductase (Mtr) (Mahapatra *et al.*, 2007). Many naphthoquinones are subversive substrates for flavoprotein disulfide reductase such as glutathione reductase, trypanothione reductase and lipoamide dehydrogenase (Salmon-Chemin *et al.*, 2001, Biot *et al.*, 2004). The functions of these enzymes involve the NAD(P)H-dependent reduction of disulfide bonds in proteins or oxidized versions of thiols such as glutathione. Glutathione is absent in *M. tuberculosis*; instead it has millimolar concentration of low molecular weight thiol mycothiol (MSH). MSH, analogous to glutathione, plays an important role in oxidative stress management and in the process is oxidized to disulfide (MSSM). Mtr helps to maintain an intracellular reducing environment by reducing MSSM back to MSH, which is essential for the growth of *M. tuberculosis* (Sareen *et al.*, 2003) and MSH-deficient mycobacteria are sensitive to oxidative stress (Rawat *et al.*, 2002). According to this hypothesis (Mahapatra *et al.*, 2007), naphthoquinones are reduced to semiquinone by Mtr and are regenerated by the reduction of oxygen to semiquinone radicals (**Figure 5.10**). In this way the naphthoquinone substrate is regenerated and the fatal redox cycle

continues. The catalytic properties of Mtr were reported using some commercial naphthoquinones as substrates (Patel & Blanchard, 1999) and this generates the possibility that naphthoquinones could be acting as substrates for disulfide reductase found in *M. tuberculosis*.

But there is no direct correlation between the substrate efficiency of naphthoquinones and their MIC values in whole cell assay (Table 5.3). This indicates that the antibacterial activity of naphthoquinones is the consequence of their activity against multiple biological targets and Mycothiol disulfide reductase is not the target for naphthoquinones. The MIC values obtained from whole cell assays were compared with  $k_{cat}/K_m$  ratio.  $K_m$  values show the substrate binding affinities and the  $k_{cat}$  values express the maximum turnover rates. The  $k_{cat}/K_m$  ratio expresses the substrate efficiency of naphthoquinones for *M. tuberculosis* Mtr. Higher  $k_{cat}/K_m$  values indicate higher substrate efficiency with Mtr. Neodiospyrin has higher  $k_{cat}/K_m$  value in comparison to Diospyrin; however it also has higher MIC which indicates no correlation between the antibacterial activity of the compounds and their specificity for Mycothiol disulfide reductase.

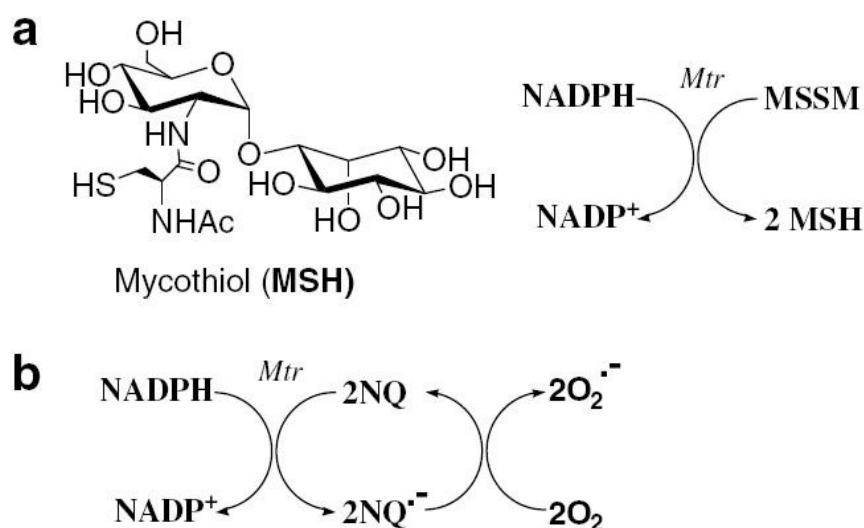


**Figure 5.10: Mycothiol reductase (Mtr) target for naphthoquinones.**

a.) Mycothiol (MSH) and its disulfide reductase: NADPH-dependent Mtr reduction of oxidized mycothiol (MSSM) to its reduced form (MSH). b.) Naphthoquinones can act as a substrate for Mtr instead of mycothiol (Mahapatra et al., 2007).

Compound	MIC ( $\mu\text{M}$ )	$k_{\text{cat}}/K_m (\times 10^5)$
1. 7-methyljuglone	3	931
2. Diospyrin	21	357
3. Neodiospyrin	27	488
4. Menadione	29	152

**Table 5.3: Substrate properties of naphthoquinones with *M. tuberculosis* Mtr (Mahapatra *et al.*, 2007).** The  $k_{\text{cat}}/K_m$  expresses the substrate efficiency of naphthoquinones for *M. tuberculosis* Mtr; higher  $k_{\text{cat}}/K_m$  values indicate higher substrate efficiency.

## 5.6 Naphthoquinones inhibit DNA gyrase

Naphthoquinones such as diospyrin and isodiospyrin have been reported to be inhibitors of *Leishmania donovani* and human type I topoisomerase (Ting *et al.*, 2003, Ray *et al.*, 1998). There have been no reports on the activity of this class of compounds against type II topoisomerases. Since naphthoquinones have antimycobacterial activity, I decided to test them against *Mycobacterial* DNA gyrase. Six different naphthoquinones: 7-methyljuglone, Diospyrin, Neodiospyrin (**Figure 5.11**), Menadione, Shinanolone, Iso-diospyrin (**Figure 5.12**) and crude extracts of *Euclea natalensis* were tested for their activity against *M. tuberculosis* DNA gyrase.

Standard supercoiling assays were performed in the presence of different concentrations of drugs. Out of all the compounds and extracts that were tested 7-methyljuglone and diospyrin were found to be the most potent inhibitors of *M. tuberculosis* DNA gyrase (**Table 5.4**). Concentration-dependent inhibition of supercoiling activity was observed with these compounds.

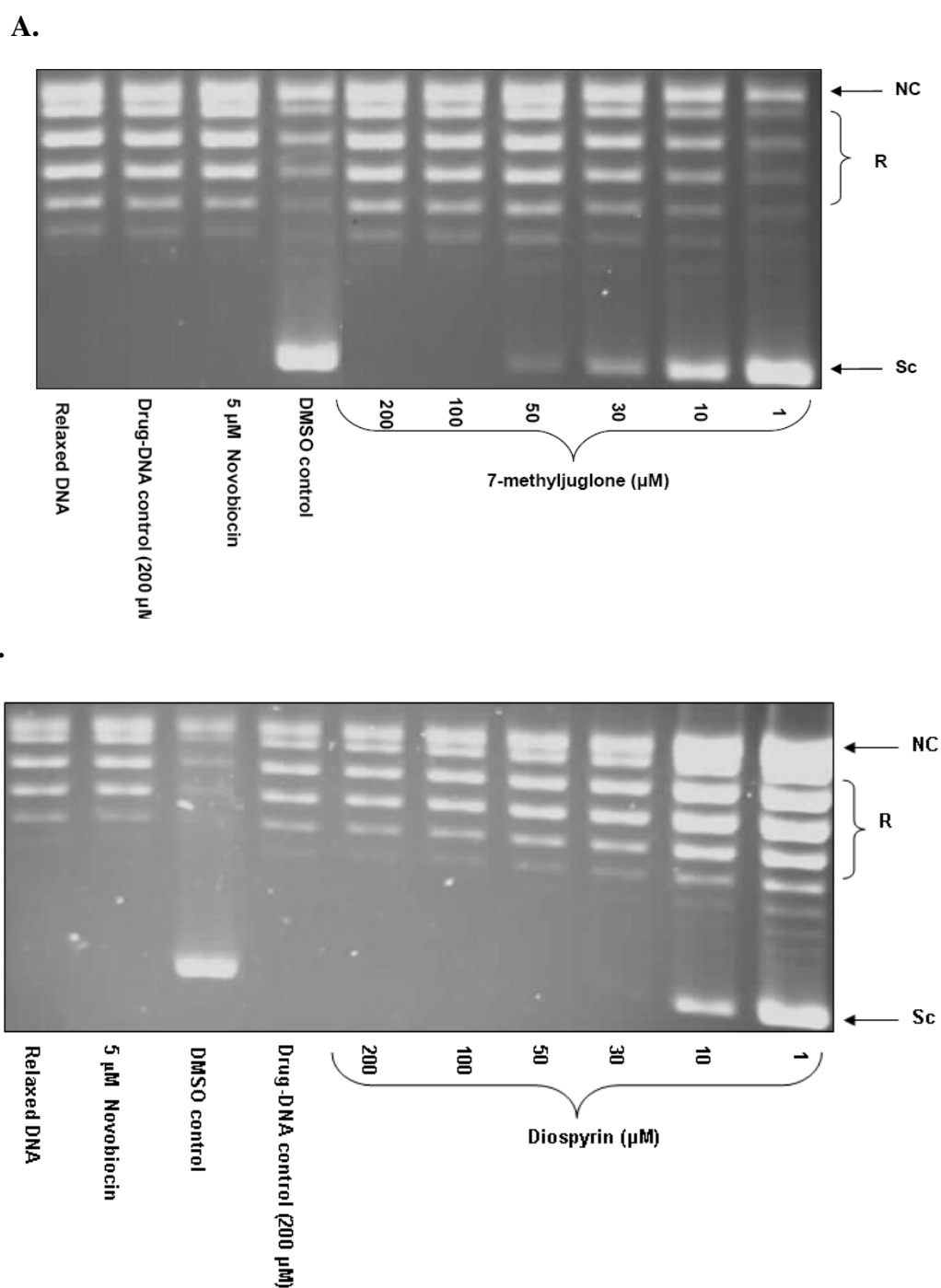


**Figure 5.11: Supercoiling inhibition assay of 7-methyljuglone (A) and diospyrin (B) against wild-type *M. tuberculosis* DNA gyrase. The final concentration of DMSO in assay is only 5% in the presence of the drug. NC: nicked Circular DNA, R: relaxed topoisomers, SC: supercoiled DNA.**

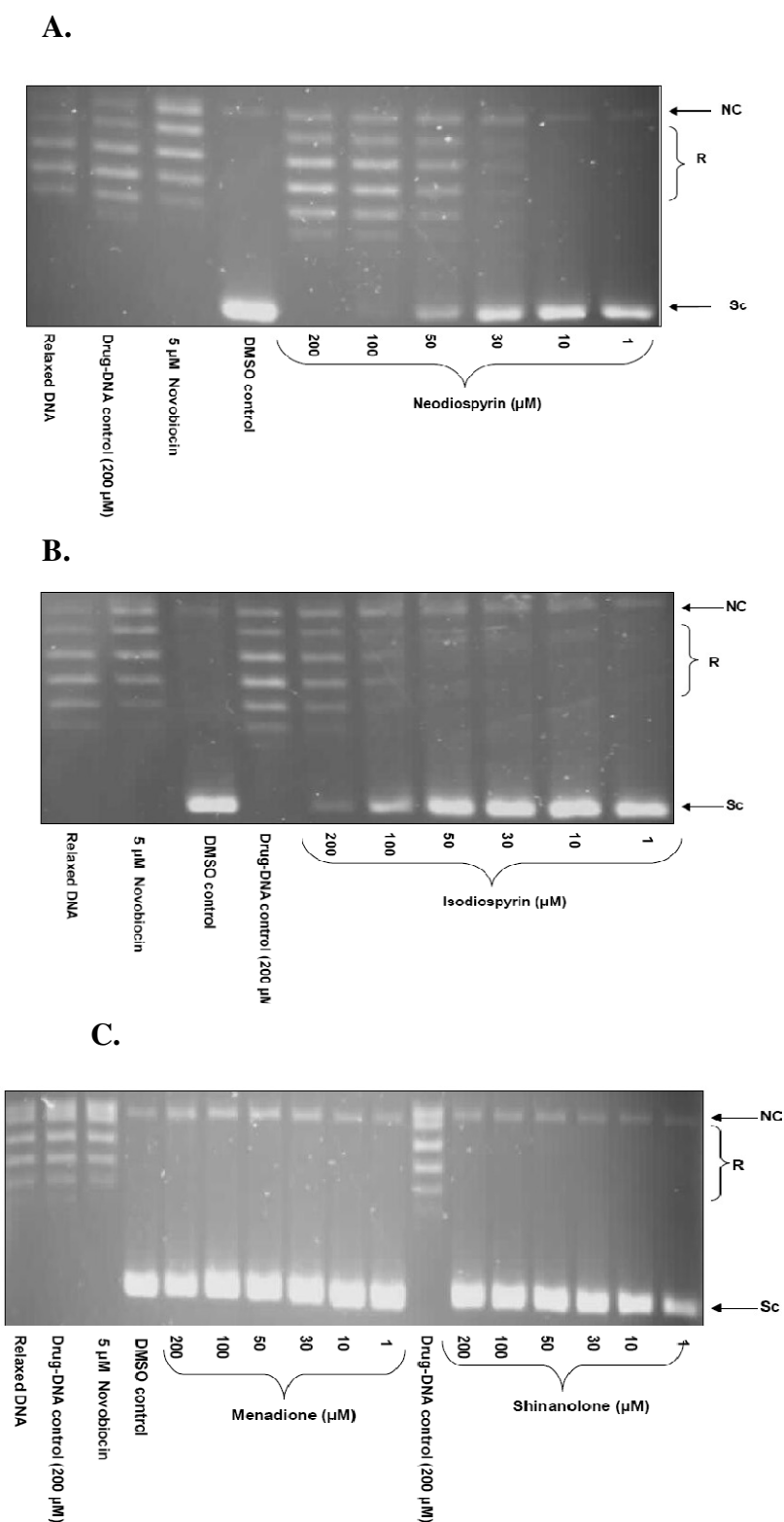


**Figure 5.12: Supercoiling inhibition assay of neodiospyrin (A), isodiospyrin (B), menadione and shinanolone (C) against wild-type *M. tuberculosis* DNA gyrase. NC: nicked Circular DNA, R: relaxed topoisomers, SC: supercoiled DNA.**

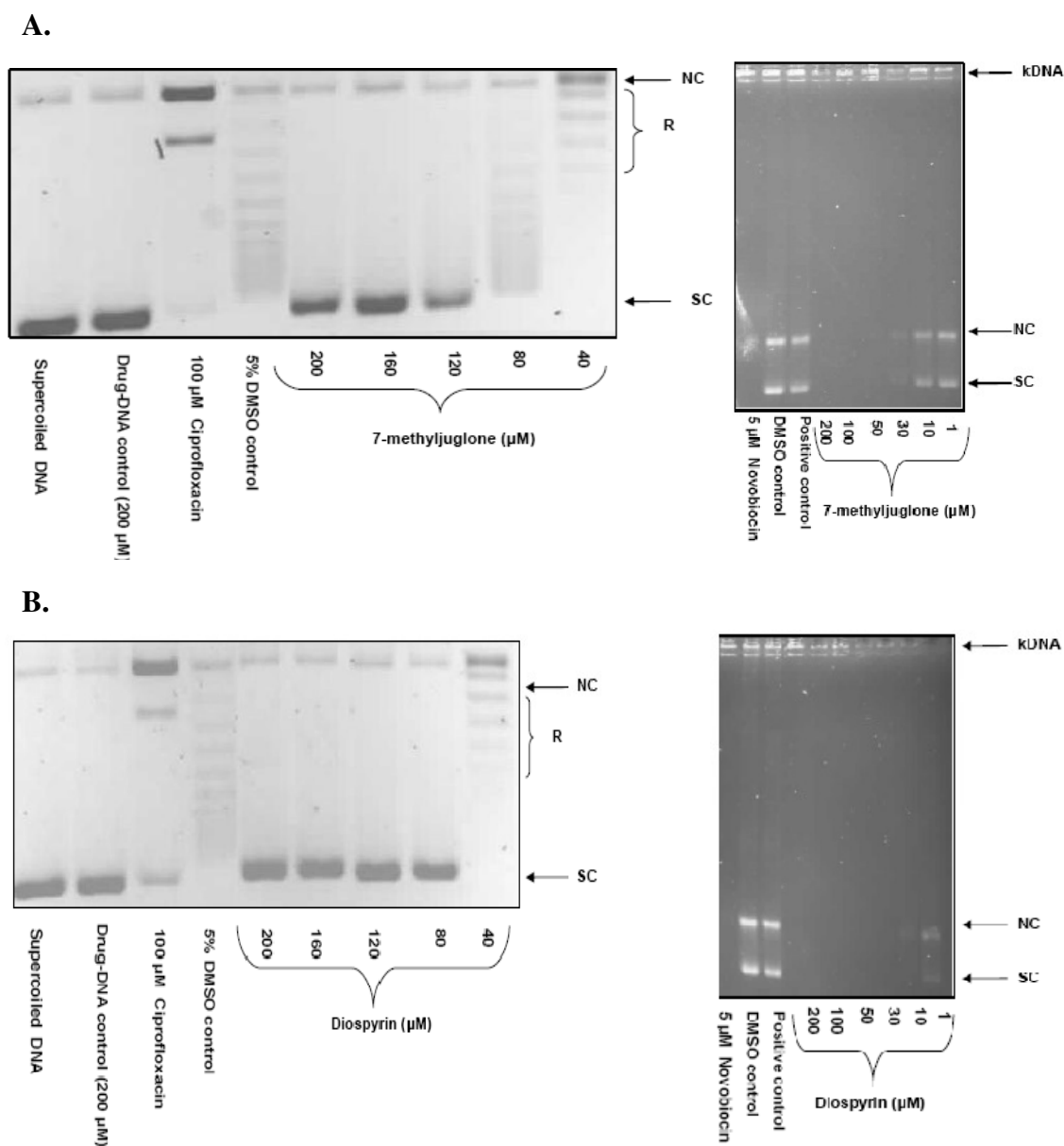


**Figure 5.13: Relaxation and decatenation inhibition assays of 7-methyljuglone (A) and diospyrin (B) respectively against *M. tuberculosis* DNA gyrase. NC: nicked Circular DNA, R: relaxed topoisomers, SC: supercoiled DNA, kDNA: catenated DNA.**

Compound	Approx IC <sub>50</sub>
1. 7-methyljuglone	10 µM
2. Diospyrin	10 µM
3. Neodiospyrin	50 µM
4. Isodiospyrin	100 µM
5. Menadione	> 200 µM
6. Shinanalone	>200 µM
7. Methanol plant extract	133.3 ng/ml*
8. Ethanol plant extract	No inhibition
9. <i>Euclea natalensis</i> crude plant extract	0.25 -2.5 µg/ml*
10. Ciprofloxacin	10 µM

**Table 5.4: DNA supercoiling IC<sub>50</sub> values for naphthoquinones.**

\*Reported in different concentration units as these are crude extracts.

7-methyljuglone and diospyrin, the most potent DNA gyrase inhibitors of all the tested compounds, have IC<sub>50</sub> of ~10 µM, comparable to the IC<sub>50</sub> of ciprofloxacin (10 µM). Besides inhibiting the DNA gyrase supercoiling activity, these compounds also inhibit DNA relaxation and decatenation activity (**Figure 5.13, Table 5.5**).

Compound	Relaxation assay	Decatenation assay
	IC <sub>50</sub>	IC <sub>50</sub>
1. 7-methyljuglone	80-120 µM	10-30 µM
2. Diospyrin	40-80 µM	1-10 µM

**Table 5.5: DNA relaxation and decatenation IC<sub>50</sub> values for naphthoquinones.**

7-methyljuglone and diospyrin also inhibit *E. coli* DNA gyrase. 7-methyljuglone inhibits the supercoiling activity of *E. coli* DNA gyrase with an IC<sub>50</sub> between 50-100 µM, while diospyrin inhibits the *E. coli* DNA gyrase supercoiling activity with an IC<sub>50</sub> between 1-10 µM (**Figure 5.14**). There is a difference in the inhibitory activity of these compounds against *E. coli* DNA gyrase unlike their inhibitory activity against *M. tuberculosis* DNA gyrase. Diospyrin is 5-10 times more effective in inhibiting the supercoiling activity of *E. coli* DNA gyrase in comparison to 7-methyljuglone.

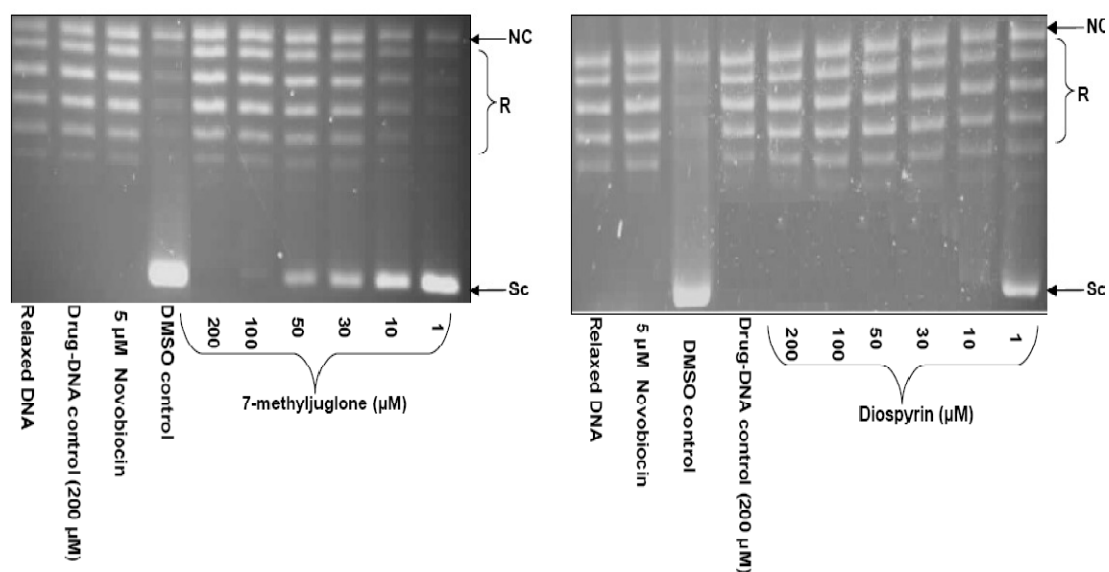


**Figure 5.14: Inhibition of *E. coli* DNA gyrase supercoiling activity in the presence of 7-methyljuglone and diospyrin. NC: nicked Circular DNA, R: relaxed topoisomers, SC: supercoiled DNA.**

As mentioned before, naphthoquinones such as diospyrin have been shown to stabilise the topoisomerase I cleavage complex in vitro (Ray *et al.*, 1998). Wild-type *M. tuberculosis* DNA gyrase, like other bacterial gyrases exhibits significant amount of cleavage activity in the presence of quinolones such as ciprofloxacin (Kampranis & Maxwell, 1998), as in the presence of quinolones the cleavage-religation equilibrium is shifted towards the cleaved form (Aubry *et al.*, 2006a). Therefore to test whether naphthoquinones inhibit the DNA gyrase activity by stabilizing the cleavage complex, DNA cleavage assays were performed in the presence of 7-methyljuglone and diospyrin. The assay was done in the presence and absence of ATP. Unlike the ciprofloxacin control in the assay, no cleaved DNA was formed either in the presence or absence of ATP (**Figure 5.15, Figure 5.16**). This observation suggests that naphthoquinones such as 7-methyljuglone and diospyrin do not inhibit the DNA gyrase activity by stabilising the cleavage complex. Thus there is difference in the mode of inhibition of topoisomerase I and DNA gyrase by naphthoquinones.

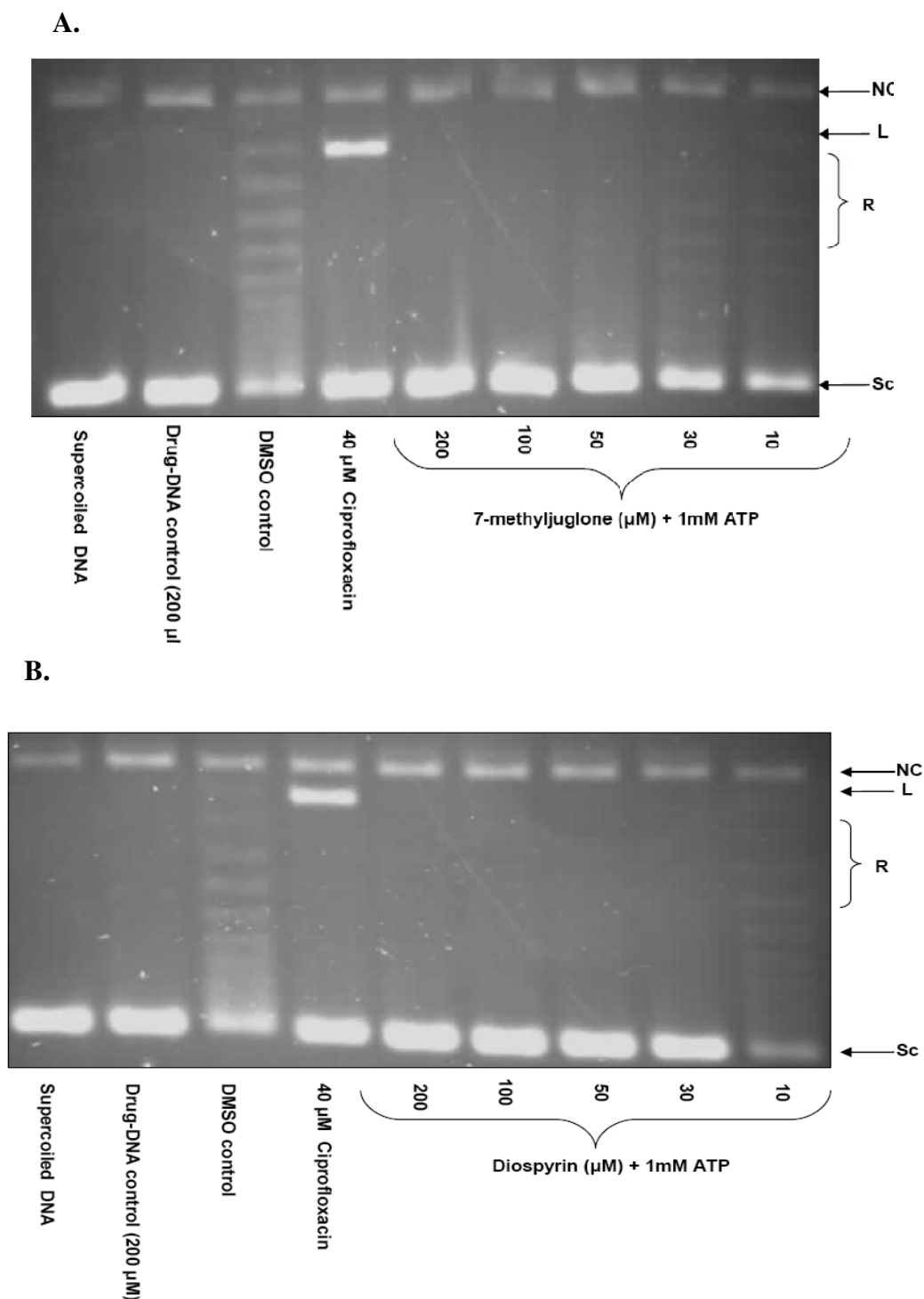


**Figure 5.15: DNA cleavage assay in the presence of different concentrations of 7-methyljuglone (A) and diospyrin (B) and in the presence of 1 mM ATP. Ciprofloxacin-induced DNA cleavage is observed in the control; but no linear DNA is observed with the DMSO control and drugs. NC: nicked Circular DNA, L: Linear DNA, R: relaxed topoisomers, SC: supercoiled DNA.**

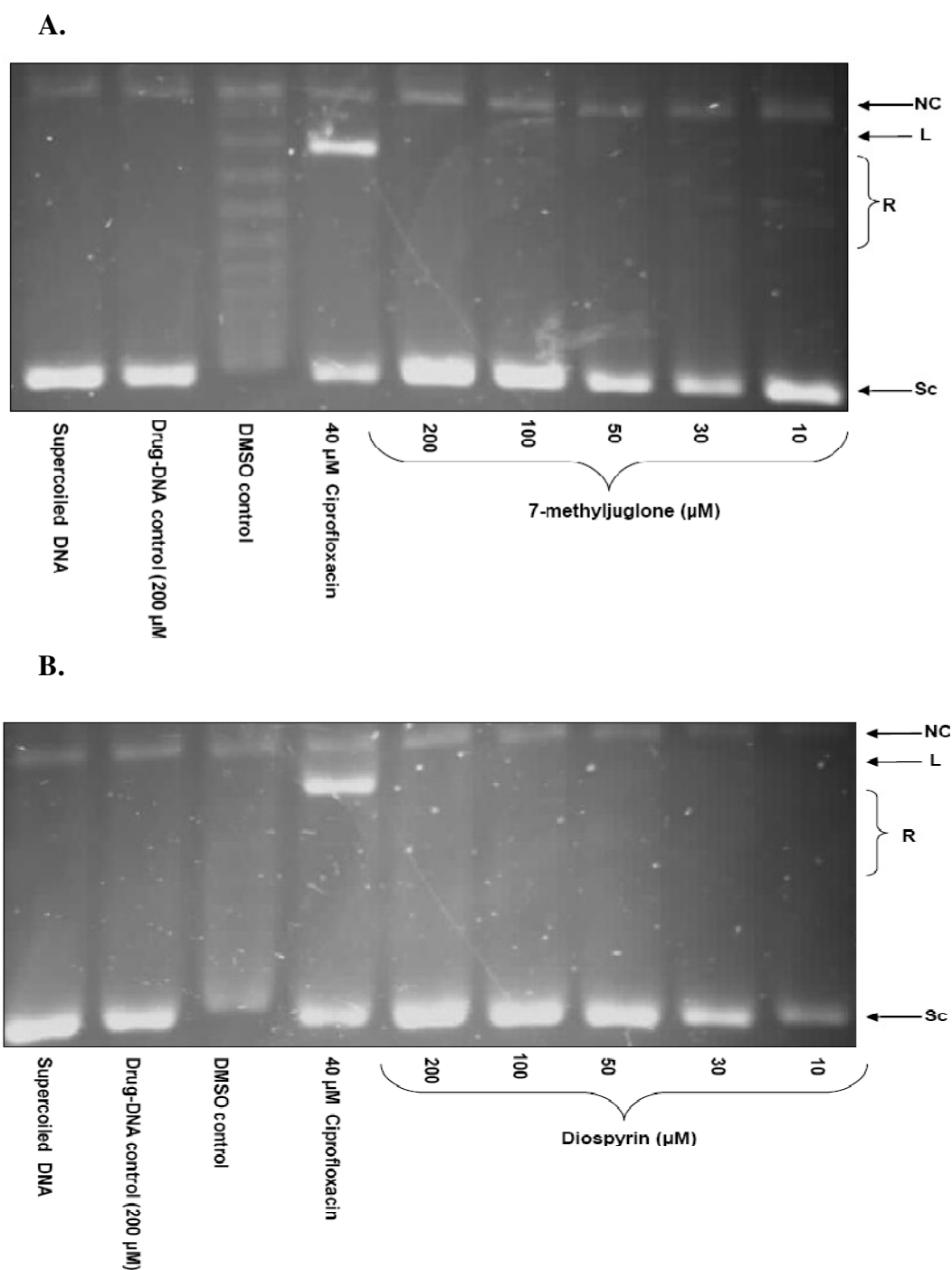


**Figure 5.16: DNA cleavage assay in the presence of 7-methyljuglone (A) and diospyrin (B) in the absence of ATP. Ciprofloxacin-induced DNA cleavage is observed in the control; but no linear DNA is observed with the DMSO control and drugs. NC: nicked Circular DNA, L: linear DNA, R: relaxed topoisomers, SC: supercoiled DNA.**

## 5.7 *E. coli* Inhibitory activity

Naphthoquinones have been shown to have antimycobacterial activity (Mahapatra *et al.*, 2007). I wanted to test if these compounds can also inhibit Gram-negative bacteria such as *E. coli*. A pilot study done on *E. coli* NR698 is shown in **Figure 5.17**. *E. coli* NR698 carries *imp4213* allele that increases the outer membrane permeability. *imp4213* allele is an in-frame deletion allele in the *imp* gene (increased membrane permeability), which encodes a protein essential for outer membrane assembly (Ruiz *et al.*, 2005). The inhibitory assay was performed in LB media. OD at 600 nm was recorded at different time points for two different concentrations of diospyrin (MIC & 10 × MIC). Similarly as a positive control, growth was recorded at different concentrations of ciprofloxacin (MIC & 10 × MIC). Appropriate DMSO controls were taken to observe the effect of the solvent. There is no apparent effect of DMSO in comparison to diospyrin. Inhibitory activity was observed at MIC & 10 × MIC for both diospyrin and ciprofloxacin.

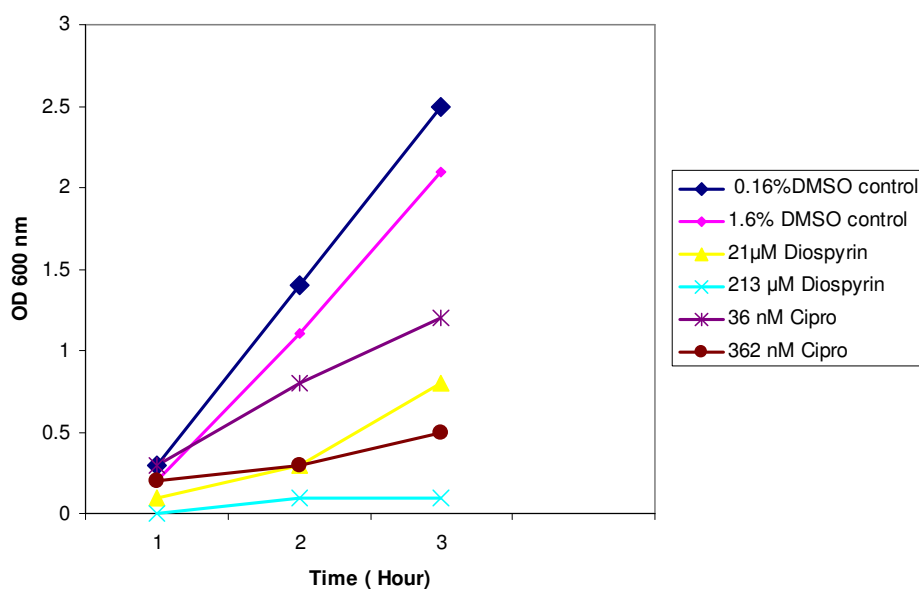


**Figure 5.17: In-vitro inhibitory activity of diospyrin against *E. coli* NR698 (Ruiz *et al.*, 2005).** 0.16% and 1.6% DMSO are equivalent to the concentration of DMSO in test samples with 21 μM (MIC) and 213 μM (10 × MIC) diospyrin. Ciprofloxacin control showed inhibitory activity at the concentration of 36 nM (MIC) and 362 nM (10 × MIC).

## 5.8 Diospyrin binding site

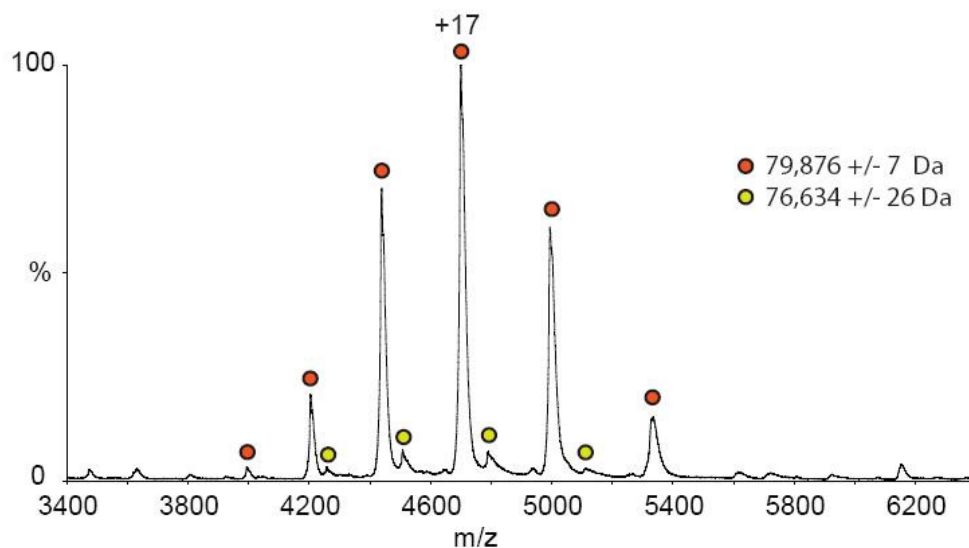
Since functional DNA gyrase exists as an A<sub>2</sub>B<sub>2</sub> complex, it is important to identify the DNA gyrase subunit to which naphthoquinones bind or interact. This information is necessary to investigate the drug-binding site and to get further insight into the mechanism of inhibition. Nanoflow-electrospray ionization mass spectrometry (nano-ESI-MS) was employed to identify the DNA gyrase subunit that is involved in interacting with diospyrin. These experiments were performed in collaboration with Dr Adam Mckay (University College London, UK). All spectra were recorded on the high mass modified ESI-ToF mass spectrometer (Waters SYNAPT HDMS) with the samples prepared in 250 mM sodium acetate (**Materials and Methods**) except in one instance when Waters LCT Premier XE was used. The experiments were performed with diospyrin (MW: 374.35 Da), due to its higher molecular weight in comparison to 7-methyljuglone (MW: 188.18 Da). It is easier to discriminate the peaks corresponding to the non-covalent binding of higher molecular weight ligands to protein on nano-ESI-MS. The diospyrin binding studies using nano-ESI-MS were performed on *M. tuberculosis* GyrA, *M. tuberculosis* GyrB, *M. tuberculosis* GyrA + GyrB, *E. coli* GyrB43 and *E. coli* GyrB47. The results of the diospyrin binding studies are summarized in **Table 5.6**.

DNA gyrase subunits	Diospyrin binding
1. <i>M. tuberculosis</i> GyrA	no diospyrin binding observed.
2. <i>M. tuberculosis</i> GyrB	diospyrin binding observed at 8-fold and 16 -fold excess of drug.
3. <i>M. tuberculosis</i> GyrA + GyrB	selective binding to GyrB observed with GyrB signals masking the GyrA profile.
4. <i>E. coli</i> GyrB43	diospyrin binding observed at 16- fold excess of drug.
5. <i>E. coli</i> GyrB47	no diospyrin binding observed.

**Table 5.6: Summary results of diospyrin binding studies using nano- ESI-MS.**

### 5.8.1 *M. tuberculosis* GyrB-diospyrin complex

*M. tuberculosis* GyrB was buffer exchanged into 250 mM sodium acetate and tested for its stability under the conditions of the mass spectrometry experiment. The mass spectrometric profile of GyrB subunit shows two different charge species. Analysis of the peaks gives a mass of 79,876 +/- 7 Da corresponding to the *M. tuberculosis* GyrB monomer (theoretically calculated MW: 79262.58 Da) and 76,634 +/- 26 Da as shown in **Figure 5.18**. The presence of the low molecular weight species could be due to truncation of *M. tuberculosis* GyrB. Despite the presence of lower molecular weight species, the molecular species with mass of 79,876 +/- 7 Da is the prominent species.

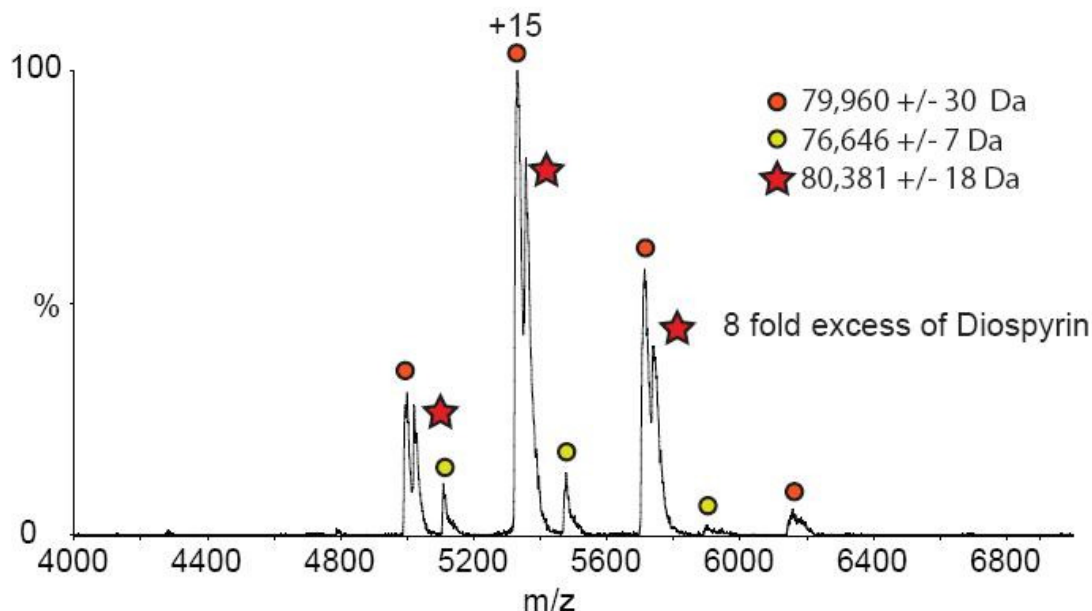
*M. tuberculosis* GyrB

**Figure 5.18:** Mass spectrometry spectrum of *M. tuberculosis* GyrB monomer (79-kDa). +17 represents the charged state of the peak.

The next step was to determine if diospyrin binds to the *M. tuberculosis* GyrB. Mass spectrometry data was collected for GyrB in the presence of an 8-fold excess of diospyrin. Three different charge species are observed with masses 79,960 +/- 30 Da; 76,646 +/- 7 Da and 80,381 +/- 18 Da as shown in **Figure 5.19**. The species with a mass of 79,960 +/- 30 Da (theoretically calculated MW: 79,262.58 Da) corresponded to the monomeric GyrB subunit without diospyrin. The experimentally determined molecular weight is more than the theoretically calculated molecular weight due to insufficient removal of either solvent and/or buffer ions during the electrospray process resulting in an increase in the measured mass as well as a broadening of the peaks in the spectrum. This has also been observed previously for other non-covalent assemblies (McKay *et al.*, 2006). The species with a molecular weight of 76,646 +/- 7 Da is also present, in the all the mass spectrometric profile of *M. tuberculosis* GyrB and is a contamination. Interestingly the third molecular species with a mass of 80,381 +/- 18 Da (theoretically calculated MW: 80,334.35 Da), corresponded to *M. tuberculosis* GyrB monomer bound with

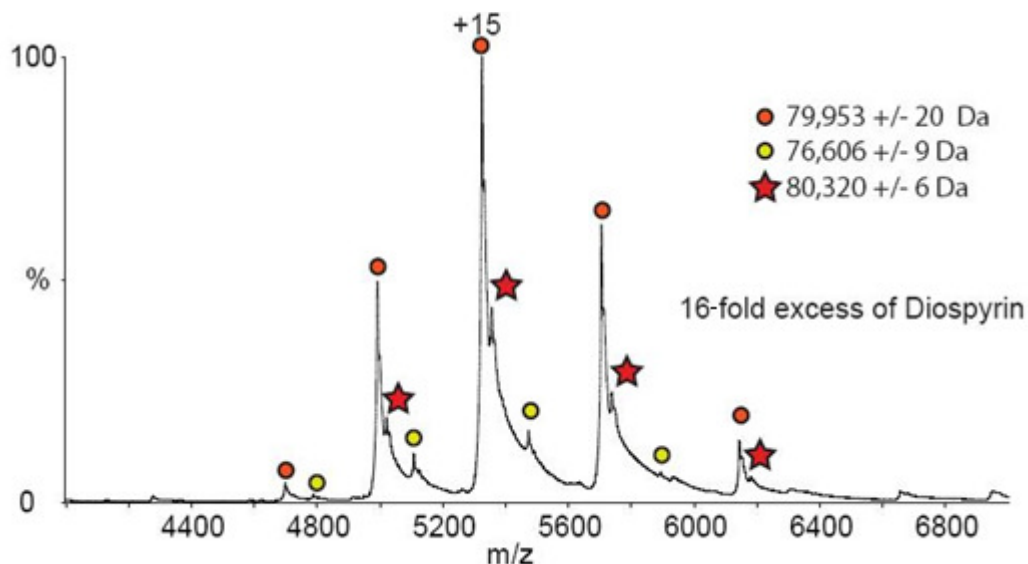
diospyrin (MW: 374.35). The peaks representing the diospyrin- bound GyrB are observed as shoulders adjacent to the peaks representing the GyrB monomer.

***M. tuberculosis* GyrB + 8-fold diospyrin**



**Figure 5.19:** Mass spectrometry spectrum of *M. tuberculosis* GyrB in the presence of an 8-fold excess of diospyrin. The coloured stars represent the shoulder peaks corresponding to the diospyrin-bound species. +15 represents the charge state of the peak.

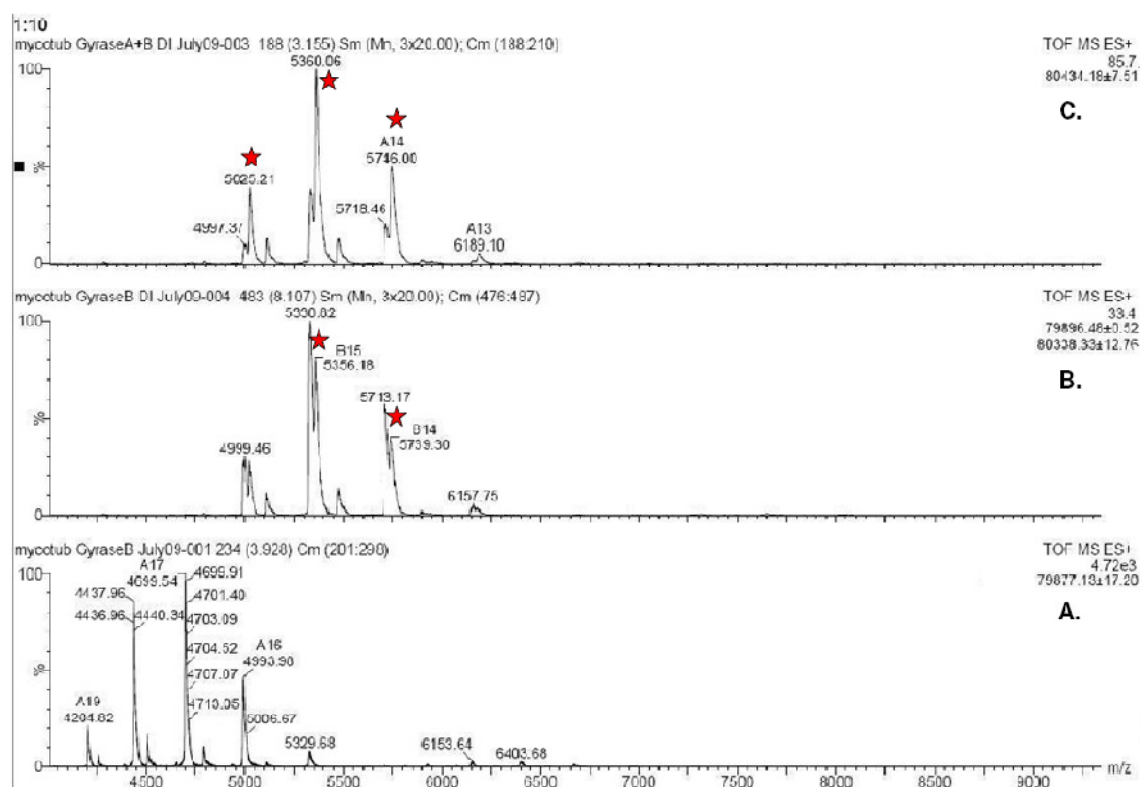
Similarly, when the same experiment was repeated in the presence of a 16-fold excess of diospyrin (**Figure 5.20**), three different charge species with a mass of 79,953 +/- 20 Da; 76,606 +/- 9 Da, 80,320 +/- 6 Da are observed as shown in **Figure 5.20**. As indicated above, the species with a mass of 79,953 +/- 20 Da (theoretically calculated MW: 79262.58 Da) and 80,320 +/- 6 Da (theoretically calculated MW: 80,327) represented the *M. tuberculosis* GyrB monomer with and without the bound diospyrin. More peaks corresponding to the drug bound protein is observed at 16-fold excess of diospyrin due to the resolution being affected by the excess DMSO and drug.

***M. tuberculosis* GyrB + 16-fold diospyrin**

**Figure 5.20:** Mass spectrometry spectrum of *M. tuberculosis* GyrB in the presence of a 16-fold excess of diospyrin. The coloured stars represent the shoulder peaks corresponding to the diospyrin-bound molecular species. +15 represent the charge state of the peak.

Similar experiments done with *M. tuberculosis* GyrA subunit revealed the dimeric states of the protein, but no peaks corresponding to the diospyrin-bound GyrA are observed. This does not completely eliminate the possibility that diospyrin binds GyrA, as it is possible that the peaks due to diospyrin binding could not be resolved due to the high molecular weight of *M. tuberculosis* GyrA (93083.13 Da) in comparison to the extremely low molecular weight of diospyrin (374.35 Da). The resolution is further affected by the excess of DMSO and drug.

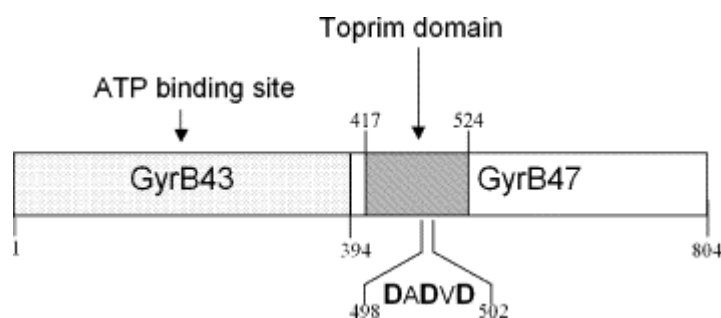
When *M. tuberculosis* GyrA and GyrB were mixed together in equimolar concentration in the presence of a 10-fold excess of diospyrin, mass spectrometry data revealed peaks of a single species with six different charged states as shown in **Figure 5.21**. Analysis of peaks gives a mass of  $80434.18 \pm 7.51$  corresponding to the diospyrin bound *M. tuberculosis* GyrB. This may be due to the masking of *M. tuberculosis* GyrA signals. The mass spectrometry data in this case was collected on Waters LCT Premier XE.



**Figure 5.21: Mass spectrometry spectra for protein-diospyrin complexes.** (A) *M. tuberculosis* GyrB; (B) GyrB in the presence of a 10-fold excess of diospyrin; (C) GyrA and GyrB mixed together in equimolar concentration in the presence of a 10-fold excess of diospyrin.

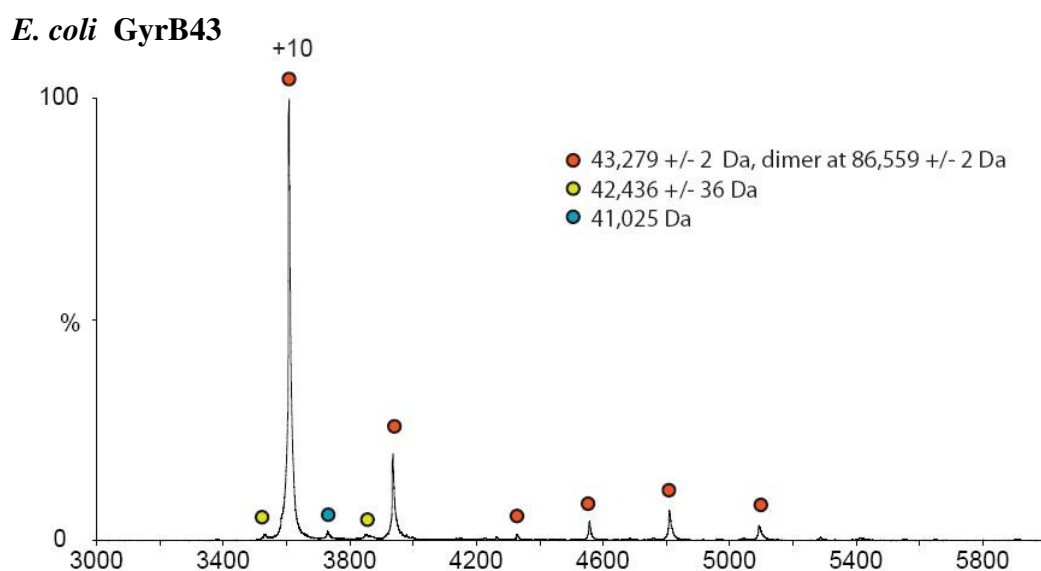
### 5.8.2 *E. coli* GyrB43-diospyrin complex

Based on the results of mass spectrometry experiments performed with *M. tuberculosis* GyrB, the next step was to identify the domain in GyrB that facilitated diospyrin binding. For this experiment the N-terminal domain of *E. coli* GyrB (GyrB43) and the C-terminal domain (GyrB47), were used (Figure 5.22). The crystal structure of *E. coli* GyrB43 with the ATP analogue ADPNP (Brino *et al.*, 2000, Wigley *et al.*, 1991) is available and has been shown to have the ATP-binding site (Ali *et al.*, 1993). GyrB47 interacts with the N-terminal domain of GyrA and forms the part of cleavage-religation domain (Brown *et al.*, 1979, Gellert *et al.*, 1979).

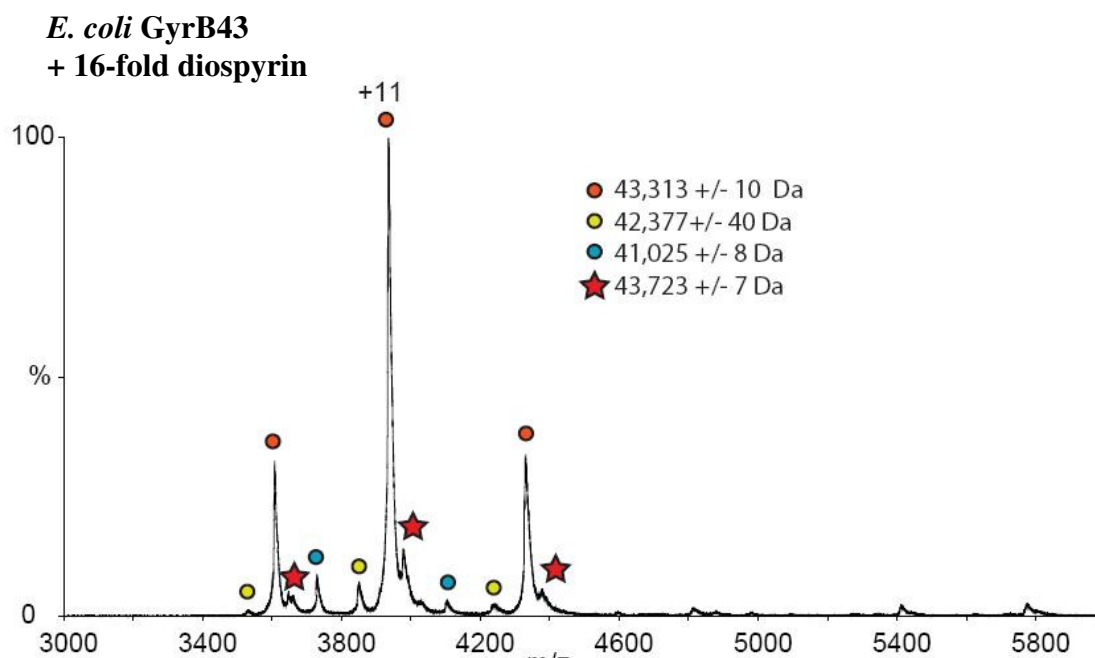


**Figure 5.22: Representation of GyrB functional domains.**

Like *M. tuberculosis* GyrB, *E. coli* GyrB43 is a monomer under the conditions of the mass spectrometry experiment. The mass spectrometric profile of *E. coli* GyrB43 subunit shows three different charge species. Analysis of peaks gives masses of 43,279  $\pm$  2 Da corresponding to the *E. coli* GyrB43 monomer (theoretically calculated MW: 43023.50 Da); 42,436  $\pm$  36 Da and 41,025 Da as shown in **Figure 5.23**. As observed in case of *M. tuberculosis* GyrB, the observed lower molecular weight species with mass of 42,436  $\pm$  36 Da and 41,025 Da may be due to the fragmentation of *E. coli* GyrB43 or contamination.



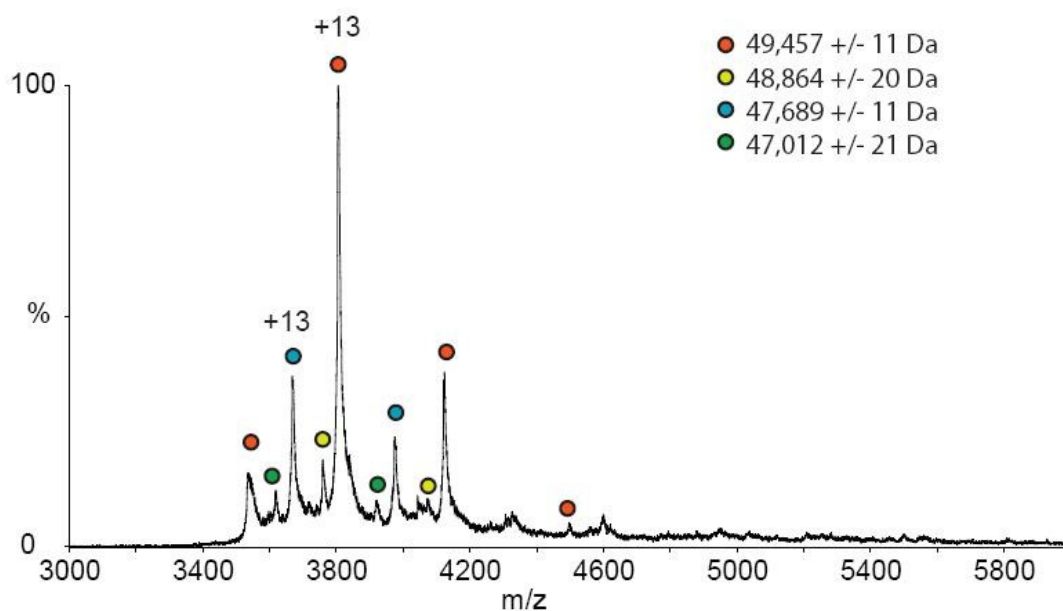
**Figure 5.23: Mass spectrometry spectrum of *E. coli* GyrB43. +10 represents the charge state of the peak.**



**Figure 5.24:** Mass spectrometry of *E. coli* GyrB43 in the presence of a 16-fold excess of diospyrin. The coloured stars represent the shoulder peaks corresponding to the diospyrin-bound species. +11 represents the charge state of the peak.

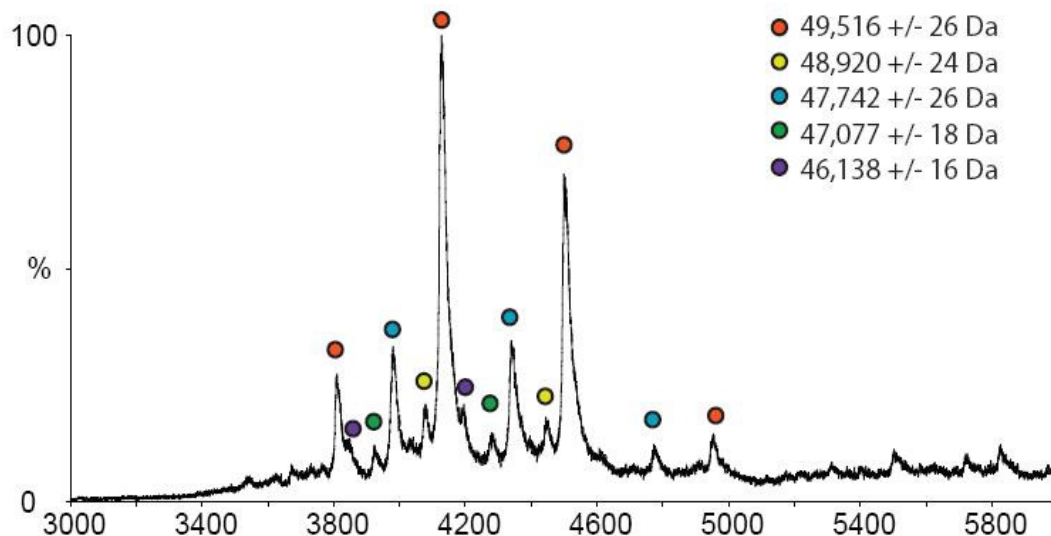
*E. coli* GyrB43 in the presence of a 16-fold excess of diospyrin, reveals a charge species in the spectrum with a mass of 43,723 +/- 7 Da corresponding to diospyrin-bound GyrB43 (theoretically calculated MW: 43687.35) in addition to the GyrB43 monomer (theoretically calculated MW: 43023.50 Da) with a mass of 43,313 +/- 10 Da; and lower molecular weight species with a mass of 42,377 +/- 40 Da and 41,025 +/- 8 Da, as shown in **Figure 5.24**.

In the case of *E. coli* GyrB47 in the absence of diospyrin, analysis of the peaks gives masses of 49,457 +/- 11 Da; 48,864 +/- 20 Da ; 47,689 +/- 11 Da and 47,012 +/- 21 Da corresponding to *E. coli* GyrB47 monomer (theoretically calculated MW: 46581.93 Da) as shown in **Figure 5.25**.

*E. coli* GyrB47

**Figure 5.25:** Mass spectrometry spectrum of *E. coli* GyrB47. **+13** represents the charge state of the peak.

In the presence of a 16-fold excess of diospyrin, no peaks corresponding to the diospyrin-bound *E. coli* GyrB47 were observed. Analysis of the peaks gives masses of 49,516 +/- 26 Da; 48,920 +/- 24 Da; 47,742 +/- 26 Da; 47,077 +/- 18 Da corresponding to the GyrB47 monomer (theoretically calculated MW: 46581.93 Da) and 46,138 +/- 16 Da (**Figure 5.26**). The peaks corresponding to 46,138 +/- 16 Da, 49,516 +/- 26 Da; 48,920 +/- 24 Da may be due to contamination. This indicates that diospyrin does not bind to *E. coli* GyrB47.

***E. coli* GyrB47 + 16-fold diospyrin**

**Figure 5.26:** Mass spectrometry spectrum of *E. coli* GyrB47 in the presence of a 16- fold excess of diospyrin.

## 5.9 Limited Proteolysis

Limited proteolysis studies have been performed to study the interaction of other DNA gyrase inhibitors such as CcdB (Kampranis *et al.*, 1999c), novobiocin (Kampranis *et al.*, 1999b), quinolones (Kampranis *et al.*, 1999c), and SD8 (Sissi *et al.*, 2010) with GyrA, GyrB and A<sub>2</sub>B<sub>2</sub>. Results from these studies have shown a characteristic proteolysis pattern for *E. coli* GyrB with the protection of the C-terminal 47-kDa domain in presence of quinolones, a 13-kDa fragment (derived from the digestion of the 43-kDa N-terminal domains) in the presence of novobiocin, and delay of a 25-kDa proteolytic fragment in the presence of SD8.

Since the ESI-MS experiments indicate the N-terminal domain of GyrB as the potential target site for diospyrin, limited trypsin proteolysis experiments were done with *M. tuberculosis* GyrB and *E. coli* GyrB43 with appropriate controls. There is an effect of diospyrin on the proteolytic profile of *M. tuberculosis* GyrB and *E. coli* GyrB43. Control experiments with *M. tuberculosis* GyrA did not show any change in the proteolytic profile of this protein.

In the case of *M. tuberculosis* GyrB, four distinct bands of ~55- kDa, ~33- kDa, ~30-kDa and ~25-kDa are observed at 5 and 10 min, with subsequent

degradation of protein in further time points. The ~33- kDa, ~30- kDa and ~25- kDa fragments may be due to further digestion of ~55- kDa fragment (**Figure 5.27**).

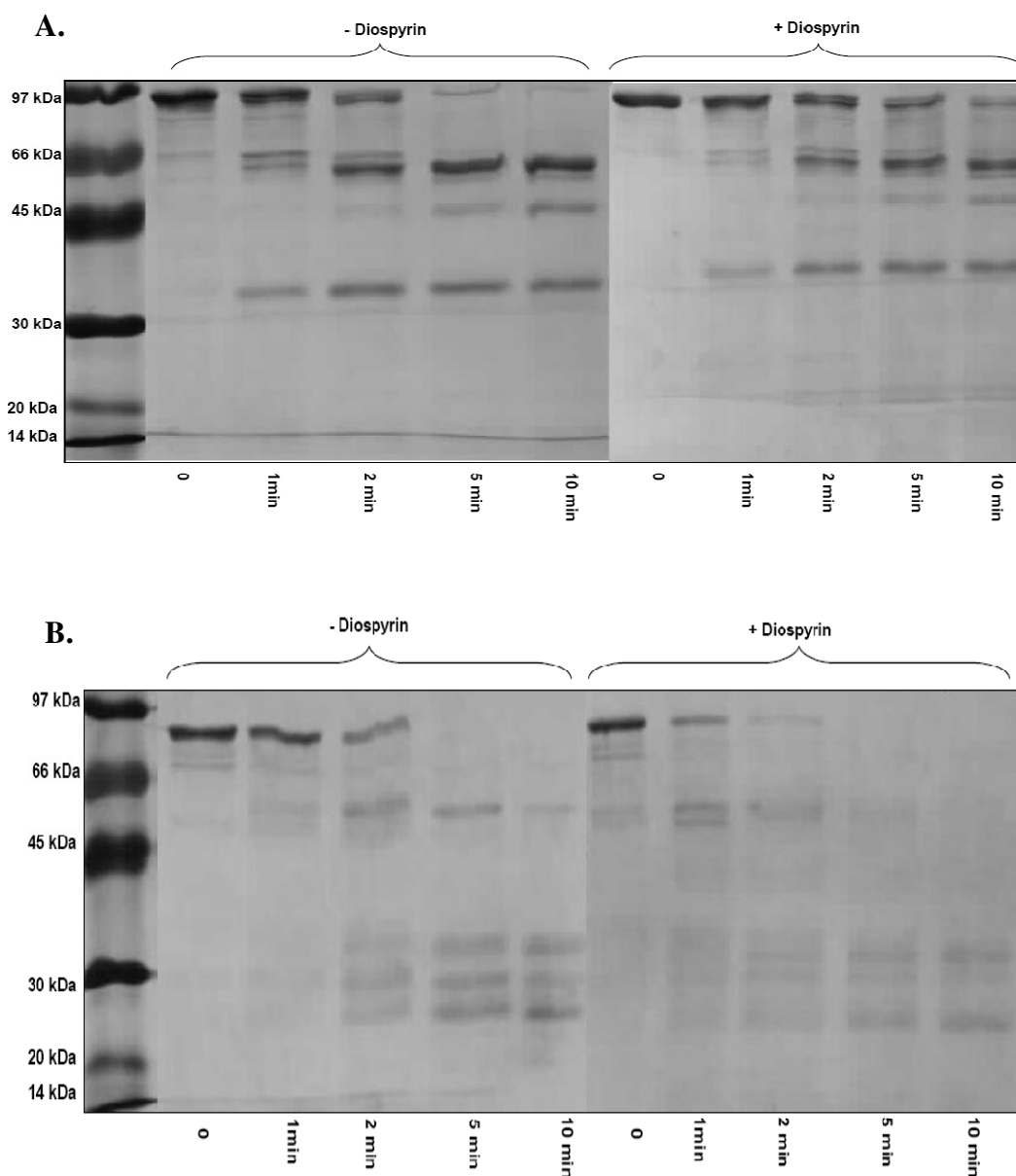


**Figure 5.27:** Tryptic digest of the *M. tuberculosis* GyrA (A) and *M. tuberculosis* GyrB (B) in the presence and absence of diospyrin. 4  $\mu$ M protein was incubated with 1  $\mu$ g/ml trypsin, at 37°C, in the presence or absence of 100  $\mu$ M diospyrin. For samples without diospyrin, DMSO was added to a final concentration of 2%. Samples were taken at various time points and subsequently analysed by SDS-PAGE.

It has been shown that it is around 20% DMSO that major stimulation in any enzyme activity is observed (Rammler, 1967); but the DMSO percentage in all the limited proteolysis experiments was not more than 2.5%. Therefore any differences observed in the digestion pattern will not be due to the effect of DMSO on the enzyme activity of trypsin. In the presence of 100  $\mu$ M diospyrin, the *M. tuberculosis* GyrB is more labile to digestion by trypsin with the disappearance of ~55-kDa band and disappearance of the other three bands. Similar experiments with *M. tuberculosis* GyrA do not show any significant differences in the proteolysis pattern, with bands of ~62-kDa, ~45-kDa and ~32-kDa observed in the absence and presence of diospyrin, as shown in **Figure 5.27**.

Trypsin digestion profiles in the case of *E. coli* GyrB43 (43-kDa) are different in the absence and presence of diospyrin at the 30 min and 60 min time points. At the 30 min time point, the ~31-kDa fragment disappears with the emergence of a ~17-kDa band, which stays on until 60 min with the complete disappearance of the ~31-kDa fragment. This pattern is similar to that observed with novobiocin, where a ~13-kDa is protected in the presence of the drug (Kampranis *et al.*, 1999b). However like *M. tuberculosis* GyrA, the *E. coli* GyrA trypsin digestion profile does not change in the presence of diospyrin. Both in the presence of DMSO and diospyrin, the characteristic bands of ~62-kDa, ~45-kDa are obtained (**Figure 5.28**).

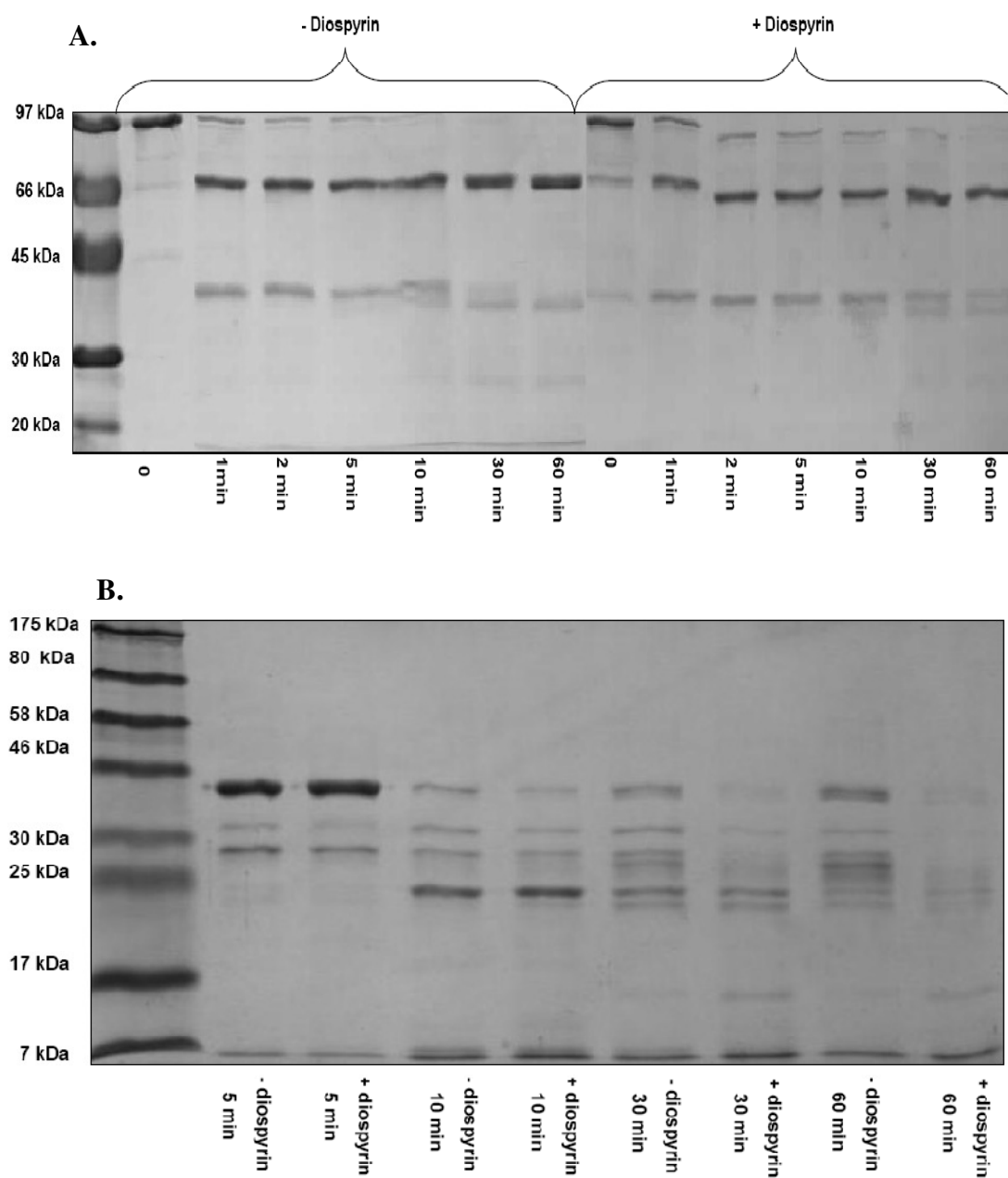


**Figure 5.28:** Tryptic digest of *E. coli* GyrA (A) and *E. coli* GyrB43 (B) in the presence and absence of diospyrin.  $4 \mu\text{M}$  of the GyrA and GyrB43 were incubated with  $1 \mu\text{g/ml}$  trypsin and  $12 \mu\text{g/ml}$  trypsin, at  $37^\circ\text{C}$ , in the presence or absence of  $100 \mu\text{M}$  diospyrin. For samples without diospyrin, DMSO was added to a final concentration of 2%. Samples were taken at various time points and subsequently analysed by SDS-PAGE.

These changes in the trypsin digestion profiles of *M. tuberculosis* GyrB, and *E. coli* GyrB43, suggest that diospyrin induces conformational changes on binding to the GyrB.

## 5.10 Surface plasmon resonance

The nano-ESI-MS and limited proteolysis experiments indicated GyrB as the potential binding site for diospyrin. Surface plasmon resonance studies under the guidance of Dr. Sandra Grieve (John Innes Centre, Norwich, UK) were performed as an alternative sensitive method to study diospyrin binding and to investigate if the diospyrin shares partially or completely the novobiocin-binding site. The diospyrin binding studies were performed with *E. coli* GyrB43, *M. tuberculosis* GyrA and GyrB subunits immobilised on to CM5 chips (carboxymethylated dextran covalently attached to a gold surface) as described in the **Material and Methods** section. The sensograms were recorded on a BIAcore T100. Initial binding studies were done with the well-characterised aminocoumarin novobiocin as a control to verify the binding properties of the immobilised protein. SPR studies carried out in the past (Kampranis *et al.*, 1999b) with novobiocin were used as the starting point.

Novobiocin binding studies, done in triplicate, clearly show drug binding to *E. coli* GyrB43 and *M. tuberculosis* GyrB with drug concentration between 20 -100 nM. Although binding was observed at different drug concentrations, regeneration with 2 M KCl was not efficient, which in turn affected the quality of the sensograms. Although 2 M KCl was reported to be the regenerating agent (Kampranis *et al.*, 1999b) the sensitivity of BIAcore T100 could detect inefficient regeneration, which may not have been detected in the past by the BIAcore 2000 system. Regeneration scouting was done with a range of recommended regeneration agents such as 10 mM glycine (pH 2, 2.5, 3), 4 M NaCl, 20 mM NaOH and 40 mM NaOH with different percentages of surfactant P20. None of the regenerations were ideal; on the contrary some of them were harsh and affected the surface of the chip. Based on the available data the apparent estimated  $K_d$  for novobiocin for *E. coli* GyrB43 and *M. tuberculosis* GyrB are in the range of  $10^{-8}$  M and  $10^{-7}$ - $10^{-8}$  M respectively (**Figure 5.29**). These  $K_d$  are consistent with the those reported in the past (Kampranis *et al.*, 1999b). The novobiocin control experiment highlighted the problem with regeneration conditions

but at the same time verified the binding efficiency of the immobilised proteins on the CM5 chip.

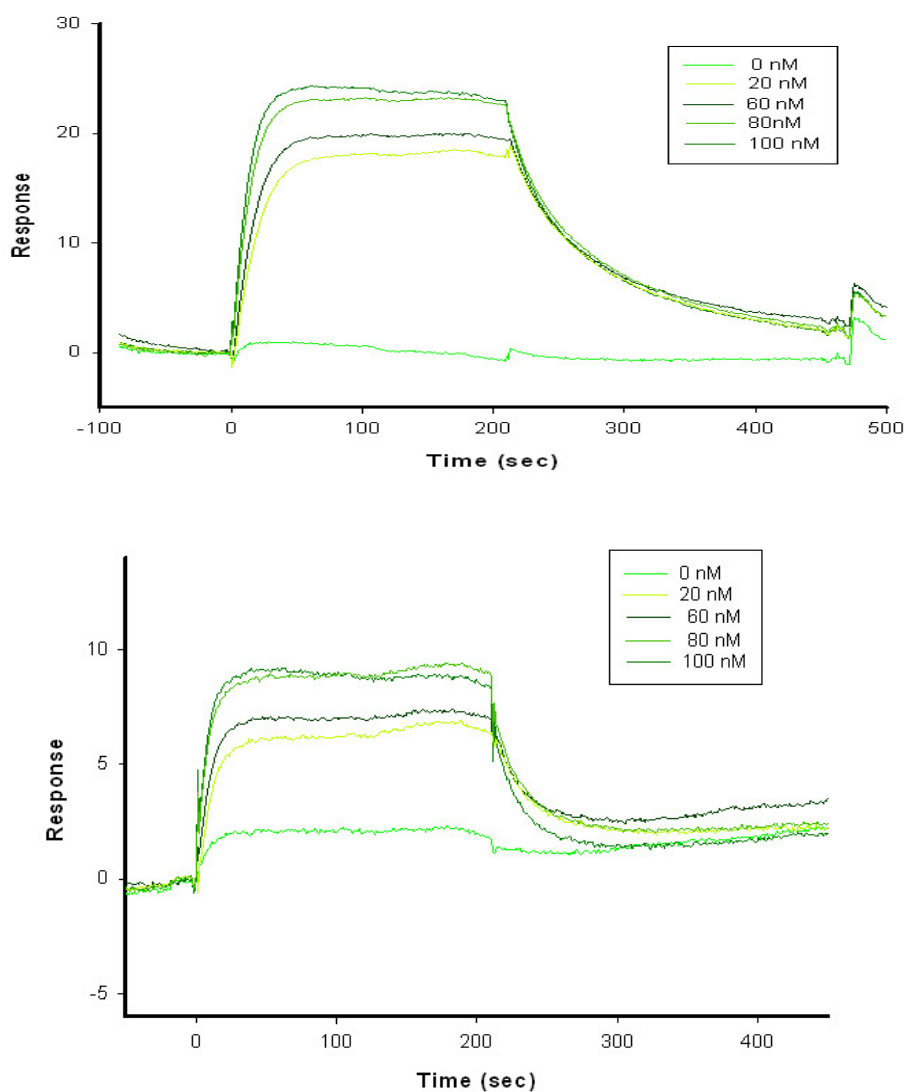


**Figure 5.29: Surface plasmon resonance data showing binding of novobiocin to *E. coli* GyrB43 (top panel) and *M. tuberculosis* GyrB (bottom panel).**

It is important to determine the regeneration conditions to make sure that binding sites are available again for ligand binding after repeated cycles of ligand injection and regeneration. Precise kinetic data cannot be obtained without efficient regeneration.

Diospyrin showed binding with *E. coli* GyrB43 with a response of 50 RU units, but like novobiocin there were issues with the regeneration. After trying a range of regeneration condition, NaOH in the concentration range of 5.0 – 5.8 mM was found to be efficient. Based on the regeneration scouting experiment 5.5 mM NaOH was used for regeneration. Sensograms obtained with 5.5 mM NaOH as the regeneration conditions were of better quality than previously, but were not ideal for kinetic studies (**Figure 5.30**). Similar studies done with *M. tuberculosis* GyrB showed diospyrin binding. Based on the available data the  $K_d$  of diospyrin can be estimated to be less than  $10^{-4}$  M. The higher  $K_d$  value is an underestimate due to poor regeneration conditions.

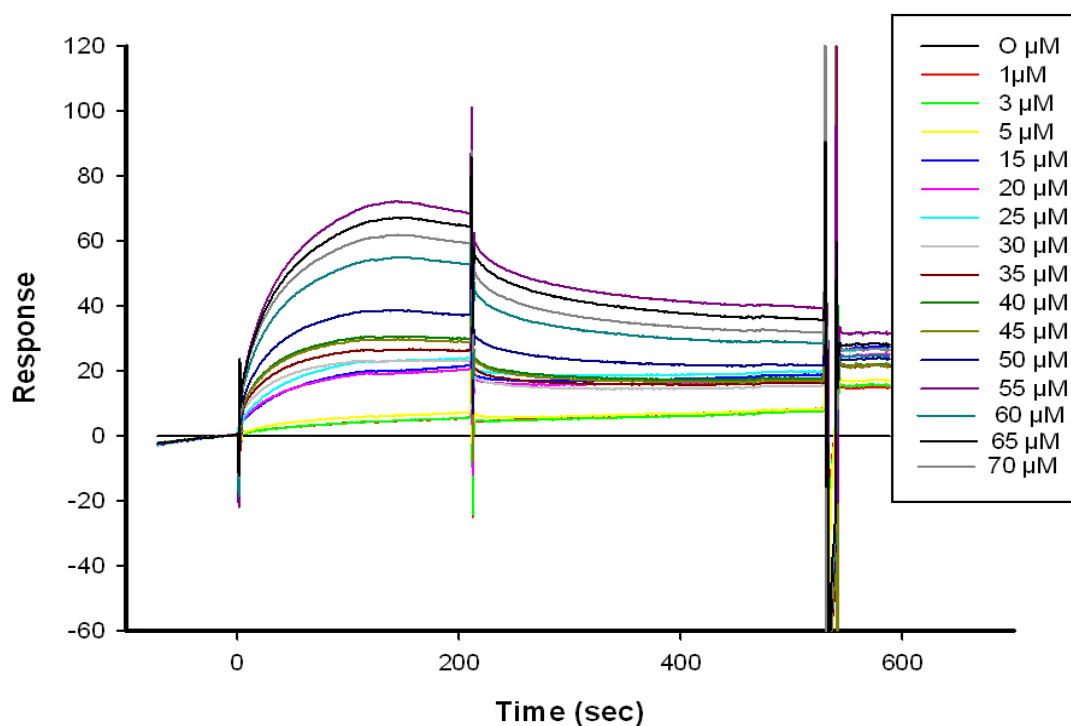


**Figure 5.30:** Surface plasmon resonance data showing binding of diospyrin to *E. coli* GyrB43.

As seen in **Figure 5.30**; diospyrin is not reaching equilibrium after a series of injections; rather a dissociation slope is seen in the sensogram which is concentration dependent. This may be due to several factors, which are as follows:

1. The complex nature of interaction between the drug and the protein, which may involve a combination of specific and non-specific interactions. The competition

between the specific and non-specific interactions may be affecting the concentration of free drug available for binding over a period of time.

2. High concentration of drug and DMSO.
3. Conformational changes in the protein induced by ligand binding (specific and non-specific binding).

With the information available about the diospyrin binding, the next focus was to investigate whether diospyrin shares partially or competes for the binding site with novobiocin. A single experiment was designed by immobilising *M. tuberculosis* GyrA in one flow cell (FC2) and *M. tuberculosis* GyrB in another (FC4). The immobilised protein quality was determined by recording binding sensograms at different concentrations of novobiocin (20 – 100 nM) as shown in **Figure 5.31**.

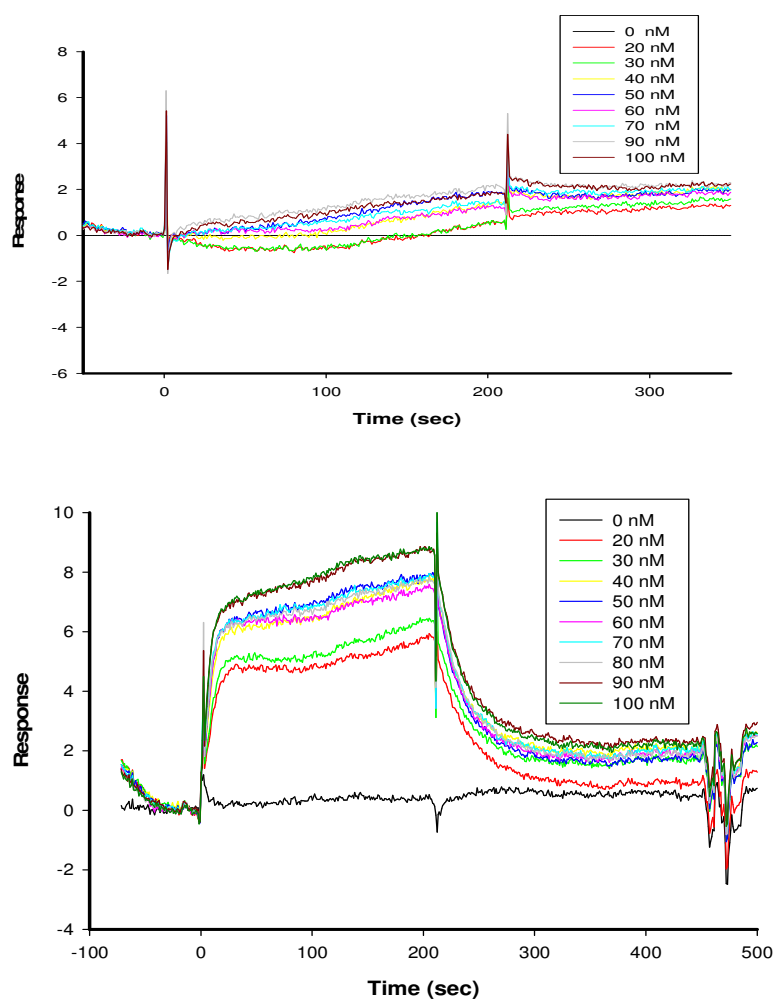


**Figure 5.31:** Surface plasmon resonance data shows novobiocin binding to *M. tuberculosis* GyrA (top panel) and GyrB (bottom panel).

As expected very little novobiocin binding was observed with *M. tuberculosis* GyrA in relation to GyrB. This was followed by a series of 100 nM novobiocin injections (80 injections, 30  $\mu\text{l}/\text{min}$ , 50 sec each) until the point of saturation, with no regeneration, followed by series of 40  $\mu\text{M}$  diospyrin injections (20 injections, 30  $\mu\text{l}/\text{min}$ , 50 sec each) as shown in the **Figure 5.32**. The idea behind the experiment was that if diospyrin shares the binding site with novobiocin then it should not show any binding with the immobilised *M. tuberculosis* GyrB saturated with novobiocin. Diospyrin binding was observed to GyrB after saturating the chip with novobiocin (**Figure 5.33**). A significant difference was also observed in the binding of diospyrin to *M. tuberculosis* GyrA and *M. tuberculosis* GyrB. Diospyrin binding was specific for *M. tuberculosis* GyrB in relation to *M. tuberculosis* GyrA as can be seen by the difference in the response unit. The weak diospyrin binding with *M. tuberculosis* GyrA may be non-specific.

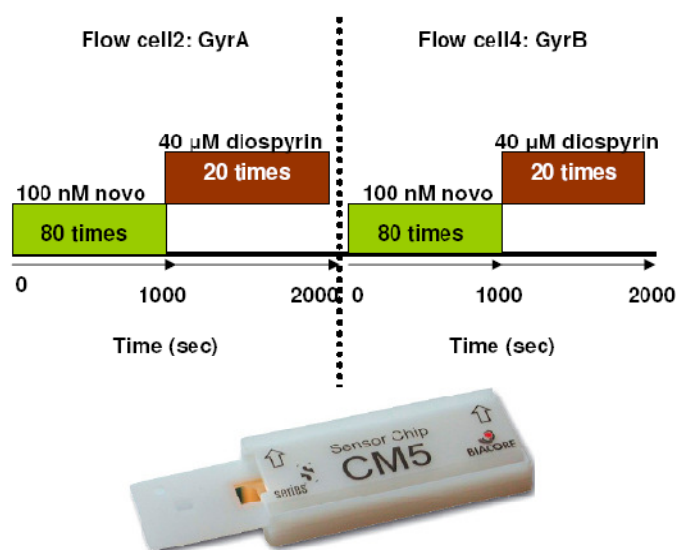


**Figure 5.32: Experimental design for studying competition between novobiocin and diospyrin.**

Thus the surface plasmon resonance experiments confirmed the finding that the GyrB N-terminal domain is the potential binding site for diospyrin and that it is different from the binding site of novobiocin.

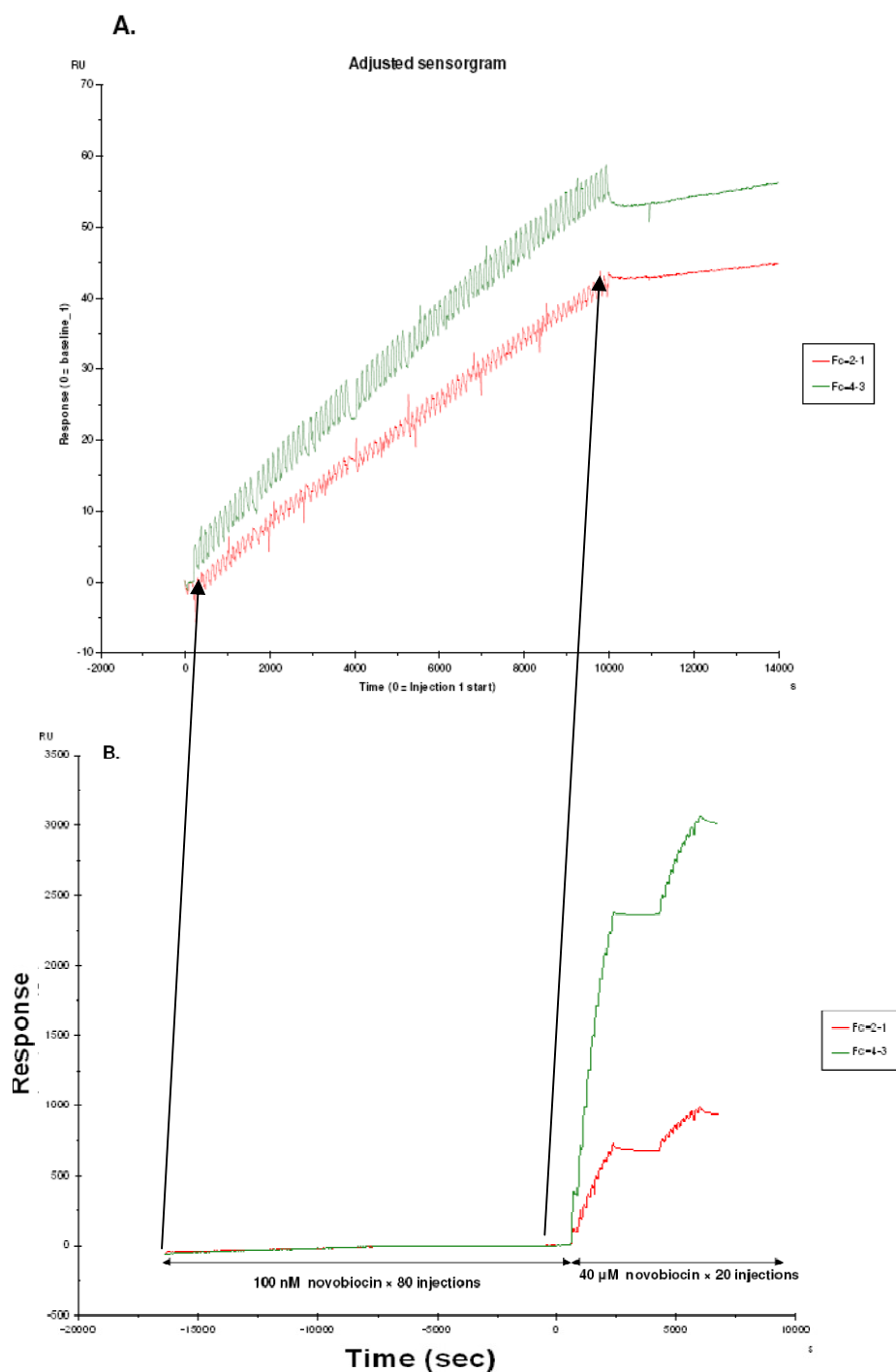


**Figure 5.33: Raw surface plasmon resonance data showing a series of 100 nM novobiocin injections (A) followed by series of diospyrin injections (B). *M. tuberculosis* GyrB (Fc4-3) preferentially binds novobiocin and diospyrin in comparison to *M. tuberculosis* GyrA.**

The SPR experiments were only able to provide approximate  $K_d$  values due to the lack of reproducible regeneration conditions. This is a significant problem and limitation with SPR when studying small molecules. The process is empirical and it varies depending up the sensitivity of the instrument. A range of regeneration conditions suggested in the SPR manual were tried. Either the regeneration was not efficient or it affected the quality of the protein on the chip.

## 5.11 ATP competition assay

ESI-MS, limited proteolysis and SPR experiments suggest that diospyrin binds to the N-terminal domain of GyrB. Diospyrin can bind to *M. tuberculosis* GyrB even after saturating it with novobiocin on the CM5 chip. This also means that novobiocin binding to *M. tuberculosis* GyrB does not affect diospyrin binding to the protein.

Since novobiocin is a competitive inhibitor of ATP, ATP-competition assays were performed in the presence of diospyrin to investigate if diospyrin competes with ATP for the ATP-binding site of GyrB. Standard supercoiling assays were performed at different concentrations of ATP, in the presence of a fixed concentration of drug, at approximately the  $IC_{50}$ . The principle of the assay is based on the fact that if a drug competes with ATP, then the supercoiling activity of the enzyme is regained with the increase in concentration of ATP.

ATP-competition assays were done with *M. tuberculosis* gyrase, with ATP concentrations from 0.02 mM – 2 mM in the presence of novobiocin (2  $\mu$ M) as a positive control, simocyclinone D8 (10  $\mu$ M) as a negative control and diospyrin (8  $\mu$ M).

As shown in **Figure 5.34**, in the absence of any drug, supercoiling activity is observed at a range of ATP concentrations. While in case of simocyclinone D8 (10  $\mu$ M), which is not a competitive inhibitor of ATP (Flatman *et al.*, 2005), no increase in supercoiling activity is observed with the increase in the concentration of ATP. Similarly in case of diospyrin, inhibition of the supercoiling activity is observed, which does not recover with increased concentrations of ATP. While in case of novobiocin, the supercoiling activity is regained with increased concentrations of

ATP. This experiment suggests that diospyrin does not inhibit the DNA gyrase activity by competing with ATP for the ATP-binding site in GyrB.

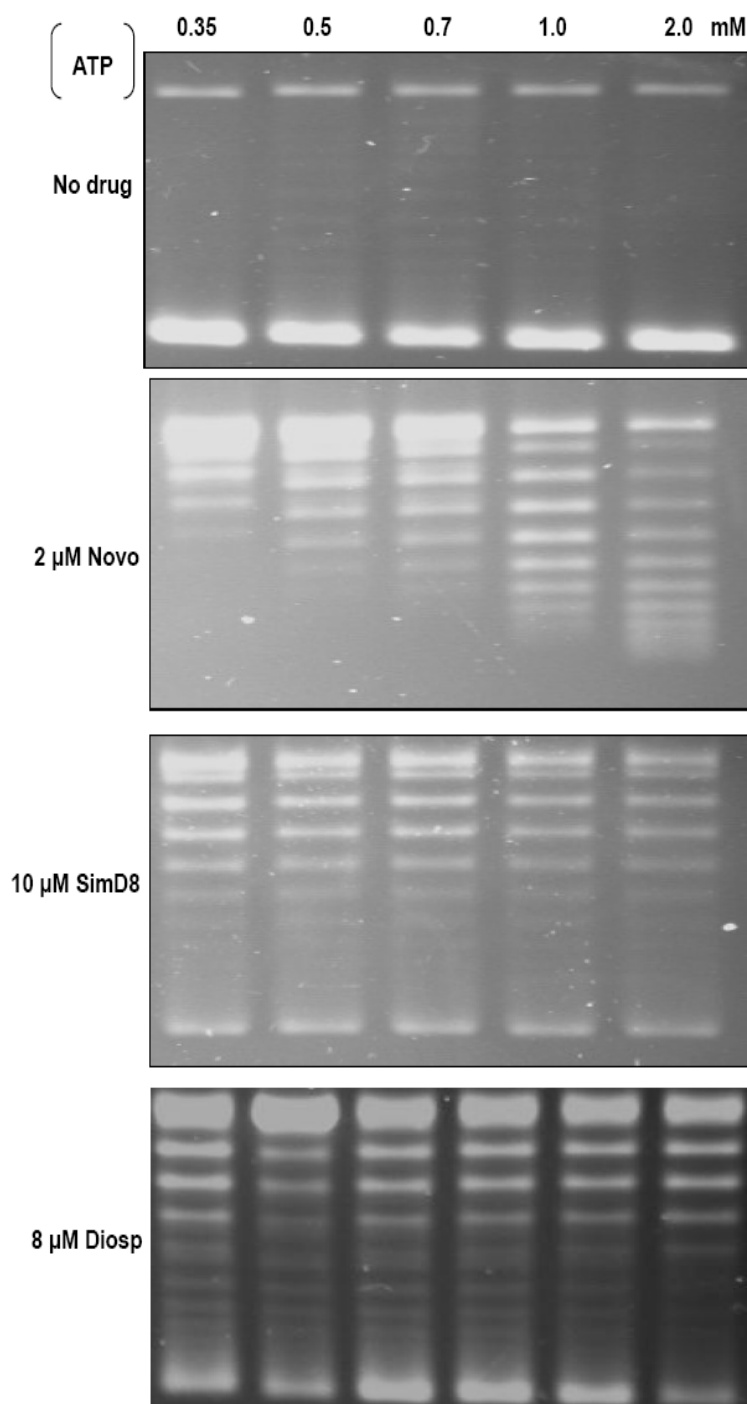


**Figure 5.34:** Effect of ATP concentration on the extent of inhibition. Samples containing the estimated  $IC_{50}$ s of the drugs were incubated in the presence of a range of ATP concentrations.

## 5.12 *M. tuberculosis* GyrB43- diospyrin complex

The results of nano-ESI-MS and surface plasmon resonance indicate that the N-terminal domain of GyrB (GyrB43) is the binding site for diospyrin. *E. coli* GyrB43-diospyrin and GyrB43-ADPNP-diospyrin co-crystallisation trials were not successful. *E. coli* GyrB24-novobiocin-diospyrin co-crystallisation (**Appendix: crystallisation conditions**) only showed the presence of novobiocin at the ATP-binding site. In-silico docking was used as an alternate approach to predict the potential binding site of diospyrin. This work was done in collaboration with Dr. Faridoon Yousafzai (John Innes Centre).

Since there is no crystal structure for *M. tuberculosis* GyrB43, a 3-dimensional model of the domain was developed based on *E. coli* GyrB43. The homology model of the N-terminus (Q48 – V466) was built by using the molecular modelling package InsightII developed by Accelrys. The amino acid sequence was initially sent to the online Fold Prediction Metaserver or GeneSilico Metaserver (Kurowski & Bujnicki, 2003) for searching a suitable template. A number of potential templates (such as PDB id: 1EI1, 1KIJ and 1S16) were identified but none of the template molecules had amino acid residues corresponding to the N-terminal residues M1 to A47 and C-terminal residues V419 - A459 of the *M. tuberculosis* GyrB. Hence these residues were excluded from the model-building process by deleting them from the amino acid sequence of the *M. tuberculosis* GyrB. After sequence alignment, 1EI1 (*E. coli* GyrB43) was chosen as a template for the entire sequence of the modeled protein, except for two regions. The first region corresponds to D263-E274, where the template molecule 1EI1 has a single insertion causing structural disturbance in the emerging model. This region was modeled using the corresponding portion of 1S16 (*E. coli* topoisomerase IV subunit B) as a template. 1S16 does not have the given insertion. The second region corresponds to a 34 amino acids insert (V300 – N333) in the *M. tuberculosis* GyrB sequence, which does not have comparable residues in the template molecule 1S16. It was modeled using residues E22-P52 of 1AQI as a template. 1AQI was returned as a top hit when the insertion sequence of *M. tuberculosis* GyrB was sent to the PDB to find a suitable template. Although, the template region of 1AQI was two residues shorter than the

insert itself, it had 41% identity and 65% similarity with the corresponding sequence V300 – N333 of the *M. tuberculosis* GyrB. Moreover, it had the correct topology i.e.  $\alpha$ -helices stacked on  $\beta$ -strands observed at the corresponding region of the template molecule 1EI1.

Once template residues were identified for the bulk of the query sequence, a crude model was developed by transferring coordinates from the template proteins to the target sequence. Those residues of the target sequence that did not receive any coordinates, because they had either no template residues or they were intentionally excluded for structural reasons, were treated as loops. A complete but unoptimised model emerged when loops were built and splices repaired. Finally the structure was optimised by removing bumps, correcting chirality and dihedral angles, particularly omega values. Bumps were removed by running energy-minimisation protocols that used the Steepest Descents and Conjugate Gradients algorithms on a constrained structure where the backbone atoms were fixed but the side-chain atoms allowed adopting any conformation. Chirality and omega angles of each residue were checked and corrected, if required, either manually or via energy minimization runs.

In-silico docking of diospyrin onto the *M. tuberculosis* GyrB43 model was carried out using the Libdock (Diller & . 2001, Rao *et al.*, 2007, Diller & Li, 2003, Diller & Merz, 2001) protocol of Discovery Studio 2.5.5, which is a modelling and simulation suite developed by Accelrys. Libdock identifies cavities in the 3-dimensional structure of a protein and treats them as potential binding sites for small molecules. Each cavity is defined by a sphere and ranked according to its diameter. Both the position and size of the spheres can be adjusted so that they are consistent with a known binding site of a protein or requisites for target small molecule. Five sites (site: 1, 2, 3, 4, 5) in *M. tuberculosis* GyrB43 model were identified as the potential sites for diospyrin docking. The five binding sites are as shown in **Figure 5.35** and are listed in the **Table 5.7**.

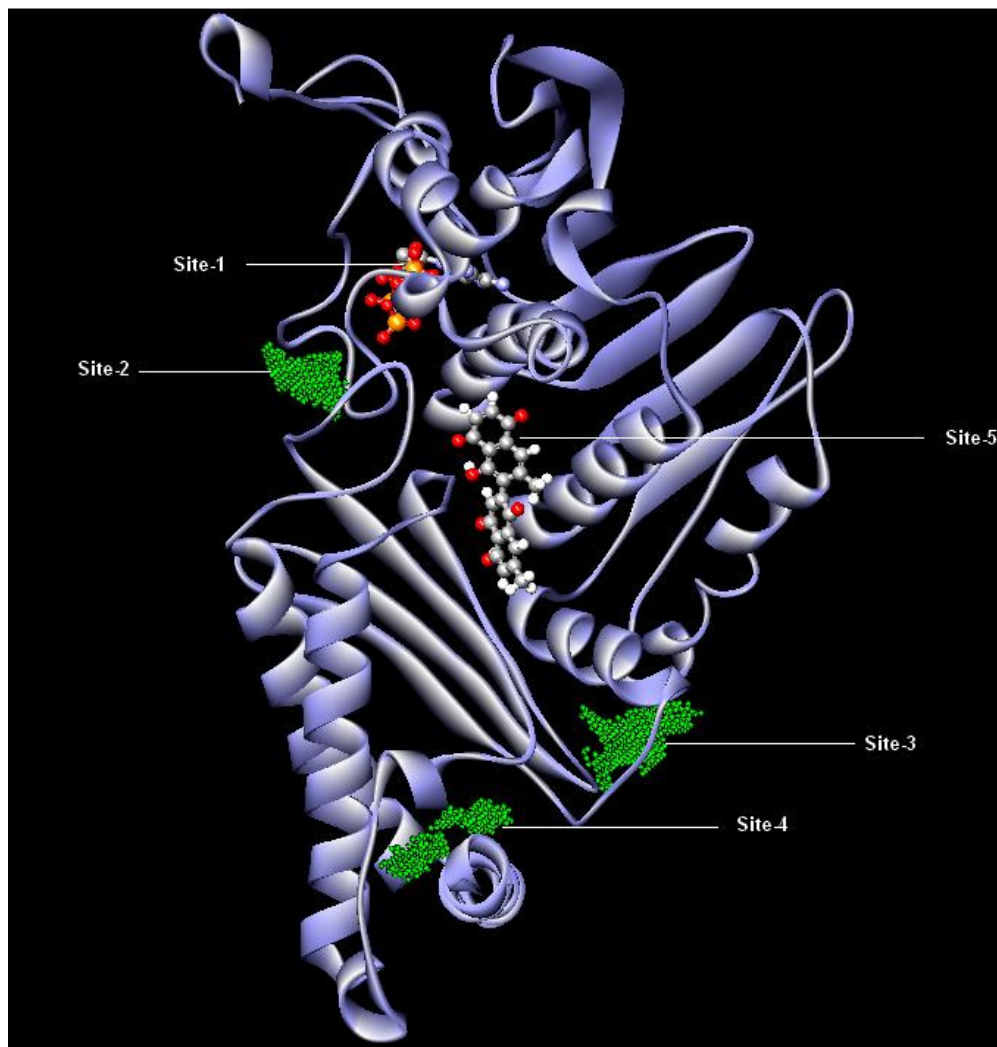


**Figure 5.35: Potential diospyrin binding sites in the model structure of *M. tuberculosis* GyrB43.** The different sites are indicated by: site-1 (with ADPNP), site-2 , site-3, site- 4, site- 5 (with diospyrin).

Docking at site-3 was unsuccessful while site-4 was too narrow to accommodate diospyrin. Site-1 was large enough to accommodate diospyrin and was identified as the ATP- binding site. The second site is close to site-1 and overlapped with it to occupy a significant portion of the common space. Initially both the sites were treated separately for docking. A total of 49 and 48 docking poses were computed at site-1 and site-2 respectively by altering the parameters in Libdock; the default parameter gave no results. The two sites (site-1 & site-2) were finally merged together because the top hits with the highest Libdock scores for the two sites were observed virtually on the edge of site-1. This merged site will be hereafter referred as

site-1+2. This was done by moving the sphere of the first site towards the second site until the later was fully encompassed. Top 2 scoring poses of the diospyrin at site-1+2 are shown in the **Figure 5.36** referred to as pose-1+2.1 and pose-1+2.2.

Both the poses are close in terms of their orientation. In Pose-1+2.1, diospyrin is making seven hydrogen bonds with Asn44, Gly75 (2 bonds), Gly99 (2 bonds), Lys100 and Val117, while in Pose-1+2.2, diospyrin is making 2 hydrogen bonds with Asn44 and Ser161. Since the biophysical (SPR, crystallography) and biochemical (ATP competitive assay) does not support the hypothesis that diospyrin binds to the ATP-binding site and therefore site-1 or site-2 or site-1+2 cannot be the potential binding site of diospyrin. However, site-5 appeared interesting as the site was originating from a deep broader cleft (**Figure 5.37**).

Docking sites in <i>M. tuberculosis</i> GyrB43	Position
Site-1	ADPNP/ATP-binding site
Site-2	Adjacent to and overlaps with site-1
Site-3	Below site-5
Site-4	Below site-3
Site-5	Predicted diospyrin-binding site

**Table 5.7: Five docking sites in the *M. tuberculosis* GyrB43 model.**

Diospyrin docking at this site was successful and the molecule was docked in the cleft with 36 poses. Libdock ranked the docking poses on a simple pair-wise score, similar to Piecewise Linear Potential (Gehlhaar *et al.*, 1995). Diospyrin does not go into the cavity but rather stays in the cleft and forms 3 hydrogen bonds with Thr294, Thr302 and His 303 as shown in **Figure 5.38**.

A second run of Libdock on the cleft rather than the cavity gave a total of 33 poses with the top hit scoring 97.9. This was done by making the site sphere relatively large and moving it away from the cavity to cover most of the cleft. This score is slightly less than the score of 101 recorded for the earlier run on site-5. In this pose diospyrin appears to forming five hydrogen bonds with neighboring amino acids Glu188, Thr295 (2 bonds) and Asn301 (2 bonds).

A.



B.

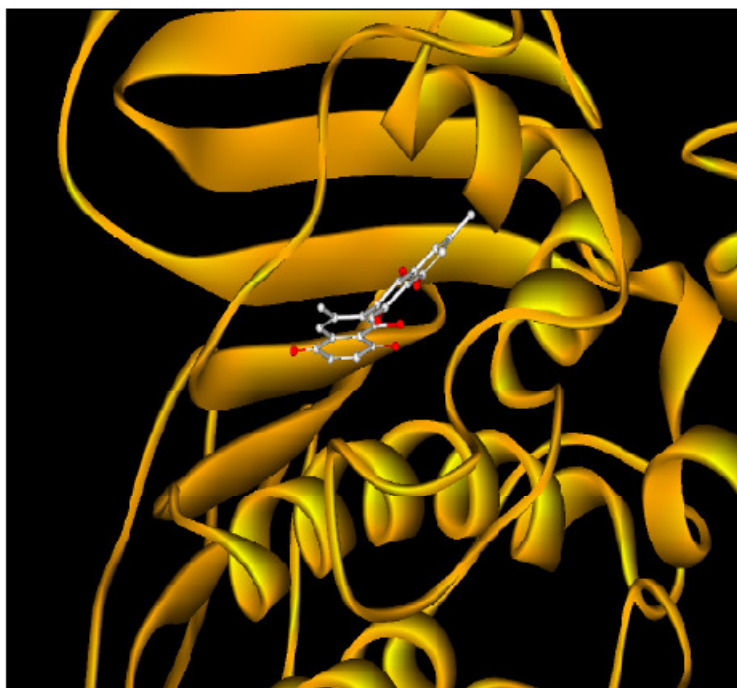


**Figure 5.36: Top 2 scoring poses of the diospyrin at site 1+2 referred to as pose-1+2.1 (A) and pose- 1+2.2 (B).**

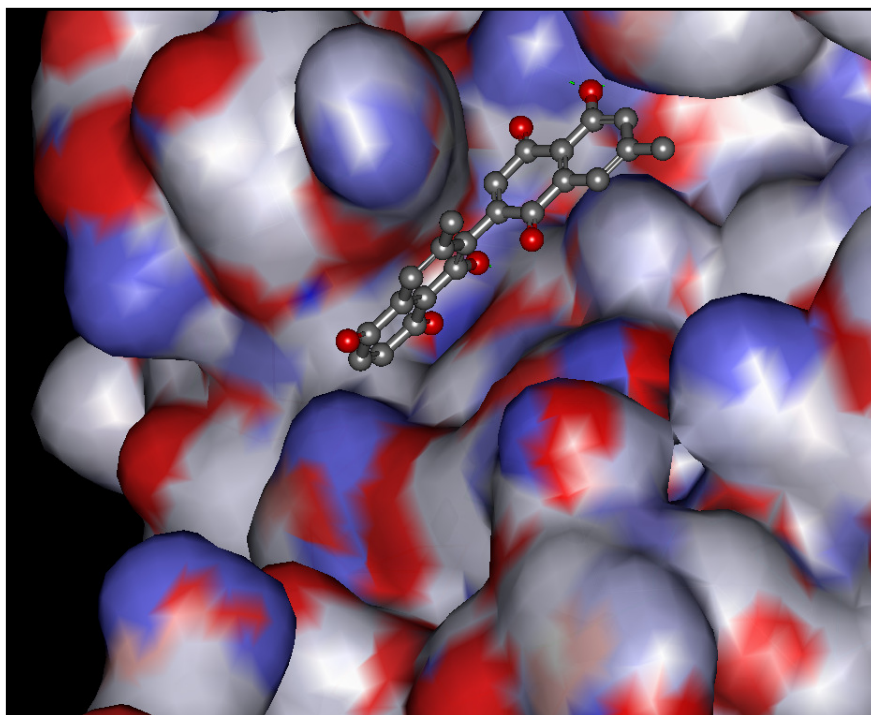


**Figure 5.37: Site-5, potential binding site for diospyrin with a deep cleft like binding pocket.**

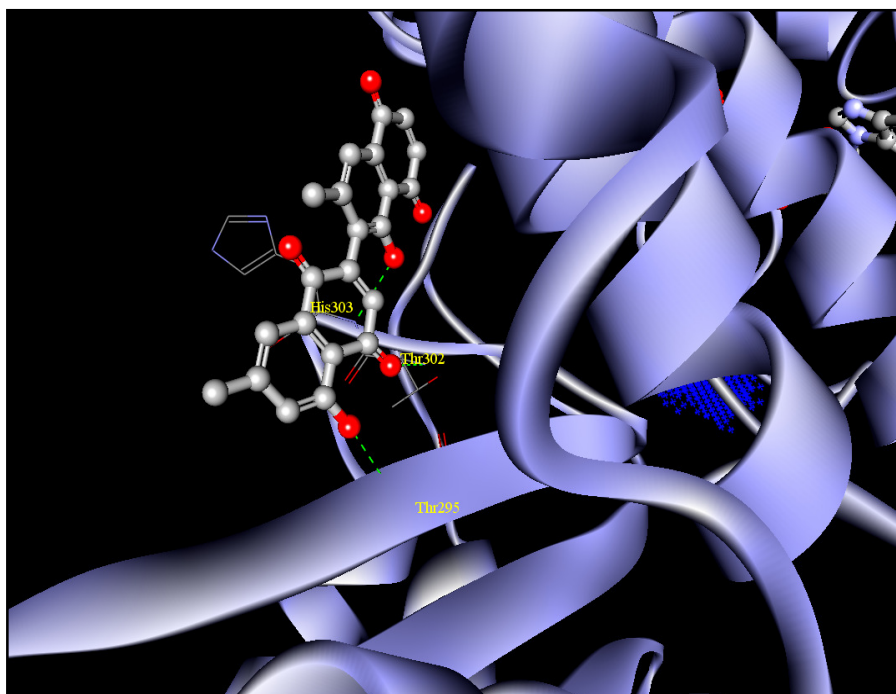


**Figure 5.38: Docked diospyrin at site-5 forming 3 hydrogen bonds with Thr294, Thr302 and His 303.**

As the biochemical and biophysical studies do not support diospyrin binding at the ATP-binding site, site-5 is preferred over site-1+2 despite the fact that Libdock scores 130 and 129 for pose-1+2.1 and pose-1+2.2, respectively, are significantly higher than 101 and 90 for the corresponding poses at site-5.

The limitation of in-silico docking as highlighted by the recent study has shown that the scoring functions of a number of docking protocols including Libdock have failed to identify the pose that is closest to the native-like pose of a binding molecule (Wang *et al.*, 2007). Although, the argument applies to different poses at a given site, it may be true for different sites as well.

## 5.13 Discussion

Representative members from three class of compounds: quinolines (chloroquine), aaptamines (1N, N-Didodecylaaptamine, Kaempferol-3-O- $\alpha$ -L-(2,3-di-E-Pcomaroyl)-rhamnoside) and naphthoquinones (7-methyljuglone, diospyrin) showed inhibitory activity against *M. tuberculosis* DNA gyrase. The compounds were screened based on standard DNA supercoiling assay. The IC<sub>50</sub> values based on DNA supercoiling assay are summarised in **Table 5.8**.

Since naphthoquinones were found to be the most potent inhibitors, I decided to study their mode of inhibition further. Diospyrin (MW: 374.35 Da) was selected for study because it has higher molecular weight in comparison to 7-methyljuglone (MW: 188.18) which is beneficial for experimental techniques such as nano-ESI-MS and SPR experiments. Chemically diospyrin is a dimeric form of 7-methyljuglone. These two molecules inhibited all three reactions of *M. tuberculosis* DNA gyrase: supercoiling, relaxation and decatenation, but diospyrin was found to be more effective in inhibiting relaxation and decatenation activity in comparison to 7-methyljuglone. The IC<sub>50</sub> values (**Table 5.9**) are not the same for all the reactions as demonstrated for other DNA gyrase inhibitors, such as albicidin which inhibits DNA supercoiling and relaxation with different IC<sub>50</sub> values (Hashimi *et al.*, 2006).

Compound	IC <sub>50</sub> (approx)
Quinolines	
Chloroquine	80 μM
Mefloquine	300 μM
Aptamines:	
1N, 4N-Didodecyl Aaptamine	~10 - 20 μM
Kaempferol-3-O-α-L-(2,3-di-E-Pcomaroyl)- rhamnoside)	200 μM
Naphthoquinones	
7-methyljuglone	10 μM
Diospyrin	10 μM
Neodiospyrin	50 μM
Isodiospyrin	100 μM
Menadione	>200 μM
Shinanalone	>200 μM

**Table 5.8: DNA supercoiling IC<sub>50</sub> values for Quinolines, Aaptamines and naphthoquinones.**

Compound	Supercoiling assay	Relaxation assay	Decatenation assay
	IC <sub>50</sub>	IC <sub>50</sub>	IC <sub>50</sub>
1. 7-methyljuglone	10 μM	80 - 120 μM	10 - 30 μM
2. Diospyrin	10 μM	40 - 80 μM	1 - 10 μM

**Table 5.9: IC<sub>50</sub> values of 7-methyljuglone and diospyrin based on supercoiling, relaxation and decatenation assay.**

These observations point to the fact that 7-methyljuglone is the active chemical scaffold which when duplicated in diospyrin increases its inhibitory activity. This hypothesis can be tested in future by designing, synthesising and testing compounds which are repetitive units of 7-methyljuglone. This may generate a new library of analogues that will be beneficial for naphthoquinone

characterisation. The activity of these molecules against *E. coli* gyrase also demonstrates that naphthoquinones can inhibit DNA gyrase from a range of bacterial species.

Based on nano-ESI-MS and SPR experiments diospyrin was shown to bind to the *E. coli* GyrB N-terminal domain (GyrB43). It does not bind at the ATP-binding site (**Figure 1.20**) as evident from the ATP competition assay and SPR experiments, ie. diospyrin is not a competitive inhibitor of ATP. DNA cleavage assays in the presence and absence of ATP indicated that it does not inhibit the enzyme activity by stabilising the cleavage complex.

Since co-crystallisation trials with *E. coli* GyrB43-diospyrin and *E. coli* GyrB43-ADPNP-diospyrin were not successful, in-silico docking of diospyrin was performed on the model of *M. tuberculosis* GyrB43 using Libdock protocol of Discovery Studio 2.5.5. Since there is no crystal structure for *M. tuberculosis* GyrB43, InsightII software developed by Accelrys was used to model the structure. According to the docking experiments the potential binding site of diospyrin is a cleft just below the ATP-binding site described as site-5 where it forms hydrogen bonds with neighboring amino acids as shown in **Figure 5.39**. This cleft below the ATP – binding site is also present in *E. coli* GyrB43 as shown in the **Figure 5.40**.

At present it is not clear how diospyrin binding at this site affects the enzyme activity. The limited proteolysis experiments with trypsin indicate conformational changes which may affect the catalytic cycle of the enzyme. There is immense scope to investigate this further as it may provide a novel mode of inhibition. One of the possibilities that were discussed while studying inhibitory activity of diospyrin was its potential to form S-conjugates (Newton & Fahey, 2002). **Table 5.10** shows the percentage of cysteine residues present in *E. coli* and *M. tuberculosis* DNA gyrase.

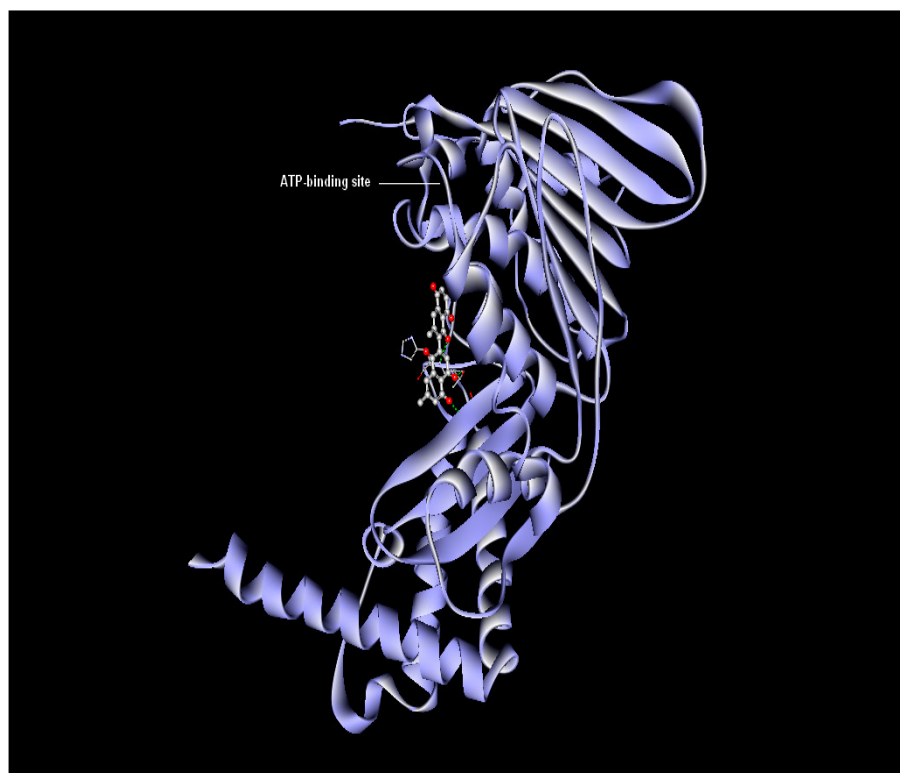


**Figure 5.39:** Potential binding site of diospyrin described as site-5 with the docked molecule. It is a cleft just below the ATP-binding site.



**Figure 5.40:** *E. coli* GyrB43 (red color) superimposed over modeled *M. tuberculosis* GyrB43 (yellow color) with diospyrin docked at site-5.

---

Protein	No: of cysteine residues	Cysteine percentage
1. <i>M. tuberculosis</i> GyrA	2	0.2%
2. <i>M. tuberculosis</i> GyrB	3	0.41%
3. <i>E. coli</i> GyrB43	2	0.5%
4. <i>M. tuberculosis</i> GyrB43	1	0.2%

**Table 5.10: Percentage of cysteine residues present in *E. coli* and *M. tuberculosis* DNA gyrase.**

According to the docking experiment there is no cysteine in the vicinity of site-5. Thus the three classes of compound were screened to discover novel DNA gyrase inhibitors. Naphthoquinones were the most potent inhibitors of DNA gyrase. Based on the biochemical data and the computer model we predict a novel binding site and speculate a novel mode of inhibition for naphthoquinones that has not been observed before for other inhibitors.

## Chapter 6: General Discussion

### 6.1 Introduction

Most of our understanding of DNA gyrase is based on the enzyme from *E. coli*, a Gram-negative bacterium, with limited information about the enzyme from other Gram-positive bacteria such as *M. tuberculosis*. The recent initiative of the TB Alliance and Bayer to conduct a global clinical development program for moxifloxacin has highlighted the significance of *M. tuberculosis* DNA gyrase as a target for the discovery and development of novel antibacterials. Moxifloxacin is a fluoroquinolone and an inhibitor of DNA gyrase. Although the GyrA and GyrB subunits of the enzyme have been successfully cloned, basic background research for this enzyme has not yet been done. Most of the studies have concentrated on studying the interaction of the enzyme with known inhibitors such as fluoroquinolones. For example, IC<sub>50</sub> values have been determined for different quinolones such as ciprofloxacin, sparfloxacin, sitafloxacin, clinafloxacin, and gatifloxacin (Aubry *et al.*, 2004, Takiff *et al.*, 1994, Onodera *et al.*, 2001).

The research described in this thesis is an attempt to understand the unique features of *M. tuberculosis* DNA gyrase and to identify potential new classes of inhibitors. It has also highlighted a general concern of sequence inconsistency across different public databases. In this research project an attempt was made to resolve inconsistency in the *M. tuberculosis* GyrB sequence.

In the first stage of the project, bioinformatics analyses were performed for *M. tuberculosis* DNA gyrase. Multiple-sequence alignment between the *M. tuberculosis* DNA gyrase with other bacterial gyrases identified the following two unique features in each of the DNA gyrase subunits: (a) prediction of the presence of 40 additional amino acids at the beginning of GyrB and (b) the presence of a predicted putative Ca<sup>2+</sup>-binding site in GyrA.

## 6.2 *M. tuberculosis* GyrB promoter analysis

The presence of 40 additional amino acids at the beginning of the GyrB N-terminus was not found in all the GyrB sequences retrieved from different databases. For example, in the case of NCBI code CAB02426 for *M. tuberculosis* H37Rv *gyrB*, the 40 additional amino acids are present. But for the same protein cross-referenced in UniProtKB/Swiss-Prot as P0C5C5 the 40 additional amino acids are absent. It was important to investigate if these 40 additional acids had any effect on the enzyme activity, which would also indicate the real starting amino acid for GyrB. The investigation was done at the level of promoter, transcript and protein analysis. RT-PCR (reverse transcriptase-PCR) performed on the RNA prepared from the crude extracts of *M. tuberculosis* cells indicated that there are two species of *gyrB* transcripts. One of the species exists because of the transcription of the sequence that includes the sequence corresponding to the 40 amino acids, while the other transcript that is transcribed from the sequence that excludes the sequence corresponding to the 40 amino acids. The presence of these species was verified by sequencing the PCR products.

Due to experimental limitations it was not possible to investigate if these 40 amino acids are present in native protein from *M. tuberculosis*. Before generating a deletion mutant (GyrB N40 $\Delta$ ), it was verified by Orbitrap analysis that the 40 additional amino acids are present in GyrB heterologously expressed in *E. coli*. The enzyme activity of the GyrB N40 $\Delta$  deletion mutant was compared with the activity of GyrB WT. There was no difference in the supercoiling, relaxation and decatenation activity of GyrB N40 $\Delta$  deletion mutant and GyrB WT. This indicated that there is no functional role of the additional 40 amino acids at the GyrB N-terminus. Based on previous work (Unniraman *et al.*, 2002) there was a possibility for the existence of promoter elements in the region that encodes the 40 amino acids at the GyrB N-terminus. This was verified by  $\beta$ -galactosidase-based activity assays in *M. smegmatis*, which confirmed the presence of promoter elements in this region. Weak promoter activity was also observed in region upstream of the 40 amino acids. Although this data is consistent with the previous publication (Unniraman *et al.*, 2002) but the promoter activity was assayed in *M. smegmatis*.

It would be interesting to repeat the same experiment in *M. tuberculosis* because sometimes *M. tuberculosis* promoters behave differently when transformed in *M. smegmatis*. Thus the data indicate that the real start codon for *M. tuberculosis* GyrB is GTG (Val) and that the additional 40 amino acids expressed in GyrB have no structural or functional significance. This information will be useful to revise the GyrB sequences available on public database. In future, mutations in the promoter elements can be made as a further proof of concept. At present, it has not been possible to identify the reason for the existence of two transcript species. This also needs further investigation, which raises the possibility of post-transcriptional modification, which has not been studied in *M. tuberculosis* with reference to *M. tuberculosis* GyrB transcripts. Genetic and biochemical studies can be performed to understand the physiological significance for the presence of two different transcript species.

### 6.3 Putative Ca<sup>2+</sup>-binding site

Another important observation from the bioinformatics analysis was the presence of a putative Ca<sup>2+</sup>-binding site in GyrA. The Ca<sup>2+</sup>-binding site '504 DVSDLEDLIAREDV 516' is present at the junction of N- and C-terminal domains of GyrA. Sequences homologues to the Ca<sup>2+</sup>-binding site are also found in *M. bovis*, *B. melitensis* and *C. diphtheria*. Interestingly, *C. diphtheria* lacks topo IV, which may suggest a relation between the presence of the Ca<sup>2+</sup>-binding site and the absence of topo IV. How DNA gyrase manages this dual role in the absence of topo IV has not been studied.

Bioinformatics analysis also demonstrated that the Ca<sup>2+</sup>-binding sequence does not follow the canonical EF-hand helix-loop-helix pattern. There are several examples of proteins in prokaryotes that do not follow the canonical definition of EF-hand Ca<sup>2+</sup>-binding sites such as the periplasmic galactose-binding protein (*Salmonella typhimurium*; PDB code: 1gcg) (Vyas *et al.*, 1987) and alginate-binding protein (*Sphingomonas* sp.; PDB code: 1kwh) (Mishima *et al.*, 2003) (**Figure 3.17**). However, like most of the EF-hand Ca<sup>2+</sup>-binding sites it exists in a pair as in the GyrA dimer.

In the absence of the complete crystal structure, two homology models for *M. tuberculosis* GyrA including the Ca<sup>2+</sup>-binding site were generated. These models (MtGyrA-1H71, MtGyrA-1BQB) were generated based on the sequence similarity of the Ca<sup>2+</sup>-binding site with two other bacterial Ca<sup>2+</sup>-binding sites (metalloprotease from *Pseudomonas sp.* and *S. aureus*). According to model MtGyrA-1H71, there is a possibility for only one Ca<sup>2+</sup> at the binding site, whereas according to the model MtGyrA-1BQB there is a possibility for two Ca<sup>2+</sup> atoms. In order to investigate these models and to study the effect of Ca<sup>2+</sup> on the enzyme activity, biochemical and site-directed mutagenesis experiments were performed.

The initial biochemical studies involved assaying the supercoiling activity of *E. coli* and *M. tuberculosis* DNA gyrase in the presence of Mg<sup>2+</sup> or Ca<sup>2+</sup>. As reported in previous studies (Aubry *et al.*, 2006a), unlike *E. coli*, *M. tuberculosis* DNA gyrase could not supercoil relaxed DNA in the presence of Ca<sup>2+</sup>. In order to identify the subunit that is important for the enzyme activity in the presence of Ca<sup>2+</sup>, the subunits between *E. coli* and *M. tuberculosis* DNA gyrase were swapped to generate a hybrid enzyme. Supercoiling activity was observed when *M. tuberculosis* GyrA and *E. coli* GyrB hybrid was assayed in the presence of 6 mM Mg<sup>2+</sup>, but no supercoiling activity was observed when the same assay was repeated in the presence of 6mM Ca<sup>2+</sup> (**Table 4.1**). This indicates that the ability of the Ca<sup>2+</sup> to support DNA supercoiling depends on the presence of *E. coli* GyrA and *M. tuberculosis* GyrA cannot substitute for it.

According to the homology models, there is possibility of at least one Ca<sup>2+</sup> in the Ca<sup>2+</sup>-binding site. Since EGTA is a specific chelator of Ca<sup>2+</sup>, GyrA was dialysed in 1 mM EGTA to remove Ca<sup>2+</sup> associated with the native protein. The effect of EGTA dialysis was a 2-3 fold loss in relaxation activity without affecting other reactions such as supercoiling and decatenation. It was possible to regain the loss in relaxation activity by external addition of Ca<sup>2+</sup> in the assay. Protein-refolding experiments were also done in the presence of EGTA to make sure that any tightly bound Ca<sup>2+</sup> is removed during protein refolding in the presence of EGTA. ICP-AES indicated a decrease in the concentration of Ca<sup>2+</sup> in the protein sample refolded in the presence of EGTA. The effect of protein refolding in the presence of EGTA was drastic which led to the loss of relaxation and decatenation activity with weak

supercoiling activity. Interestingly, relaxation and decatenation activities are associated with topo IV, which is absent in case of *M. tuberculosis*.

Based on the *M. tuberculosis* GyrA model described previously, site-directed mutagenesis experiments were performed. For the quadruple mutation (D504A, E508A, D509A, E514A) in the putative Ca<sup>2+</sup>-binding site, incomplete supercoiling activity was observed. There was no effect of these mutations on the relaxation and decatenation activity of the enzyme. By CD experiments, it was verified that this effect is not due to protein misfolding. Further investigation into the weak supercoiling activity revealed that the mutations have affected DNA wrapping. This effect could be due to the loss of Ca<sup>2+</sup> at the Ca<sup>2+</sup>-binding site due to the mutations. Thus, there is a functional significance of the Ca<sup>2+</sup> and the Ca<sup>2+</sup>-binding site.

In order to explain the significance of Ca<sup>2+</sup> and the Ca<sup>2+</sup>-binding site, a model is proposed. The proposed model is based on the established model for DNA wrapping around the GyrA C-terminal with slight modification due to the presence of the Ca<sup>2+</sup>-binding site in *M. tuberculosis* GyrA.

The model is based on the assumption that Ca<sup>2+</sup> may act as a pivot or regulator that controls the flexibility of the arm / linker connecting the GyrA N- and C-terminal domains. It has been suggested in previous studies that the linkage between the N- and C-terminal regions may be flexible (Corbett *et al.*, 2004). This flexible arm has the Ca<sup>2+</sup>-binding site as demonstrated by the bioinformatics and biochemical studies. The conformation of the GyrA C-terminal domain is important for DNA supercoiling (Corbett *et al.*, 2004, Costenaro *et al.*, 2005).

The DNA wrapping process is a cycle of events in the following sequence (**Figure 6.1**):

1. **Arms-down:** In the native state, Ca<sup>2+</sup> coordinated by the Ca<sup>2+</sup>-binding site of *M. tuberculosis* GyrA keeps the C-terminal domain down at each side of the dimer away from the cleavage active site. In this stage, DNA gyrase is ready to catalyse DNA supercoiling or DNA relaxation /decatenation. In a previous study (Costenaro *et al.*, 2005) it has been suggested that such a conformation would minimise the obstruction of relaxation and decatenation by the C-

terminal domains and this could be their actual conformation with GyrA during these reactions.

2. **Arms-up:** A<sub>2</sub>B<sub>2</sub> tetramerisation followed by DNA wrapping around the C-terminal moves the arm upwards to make protein-DNA contacts between the G-segment and the cleavage active site. Therefore the initiation of supercoiling will be the binding of DNA which will move the arms having the Ca<sup>2+</sup>-binding site up towards the cleavage active site in order to facilitate the introduction of the T segment. It has been previously reported that a large conformational change is induced in the enzyme upon DNA binding (Costenaro *et al.*, 2005).
3. **Arms-down:** Near the end of the catalytic cycle, when the T-segment is about to leave the C-gate, the DNA induces conformational changes in the arm which again brings it down to its native state, away from the cleavage active site. At this stage, the enzyme is again ready for either supercoiling or relaxation / decatenation.

Thus, Ca<sup>2+</sup> may help to maintain *M. tuberculosis* DNA gyrase in a state, which would favour all the topological reactions. In the absence of topo IV in *M. tuberculosis*, this may be important to keep the enzyme in a state ready for both supercoiling and relaxation/decatenation reactions. In the case of bacterial species such as *E. coli*, lacking the Ca<sup>2+</sup>-binding site and having a topo IV, the relaxation activity and decatenation activity is weaker in comparison to *M. tuberculosis* DNA gyrase. This may be due to the more flexible nature of the arms due to the absence of Ca<sup>2+</sup>, which is stabilised by Ca<sup>2+</sup> in case of *M. tuberculosis* DNA gyrase away from the cleavage active site. The flexibility of these linkers is evident from the absence of this region in the recent crystal structures of GyrA N-terminus (PDB code: 3ILW; 3IFZ).

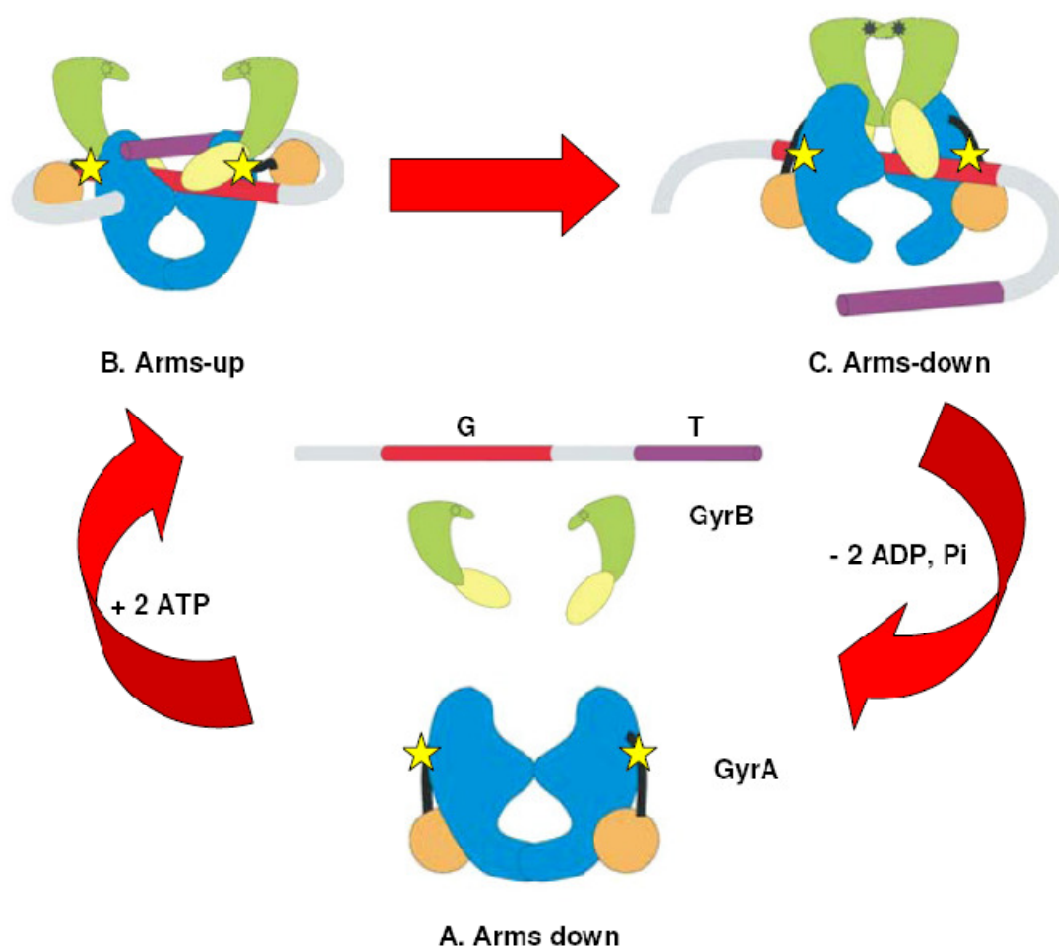


**Figure 6.1: Down-UP-Down arm model (DUDAM) proposed for the regulation of DNA supercoiling. *Black asterix: ATP, yellow stars:  $\text{Ca}^{2+}$ .***

This model can explain the experimental observations. In the biochemical, experiments following two observations were made:

- 1. Weak supercoiling activity by the quadruple mutation (GyrA D504A, E508A, D509A, E514A) without significantly affecting the relaxation and decatenation activity.**

The mutations made the arms less flexible in comparison to the native protein due to both the loss of  $\text{Ca}^{2+}$  and the mutation of acidic amino acids to alanine. Because of this, the arms cannot efficiently assist the DNA wrapping around the C-terminal domain. I have experimentally demonstrated

that the mutations have an effect on DNA wrapping. Since DNA wrapping is only important for supercoiling, the mutations have no effect on the relaxation and the decatenation activity of the enzyme. I propose that the arms are held in a conformation unsuitable for DNA supercoiling, but DNA relaxation and decatenation can still occur (**Figure 6.2**).

**2. EGTA dialysis and refolding lead to loss of the relaxation and decatenation activity.**

EGTA is a specific chelator of  $\text{Ca}^{2+}$ . When GyrA is refolded in the presence of EGTA, any  $\text{Ca}^{2+}$  tightly bound to the GyrA subunit will be removed by EGTA and presumably, the refolded protein will be without any  $\text{Ca}^{2+}$ . Due to the loss of  $\text{Ca}^{2+}$  from the  $\text{Ca}^{2+}$ -binding site, the favoured position for the arms is up and close to cleavage active site, which may obstruct relaxation/decatenation activity. As a result, the enzyme can catalyse DNA supercoiling, but it is weaker than the native protein. This is because there is no  $\text{Ca}^{2+}$  to provide additional stability or appropriate conformation to the arms during the process of DNA supercoiling. Interestingly, weaker relaxation activity has also been observed when the protein was dialysed in EGTA (no refolding), which can be regained by addition of  $\text{Ca}^{2+}$  in the assay. This indicates that EGTA dialysis alone is not sufficient to remove all the  $\text{Ca}^{2+}$ . This method is also not reproducible as there are factors associated with protein batch and chelation of  $\text{Ca}^{2+}$  by EGTA (**Figure 6.2**).

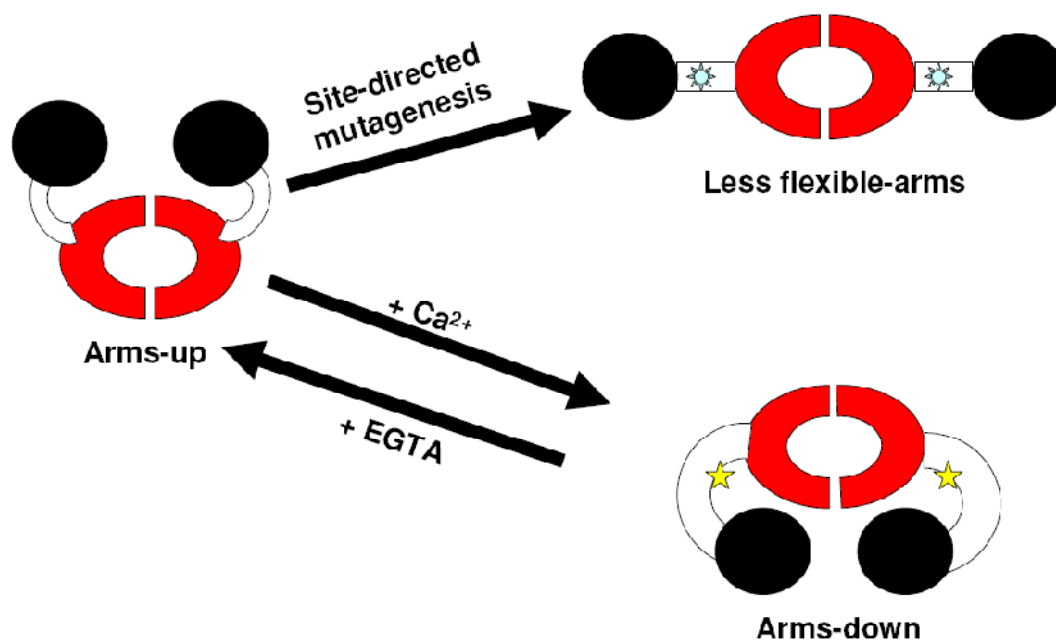


**Figure 6.2:** Conformational changes in *M. tuberculosis* GyrA due to quadruple mutation (GyrA D504A, E508A, D509A, E514A),  $\text{Ca}^{2+}$  and EGTA. Yellow stars:  $\text{Ca}^{2+}$ .

Limited proteolysis experiments with trypsin also demonstrated that  $\text{Ca}^{2+}$  induces conformational changes in GyrA and that this effect is specific. One of the differences is the disappearance of a 47-kDa band in the presence of  $\text{Ca}^{2+}$ . Edman sequencing confirmed that the 47-kDa band included the  $\text{Ca}^{2+}$ -binding site.

Due to the significance of the  $\text{Ca}^{2+}$ -binding site, virtual screening was done with AutoDock Vina v1.0.2 using the NCI diversity II dataset from the ZINC database. Compounds ZINC13130018 and ZINC1639634 inhibit the supercoiling and relaxing activity of the enzyme and has an in-vitro MIC of  $\sim 50 \mu\text{M}$  against *M. tuberculosis*.

In future, cross-linking and Fluorescence Resonance Energy Transfer (FRET) studies could be done to demonstrate how  $\text{Ca}^{2+}$  can control the flexibility of the arm connecting N- and C-terminal domain. Cross-linking studies can be performed before performing FRET studies. The arms/GyrA C-terminal domain can be cross-linked to GyrA N-terminal in arms down conformation as shown in **Figure 6.1 A**. For cross-

linking studies, all the cysteines in GyrA will have to be substituted by alanines and new cysteine residues will have to be introduced at the site of cross-linking. The cross-linking studies will provide information about the significance of the flexible arm and its effect on the supercoiling activity of enzyme. FRET studies can be performed by labelling the C-terminal domain with a fluorophore and the GyrA N-terminal domain that makes contact with C-terminal domain with a quencher. Cross-linked protein can act as a control for the FRET experiment. FRET experiments will be helpful to study the flexibility of the arms/ linkers and the effect of DNA and  $\text{Ca}^{2+}$  on it.

The significance of the  $\text{Ca}^{2+}$ -binding site can also be investigated by studying the effect of EGTA dialysis on the relaxation activity of the GyrA N-terminal domain without the putative  $\text{Ca}^{2+}$ -binding site. Isothermal titration calorimetry (ITC) can also be performed to determine the kinetics of  $\text{Ca}^{2+}$ -binding at the predicted site in GyrA. Further work also needs to be done to determine the  $\text{IC}_{50}$ s for ZINC13130018 and ZINC1639634. Since the quadruple mutant (GyrA D504A, E508A, D509A, E514A) has mutations in the  $\text{Ca}^{2+}$ -binding site, these two compounds can also be assayed against it to see if there is any difference in their  $\text{IC}_{50}$ .

## 6.4 Novel DNA gyrase inhibitors

The main focus of my project was to identify novel inhibitors of *M. tuberculosis* DNA gyrase. I decided to investigate selected classes of compounds that have published information about their antibacterial activity. These compounds also did not have any information about their possible targets. There were two advantages of this method. The first advantage is that since these compounds have already been shown to have antibacterial activity, I know that they have biological activity and can enter the bacterial cell. The other advantage is that if any of these compounds exhibit inhibitory activity against DNA gyrase, then it is likely that the collaborators would be able to perform synthetic chemistry on the selected molecule to design better inhibitors. I selected three classes of compound: quinolines, aaptamines and naphthoquinones for study. Aaptamines and naphthoquinones (Gul *et al.*, 2006,

Mahapatra *et al.*, 2007) were selected because these classes of compound have been shown to have anti-mycobacterial activity but no information is available about their cellular target. Similarly quinolines, the anti-malarial drugs have been shown to induce cross-resistance to fluoroquinolones by generating mutations in DNA gyrase and topo IV (Davidson *et al.*, 2008). Out of all the three classes of compounds, naphthoquinones were found to be most effective and were studied in detail.

Initial studies involved IC<sub>50</sub> determination for representative compounds. Two representative quinolines, chloroquine and mefloquine, were assayed for their activity against *M. tuberculosis* DNA gyrase. Chloroquine inhibited the supercoiling and relaxation activity with an IC<sub>50</sub> of 80 µM and mefloquine inhibited both the reaction with an IC<sub>50</sub> of 300 µM. Interestingly, chloroquine exhibited DNA cleavage in the absence of ATP. But its DNA cleavage activity was weaker than ciprofloxacin. These preliminary results are promising to develop quinolines for antimycobacterials. Previous reports on quinoline induced cross-resistance to fluoroquinolone also indicate possible interaction between quinolines and DNA gyrase (Davidson *et al.*, 2008). In many parts of the world, TB and malaria are endemic. Population genetic studies in these areas can be done in future to establish correlation between the cases of malaria and TB.

Aaptamines are related to quinolines, possess antimycobacterial activity (Pettit *et al.*, 2004) and are predicted to interact with topoisomerases. Therefore I decided to assay seven aaptamine derivatives and marine extracts to study their effect on the activity of *M. tuberculosis* DNA gyrase. Out of all the compounds that were tested, 1N,4N-didodecyl aaptamine (**Figure 5.6**) is a good inhibitor of *M. tuberculosis* DNA gyrase (IC<sub>50</sub>~10-20 µM). Thus aaptamines can be developed to specifically target *M. tuberculosis* DNA gyrase.

The naphthoquinone class have been studied in detail in relation to a broad range of biological activities that can be exploited for the design of new antibacterial (Mahapatra *et al.*, 2007), anti-leishmaniasis (Ray *et al.*, 1998, Yardley *et al.*, 1996) and antitumor compounds (Ting *et al.*, 2003, Hazra *et al.*, 1984). Although there is no established target for naphthoquinones, the predicted targets are the electron transport chain and mycothiol disulfide reductase in *M. tuberculosis*. Nine different

compounds and plant extracts were tested against *M. tuberculosis* DNA gyrase supercoiling. 7-methyljuglone and diospyrin were the most potent DNA gyrase inhibitors of all the tested compounds. These compounds have an IC<sub>50</sub> of ~10 μM, comparable to the IC<sub>50</sub> of ciprofloxacin (10 μM) in a supercoiling assay. These compounds also inhibit DNA relaxation and decatenation activity.

Besides *M. tuberculosis* DNA gyrase, 7-methyljuglone and diospyrin also inhibited *E. coli* DNA gyrase supercoiling activity with an IC<sub>50</sub> between 50-100 μM and 1-10 μM respectively. Diospyrin (MW: 374.35 Da) was selected for further study because it has higher molecular weight in comparison to 7-methyljuglone (MW: 188.18 Da), which is beneficial for experimental techniques such as nano-ESI-MS and SPR experiments. DNA cleavage assays in the presence and absence of ATP indicated that diospyrin does not inhibit the enzyme activity by stabilising the cleavage complex.

In order to identify the potential binding site for diospyrin, two different biophysical techniques (SPR, nano-ESI-MS) were used. Both of these techniques confirmed that the GyrB N-terminus is the potential target site for diospyrin. Co-crystallisation trials with *E. coli* GyrB43-diospyrin and *E. coli* GyrB43-ADPNP-diospyrin were not successful and *E. coli* GyrB24-novobiocin-diospyrin crystals diffraction data did not show bound diospyrin (**Appendix**). In the absence of a crystal structure, in-silico docking for diospyrin was performed on the model of *M. tuberculosis* GyrB43 using Libdock protocol of Discovery Studio 2.5.5. According to the docking experiments, the potential binding site of diospyrin is a cleft just below the ATP-binding site. Using an ATP competition assay and SPR experiments I have shown that diospyrin does not bind at the ATP-binding site. Although now we know the target site for diospyrin, it is not clear how diospyrin binding at this site affects the enzyme activity. The limited proteolysis experiments with trypsin indicate conformational changes which may affect the catalytic cycle of the enzyme.

In future, site-directed mutagenesis experiments can be done to mutate the predicted amino acids involved in diospyrin-binding (Glu188, Thr295, Asn301, Thr294, Thr302 and His 303) and to study if there is any change in the IC<sub>50</sub> for diospyrin. GyrB43-diospyrin co-crystallisation trials can also be carried out by

identifying new crystallization conditions from fresh screens. In order to obtain kinetic data for diospyrin-binding, isothermal titration calorimetry (ITC) can also be performed.

*M. tuberculosis* DNA gyrase is a potential target for discovering novel antibacterial. In this project I used different approaches to achieve this goal. One of the methods was based on the virtual screening at a unique site (putative Ca<sup>2+</sup>-binding site) in the protein and another was investigating the activity of compounds against *M. tuberculosis* DNA gyrase, which have already been reported as antimycobacterials with no information about their target. There are different approaches for addressing antibacterial drug discovery. The important goal is to find new drugs and therapies that can address the problem of epidemics like tuberculosis. This can be addressed by exploring sources for new drugs and understanding the molecular mechanism behind drug resistance. Drug resistance to several established targets is common across different bacterial species. For example DNA gyrase and fluoroquinolone resistance and rifampicin resistance and alterations in *rpoB* cluster I in *S. pneumoniae*, *E. coli* and *M. tuberculosis* (Enright *et al.*, 1998). I would like to finish with a quote from the TB Alliance 2009 report that highlights the challenge in discovering the most convenient, quick and timeless therapy for tuberculosis.

**“The precious hopes of new drugs stand in stark contrast to the grim reality of the TB epidemic. TB still kills 5,000 people every day... and the problem is getting worse. TB anywhere is TB everywhere”.**

*-TB ALLIANCE 2009 Annual Report*

## APPENDIX

## Crystallisation trials

Protein	Reagent conditions	Crystals
<i>M. tuberculosis</i> GyrA	0.2 M Sodium sulphate, 0.1M Bis Tris propane (pH 6.5), 20% w/v PEG 3350 0.2 M Sodium malonate, 0.1 M Bis Tris propane (pH 6.5), 20% w/v PEG 3350 0.2 M Lithium sulphate, 0.1 M Tris.HCl (pH 8.5), 30% (w/v) PEG 4000 0.2 M tri-Sodium citrate, 20% w/v PEG 3350	Needles
<i>M. tuberculosis</i> GyrB	0.2M Sodium formate, 20% w/v PEG 3350, 0.1M Bis Tris propane (pH 6.5) 0.2M Sodium acetate, 20% w/v PEG 3350, 0.1M Bis Tris propane (pH 6.5)	Plates
<i>M. tuberculosis</i> GyrB N40Δ	0.02 M Calcium chloride, 0.1 M Sodium acetate (pH 4.6), 30 %(v/v) MPD 0.2 M Ammonium sulfate. 30 % (w/v) PEG 4000	Needles
<i>E. coli</i> GyrB43 + 1 mM ADPNP & <i>E. coli</i> GyrB43+ 1 mM ADPNP + 1mM Diospyrin	0.1 M HEPES (pH 7.5), 4-9% PEG400, 0.2 M ammonium sulfate	Clear drops
<i>E. coli</i> GyrB24+ 1 mM novobiocin & <i>E. coli</i> GyrB24 + 1 mM novobiocin + 1 mM diospyrin	20% - 21% PEG 550 MME, 100 mM MES pH 6.5	Plates/ Needles



*E. coli GyrB24-novobiocin*

(20% PEG 550 MME, 100 mM MES pH 6.5)



*E. coli GyrB24-novobiocin-diospyrin*

(21% PEG 550 MME, 100 mM MES pH 6.5)

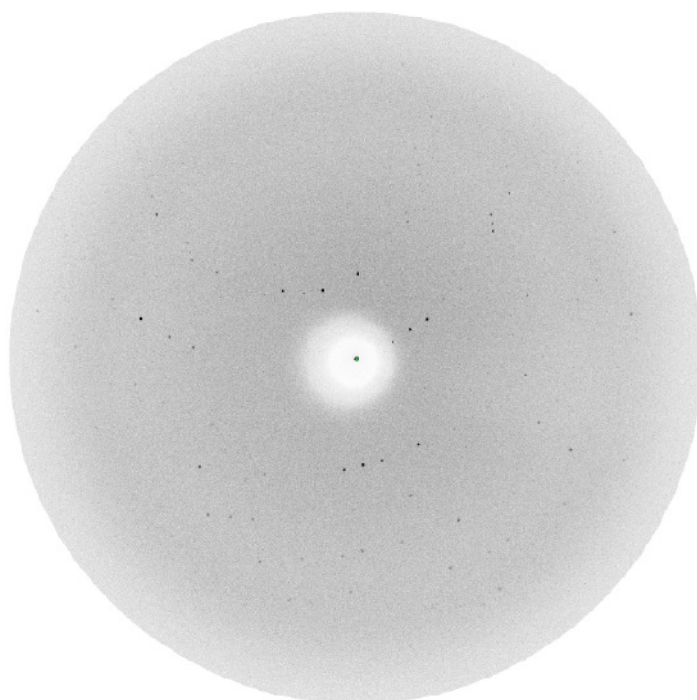


*E. coli GyrB24-novobiocin-diospyrin*

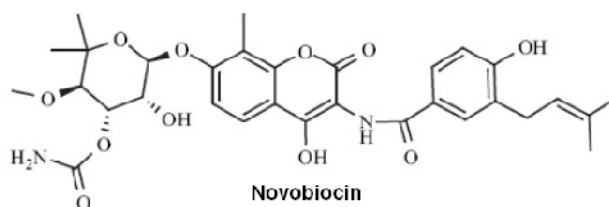
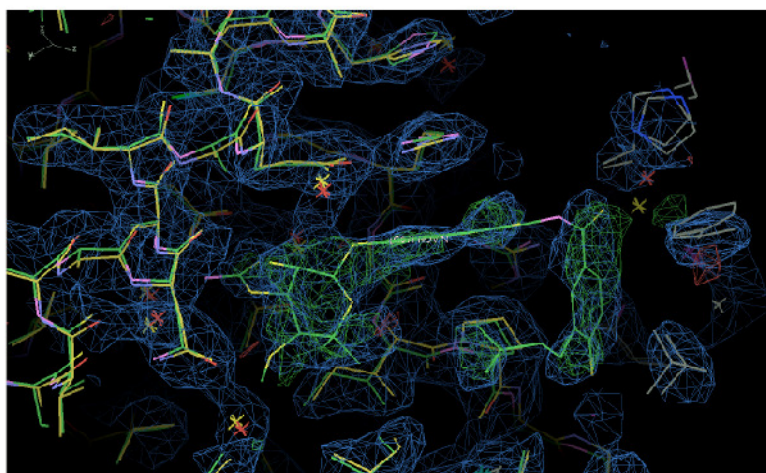
(20% PEG 550 MME, 100 mM MES pH 6.5)

**Co-Crystals of *E. coli* GyrB24-novobiocin-diospyrin and *E. coli* GyrB24-novobiocin**

A.



B.



**Diffraction data for *E. coli* GyrB24-novobiocin-diospyrin co-crystals.** (A) *The crystal diffraction pattern at 2.8 Å* (B) *Electron density only showing novobiocin binding. Diospyrin molecule was not observed.*

## ABBREVIATIONS

Å	Angstrom ( $10^{-10}$ m)
ATP	Adenosine triphosphate
CD	Circular dichroism
DMSO	Dimethylsulfoxide
DNA	Deoxyribonucleic acid
DTT	Dithiothreitol
EDTA	Ethylenediaminetetraacetic acid
EGTA	Ethylene glycol tetraacetic acid
HEPES	4-(2-Hydroxyethyl)piperazine-1 ethanesulfonic acid
ICP-AES	Inductively coupled plasma atomic emission spectroscopy
IPTG	Isopropyl- $\beta$ -D-thiogalactopyranoside
kDa	Kilo Dalton
LB	Luria Bertani media
MS	Mass spectrometry
MIC	Minimum inhibitory concentration
MPC	Mutant prevention concentration
MurI	Glutamate racemase
Nano-ESI	Nanoflow electrospray ionisation
ONP	o-nitrophenol
ONPG	o-Nitrophenyl- $\beta$ -D-galactopyranoside
PAGE	Polyacrylamide gel electrophoresis
PCR	Polymerase chain reaction
PEG	Polyethylene glycol
PDB	Protein data bank
Rpm	Revolutions per minute
RT-PCR	Reverse transcription-polymerase chain reaction
SAB	Sample application buffer
SDM	Site-directed mutagenesis
SPR	Surface plasmon resonance
TAE	Tris base, acetic acid and EDTA.
TB	Tuberculosis
Tris	Tris (hydroxymethyl)aminomethane
Tw	Twist
Wr	Writhe
SDS	Sodium dodecyl sulfate

---

## REFERENCES

- (2009) Screening we can believe in. In: Nat Chem Biol. Nature Publishing Group, pp. 127-127.
- Adachi, T., M. Mizuuchi, E. A. Robinson, E. Appella, M. H. O'Dea, M. Gellert & K. Mizuuchi, (1987) DNA sequence of the E. coli gyrB gene: application of a new sequencing strategy. *Nucleic Acids Res* **15**: 771-784.
- Adams, D. E., E. M. Shekhtman, E. L. Zechiedrich, M. B. Schmid & N. R. Cozzarelli, (1992) The role of topoisomerase IV in partitioning bacterial replicons and the structure of catenated intermediates in DNA replication. *Cell* **71**: 277-288.
- Agarwal, N., T. R. Raghunand & W. R. Bishai, (2006) Regulation of the expression of whiB1 in Mycobacterium tuberculosis: role of cAMP receptor protein. *Microbiology* **152**: 2749-2756.
- Aghajari, N., F. V. Petegem, V. Villeret, J.-P. Chessa, C. Gerday, R. Haser & J. V. Beeumen, (2003) Crystal structures of a psychrophilic metalloprotease reveal new insights into catalysis by cold-adapted proteases. *Proteins: Structure, Function, and Genetics* **50**: 636-647.
- Ali, J. A., A. P. Jackson, A. J. Howells & A. Maxwell, (1993) The 43-kilodalton N-terminal fragment of the DNA gyrase B protein hydrolyzes ATP and binds coumarin drugs. *Biochemistry* **32**: 2717-2724.
- Andersson, S. G. E. & P. M. Sharp, (1996) Codon usage in the Mycobacterium tuberculosis complex. *Microbiology* **142**: 915-925.
- Andrew, R. G. & R. A. Raphael, (1987) A new total synthesis of aaptamine. *Tetrahedron* **43**: 4803-4816.
- Angehrn, P., S. Buchmann, C. Funk, E. Goetschi, H. Gmuender, P. Hebeisen, D. Kostrewa, H. Link, T. Luebbers, R. Masciadri, J. Nielsen, P. Reindl, F. Ricklin, A. Schmitt-Hoffmann & F. P. Theil, (2004) New antibacterial agents derived from the DNA gyrase inhibitor cyclothialidine. *J Med Chem* **47**: 1487-1513.
- Annamalai, T., N. Dani, B. Cheng & Y.-C. Tse-Dinh, (2009) Analysis of DNA relaxation and cleavage activities of recombinant Mycobacterium tuberculosis DNA topoisomerase I from a new expression and purification protocol. *BMC Biochemistry* **10**: 18.
- Appelbaum, P. C. & P. A. Hunter, (2000) The fluoroquinolone antibacterials: past, present and future perspectives. *International Journal of Antimicrobial Agents* **16**: 5-15.
- Aravind, L., D. D. Leipe & E. V. Koonin, (1998) Toprim--a conserved catalytic domain in type IA and II topoisomerases, DnaG-type primases, OLD family nucleases and RecR proteins. *Nucleic Acids Res* **26**: 4205-4213.
- Aubry, A., L. Mark Fisher, V. Jarlier & E. Cambau, (2006a) First functional characterization of a singly expressed bacterial type II topoisomerase: The enzyme from Mycobacterium tuberculosis. *Biochemical and Biophysical Research Communications* **348**: 158-165.

- Aubry, A., X. S. Pan, L. M. Fisher, V. Jarlier & E. Cambau, (2004) Mycobacterium tuberculosis DNA gyrase: interaction with quinolones and correlation with antimycobacterial drug activity. *Antimicrob Agents Chemother* **48**: 1281-1288.
- Aubry, A., N. Veziris, E. Cambau, C. Truffot-Pernot, V. Jarlier & L. M. Fisher, (2006b) Novel gyrase mutations in quinolone-resistant and -hypersusceptible clinical isolates of Mycobacterium tuberculosis: functional analysis of mutant enzymes. *Antimicrob Agents Chemother* **50**: 104-112.
- Bahassi, E. M., M. H. O'Dea, N. Allali, J. Messens, M. Gellert & M. Couturier, (1999) Interactions of CcdB with DNA gyrase. Inactivation of Gyra, poisoning of the gyrase-DNA complex, and the antidote action of CcdA. *J Biol Chem* **274**: 10936-10944.
- Bahassi, E. M., M. A. Salmon, L. Van Melderen, P. Bernard & M. Couturier, (1995) F plasmid CcdB killer protein: ccdB gene mutants coding for non-cytotoxic proteins which retain their regulatory functions. *Mol Microbiol* **15**: 1031-1037.
- Banbula, A., J. Potempa, J. Travis, C. Fernandez-Catalén, K. Mann, R. Huber, W. Bode & F. J. Medrano, (1998) Amino-acid sequence and three-dimensional structure of the Staphylococcus aureus metalloproteinase at 1.72 Å resolution. *Structure* **6**: 1185-1193.
- Bapela, N. B., N. Lall, P. B. Fourie, S. G. Franzblau & C. E. J. Van Rensburg, (2006) Activity of 7-methyljuglone in combination with antituberculous drugs against Mycobacterium tuberculosis. *Phytomedicine* **13**: 630-635.
- Barnard, F. M. & A. Maxwell, (2001) Interaction between DNA gyrase and quinolones: effects of alanine mutations at GyrA subunit residues Ser(83) and Asp(87). *Antimicrob Agents Chemother* **45**: 1994-2000.
- Bates, A. D., J. M. Berger & A. Maxwell, (2010) The ancestral role of ATP hydrolysis in type II topoisomerases : prevention of DNA double-strand breaks. *unpublished*: 1-29.
- Bates, A. D. & A. Maxwell, (2005) *DNA Topology*. Oxford University Press.
- Baumann, U., S. Wu, K. Flaherty & B. D. McKay, (1993) Three-dimensional structure of the alkaline protease of Pseudomonas aeruginosa: a two-domain protein with a calcium binding parallel beta roll motif. *The EMBO Journal* **12**: 3357-3364.
- Bauquerez, R., L. Blanc, A. Bierrenbach, A. Brands, K. Ciceri, D. Falzon, K. Floyd, P. Glaziou, C. Gunneberg, T. Hiatt, M. Hosseini, A. Pantoja, M. Uplekar, C. Watt & A. Wright, (2009) Global Tuberculosis Control 2009 Epidemiology, Strategy, Financing. In. Geneva: WHO, pp. 303.
- Bax, B. D., P. F. Chan, D. S. Eggleston, A. Fosberry, D. R. Gentry, F. Gorrec, I. Giordano, M. M. Hann, A. Hennessy, M. Hibbs, J. Huang, E. Jones, J. Jones, K. K. Brown, C. J. Lewis, E. W. May, M. R. Saunders, O. Singh, C. E. Spitzfaden, C. Shen, A. Shillings, A. F. Theobald, A. Wohlkonig, N. D. Pearson & M. N. Gwynn, (2010) Type IIA topoisomerase inhibition by a new class of antibacterial agents. *Nature* **466**: 935-940
- Bellon, S., J. D. Parsons, Y. Wei, K. Hayakawa, L. L. Swenson, P. S. Charifson, J. A. Lippke, R. Aldape & C. H. Gross, (2004) Crystal Structures of Escherichia coli Topoisomerase IV ParE Subunit (24 and 43 Kilodaltons): a Single

- Residue Dictates Differences in Novobiocin Potency against Topoisomerase IV and DNA Gyrase. *Antimicrob. Agents Chemother.* **48**: 1856-1864.
- Belova, G. I., R. Prasad, S. A. Kozyavkin, J. A. Lake, S. H. Wilson & A. I. Slesarev, (2001) A type IB topoisomerase with DNA repair activities. *Proceedings of the National Academy of Sciences of the United States of America* **98**: 6015-6020.
- Bergerat, A., B. de Massy, D. Gadelle, P. C. Varoutas, A. Nicolas & P. Forterre, (1997) An atypical topoisomerase II from Archaea with implications for meiotic recombination. *Nature* **386**: 414-417.
- Bergerat, A., D. Gadelle & P. Forterre, (1994) Purification of a DNA topoisomerase II from the hyperthermophilic archaeon *Sulfolobus shibatae*. A thermostable enzyme with both bacterial and eucaryal features. *Journal of Biological Chemistry* **269**: 27663-27669.
- Bermudez, L. E., P. Kolonoski, M. Wu, P. A. Aralar, C. B. Inderlied & L. S. Young, (1999) Mefloquine Is Active In Vitro and In Vivo against Mycobacterium avium Complex. *Antimicrob. Agents Chemother.* **43**: 1870-1874.
- Bernard, P. & M. Couturier, (1992) Cell killing by the F plasmid CcdB protein involves poisoning of DNA-topoisomerase II complexes. *J Mol Biol* **226**: 735-745.
- Bernard, P., K. E. Kezdy, L. Van Melderen, J. Steyaert, L. Wyns, M. L. Pato, P. N. Higgins & M. Couturier, (1993) The F plasmid CcdB protein induces efficient ATP-dependent DNA cleavage by gyrase. *J Mol Biol* **234**: 534-541.
- Bhaduri, T., T. K. Bagui, D. Sikder & V. Nagaraja, (1998) DNA Topoisomerase I from Mycobacterium smegmatis. *Journal of Biological Chemistry* **273**: 13925-13932.
- Bhaduri, T., S. Basak, D. Sikder & V. Nagaraja, (2000) Inhibition of Mycobacterium smegmatis topoisomerase I by specific oligonucleotides. *FEBS Letters* **486**: 126-130.
- Biot, C., H. Bauer, R. H. Schirmer & E. Davioud-Charvet, (2004) 5-Substituted Tetrazoles as Bioisosteres of Carboxylic Acids. Bioisosterism and Mechanistic Studies on Glutathione Reductase Inhibitors as Antimalarials. *Journal of Medicinal Chemistry* **47**: 5972-5983.
- Boros, I., G. Posfai & P. Venetianer, (1984) High-copy-number derivatives of the plasmid cloning vector pBR322. *Gene* **30**: 257-260.
- Bowling, J. J., H. K. Pennaka, K. Ivey, S. Wahyuono, M. Kelly, R. F. Schinazi, F. A. Valeriote, D. E. Graves & M. T. Hamann, (2008) Antiviral and Anticancer Optimization Studies of the DNA-binding Marine Natural Product Aaptamine. *Chemical Biology & Drug Design* **71**: 205-215.
- Boyd, L. B., R. L. Atmar, G. L. Randall, R. J. Hamill, D. Steffen & L. Zechiedrich, (2008) Increased fluoroquinolone resistance with time in Escherichia coli from >17,000 patients at a large county hospital as a function of culture site, age, sex, and location. *BMC Infect Dis* **8**: 4.
- Bradford, M. M., (1976) A rapid and sensitive method for the quantitation of microgram quantities of protein utilizing the principle of protein-dye binding. *Anal Biochem* **72**: 248-254.
- Brino, L., D. Moras, A. Urzhumtsev, M. Mousli, C. Bronner, A. Mitschler & P. Oudet, (2000) Dimerization of Escherichia coli DNA-gyrase B Provides a

- Structural Mechanism for Activating the ATPase Catalytic Center. *Journal of Biological Chemistry* **275**: 9468-9475.
- Brooks, B. R., R. E. Bruccoleri, B. D. Olafson, D. J. States, S. Swaminathan & M. Karplus, (1983) CHARMM: A program for macromolecular energy, minimization, and dynamics calculations. *Journal of Computational Chemistry* **4**: 187-217.
- Brown, P. O., C. L. Peebles & N. R. Cozzarelli, (1979) A topoisomerase from *Escherichia coli* related to DNA gyrase. *Proceedings of the National Academy of Sciences of the United States of America* **76**: 6110-6114.
- Buhler, C., J. H. G. Lebbink, C. Bocs, R. Ladenstein & P. Forterre, (2001) DNA Topoisomerase VI Generates ATP-dependent Double-strand Breaks with Two-nucleotide Overhangs. *Journal of Biological Chemistry* **276**: 37215-37222.
- Champoux, J. J., (2001) DNA TOPOISOMERASES: Structure, Function, and Mechanism. *Annual Review of Biochemistry* **70**: 369-413.
- Champoux, J. J. & R. Dulbecco, (1972) An Activity from Mammalian Cells That Untwists Superhelical DNA—A Possible Swivel For DNA Replication. *Proceedings of the National Academy of Sciences of the United States of America* **69**: 143-146.
- Chatterji, M., S. Sengupta & V. Nagaraja, (2003) Chromosomally encoded gyrase inhibitor GyrI protects *Escherichia coli* against DNA-damaging agents. *Arch Microbiol* **180**: 339-346.
- Chatterji, M., S. Unniraman, A. Maxwell & V. Nagaraja, (2000) The additional 165 amino acids in the B protein of *Escherichia coli* DNA gyrase have an important role in DNA binding. *J Biol Chem* **275**: 22888-22894.
- Cheng, C., P. Kussie, N. Pavletich & S. Shuman, (1998) Conservation of Structure and Mechanism between Eukaryotic Topoisomerase I and Site-Specific Recombinases. *Cell* **92**: 841-850.
- Chusri, S., I. Villanueva, S. P. Voravuthikunchai & J. Davies, (2009) Enhancing antibiotic activity: a strategy to control *Acinetobacter* infections. *Journal of Antimicrobial Chemotherapy* **64**: 1203-1211.
- Clayton, D. A. & J. Vinograd, (1967) Circular Dimer and Catenate Forms of Mitochondrial DNA in Human Leukaemic Leucocytes. *Nature* **216**: 652-657.
- Corbett, K. D., P. Benedetti & J. M. Berger, (2007) Holoenzyme assembly and ATP-mediated conformational dynamics of topoisomerase VI. *Nat Struct Mol Biol* **14**: 611-619.
- Corbett, K. D. & J. M. Berger, (2003) Structure of the topoisomerase VI-B subunit: implications for type II topoisomerase mechanism and evolution. *EMBO J* **22**: 151-163.
- Corbett, K. D. & J. M. Berger, (2004) Structure, molecular mechanisms, and evolutionary relationships in DNA topoisomerases. *Annual Review of Biophysics and Biomolecular Structure* **33**: 95-118.
- Corbett, K. D., A. J. Schoeffler, N. D. Thomsen & J. M. Berger, (2005) The Structural Basis for Substrate Specificity in DNA Topoisomerase IV. *Journal of Molecular Biology* **351**: 545-561.

- Corbett, K. D., R. K. Shultzaberger & J. M. Berger, (2004) The C-terminal domain of DNA gyrase A adopts a DNA-bending beta-pinwheel fold. *Proc Natl Acad Sci U S A* **101**: 7293-7298.
- Cortes, F., N. Pastor, S. Mateos & I. Dominguez, (2003) Roles of DNA topoisomerases in chromosome segregation and mitosis. *Mutat Res* **543**: 59-66.
- Costenaro, L., J. G. Grossmann, C. Ebel & A. Maxwell, (2005) Small-angle X-ray scattering reveals the solution structure of the full-length DNA gyrase a subunit. *Structure* **13**: 287-296.
- Critchlow, S. E. & A. Maxwell, (1996) DNA cleavage is not required for the binding of quinolone drugs to the DNA gyrase-DNA complex. *Biochemistry* **35**: 7387-7393.
- Crumplin, G. C. & J. T. Smith, (1975) Nalidixic acid: an antibacterial paradox. *Antimicrob Agents Chemother* **8**: 251-261.
- Danelishvili, L., M. Wu, L. S. Young & L. E. Bermudez, (2005) Genomic Approach to Identifying the Putative Target of and Mechanisms of Resistance to Mefloquine in Mycobacteria. *Antimicrob. Agents Chemother.* **49**: 3707-3714.
- Dao-Thi, M. H., L. Van Melderren, E. De Genst, H. Afif, L. Buts, L. Wyns & R. Loris, (2005) Molecular basis of gyrase poisoning by the addiction toxin CcdB. *J Mol Biol* **348**: 1091-1102.
- Dar, A., D. Prusty, N. Mondal & S. K. Dhar, (2009) A Unique 45-Amino-Acid Region in the Toprim Domain of Plasmodium falciparum Gyrase B Is Essential for Its Activity. *Eukaryotic Cell* **8**: 1759-1769.
- Dar, A., A. Sharma, N. Mondal & S. K. Dhar, (2007) Molecular Cloning of Apicoplast-Targeted Plasmodium falciparum DNA Gyrase Genes: Unique Intrinsic ATPase Activity and ATP-Independent Dimerization of PfGyrB Subunit. *Eukaryotic Cell* **6**: 398-412.
- Davidson, R. J., I. Davis, B. M. Willey, K. Rizg, S. Bolotin, V. Porter, J. Polsky, N. Daneman, A. McGeer, P. Yang, D. Scolnik, R. Rowsell, O. Imas & M. S. Silverman, (2008) Antimalarial Therapy Selection for Quinolone Resistance among Escherichia coli in the Absence of Quinolone Exposure, in Tropical South America. *PLoS ONE* **3**: e2727.
- De Jonge, N., A. Garcia-Pino, L. Buts, S. Haesaerts, D. Charlier, K. Zangger, L. Wyns, H. De Greve & R. Loris, (2009) Rejuvenation of CcdB-poisoned gyrase by an intrinsically disordered protein domain. *Mol Cell* **35**: 154-163.
- DiGate, R. J. & K. J. Marians, (1988) Identification of a potent decatenating enzyme from Escherichia coli. *Journal of Biological Chemistry* **263**: 13366-13373.
- Diller, D. J. & K. M. M. . (2001) High throughput docking for library design and library prioritization. *Proteins: Structure, Function, and Genetics* **43**: 113-124.
- Diller, D. J. & R. Li, (2003) Kinases, Homology Models, and High Throughput Docking. *Journal of Medicinal Chemistry* **46**: 4638-4647.
- Diller, D. J. & K. M. Merz, Jr., (2001) High throughput docking for library design and library prioritization. *Proteins* **43**: 113-124.
- Dong, K. C. & J. M. Berger, (2007) Structural basis for gate-DNA recognition and bending by type IIA topoisomerases. *Nature* **450**: 1201-1205.

- Drlica, K., (2003) The mutant selection window and antimicrobial resistance. *J Antimicrob Chemother* **52**: 11-17.
- Drlica, K., M. Malik, R. J. Kerns & X. Zhao, (2008) Quinolone-mediated bacterial death. *Antimicrob Agents Chemother* **52**: 385-392.
- Duquesne, S., D. Destoumieux-Garzon, J. Peduzzi & S. Rebuffat, (2007) Microcins, gene-encoded antibacterial peptides from enterobacteria. *Nat Prod Rep* **24**: 708-734.
- Dutta, R. & M. Inouye, (2000) GHKL, an emergent ATPase/kinase superfamily. *Trends Biochem Sci* **25**: 24-28.
- Dwyer, D. J., M. A. Kohanski, B. Hayete & J. J. Collins, (2007) Gyrase inhibitors induce an oxidative damage cellular death pathway in *Escherichia coli*. *Mol Syst Biol* **3**: 91.
- Edgar, R. C., (2004a) MUSCLE: a multiple sequence alignment method with reduced time and space complexity. *BMC Bioinformatics* **5**: 113.
- Edgar, R. C., (2004b) MUSCLE: multiple sequence alignment with high accuracy and high throughput. *Nucleic Acids Res* **32**: 1792-1797.
- Edwards, M. J., (2009) The mode of action of simocyclinone D8; a novel inhibitor of DNA gyrase. In: *Biological Chemistry*. University of East Anglia, pp. 199.
- Edwards, M. J., R. H. Flatman, L. A. Mitchenall, C. E. Stevenson, T. B. Le, T. A. Clarke, A. R. McKay, H. P. Fiedler, M. J. Buttner, D. M. Lawson & A. Maxwell, (2009) A crystal structure of the bifunctional antibiotic simocyclinone D8, bound to DNA gyrase. *Science* **326**: 1415-1418.
- Emsley, P. & K. Cowtan, (2004) Coot: model-building tools for molecular graphics. *Acta Crystallogr D Biol Crystallogr* **60**: 2126-2132.
- Enright, M., P. Zawadzki, P. Pickerill & C. G. Dowson, (1998) Molecular evolution of rifampicin resistance in *Streptococcus pneumoniae*. *Microb Drug Resist* **4**: 65-70.
- Evans-Roberts, K. M., C. Breuer, M. K. Wall, K. Sugimoto-Shirasu & A. Maxwell, (2010) *Arabidopsis thaliana* GYRB3 does not encode a DNA gyrase subunit. *PLoS One* **5**: e9899.
- Evers, A. & G. Klebe, (2004a) Ligand-Supported Homology Modeling of G-Protein-Coupled Receptor Sites: Models Sufficient for Successful Virtual Screening13. *Angewandte Chemie International Edition* **43**: 248-251.
- Evers, A. & G. Klebe, (2004b) Successful Virtual Screening for a Submicromolar Antagonist of the Neurokinin-1 Receptor Based on a Ligand-Supported Homology Model. *Journal of Medicinal Chemistry* **47**: 5381-5392.
- Fairall, L., S. Martin & D. Rhodes, (1989) The DNA binding site of the *Xenopus* transcription factor IIIA has a non-B-form structure. *The EMBO Journal* **8**: 1 809 - 1817.
- Feng-Jui, C. & L. Hsiu-Jung, ( 2003 ) Molecular mechanisms of fluoroquinolone resistance. *J Microbiol Immunol Infect* **36**: 1-9.
- Flatman, R. H., A. J. Howells, L. Heide, H.-P. Fiedler & A. Maxwell, (2005) Simocyclinone D8, an Inhibitor of DNA Gyrase with a Novel Mode of Action. *Antimicrob. Agents Chemother.* **49**: 1093-1100.
- Foley, M. & L. Tilley, (1998) Quinoline Antimalarials: Mechanisms of Action and Resistance and Prospects for New Agents. *Pharmacology & Therapeutics* **79**: 55-87.

- Frothingham, R., (1995) Differentiation of strains in Mycobacterium tuberculosis complex by DNA sequence polymorphisms, including rapid identification of *M. bovis* BCG. *J. Clin. Microbiol.* **33**: 840-844.
- Fu, G., J. Wu, W. Liu, D. Zhu, Y. Hu, J. Deng, X. E. Zhang, L. Bi & D. C. Wang, (2009) Crystal structure of DNA gyrase B' domain sheds lights on the mechanism for T-segment navigation. *Nucleic Acids Res* **37**: 5908-5916.
- Garbe, T. R., (2004) Co-induction of methyltransferase RvO560c by naphthoquinones and fibric acids suggests attenuation of isoprenoid quinone action in Mycobacterium tuberculosis. *Canadian Journal of Microbiology* **50**: 771-778.
- Garrido, M. C., M. Herrero, R. Kolter & F. Moreno, (1988) The export of the DNA replication inhibitor Microcin B17 provides immunity for the host cell. *EMBO J* **7**: 1853-1862.
- Gasteiger, E., A. Gattiker, C. Hoogland, I. Ivanyi, R. D. Appel & A. Bairoch, (2003) ExPASy: the proteomics server for in-depth protein knowledge and analysis. *Nucl. Acids Res.* **31**: 3784-3788.
- Gatto, B., G. Capranico & M. Palumbo, (1999) Drugs acting on DNA topoisomerases: recent advances and future perspectives. *Curr Pharm Des* **5**: 195-215.
- Gehlhaar, D. K., G. M. Verkhivker, P. A. Rejto, C. J. Sherman, D. R. Fogel, L. J. Fogel & S. T. Freer, (1995) Molecular recognition of the inhibitor AG-1343 by HIV-1 protease: conformationally flexible docking by evolutionary programming. *Chemistry & Biology* **2**: 317-324.
- Gellert, M., L. M. Fisher & M. H. O'Dea, (1979) DNA gyrase: purification and catalytic properties of a fragment of gyrase B protein. *Proceedings of the National Academy of Sciences of the United States of America* **76**: 6289-6293.
- Gellert, M., K. Mizuuchi, M. H. O'Dea & H. A. Nash, (1976) DNA gyrase: an enzyme that introduces superhelical turns into DNA. *Proc Natl Acad Sci U S A* **73**: 3872-3876.
- Gifford, J. L., M. P. Walsh & H. J. Vogel, (2007) Structures and metal-ion-binding properties of the Ca<sup>2+</sup>-binding helix-loop-helix EF-hand motifs. *Biochem J* **405**: 199-221.
- Ginalski, K., A. Elofsson, D. Fischer & L. Rychlewski, (2003) 3D-Jury: a simple approach to improve protein structure predictions. *Bioinformatics* **19**: 1015-1018.
- Goetschi, E., P. Angehrn, H. Gmuender, P. Hebeisen, H. Link, R. Masciadri & J. Nielsen, (1993) Cyclothialidine and its congeners: a new class of DNA gyrase inhibitors. *Pharmacol Ther* **60**: 367-380.
- Goodsell, D. S., G. M. Morris & A. J. Olson, (1996) Automated docking of flexible ligands: Applications of autodock. *Journal of Molecular Recognition* **9**: 1-5.
- Gormley, N. A., G. Orphanides, A. Meyer, P. M. Cullis & A. Maxwell, (1996) The interaction of coumarin antibiotics with fragments of DNA gyrase B protein. *Biochemistry* **35**: 5083-5092.
- Goswitz, J. J., K. E. Willard, C. E. Fasching & L. R. Peterson, (1992) Detection of gyrA gene mutations associated with ciprofloxacin resistance in methicillin-resistant *Staphylococcus aureus*: analysis by polymerase chain reaction and

- automated direct DNA sequencing. *Antimicrob Agents Chemother* **36**: 1166-1169.
- Grabarek, Z., (2006) Structural Basis for Diversity of the EF-hand Calcium-binding Proteins. *Journal of Molecular Biology* **359**: 509-525.
- Greenfield, N. J., (2006a) Using circular dichroism collected as a function of temperature to determine the thermodynamics of protein unfolding and binding interactions. *Nat Protoc* **1**: 2527-2535.
- Greenfield, N. J., (2006b) Using circular dichroism spectra to estimate protein secondary structure. *Nat Protoc* **1**: 2876-2890.
- Gross, C. H., J. D. Parsons, T. H. Grossman, P. S. Charifson, S. Bellon, J. Jernee, M. Dwyer, S. P. Chambers, W. Markland, M. Botfield & S. A. Raybuck, (2003) Active-Site Residues of Escherichia coli DNA Gyrase Required in Coupling ATP Hydrolysis to DNA Supercoiling and Amino Acid Substitutions Leading to Novobiocin Resistance. *Antimicrob. Agents Chemother.* **47**: 1037-1046.
- Guillemin, I., V. Jarlier & E. Cambau, (1998) Correlation between quinolone susceptibility patterns and sequences in the A and B subunits of DNA gyrase in mycobacteria. *Antimicrob Agents Chemother* **42**: 2084-2088.
- Guillemin, I., W. Sougakoff, E. Cambau, V. Revel-Viravau, N. Moreau & V. Jarlier, (1999) Purification and inhibition by quinolones of DNA gyrases from Mycobacterium avium, Mycobacterium smegmatis and Mycobacterium fortuitum bv. peregrinum. *Microbiology* **145**: 2527-2532.
- Gul, W., N. L. Hammond, M. Yousaf, J. J. Bowling, R. F. Schinazi, S. S. Wirtz, G. de Castro Andrews, C. Cuevas & M. T. Hamann, (2006) Modification at the C9 position of the marine natural product isoaptamine and the impact on HIV-1, mycobacterial, and tumor cell activity. *Bioorganic & Medicinal Chemistry* **14**: 8495-8505.
- Hanai, R., P. R. Caron & J. C. Wang, (1996) Human TOP3: a single-copy gene encoding DNA topoisomerase III. *Proceedings of the National Academy of Sciences of the United States of America* **93**: 3653-3657.
- Hashimi, S. M., G. Huang, A. Maxwell & R. G. Birch, (2008) DNA Gyrase from the Albicidin Producer Xanthomonas albilineans Has Multiple-Antibiotic-Resistance and Unusual Enzymatic Properties. *Antimicrob. Agents Chemother.* **52**: 1382-1390.
- Hashimi, S. M., M. K. Wall, A. B. Smith, A. Maxwell & R. G. Birch, (2006) The Phytotoxin Albicidin is a Novel Inhibitor of DNA Gyrase. *Antimicrob. Agents Chemother.* **51**: 181-187.
- Haydel, S. E., W. H. Benjamin, Jr., N. E. Dunlap & J. E. Clark-Curtiss, (2002) Expression, Autoregulation, and DNA Binding Properties of the Mycobacterium tuberculosis TrcR Response Regulator. *J. Bacteriol.* **184**: 2192-2203.
- Hazra, B., R. Ghosh, A. Banerjee, G. C. Kirby, D. C. Warhurst & J. D. Phillipson, (1995) In vitro antiplasmodial effects of diospyrin, a plant-derived naphthoquinoid, and a novel series of derivatives. *Phytotherapy Research* **9**: 72-74.
- Hazra, B., P. Sur, D. K. Roy, B. Sur & A. Banerjee, (1984) Biological activity of diospyrin towards Ehrlich ascites carcinoma in Swiss A mice. *Planta Med* **50**: 295-297.

- Heddle, J. G., S. J. Blance, D. B. Zamble, F. Hollfelder, D. A. Miller, L. M. Wentzell, C. T. Walsh & A. Maxwell, (2001) The antibiotic microcin B17 is a DNA gyrase poison: characterisation of the mode of inhibition. *J Mol Biol* **307**: 1223-1234.
- Heddle, J. G., S. Mittelheiser, A. Maxwell & N. H. Thomson, (2004) Nucleotide binding to DNA gyrase causes loss of DNA wrap. *J Mol Biol* **337**: 597-610.
- Hegde, S. S., M. W. Vetting, S. L. Roderick, L. A. Mitchenall, A. Maxwell, H. E. Takiff & J. S. Blanchard, (2005) A fluoroquinolone resistance protein from *Mycobacterium tuberculosis* that mimics DNA. *Science* **308**: 1480-1483.
- Herrero, M. & F. Moreno, (1986) Microcin B17 blocks DNA replication and induces the SOS system in *Escherichia coli*. *J Gen Microbiol* **132**: 393-402.
- Hiasa, H., R. J. DiGate & K. J. Mariani, (1994) Decatenating activity of *Escherichia coli* DNA gyrase and topoisomerases I and III during *oriC* and pBR322 DNA replication in vitro. *Journal of Biological Chemistry* **269**: 2093-2099.
- Hockings, S. C. & A. Maxwell, (2002) Identification of four GyrA residues involved in the DNA breakage-reunion reaction of DNA gyrase. *J Mol Biol* **318**: 351-359.
- Holdgate, G. A., A. Tunnicliffe, W. H. Ward, S. A. Weston, G. Rosenbrock, P. T. Barth, I. W. Taylor, R. A. Pauptit & D. Timms, (1997) The entropic penalty of ordered water accounts for weaker binding of the antibiotic novobiocin to a resistant mutant of DNA gyrase: a thermodynamic and crystallographic study. *Biochemistry* **36**: 9663-9673.
- Holzenkampfer, M., M. Walker, A. Zeeck, J. Schimana & H. P. Fiedler, (2002) Simocyclinones, novel cytostatic angucyclinone antibiotics produced by *Streptomyces antibioticus* Tu 6040 II. Structure elucidation and biosynthesis. *J Antibiot (Tokyo)* **55**: 301-307.
- Hopewell, R., M. Oram, R. Briesewitz & L. M. Fisher, (1990) DNA cloning and organization of the *Staphylococcus aureus* *gyrA* and *gyrB* genes: close homology among gyrase proteins and implications for 4-quinolone action and resistance. *J Bacteriol* **172**: 3481-3484.
- Hsieh, T. J., T. J. Yen, T. S. Lin, H. T. Chang, S. Y. Huang, C. H. Hsu, L. Farh & N. L. Chan, (2010) Twisting of the DNA-binding surface by a beta-strand-bearing proline modulates DNA gyrase activity. *Nucleic Acids Res* **38**: 4173-4181.
- Huang, Y.-Y., J.-Y. Deng, J. Gu, Z.-P. Zhang, A. Maxwell, L.-J. Bi, Y.-Y. Chen, Y.-F. Zhou, Z.-N. Yu & X.-E. Zhang, (2006) The key DNA-binding residues in the C-terminal domain of *Mycobacterium tuberculosis* DNA gyrase A subunit (GyrA). *Nucl. Acids Res.* **34**: 5650-5659.
- Hudson, B. & J. Vinograd, (1967) Catenated Circular DNA Molecules in HeLa Cell Mitochondria. *Nature* **216**: 647-652.
- Hunter, M. J. & W. J. Chazin, (1998) High Level Expression and Dimer Characterization of the S100 EF-hand Proteins, Migration Inhibitory Factor-related Proteins 8 and 14. *Journal of Biological Chemistry* **273**: 12427-12435.
- Irwin, J. J. & B. K. Shoichet, (2004) ZINC – A Free Database of Commercially Available Compounds for Virtual Screening. *Journal of Chemical Information and Modeling* **45**: 177-182.

- Jackson, A. P. & A. Maxwell, (1993) Identifying the catalytic residue of the ATPase reaction of DNA gyrase. *Proc Natl Acad Sci U S A* **90**: 11232-11236.
- Jain, V., S. Sujatha, A. K. Ojha & D. Chatterji, (2005) Identification and characterization of rel promoter element of Mycobacterium tuberculosis. *Gene* **351**: 149-157.
- Janda, K. D., (1994) Tagged versus untagged libraries: methods for the generation and screening of combinatorial chemical libraries. *Proceedings of the National Academy of Sciences of the United States of America* **91**: 10779-10785.
- Jang, K. H., S.-C. Chung, J. Shin, S.-H. Lee, T.-I. Kim, H.-S. Lee & K.-B. Oh, (2007) Aaptamines as sortase A inhibitors from the tropical sponge Aaptos aaptos. *Bioorganic & Medicinal Chemistry Letters* **17**: 5366-5369.
- Janin, Y. L., (2007) Antituberculosis drugs: ten years of research. *Bioorg Med Chem* **15**: 2479-2513.
- Jayaprakash, S., Y. Iso, B. Wan, Scott G. Franzblau & Alan P. Kozikowski, (2006) Design, Synthesis, and SAR Studies of Mefloquine-Based Ligands as Potential Antituberculosis Agents. *ChemMedChem* **1**: 593-597.
- Jones, D. T., (1999) Protein secondary structure prediction based on position-specific scoring matrices. *Journal of Molecular Biology* **292**: 195-202.
- Jou, R., W. L. Huang & C. Y. Chiang, (2008) Human tuberculosis caused by Mycobacterium bovis, Taiwan. *Emerging infectious diseases* **14**: 515-517.
- Kampranis, S. C., A. D. Bates & A. Maxwell, (1999a) A model for the mechanism of strand passage by DNA gyrase. *Proc Natl Acad Sci U S A* **96**: 8414-8419.
- Kampranis, S. C., N. A. Gormley, R. Tranter, G. Orphanides & A. Maxwell, (1999b) Probing the binding of coumarins and cyclothialidines to DNA gyrase. *Biochemistry* **38**: 1967-1976.
- Kampranis, S. C., A. J. Howells & A. Maxwell, (1999c) The interaction of DNA gyrase with the bacterial toxin CcdB: evidence for the existence of two gyrase-CcdB complexes. *J Mol Biol* **293**: 733-744.
- Kampranis, S. C. & A. Maxwell, (1996) Conversion of DNA gyrase into a conventional type II topoisomerase. *Proc Natl Acad Sci U S A* **93**: 14416-14421.
- Kampranis, S. C. & A. Maxwell, (1998) The DNA gyrase-quinolone complex. ATP hydrolysis and the mechanism of DNA cleavage. *J Biol Chem* **273**: 22615-22626.
- Kawasaki, H., S. Nakayama & R. H. Kretsinger, (1998) Classification and evolution of EF-hand proteins. *BioMetals* **11**: 277-295.
- Keeney, S., C. N. Giroux & N. Kleckner, (1997) Meiosis-specific DNA double-strand breaks are catalyzed by Spo11, a member of a widely conserved protein family. *Cell* **88**: 375-384.
- Kelley, L. A. & M. J. E. Sternberg, (2009) Protein structure prediction on the Web: a case study using the Phyre server. *Nat. Protocols* **4**: 363-371.
- Khodursky, A. B. & N. R. Cozzarelli, (1998) The mechanism of inhibition of topoisomerase IV by quinolone antibacterials. *J Biol Chem* **273**: 27668-27677.
- Kocagoz, T., C. J. Hackbarth, I. Unsal, E. Y. Rosenberg, H. Nikaido & H. F. Chambers, (1996) Gyrase mutations in laboratory-selected, fluoroquinolone-

- resistant mutants of *Mycobacterium tuberculosis* H37Ra. *Antimicrob Agents Chemother* **40**: 1768-1774.
- Krah, R., S. A. Kozyavkin, A. I. Slesarev & M. Gellert, (1996) A two-subunit type I DNA topoisomerase (reverse gyrase) from an extreme hyperthermophile. *Proceedings of the National Academy of Sciences of the United States of America* **93**: 106-110.
- Kretsinger, R. H. & C. E. Nockolds, (1973) Carp Muscle Calcium-binding Protein. *Journal of Biological Chemistry* **248**: 3313-3326.
- Kumar, D., B. S. Srivastava & R. Srivastava, (1998) Genetic rearrangements leading to disruption of heterologous gene expression in mycobacteria: An observation with *Escherichia coli* [beta]-galactosidase in *Mycobacterium smegmatis* and its implication in vaccine development. *Vaccine* **16**: 1212-1215.
- Kurowski, M. A. & J. M. Bujnicki, (2003) GeneSilico protein structure prediction meta-server. *Nucleic Acids Res* **31**: 3305-3307.
- Lafitte, D., V. Lamour, P. O. Tsvetkov, A. A. Makarov, M. Klich, P. Deprez, D. Moras, C. Briand & R. Gilli, (2002) DNA gyrase interaction with coumarin-based inhibitors: the role of the hydroxybenzoate isopentenyl moiety and the 5'-methyl group of the noviose. *Biochemistry* **41**: 7217-7223.
- Lall, N. & J. J. M. Meyer, (2001) Inhibition of drug-sensitive and drug-resistant strains of *Mycobacterium tuberculosis* by diospyrin, isolated from *Euclea natalensis*. *Journal of Ethnopharmacology* **78**: 213-216.
- Lamour, V., L. Hoermann, J. M. Jeltsch, P. Oudet & D. Moras, (2002) An open conformation of the *Thermus thermophilus* gyrase B ATP-binding domain. *J Biol Chem* **277**: 18947-18953.
- Laponogov, I., M. K. Sohi, D. A. Veselkov, X. S. Pan, R. Sawhney, A. W. Thompson, K. E. McAuley, L. M. Fisher & M. R. Sanderson, (2009) Structural insight into the quinolone-DNA cleavage complex of type IIA topoisomerases. *Nat Struct Mol Biol* **16**: 667-669.
- Larghi, E. L., M. L. Bohn & T. S. Kaufman, (2009) Aaptamine and related products. Their isolation, chemical syntheses, and biological activity. *Tetrahedron* **65**: 4257-4282.
- Larkin, M. A., G. Blackshields, N. P. Brown, R. Chenna, P. A. McGettigan, H. McWilliam, F. Valentin, I. M. Wallace, A. Wilm, R. Lopez, J. D. Thompson, T. J. Gibson & D. G. Higgins, (2007) Clustal W and Clustal X version 2.0. *Bioinformatics* **23**: 2947-2948.
- Laskowski, A. R., W. M. MacArthur, S. D. Moss & M. J. Thornton, (1993) PROCHECK: a program to check the stereochemical quality of protein structures. *Journal of Applied Crystallography* **26**: 283-291
- Le, T. B., H. P. Fiedler, C. D. den Hengst, S. K. Ahn, A. Maxwell & M. J. Buttner, (2009) Coupling of the biosynthesis and export of the DNA gyrase inhibitor simocyclinone in *Streptomyces antibioticus*. *Mol Microbiol* **72**: 1462-1474.
- Leelaram, M. N., N. Suneetha, V. Nagaraja & R. Manjunath, (2010) A new ELISA plate based microtiter well assay for mycobacterial topoisomerase I for the direct screening of enzyme inhibitory monoclonal antibody supernatants. *Journal of Immunological Methods* **357**: 26-32.

- Leslie, A. G., (2006) The integration of macromolecular diffraction data. *Acta Crystallogr D Biol Crystallogr* **62**: 48-57.
- Lewis, R. J., O. M. Singh, C. V. Smith, T. Skarzynski, A. Maxwell, A. J. Wonacott & D. B. Wigley, (1996) The nature of inhibition of DNA gyrase by the coumarins and the cyclothialidines revealed by X-ray crystallography. *EMBO J* **15**: 1412-1420.
- Li, Z., A. Mondragón & R. J. DiGate, (2001) The Mechanism of Type IA Topoisomerase-Mediated DNA Topological Transformations. *Molecular Cell* **7**: 301-307.
- Lisby, M., J. R. Olesen, C. Skouboe, B. O. Krogh, T. Straub, F. Boege, S. Velmurugan, P. M. Martensen, A. H. Andersen, M. Jayaram, O. Westergaard & B. R. Knudsen, (2001) Residues within the N-terminal Domain of Human Topoisomerase I Play a Direct Role in Relaxation\*. *Journal of Biological Chemistry* **276**: 20220-20227.
- Liu, L. F., R. E. Depew & J. C. Wang, (1976) Knotted single-stranded DNA rings: A novel topological isomer of circular single-stranded DNA formed by treatment with Escherichia coli [omega] protein. *Journal of Molecular Biology* **106**: 439-452.
- Liu, L. F., L. Perkocha, R. Calendar & J. C. Wang, (1981) Knotted DNA from bacteriophage capsids. *Proceedings of the National Academy of Sciences of the United States of America* **78**: 5498-5502.
- Liu, L. F. & J. C. Wang, (1978a) DNA-DNA gyrase complex: the wrapping of the DNA duplex outside the enzyme. *Cell* **15**: 979-984.
- Liu, L. F. & J. C. Wang, (1978b) Micrococcus luteus DNA gyrase: active components and a model for its supercoiling of DNA. *Proc Natl Acad Sci U S A* **75**: 2098-2102.
- Liu, L. F. & J. C. Wang, (1987) Supercoiling of the DNA template during transcription. *Proc Natl Acad Sci U S A* **84**: 7024-7027.
- Loris, R., M. H. Dao-Thi, E. M. Bahassi, L. Van Melderen, F. Poortmans, R. Liddington, M. Couturier & L. Wyns, (1999) Crystal structure of CcdB, a topoisomerase poison from E. coli. *J Mol Biol* **285**: 1667-1677.
- Lue, N., A. Sharma, A. Mondragón & J. C. Wang, (1995) A 26 kDa yeast DNA topoisomerase I fragment: crystallographic structure and mechanistic implications. *Structure* **3**: 1315-1322.
- Lynn, R., G. Giaever, S. L. Swanberg & J. C. Wang, (1986) Tandem regions of yeast DNA topoisomerase II share homology with different subunits of bacterial gyrase. *Science* **233**: 647-649.
- Madhusudan, K. & V. Nagaraja, (1995) Mycobacterium smegmatis DNA gyrase: cloning and overexpression in Escherichia coli. *Microbiology* **141** ( Pt 12): 3029-3037.
- Madhusudan, K., V. Ramesh & V. Nagaraja, (1994) Molecular cloning of gyrA and gyrB genes of Mycobacterium tuberculosis: analysis of nucleotide sequence. *Biochem Mol Biol Int* **33**: 651-660.
- Mahapatra, A., S. P. N. Mativandlela, B. Binneman, P. B. Fourie, C. J. Hamilton, J. J. M. Meyer, F. van der Kooy, P. Houghton & N. Lall, (2007) Activity of 7-methyljuglone derivatives against Mycobacterium tuberculosis and as

- subversive substrates for mycothiol disulfide reductase. *Bioorganic & Medicinal Chemistry* **15**: 7638-7646.
- Malik, M. & K. Drlica, (2006) Moxifloxacin lethality against Mycobacterium tuberculosis in the presence and absence of chloramphenicol. *Antimicrob Agents Chemother* **50**: 2842-2844.
- Marians, K. J. & H. Hiasa, (1997) Mechanism of quinolone action. A drug-induced structural perturbation of the DNA precedes strand cleavage by topoisomerase IV. *J Biol Chem* **272**: 9401-9409.
- Martinez-Martinez, L., A. Pascual & G. A. Jacoby, (1998) Quinolone resistance from a transferable plasmid. *Lancet* **351**: 797-799.
- Matrat, S., N. Veziris, C. Mayer, V. Jarlier, C. Truffot-Pernot, J. Camuset, E. Bouvet, E. Cambau & A. Aubry, (2006) Functional analysis of DNA gyrase mutant enzymes carrying mutations at position 88 in the A subunit found in clinical strains of Mycobacterium tuberculosis resistant to fluoroquinolones. *Antimicrob Agents Chemother* **50**: 4170-4173.
- Maxwell, A., (1997) DNA gyrase as a drug target. *Trends Microbiol* **5**: 102-109.
- Maxwell, A. & D. M. Lawson, (2003) The ATP-binding site of type II topoisomerases as a target for antibacterial drugs. *Curr Top Med Chem* **3**: 283-303.
- McCoy, A. J., R. W. Grosse-Kunstleve, P. D. Adams, M. D. Winn, L. C. Storoni & R. J. Read, (2007) Phaser crystallographic software. *J Appl Crystallogr* **40**: 658-674.
- McKay, A. R., B. T. Ruotolo, L. L. Ilag & C. V. Robinson, (2006) Mass Measurements of Increased Accuracy Resolve Heterogeneous Populations of Intact Ribosomes. *Journal of the American Chemical Society* **128**: 11433-11442.
- Mdluli, K. & Z. Ma, (2007) Mycobacterium tuberculosis DNA gyrase as a target for drug discovery. *Infect Disord Drug Targets* **7**: 159-168.
- Merens, A., S. Matrat, A. Aubry, C. Lascols, V. Jarlier, C. J. Soussy, J. D. Cavallo & E. Cambau, (2009) The pentapeptide repeat proteins MfpAMt and QnrB4 exhibit opposite effects on DNA gyrase catalytic reactions and on the ternary gyrase-DNA-quinolone complex. *J Bacteriol* **191**: 1587-1594.
- Michiels, J., C. Xi, J. Verhaert & J. Vanderleyden, (2002) The functions of Ca<sup>2+</sup> in bacteria: a role for EF-hand proteins? *Trends in Microbiology* **10**: 87-93.
- Miller, A. A., G. L. Bundy, J. E. Mott, J. E. Skepner, T. P. Boyle, D. W. Harris, A. E. Hromockyj, K. R. Marotti, G. E. Zurenko, J. B. Munzner, M. T. Sweeney, G. F. Bammert, J. C. Hamel, C. W. Ford, W. Z. Zhong, D. R. Graber, G. E. Martin, F. Han, L. A. Dolak, E. P. Seest, J. C. Ruble, G. M. Kamilar, J. R. Palmer, L. S. Banitt, A. R. Hurd & M. R. Barbachyn, (2008) Discovery and characterization of QPT-1, the progenitor of a new class of bacterial topoisomerase inhibitors. *Antimicrob Agents Chemother* **52**: 2806-2812.
- Mishima, Y., K. Momma, W. Hashimoto, B. Mikami & K. Murata, (2003) Crystal Structure of AlgQ2, a Macromolecule (Alginate)-binding Protein of Sphingomonas sp. A1, Complexed with an Alginate Tetrasaccharide at 1.6-Å Resolution. *Journal of Biological Chemistry* **278**: 6552-6559.

- Montero, C., G. Mateu, R. Rodriguez & H. Takiff, (2001) Intrinsic resistance of *Mycobacterium smegmatis* to fluoroquinolones may be influenced by new pentapeptide protein MfpA. *Antimicrob Agents Chemother* **45**: 3387-3392.
- Morais Cabral, J. H., A. P. Jackson, C. V. Smith, N. Shikotra, A. Maxwell & R. C. Liddington, (1997) Crystal structure of the breakage-reunion domain of DNA gyrase. *Nature* **388**: 903-906.
- Nakada, N., H. Gmunder, T. Hirata & M. Arisawa, (1994) Mechanism of inhibition of DNA gyrase by cyclothialidine, a novel DNA gyrase inhibitor. *Antimicrob Agents Chemother* **38**: 1966-1973.
- Nakada, N., H. Shimada, T. Hirata, Y. Aoki, T. Kamiyama, J. Watanabe & M. Arisawa, (1993) Biological characterization of cyclothialidine, a new DNA gyrase inhibitor. *Antimicrob Agents Chemother* **37**: 2656-2661.
- Nakamura, H., J. i. Kobayashi, Y. Ohizumi & Y. Hirata, (1982) Isolation and structure of aaptamine a novel heteroaromatic substance possessing [alpha]-blocking activity from the sea sponge. *Tetrahedron Letters* **23**: 5555-5558.
- Nakamura, H., J. i. Kobayashi, Y. Ohizumi & Y. Hirata, (1987) Physiologically active marine natural products from *Prolifera*. Part 10. Aaptamines. Novel benzo[de][1,6]naphthyridines from the Okinawan marine sponge *Aptos aaptos*. *J Chem Soc Perkin Trans 1*: 173-176.
- Nakanishi, A., S. Imajoh-Ohmi & F. Hanaoka, (2002) Characterization of the interaction between DNA gyrase inhibitor and DNA gyrase of *Escherichia coli*. *J Biol Chem* **277**: 8949-8954.
- Nakanishi, A., T. Oshida, T. Matsushita, S. Imajoh-Ohmi & T. Ohnuki, (1998) Identification of DNA gyrase inhibitor (GyrI) in *Escherichia coli*. *J Biol Chem* **273**: 1933-1938.
- Neumann, S., W. Huang, S. Titus, G. Krause, G. Kleinau, A. T. Alberobello, W. Zheng, N. T. Southall, J. Inglese, C. P. Austin, F. S. Celi, O. Gavrilova, C. J. Thomas, B. M. Raaka & M. C. Gershengorn, (2009) Small-molecule agonists for the thyrotropin receptor stimulate thyroid function in human thyrocytes and mice. *Proceedings of the National Academy of Sciences* **106**: 12471-12476.
- Newton, G. & R. Fahey, (2002) Mycothiol biochemistry. *Archives of Microbiology* **178**: 388-394.
- Nitiss, J. L., J. Zhou, A. Rose, Y. Hsiung, K. C. Gale & N. Osheroff, (1998) The Bis(naphthalimide) DMP-840 Causes Cytotoxicity by Its Action against Eukaryotic Topoisomerase II $\dagger$ . *Biochemistry* **37**: 3078-3085.
- Noble, C. G. & A. Maxwell, (2002) The role of GyrB in the DNA cleavage-religation reaction of DNA gyrase: a proposed two metal-ion mechanism. *J Mol Biol* **318**: 361-371.
- Nordmann, P. & L. Poirel, (2005) Emergence of plasmid-mediated resistance to quinolones in Enterobacteriaceae. *J Antimicrob Chemother* **56**: 463-469.
- Oblak, M., M. Kotnik & T. Solmajer, (2007) Discovery and development of ATPase inhibitors of DNA gyrase as antibacterial agents. *Curr Med Chem* **14**: 2033-2047.
- Onodera, Y., M. Tanaka & K. Sato, (2001) Inhibitory activity of quinolones against DNA gyrase of *Mycobacterium tuberculosis*. *J Antimicrob Chemother* **47**: 447-450.

- Oppegard, L. M., B. L. Hamann, K. R. Streck, K. C. Ellis, H. P. Fiedler, A. B. Khodursky & H. Hiasa, (2009) In vivo and in vitro patterns of the activity of simocyclinone D8, an angucyclinone antibiotic from *Streptomyces antibioticus*. *Antimicrob Agents Chemother* **53**: 2110-2119.
- Orr, E. & W. L. Staudenbauer, (1982) *Bacillus subtilis* DNA gyrase: purification of subunits and reconstitution of supercoiling activity. *J Bacteriol* **151**: 524-527.
- Ostrov, D. A., J. A. Hernandez Prada, P. E. Corsino, K. A. Finton, N. Le & T. C. Rowe, (2007) Discovery of Novel DNA Gyrase Inhibitors by High-Throughput Virtual Screening. *Antimicrob. Agents Chemother.* **51**: 3688-3698.
- Parish, T., J. Turner & N. Stoker, (2001) *amiA* is a negative regulator of acetamidase expression in *Mycobacterium smegmatis*. *BMC Microbiology* **1**: 19.
- Patel, M. P. & J. S. Blanchard, (1999) Expression, Purification, and Characterization of *Mycobacterium tuberculosis* Mycothione Reductase<sup>†</sup>. *Biochemistry* **38**: 11827-11833.
- Payot, S., A. Cloeckeaert & E. Chaslus-Dancla, (2002) Selection and Characterization of Fluoroquinolone-Resistant Mutants of *Campylobacter jejuni* Using Enrofloxacin. *Microbial Drug Resistance* **8**: 335-343.
- Pelletier, J. C. & M. P. Cava, (1985) Synthesis of aaptamine, a novel marine alkaloid. *Tetrahedron Letters* **26**: 1259-1260.
- Perichon, B., P. Courvalin & M. Galimand, (2007) Transferable resistance to aminoglycosides by methylation of G1405 in 16S rRNA and to hydrophilic fluoroquinolones by QepA-mediated efflux in *Escherichia coli*. *Antimicrob Agents Chemother* **51**: 2464-2469.
- Pettit, G. R., H. Hoffmann, D. L. Herald, P. M. Blumberg, E. Hamel, J. M. Schmidt, Y. Chang, R. K. Pettit, N. E. Lewin & L. V. Pearce, (2004) Antineoplastic Agents. 499. Synthesis of Hystatin 2 and Related 1H-Benzo[de][1,6]-naphthyridinium Salts from Aaptamine1. *Journal of Medicinal Chemistry* **47**: 1775-1782.
- Pierrat, O. A. & A. Maxwell, (2003) The action of the bacterial toxin microcin B17. Insight into the cleavage-religation reaction of DNA gyrase. *J Biol Chem* **278**: 35016-35023.
- Piton, J., S. Petrella, M. Delarue, G. André-Leroux, V. Jarlier, A. Aubry & C. Mayer, (2010) Structural Insights into the Quinolone Resistance Mechanism of *Mycobacterium tuberculosis* DNA Gyrase. *PLoS One* **5**: e12245.
- Pojer, F., S. M. Li & L. Heide, (2002) Molecular cloning and sequence analysis of the clorobiocin biosynthetic gene cluster: new insights into the biosynthesis of aminocoumarin antibiotics. *Microbiology* **148**: 3901-3911.
- Pujol, J., (1990.) Nature Africa. *The Herbalist Handbook*. Jean Pujol Natural Healers Foundation, Durban: 40-57.
- Rammler, D. H., (1967) The effect of DMSO on several enzyme systems. *Annals of the New York Academy of Sciences* **141**: 291-299.
- Rao, S. N., M. S. Head, A. Kulkarni & J. M. LaLonde, (2007) Validation Studies of the Site-Directed Docking Program LibDock. *Journal of Chemical Information and Modeling* **47**: 2159-2171.

- Ravasi, T., K. Hsu, J. Goyette, K. Schroder, Z. Yang, F. Rahimi, L. P. Miranda, P. F. Alewood, D. A. Hume & C. Geczy, (2004) Probing the S100 protein family through genomic and functional analysis. *Genomics* **84**: 10-22.
- Ravulapalli, R., B. G. Diaz, R. L. Campbell & P. L. Davies, (2005) Homodimerization of calpain 3 penta-EF-hand domain. *Biochem. J.* **388**: 585-591.
- Rawat, M., G. L. Newton, M. Ko, G. J. Martinez, R. C. Fahey & Y. Av-Gay, (2002) Mycothiol-Deficient Mycobacterium smegmatis Mutants Are Hypersensitive to Alkylating Agents, Free Radicals, and Antibiotics. *Antimicrob. Agents Chemother.* **46**: 3348-3355.
- Ray, S., B. Hazra, B. Mitra, A. Das & H. K. Majumder, (1998) Diospyrin, A Bisnaphthoquinone: A Novel Inhibitor of Type I DNA Topoisomerase of Leishmania donovani. *Mol Pharmacol* **54**: 994-999.
- Redinbo, M. R., J. J. Champoux & W. G. J. Hol, (2000) Novel Insights into Catalytic Mechanism from a Crystal Structure of Human Topoisomerase I in Complex with DNA<sup>†</sup>. *Biochemistry* **39**: 6832-6840.
- Redinbo, M. R., L. Stewart, P. Kuhn, J. J. Champoux, W. G. Hol, nbsp & J., (1998) Crystal Structures of Human Topoisomerase I in Covalent and Noncovalent Complexes with DNA. *Science* **279**: 1504-1513.
- Reece, R. J. & A. Maxwell, (1989) Tryptic fragments of the Escherichia coli DNA gyrase A protein. *J. Biol. Chem.* **264**: 19648-19653.
- Reece, R. J. & A. Maxwell, (1991) The C-terminal domain of the Escherichia coli DNA gyrase A subunit is a DNA-binding protein. *Nucleic Acids Res* **19**: 1399-1405.
- Richter, S. N., G. Giaretta, V. Comuzzi, E. Leo, L. A. Mitchenall, L. M. Fisher, A. Maxwell & M. Palumbo, (2007) Hot-spot consensus of fluoroquinolone-mediated DNA cleavage by Gram-negative and Gram-positive type II DNA topoisomerases. *Nucleic Acids Res* **35**: 6075-6085.
- Rigden, D. J. & M. Y. Galperin, (2004) The DxDxDG Motif for Calcium Binding: Multiple Structural Contexts and Implications for Evolution. *Journal of Molecular Biology* **343**: 971-984.
- Rigden, D. J., M. J. Jedrzejewski, O. V. Moroz & M. Y. Galperin, (2003) Structural diversity of calcium-binding proteins in bacteria: single-handed EF-hands? *Trends in Microbiology* **11**: 295-297.
- Robicsek, A., G. A. Jacoby & D. C. Hooper, (2006a) The worldwide emergence of plasmid-mediated quinolone resistance. *Lancet Infect Dis* **6**: 629-640.
- Robicsek, A., J. Strahilevitz, G. A. Jacoby, M. Macielag, D. Abbanat, C. H. Park, K. Bush & D. C. Hooper, (2006b) Fluoroquinolone-modifying enzyme: a new adaptation of a common aminoglycoside acetyltransferase. *Nat Med* **12**: 83-88.
- Roca, J., (1995) The mechanisms of DNA topoisomerases. *Trends in Biochemical Sciences* **20**: 156-160.
- Roca, J. & J. C. Wang, (1992) The capture of a DNA double helix by an ATP-dependent protein clamp: A key step in DNA transport by type II DNA topoisomerases. *Cell* **71**: 833-840.
- Ross Kelly, T. & M. P. Maguire, (1985) A synthesis of aaptamine. *Tetrahedron* **41**: 3033-3036.

- Ruiz, N., B. Falcone, D. Kahne & T. J. Silhavy, (2005) Chemical Conditionality: A Genetic Strategy to Probe Organelle Assembly. *Cell* **121**: 307-317.
- Ruthenburg, A. J., D. M. Graybosch, J. C. Huetsch & G. L. Verdine, (2005) A superhelical spiral in the Escherichia coli DNA gyrase A C-terminal domain imparts unidirectional supercoiling bias. *J Biol Chem* **280**: 26177-26184.
- Rutherford, K., J. Parkhill, J. Crook, T. Horsnell, P. Rice, M.-A. Rajandream & B. Barrell, (2000) Artemis: sequence visualization and annotation. *Bioinformatics* **16**: 944-945.
- Rybenkov, V. V., C. Ullsperger, A. V. Vologodskii & N. R. Cozzarelli, (1997) Simplification of DNA topology below equilibrium values by type II topoisomerases. *Science* **277**: 690-693.
- Sadiq, A. A., M. R. Patel, B. A. Jacobson, M. Escobedo, K. Ellis, L. M. Oppgaard, H. Hiasa & R. A. Kratzke, (2010) Anti-proliferative effects of simocyclinone D8 (SD8), a novel catalytic inhibitor of topoisomerase II. *Invest New Drugs* **28**: 20-25.
- Salmon-Chemin, L., E. Buisine, V. Yardley, S. Kohler, M.-A. Debreu, V. Landry, C. Sergheraert, S. L. Croft, R. L. Krauth-Siegel & E. Davioud-Charvet, (2001) 2- and 3-Substituted 1,4-Naphthoquinone Derivatives as Subversive Substrates of Trypanothione Reductase and Lipoamide Dehydrogenase from Trypanosoma cruzi: Synthesis and Correlation between Redox Cycling Activities and in Vitro Cytotoxicity. *Journal of Medicinal Chemistry* **44**: 548-565.
- Sambrook, J., F. E. Fritsch & T. Maniatis, (1989) Molecular cloning: a laboratory manual. . *Cold Spring Harbor Press. Cold Spring Harbor*.
- Sareen, D., G. L. Newton, R. C. Fahey & N. A. Buchmeier, (2003) Mycothiol Is Essential for Growth of Mycobacterium tuberculosis Erdman. *J. Bacteriol.* **185**: 6736-6740.
- Schimana, J., H. P. Fiedler, I. Groth, R. Sussmuth, W. Beil, M. Walker & A. Zeeck, (2000) Simocyclinones, novel cytostatic angucyclinone antibiotics produced by Streptomyces antibioticus Tu 6040. I. Taxonomy, fermentation, isolation and biological activities. *J Antibiot (Tokyo)* **53**: 779-787.
- Schimana, J., M. Walker, A. Zeeck & P. Fiedler, (2001) Simocyclinones: diversity of metabolites is dependent on fermentation conditions. *J Ind Microbiol Biotechnol* **27**: 144-148.
- Schoeffler, A. J. & J. M. Berger, (2008) DNA topoisomerases: harnessing and constraining energy to govern chromosome topology. *Quarterly Reviews of Biophysics* **41**: 41-101.
- Schoeffler, A. J., A. P. May & J. M. Berger, (2010) A domain insertion in Escherichia coli GyrB adopts a novel fold that plays a critical role in gyrase function. *Nucleic Acids Res.*
- Sengupta, S., S. Ghosh & V. Nagaraja, (2008) Moonlighting function of glutamate racemase from Mycobacterium tuberculosis: racemization and DNA gyrase inhibition are two independent activities of the enzyme. *Microbiology* **154**: 2796-2803.
- Sengupta, S. & V. Nagaraja, (2008a) Inhibition of DNA gyrase activity by Mycobacterium smegmatis MurI. *FEMS Microbiol Lett* **279**: 40-47.

- Sengupta, S. & V. Nagaraja, (2008b) YacG from *Escherichia coli* is a specific endogenous inhibitor of DNA gyrase. *Nucleic Acids Res* **36**: 4310-4316.
- Sengupta, S., M. Shah & V. Nagaraja, (2006) Glutamate racemase from *Mycobacterium tuberculosis* inhibits DNA gyrase by affecting its DNA-binding. *Nucl. Acids Res.* **34**: 5567-5576.
- Shakkeed, Z., D. Rabinovich, W. B. T. Cruse, E. Egert, O. Kennard, G. Sala, S. A. Salisbury & M. A. Viswamitra, (1981) Crystalline A-DNA: The X-Ray Analysis of the Fragment d(G-G-T-A-T-A-C-C). *Proceedings of the Royal Society of London. Series B. Biological Sciences* **213**: 479-487.
- Shen, Y.-C., T.-T. Lin, J.-H. Sheu & C.-Y. Duh, (1999) Structures and Cytotoxicity Relationship of Isoaaptamine and Aaptamine Derivatives. *Journal of Natural Products* **62**: 1264-1267.
- Sierra, J. M., L. Martinez-Martinez, F. Vazquez, E. Giralt & J. Vila, (2005) Relationship between Mutations in the *gyrA* Gene and Quinolone Resistance in Clinical Isolates of *Corynebacterium striatum* and *Corynebacterium amycolatum*. *Antimicrob. Agents Chemother.* **49**: 1714-1719.
- Sikder, D. & V. Nagaraja, (2000) Determination of the recognition sequence of *Mycobacterium smegmatis* topoisomerase I on mycobacterial genomic sequences. *Nucl. Acids Res.* **28**: 1830-1837.
- Sikder, D. & V. Nagaraja, (2001) A novel bipartite mode of binding of *M. smegmatis* topoisomerase I to its recognition sequence. *Journal of Molecular Biology* **312**: 347-357.
- Sikder, D., S. Unniraman, T. Bhaduri & V. Nagaraja, (2001) Functional cooperation between topoisomerase I and single strand DNA-binding protein. *Journal of Molecular Biology* **306**: 669-679.
- Sissi, C., A. Chemello, E. Vazquez, L. A. Mitchenall, A. Maxwell & M. Palumbo, (2008) DNA gyrase requires DNA for effective two-site coordination of divalent metal ions: further insight into the mechanism of enzyme action. *Biochemistry* **47**: 8538-8545.
- Sissi, C., E. Perdon, E. Domenici, A. Feriani, A. J. Howells, A. Maxwell & M. Palumbo, (2001) Ciprofloxacin affects conformational equilibria of DNA gyrase A in the presence of magnesium ions. *J Mol Biol* **311**: 195-203.
- Sissi, C., E. Vazquez, A. Chemello, L. A. Mitchenall, A. Maxwell & M. Palumbo, (2010) Mapping Simocyclinone D8 Interaction with DNA Gyrase: Evidence for a New Binding Site on GyrB. *Antimicrob. Agents Chemother.* **54**: 213-220.
- Slesarev, A. I., K. O. Stetter, J. A. Lake, M. Gellert, R. Krah & S. A. Kozyavkin, (1993) DNA topoisomerase V is a relative of eukaryotic topoisomerase I from a hyperthermophilic prokaryote. *Nature* **364**: 735-737.
- Smith, C. V. & A. Maxwell, (1998) Identification of a residue involved in transition-state stabilization in the ATPase reaction of DNA gyrase. *Biochemistry* **37**: 9658-9667.
- Smith, H. J., K. A. Nichol, D. J. Hoban & G. G. Zhanel, (2003) Stretching the mutant prevention concentration (MPC) beyond its limits. *J Antimicrob Chemother* **51**: 1323-1325.
- Srivastava, R., D. Kumar, P. Subramaniam & B. S. Srivastava, (1997) [beta]-Galactosidase Reporter System in *Mycobacteria* and Its Application in Rapid

- Antimycobacterial Drug Screening. *Biochemical and Biophysical Research Communications* **235**: 602-605.
- Steck, T. R. & K. Drlica, (1984) Bacterial chromosome segregation: evidence for DNA gyrase involvement in decatenation. *Cell* **36**: 1081-1088.
- Stewart, L., G. C. Ireton & J. J. Champoux, (1996) The Domain Organization of Human Topoisomerase I. *Journal of Biological Chemistry* **271**: 7602-7608.
- Stewart, L., M. R. Redinbo, X. Qiu, W. G. Hol, nbsp, J. & J. J. Champoux, (1998) A Model for the Mechanism of Human Topoisomerase I. *Science* **279**: 1534-1541.
- Stuchinskaya, T., L. A. Mitchenall, A. J. Schoeffler, K. D. Corbett, J. M. Berger, A. D. Bates & A. Maxwell, (2009) How do type II topoisomerases use ATP hydrolysis to simplify DNA topology beyond equilibrium? Investigating the relaxation reaction of nonsupercoiling type II topoisomerases. *J Mol Biol* **385**: 1397-1408.
- Takiff, H. E., L. Salazar, C. Guerrero, W. Philipp, W. M. Huang, B. Kreiswirth, S. T. Cole, W. R. Jacobs, Jr. & A. Telenti, (1994) Cloning and nucleotide sequence of Mycobacterium tuberculosis gyrA and gyrB genes and detection of quinolone resistance mutations. *Antimicrob. Agents Chemother.* **38**: 773-780.
- Taneja, B., A. Patel, A. Slesarev & A. Mondragon, (2006) Structure of the N-terminal fragment of topoisomerase V reveals a new family of topoisomerases. *EMBO J* **25**: 398-408.
- Tazi, J., N. Bakkour, J. Soret, L. Zekri, B. Hazra, W. Laine, B. Baldeyrou, A. Lansiaux & C. Bailly, (2005) Selective Inhibition of Topoisomerase I and Various Steps of Spliceosome Assembly by Diospyrin Derivatives. *Molecular Pharmacology* **67**: 1186-1194.
- Theobald, U., J. Schimana & H. P. Fiedler, (2000) Microbial growth and production kinetics of Streptomyces antibioticus Tu 6040. *Antonie Van Leeuwenhoek* **78**: 307-313.
- Thompson, J., C. B. Pratt, C. F. Stewart, L. Avery, L. Bowman, W. C. Zamboni & A. Pappo, (1999) Phase I study of DMP 840 in pediatric patients with refractory solid tumors. *Investigational New Drugs* **16**: 45-49.
- Ting, C.-Y., C.-T. Hsu, H.-T. Hsu, J.-S. Su, T.-Y. Chen, W.-Y. Tarn, Y.-H. Kuo, J. Whang-Peng, L. F. Liu & J. Hwang, (2003) Isodiospyrin as a novel human DNA topoisomerase I inhibitor. *Biochemical Pharmacology* **66**: 1981-1991.
- Tran, J. H., G. A. Jacoby & D. C. Hooper, (2005a) Interaction of the plasmid-encoded quinolone resistance protein Qnr with Escherichia coli DNA gyrase. *Antimicrob Agents Chemother* **49**: 118-125.
- Tran, J. H., G. A. Jacoby & D. C. Hooper, (2005b) Interaction of the plasmid-encoded quinolone resistance protein QnrA with Escherichia coli topoisomerase IV. *Antimicrob Agents Chemother* **49**: 3050-3052.
- Trask, D. K. & M. T. Muller, (1983) Biochemical characterization of topoisomerase I purified from avian erythrocytes. *Nucleic Acids Res* **11**: 2779-2800.
- Trefzer, A., S. Pelzer, J. Schimana, S. Stockert, C. Bihlmaier, H. P. Fiedler, K. Welzel, A. Vente & A. Bechthold, (2002) Biosynthetic gene cluster of simocyclinone, a natural multihybrid antibiotic. *Antimicrob Agents Chemother* **46**: 1174-1182.

- Tretter, E. M., A. J. Schoeffler, S. R. Weisfield & J. M. Berger, (2010) Crystal structure of the DNA gyrase GyrA N-terminal domain from *Mycobacterium tuberculosis*. *Proteins: Structure, Function, and Bioinformatics* **78**: 492-495.
- Tse-Dinh, Y. C., (2007) Exploring DNA topoisomerases as targets of novel therapeutic agents in the treatment of infectious diseases. *Infect Disord Drug Targets* **7**: 3-9.
- Tse, Y.-c. & J. C. Wang, (1980) *E. coli* and *M. luteus* DNA topoisomerase I can catalyze catenation or decatenation of double-stranded DNA rings. *Cell* **22**: 269-276.
- Tse, Y. C., K. Kirkegaard & J. C. Wang, (1980) Covalent bonds between protein and DNA. Formation of phosphotyrosine linkage between certain DNA topoisomerases and DNA. *J Biol Chem* **255**: 5560-5565.
- Unniraman, S., M. Chatterji & V. Nagaraja, (2002) DNA Gyrase Genes in *Mycobacterium tuberculosis*: a Single Operon Driven by Multiple Promoters. *J. Bacteriol.* **184**: 5449-5456.
- van der Kooy, F., J. J. M. Meyer & N. Lall, (2006) Antimycobacterial activity and possible mode of action of newly isolated neodiospyrin and other naphthoquinones from *Euclea natalensis*. *South African Journal of Botany* **72**: 349-352.
- Van Wyk, B. & P. Van Wyk, (1997) Field Guide to Trees of Southern Africa. *McKenzie, Cape Town*, : 184.
- Vizan, J. L., C. Hernandez-Chico, I. del Castillo & F. Moreno, (1991) The peptide antibiotic microcin B17 induces double-strand cleavage of DNA mediated by *E. coli* DNA gyrase. *EMBO J* **10**: 467-476.
- Von Groll, A., A. Martin, P. Jureen, S. Hoffner, P. Vandamme, F. Portaels, J. C. Palomino & P. A. da Silva, (2009) Fluoroquinolone resistance in *Mycobacterium tuberculosis* and mutations in *gyrA* and *gyrB*. *Antimicrob Agents Chemother* **53**: 4498-4500.
- Vyas, N. K., M. N. Vyas & F. A. Quioco, (1987) A novel calcium binding site in the galactose-binding protein of bacterial transport and chemotaxis. *Nature* **327**: 635-638.
- Wall, M. K., L. A. Mitchenall & A. Maxwell, (2004) *Arabidopsis thaliana* DNA gyrase is targeted to chloroplasts and mitochondria. *Proc Natl Acad Sci U S A* **101**: 7821-7826.
- Wang, B., L. M. Westerhoff & K. M. Merz, (2007) A Critical Assessment of the Performance of Protein–Ligand Scoring Functions Based on NMR Chemical Shift Perturbations. *Journal of Medicinal Chemistry* **50**: 5128-5134.
- Wang, J. C., (1971) Interaction between DNA and an *Escherichia coli* protein omega. *J Mol Biol* **55**: 523-533.
- Wang, J. C., (1985) DNA topoisomerases. *Annu Rev Biochem* **54**: 665-697.
- Wang, J. C., (1998) Moving one DNA double helix through another by a type II DNA topoisomerase: the story of a simple molecular machine. *Q Rev Biophys* **31**: 107-144.
- Wang, J. C., (2002) Cellular roles of DNA topoisomerases: a molecular perspective. *Nat Rev Mol Cell Biol* **3**: 430-440.
- Watson, J. D. & F. H. C. Crick, (1953) Molecular Structure of Nucleic Acids: A Structure for Deoxyribose Nucleic Acid. *Nature* **171**: 737-738.

- Wigley, D. B., G. J. Davies, E. J. Dodson, A. Maxwell & G. Dodson, (1991) Crystal structure of an N-terminal fragment of the DNA gyrase B protein. *Nature* **351**: 624-629.
- Williams, N. L., A. J. Howells & A. Maxwell, (2001) Locking the ATP-operated clamp of DNA gyrase: probing the mechanism of strand passage. *J Mol Biol* **306**: 969-984.
- Williams, N. L. & A. Maxwell, (1999a) Locking the DNA gate of DNA gyrase: investigating the effects on DNA cleavage and ATP hydrolysis. *Biochemistry* **38**: 14157-14164.
- Williams, N. L. & A. Maxwell, (1999b) Probing the two-gate mechanism of DNA gyrase using cysteine cross-linking. *Biochemistry* **38**: 13502-13511.
- Woldringh, C. & N. Nanninga, (1985) *Structure of nucleoid and cytoplasm in the intact cell*. Academic Press, London.
- Worcel, A. & E. Burgi, (1972) On the structure of the folded chromosome of *Escherichia coli*. *J Mol Biol* **71**: 127-147.
- Yamane, K., J. Wachino, S. Suzuki & Y. Arakawa, (2008) Plasmid-mediated qepA gene among *Escherichia coli* clinical isolates from Japan. *Antimicrob Agents Chemother* **52**: 1564-1566.
- Yang, F., G. Lu & H. Rubin, (1996) Cloning, expression, purification and characterization of DNA topoisomerase I of *Mycobacterium tuberculosis*. *Gene* **178**: 63-69.
- Yang, K., (2001) Prokaryotic calmodulins: recent developments and evolutionary implications. *J Mol Microbiol Biotechnol* **3**: 457-459.
- Yardley, V., D. Snowdon, S. Croft & B. Hazra, (1996) In vitro activity of Diospyrin and Derivatives against *Leishmania donovani*, *Trypanosoma cruzi* and *Trypanosoma brucei brucei*. *Phytotherapy Research* **10**: 559-562.
- Yoshida, H., M. Bogaki, M. Nakamura & S. Nakamura, (1990) Quinolone resistance-determining region in the DNA gyrase gyrA gene of *Escherichia coli*. *Antimicrob Agents Chemother* **34**: 1271-1272.
- Yoshida, H., M. Bogaki, M. Nakamura, L. M. Yamanaka & S. Nakamura, (1991) Quinolone resistance-determining region in the DNA gyrase gyrB gene of *Escherichia coli*. *Antimicrob Agents Chemother* **35**: 1647-1650.
- Young, D. B., M. D. Perkins, K. Duncan & C. E. Barry, 3rd, (2008) Confronting the scientific obstacles to global control of tuberculosis. *J Clin Invest* **118**: 1255-1265.
- Zechiedrich, E. L., A. B. Khodursky & N. R. Cozzarelli, (1997) Topoisomerase IV, not gyrase, decatenates products of site-specific recombination in *Escherichia coli*. *Genes & Development* **11**: 2580-2592.
- Zhou, J., Y. Dong, X. Zhao, S. Lee, A. Amin, S. Ramaswamy, J. Domagala, J. M. Musser & K. Drlica, (2000) Selection of antibiotic-resistant bacterial mutants: allelic diversity among fluoroquinolone-resistant mutations. *J Infect Dis* **182**: 517-525.
- Zhou, Y., W. Yang, M. Kirberger, H.-W. Lee, G. Ayalasomayajula & J. J. Yang, (2006) Prediction of EF-hand calcium-binding proteins and analysis of bacterial EF-hand proteins. *Proteins: Structure, Function, and Bioinformatics* **65**: 643-655.

- Zimmerman, S. B., (2006) Shape and compaction of Escherichia coli nucleoids. *J Struct Biol* **156**: 255-261.